

RADIOLOGY AND ONCOLOGY

vol.51 no.4

december 2017



NOVO



Cilja na 2 procesa nastanka CINV* v 1 odmerku
Zagotavlja učinkovito 5-dnevno preprečevanje CINV¹⁻⁵

En odmerek Dvojno delovanje 5-dnevno preprečevanje¹⁻⁵

Akynzeo[®]
netupitant/palonosetron

* CINV: Chemotherapy-induced nausea and vomiting
[Slabost in bruhanje povzročena s kemoterapijo]

1. Aapro M et al. Ann Oncol. 2014 Jul;25(7):1328-33.
2. Hesketh et al. Ann Oncol. 2014 Jul;25(7):1340-46.
3. Gralla RJ et al. Ann Oncol. 2014 Jul;25(7):1333-39.
4. Rojas C et al. Eur J Pharmacol. 2014 Jan 5;572:26-37.
5. Akynzeo SmPC, junij 2016

SKRAJŠAN POVZETEK GLAVNIH ZNAČILNOSTI ZDRAVILA

▼ Za to zdravilo se izvaja dodatno spremljanje varnosti. Tako bodo hitreje na voljo nove informacije o njegovi varnosti. Zdravstvene delavce naprošamo, da poročajo o katerem koli domnevnem neželenem učinku zdravila.

Akynzeo 300 mg/0,5 mg trde kapsule (netupitant/palonosetron)

TERAPEVTSKE INDIKACIJE Pri odraslih za preprečevanje akutne in zakasnjene navzee in bruhanja, povezanih z zelo emetogeno kemoterapijo na osnovi cisplatina za zdravljenje raka ter z zmerno emetogeno kemoterapijo za zdravljenje raka. **ODMERJANJE IN NAČIN UPORABE** Eno 300 mg/0,5 mg kapsulo je treba dati približno eno uro pred začetkom vsakega cikla kemoterapije. Trdo kapsulo je treba pogoltniti celo. Kapsulo je mogoče vzeti s hrano ali brez nje. Priporočeni peroralni odmerek deksametazona je treba ob sočasni uporabi z Akynzeom zmanjšati za približno 50 %. Prilagoditev odmerka pri starejših bolnikih ni potrebna. Pri uporabi tega zdravila pri bolnikih, starejših od 75 let, je potrebna previdnost zaradi daljšega razpolovnega časa zdravilnih učinkovin in omejenih izkušenj s to populacijo. Varnost in učinkovitost Akynzea pri pediatrični populaciji nista bili dokazani. Prilagoditev odmerka pri bolnikih z blago do hudo okvaro ledvic predvidoma ni potrebna. Potrebno se je izogibati uporabi Akynzea pri bolnikih s končnim stadijem bolezni ledvic, ki potrebujejo hemodializo. Pri bolnikih z blago ali zmerno okvaro jeter (stopnje 5-8 po lestvici Child-Pugh) prilagoditev odmerka ni potrebna. Pri bolnikih s hudo okvaro jeter (stopnja ≥ 9 po lestvici Child-Pugh) je treba Akynzeo uporabljati previdno. **KONTRAINDIKACIJE** Preobčutljivost na zdravilni učinkovini ali katero koli pomožno snov, nosečnost. **POSEBNA OPOZORILA IN PREVIDNOSTNI UKREPI** Ker lahko palonosetron podaljša čas prehoda skozi debelo črevo, je treba bolnike z anamnezo zaprja ali znaki subakutne zapore črevesa po dajanju zdravila spremljati. Pri uporabi antagonistov 5-HT₃ samih ali v kombinaciji z drugimi serotonergičnimi zdravili (vključno s selektivnimi zaviralci ponovnega privzema serotonina (SSRI) in zaviralci ponovnega privzema serotonina in noradrenalina (SNRI)) so poročali o serotoninskem sindromu. Priporočamo ustrezno opazovanje bolnikov glede simptomov, podobnih kot pri serotoninskem sindromu. Ker Akynzeo vsebuje antagonist receptorjev 5-HT₃, je potrebna previdnost pri sočasni uporabi z zdravili, ki podaljšujejo interval QT, ali pri bolnikih, ki so razvili podaljšan interval QT, oziroma je verjetno, da ga bodo. Tega zdravila ne smemo uporabljati za preprečevanje navzee in bruhanja v dneh po kemoterapiji, razen v povezavi z dajanjem naslednjega cikla kemoterapije. Ne smemo ga uporabljati za zdravljenje navzee in bruhanja po kemoterapiji. Pri bolnikih s hudo okvaro jeter je potrebna previdnost, saj je za te bolnike na voljo malo podatkov. To zdravilo je treba uporabljati previdno pri bolnikih, ki sočasno peroralno prejemajo zdravilne učinkovine, ki se primarno presnavljajo prek CYP3A4 in imajo ozko terapevtsko območje. Netupitant je zmeren zaviralec CYP3A4 in lahko poveča izpostavljenost kemoterapevtskim zdravilom, ki so substrati za CYP3A4, npr. docetaksel. Zaradi tega je treba bolnike spremljati glede povečane toksičnosti kemoterapevtskih zdravil, ki so substrati za CYP3A4, vključno z irinotekanom. Poleg tega lahko netupitant vpliva tudi na učinkovitost kemoterapevtskih zdravil, pri katerih je potrebna aktivacija prek presnove s CYP3A4. Akynzeo vsebuje sorbitol in saharozo. Bolniki z redko dedno intoleranco za fruktozo, malabsorpcijo glukoze/galaktoze ali pomanjkanjem saharoza-izomaltoze ne smejo jemati tega zdravila. Poleg tega lahko vsebuje tudi sledi lecitina, pridobljenega iz soje. Zaradi tega je treba bolnike z znano preobčutljivostjo na arašide

ali sojo skrbno spremljati glede znakov alergijske reakcije. Ženske v rodni dobi ne smejo biti noseče ali zanosit med zdravljenjem z Akynzeom. Pred začetkom zdravljenja je treba opraviti test nosečnosti pri vseh ženskah, ki še niso imele menopavze. Ženske v rodni dobi morajo uporabljati učinkovito kontracepcijo med zdravljenjem in še do en mesec po njem. Akynzeo je kontraindiciran med nosečnostjo. Med zdravljenjem z Akynzeom in še 1 mesec po zadnjem odmerku je treba prenehati z dojenjem. **INTERAKCIJE** Ob sočasni uporabi Akynzea z drugim zaviralcem CYP3A4 lahko pride do zvišanja plazemskih koncentracij netupitanta. Pri sočasni uporabi Akynzea in zdravil, ki spodbujajo delovanje CYP3A4, lahko pride do znižanja plazemskih koncentracij netupitanta, kar lahko privede do zmanjšane učinkovitosti. Akynzeo lahko zviša plazemske koncentracije sočasno uporabljenih zdravil, ki se presnavljajo prek CYP3A4. Ob sočasnem dajanju deksametazona z Akynzeom je treba peroralni odmerek deksametazona zmanjšati za približno 50 %. Ob sočasnem dajanju z Akynzeom se je izpostavljenost docetakselu in etopozidu povečala za 37 % oziroma 21 %. Pri ciklofosfamidu po sočasnem dajanju netupitanta niso opazili konsistentnih učinkov. Pri eritromicinu, midazolamu ali drugih benzodiazepinih, ki se presnavljajo prek CYP3A4 (alprazolam, triazolam), je treba ob sočasnem dajanju Akynzea upoštevati možne učinke njihovih zvišanih plazemskih koncentracij. Pri sočasnem dajanju Akynzea z močnimi zaviralci CYP3A4 (npr. ketokonazol) je potrebna previdnost, sočasnemu dajanju z močnimi spodbujevalci CYP3A4 (npr. rifampicin) pa se je treba izogibati. Priporočamo previdnost pri uporabi netupitanta v kombinaciji s peroralnim substratom encima UGT2B7 (npr. zidovudin, valprojska kislina, morfin), ker *in vitro* podatki kažejo, da netupitant zavira UGT2B7. Priporočamo previdnost pri kombiniranju netupitanta z digoksinom ali drugimi substrati P-gp, kot sta dabigatran ali kolhicin, ker podatki *in vitro* kažejo, da je netupitant zaviralec P-gp. **NEŽELENI UČINKI** Pogosti ($\geq 1/100$ do $< 1/10$): glavobol, zaprtje, utrujenost. Občasni ($\geq 1/1.000$ do $< 1/100$): nevtropenija, levkocitoza, zmanjšan apetit, nespečnost, omotica, vrtoglavica, atrijski blok prve stopnje, kardiomiopatija, motnja prevarjanja, hipertenzija, kolcanje, bolečina v trebuhu, driska, dispneja, naperjanje, navzea, alopecija, urtikarija, astenija, zvišane jetrne transaminaze, zvišana alkalna fosfataza v krvi, zvišan kreatinin v krvi, podaljšanje QT na elektrokardiogramu. Redki ($\geq 1/10.000$ do $< 1/1.000$): cistitis, levkopenija, limfocitoza, hipokalemija, akutna psihoza, sprememba razpoloženja, motnja spanja, hipestezijska, konjunktivitis, zamegljen vid, aritmija, atrijski blok druge stopnje, kračni blok, popuščanje mitralne zaklopke, miokardna ishemija, ventrikularne extrasistole, hipotenzija, disgagija, obložen jezik, bolečina v hrbtu, občutek vročine, nekardialna bolečina v prsnem košu, nenormalen okus zdravila, zvišan bilirubin v krvi, zvišana kreatin fosfokinaza MB v krvi, depresija segmenta ST na elektrokardiogramu, nenormalen segment ST-T na elektrokardiogramu, zvišan troponin. **Vrsta ovojnine in vsebina:** Škatla z eno kapsulo v prebršenem omotu iz aluminija. **Režim izdaj:** Rp Imetnik dovoljenja za promet: Helsinn Birex Pharmaceuticals Ltd, Damastown, Mulhuddart, Dublin 15, Irska AKY-062016

Pred predpisovanjem in uporabo zdravila prosimo preberite celoten povzetek glavnih značilnosti zdravila!

Samo za strokovno javnost!
AKY0816-01, avgust 2016

 **PharmaSwiss**
Choose More Life

Odgovoren za trženje v Sloveniji:
PharmaSwiss d.o.o., Brodšiče 32, 1236 Trzin
telefon: +386 1 236 47 00, faks: +386 1 283 58 10

 **HEL SIN N**
Building quality cancer care together



Publisher

Association of Radiology and Oncology

Affiliated with

Slovenian Medical Association – Slovenian Association of Radiology, Nuclear Medicine Society,
Slovenian Society for Radiotherapy and Oncology, and Slovenian Cancer Society
Croatian Medical Association – Croatian Society of Radiology
Societas Radiologorum Hungarorum
Friuli-Venezia Giulia regional groups of S.I.R.M.
Italian Society of Medical Radiology

Aims and scope

Radiology and Oncology is a journal devoted to publication of original contributions in diagnostic and interventional radiology, computerized tomography, ultrasound, magnetic resonance, nuclear medicine, radiotherapy, clinical and experimental oncology, radiobiology, radiophysics and radiation protection.

Editor-in-Chief

Gregor Serša, Institute of Oncology Ljubljana,
Department of Experimental Oncology, Ljubljana,
Slovenia

Executive Editor

Viljem Kovač, Institute of Oncology Ljubljana,
Department of Radiation Oncology, Ljubljana, Slovenia

Editorial Board

Sotirios Bisdas, National Hospital for Neurology
and Neurosurgery, University College London
Hospitals, London, UK

Karl H. Bohuslavizki, Facharzt für
Nuklearmedizin, Hamburg, Germany

Serena Bonin, University of Trieste, Department of
Medical Sciences, Trieste, Italy

Boris Brkljačić, University Hospital “Dubrava”,
Department of Diagnostic and Interventional
Radiology, Zagreb, Croatia

Luca Campana, Veneto Institute of Oncology
(IOV-IRCCS), Padova, Italy

Christian Dittreich, Kaiser Franz Josef - Spital,
Vienna, Austria

Metka Filipič, National Institute of Biology,
Department of Genetic Toxicology and Cancer Biology,
Ljubljana, Slovenia

Maria Gódehy, National Institute of Oncology,
Budapest, Hungary

Janko Kos, University of Ljubljana, Faculty of
Pharmacy, Ljubljana, Slovenia

Robert Jeraj, University of Wisconsin, Carbone
Cancer Center, Madison, Wisconsin, USA

Advisory Committee

Tullio Girdali, University of Trieste, Faculty of
Medicine and Psychology, Trieste, Italy

Vassil Hadjidekov, Medical University,
Department of Diagnostic Imaging, Sofia, Bulgaria

Deputy Editors

Andrej Čör, University of Primorska, Faculty of
Health Science, Izola, Slovenia

Maja Čemažar, Institute of Oncology Ljubljana,
Department of Experimental Oncology, Ljubljana,
Slovenia

Igor Kocijančič, University Medical Centre
Ljubljana, Institute of Radiology, Ljubljana, Slovenia

Karmen Stanič, Institute of Oncology Ljubljana,
Department of Radiation Oncology, Ljubljana, Slovenia

Primož Strojjan, Institute of Oncology Ljubljana,
Department of Radiation Oncology, Ljubljana, Slovenia

Tamara Lah Turnšek, National Institute of
Biology, Ljubljana, Slovenia

Damijan Miklavčič, University of Ljubljana,
Faculty of Electrical Engineering, Ljubljana, Slovenia

Luka Milas, UT M. D. Anderson Cancer Center,
Houston, USA

Damir Miletić, Clinical Hospital Centre Rijeka,
Department of Radiology, Rijeka, Croatia

Håkan Nyström, Skandionkliniken,
Uppsala, Sweden

Maja Osmak, Ruder Bošković Institute,
Department of Molecular Biology, Zagreb, Croatia

Dušan Pavčnik, Dotter Interventional Institute,
Oregon Health Science University, Oregon,
Portland, USA

Geoffrey J. Pilkington, University of
Portsmouth, School of Pharmacy and Biomedical
Sciences, Portsmouth, UK

Ervin B. Podgoršak, McGill University,
Montreal, Canada

Matthew Podgorsak, Roswell Park Cancer
Institute, Departments of Biophysics and Radiation
Medicine, Buffalo, NY, USA

Marko Hočevar, Institute of Oncology Ljubljana,
Department of Surgical Oncology, Ljubljana, Slovenia

Miklós Kásler, National Institute of Oncology,
Budapest, Hungary

Csaba Polgar, National Institute of Oncology,
Budapest, Hungary

Dirk Rades, University of Lubeck, Department of
Radiation Oncology, Lubeck, Germany

Mirjana Rajer, Institute of Oncology Ljubljana,
Department of Radiation Oncology, Ljubljana, Slovenia

Luis Souhami, McGill University, Montreal,
Canada

Borut Štabuc, University Medical Centre Ljubljana,
Department of Gastroenterology, Ljubljana, Slovenia

Katarina Šurlan Popovič, University Medical
Center Ljubljana, Clinical Institute of Radiology,
Ljubljana, Slovenia

Justin Teissié, CNRS, IPBS, Toulouse, France

Gillian M. Tozer, University of Sheffield,
Academic Unit of Surgical Oncology, Royal
Hallamshire Hospital, Sheffield, UK

Andrea Veronesi, Centro di Riferimento
Oncologico - Aviano, Division of Medical Oncology,
Aviano, Italy

Branko Zakotnik, Institute of Oncology Ljubljana,
Department of Medical Oncology, Ljubljana, Slovenia

Stojan Plesničar, Institute of Oncology Ljubljana,
Department of Radiation Oncology, Ljubljana, Slovenia

Tomaž Benulič, Institute of Oncology Ljubljana,
Department of Radiation Oncology, Ljubljana, Slovenia

Editorial office

Radiology and Oncology

Zaloška cesta 2

P. O. Box 2217

SI-1000 Ljubljana

Slovenia

Phone: +386 1 5879 369

Phone/Fax: +386 1 5879 434

E-mail: gsera@onko-i.si

Copyright © Radiology and Oncology. All rights reserved.

Reader for English

Vida Kološa

Secretary

Mira Klemenčič

Zvezdana Vukmirović

Design

Monika Fink-Serša, Samo Rován, Ivana Ljubanović

Layout

Matjaž Lužar

Printed by

Tiskarna Ozimek, Slovenia

Published quarterly in 400 copies

Beneficiary name: DRUŠTVO RADIOLOGIJE IN ONKOLOGIJE

Zaloška cesta 2

1000 Ljubljana

Slovenia

Beneficiary bank account number: SI56 02010-0090006751

IBAN: SI56 0201 0009 0006 751

Our bank name: Nova Ljubljanska banka, d.d.,

Ljubljana, Trg republike 2,

1520 Ljubljana; Slovenia

SWIFT: LJBASIX

Subscription fee for institutions EUR 100, individuals EUR 50

The publication of this journal is subsidized by the Slovenian Research Agency.

Indexed and abstracted by:

- *Celdes*
- *Chemical Abstracts Service (CAS)*
- *Chemical Abstracts Service (CAS) - SciFinder*
- *CNKI Scholar (China National Knowledge Infrastructure)*
- *CNPIEC*
- *DOAJ*
- *EBSCO - Biomedical Reference Collection*
- *EBSCO - Cinahl*
- *EBSCO - TOC Premier*
- *EBSCO Discovery Service*
- *Elsevier - EMBASE*
- *Elsevier - SCOPUS*
- *Google Scholar*
- *J-Gate*
- *JournalTOCs*
- *Naviga (Softweco)*
- *Primo Central (ExLibris)*
- *ProQuest - Advanced Technologies Database with Aerospace*
- *ProQuest - Health & Medical Complete*
- *ProQuest - Illustrata: Health Sciences*
- *ProQuest - Illustrata: Technology*
- *ProQuest - Medical Library*
- *ProQuest - Nursing & Allied Health Source*
- *ProQuest - Pharma Collection*
- *ProQuest - Public Health*
- *ProQuest - Science Journals*
- *ProQuest - SciTech Journals*
- *ProQuest - Technology Journals*
- *PubMed*
- *PubsHub*
- *ReadCube*
- *SCImago (SJR)*
- *Summon (Serials Solutions/ProQuest)*
- *TDOne (TDNet)*
- *Thomson Reuters - Journal Citation Reports/Science Edition*
- *Thomson Reuters - Science Citation Index Expanded*
- *Ulrich's Periodicals Directory/ulrichsweb*
- *WorldCat (OCLC)*

This journal is printed on acid-free paper

On the web: ISSN 1581-3207

<http://www.degruyter.com/view/j/raon>

<http://www.radioloncol.com>

contents

review

- 369 **Carcinogenesis induced by low-dose radiation**
Igor Piotrowski, Katarzyna Kulcenty, Wiktoria Maria Suchorska, Agnieszka Skrobata, Małgorzata Skórska, Marta Kruszyna-Mochalska, Anna Kowalik, Weronika Jackowiak, Julian Malicki

nuclear medicine

- 378 **Clinical significance of fluorine-18-fluorodeoxyglucose positron emission tomography/computed tomography in the follow-up of colorectal cancer: searching off approaches increasing specificity for detection of recurrence**
Semra Ince, Kursat Okuyucu, Oguz Hancerliogullari, Engin Alagoz, Huseyin San, Nuri Arslan

radiology

- 386 **Is there a role for contrast-enhanced ultrasound in the detection and biopsy of MRI only visible breast lesions?**
Aki Nykänen, Otso Arponen, Anna Sutela, Ritva Vanninen, Mazen Sudah
- 393 **Baseline tumor Lipiodol uptake after transarterial chemoembolization for hepatocellular carcinoma: identification of a threshold value predicting tumor recurrence**
Yusuke Matsui, Masahiro Horikawa, Younes Jahangiri Noudeh, John A. Kaufman, Kenneth J. Kolbeck, Khashayar Farsad
- 401 **The relationship between chondromalacia patella, medial meniscal tear and medial periarticular bursitis in patients with osteoarthritis**
Mustafa Resorlu, Davut Doner, Ozan Karatag, Canan Akgun Toprak

experimental oncology

- 407 **Phytotherapeutics oridonin and ponocidin show additive effects combined with irradiation in pancreatic cancer *in vitro***
Jakob Liermann, Patrick Naumann, Franco Fortunato, Thomas E. Schmid, Klaus-Josef Weber, Jürgen Debus, Stephanie E. Combs
- 415 **Focused transhepatic electroporation mediated by hypersaline infusion through the portal vein in rat model. Preliminary results on differential conductivity**
Clara Pañella, Quim Castellví, Xavier Moll, Rita Quesada, Alberto Villanueva, Mar Iglesias, Dolores Naranjo, Patricia Sánchez-Velázquez, Anna Andaluz, Luís Grande, Antoni Ivorra, Fernando Burdío

- 422 **Minimally invasive electrochemotherapy procedure for treating nasal duct tumors in dogs using a single needle electrode**

Felipe Maglietti, Matías Tellado, Nahuel Olaiz, Sebastian Michinski, Guillermo Marshall

- 431 **Metformin enhanced *in vitro* radiosensitivity associates with G2/M cell cycle arrest and elevated adenosine-5'-monophosphate-activated protein kinase levels in glioblastoma**

Sebastian Adeberg, Denise Bernhardt, Semi B. Harrabi, Nils H. Nicolay, Juliane Hörner-Rieber, Laila König, Michael Repka, Angela Mohr, Amir Abdollahi, Klaus-Josef Weber, Juergen Debus, Stefan Rieken

clinical oncology

- 438 **Evaluation of deformable image registration (DIR) methods for dose accumulation in nasopharyngeal cancer patients during radiotherapy**

Wannapha Nobnop, Imjai Chitapanarux, Hudsaleark Neamin, Somsak Wanwilairat, Vicharn Lorvidhaya, Taweap Sanghangthum

- 447 **Long term results of radiotherapy in vulvar cancer patients in Slovenia between 1997-2004**

Helena Barbara Zobec Logar

- 455 **Association between SLC19A1 gene polymorphism and high dose methotrexate toxicity in childhood acute lymphoblastic leukaemia and non Hodgkin malignant lymphoma: introducing a haplotype based approach**

Barbara Faganel Kotnik, Janez Jazbec, Petra Bohanec Grabar, Cristina Rodriguez-Antona, Vita Dolžan

- 463 **Impact on radiation dose and volume V57 Gy of the brain on recurrence and survival of patients with glioblastoma multiformae**

Igor Stojkovski, Valentina Krstevska, Snezhana Smichkoska

radiophysics

- 469 **Quality assurance procedures based on dosimetric, gamma analysis as a fast reliable tool for commissioning brachytherapy treatment planning systems**

Grzegorz Zwierzchowski, Grzegorz Bieledda, Janusz Skowronek

| *slovenian abstracts*

Carcinogenesis induced by low-dose radiation

Igor Piotrowski¹, Katarzyna Kulcenty^{1,2}, Wiktoria Maria Suchorska^{1,2}, Agnieszka Skrobata^{2,3}, Małgorzata Skórska³, Marta Kruszyna-Mochalska^{2,3}, Anna Kowalik³, Weronika Jackowiak⁴, Julian Malicki^{2,3}

¹ Radiobiology Laboratory, Department of Medical Physics, Greater Poland Cancer Centre, Poznań, Poland

² Department of Electroradiology, University of Medical Sciences, Poznań, Poland

³ Department of Medical Physics, Greater Poland Cancer Centre, Poznań, Poland

⁴ Radiotherapy Ward I, Greater Poland Cancer Centre, Poznań, Poland

Radiol Oncol 2017; 51(4): 369-377.

Received 4 July 2017

Accepted 25 September 2017

Correspondence to: Dr. Katarzyna Kulcenty, Radiobiology Laboratory, Department of Medical Physics, Greater Poland Cancer Centre, Garbary 15 Street, Poznań, Poland. E-mail: katarzyna.kulcenty@wco.pl

Igor Piotrowski and Katarzyna Kulcenty contributed equally to this work.

Disclosure: No potential conflicts of interest were disclosed.

Background. Although the effects of high dose radiation on human cells and tissues are relatively well defined, there is no consensus regarding the effects of low and very low radiation doses on the organism. Ionizing radiation has been shown to induce gene mutations and chromosome aberrations which are known to be involved in the process of carcinogenesis. The induction of secondary cancers is a challenging long-term side effect in oncologic patients treated with radiation. Medical sources of radiation like intensity modulated radiotherapy used in cancer treatment and computed tomography used in diagnostics, deliver very low doses of radiation to large volumes of healthy tissue, which might contribute to increased cancer rates in long surviving patients and in the general population. Research shows that because of the phenomena characteristic for low dose radiation the risk of cancer induction from exposure of healthy tissues to low dose radiation can be greater than the risk calculated from linear no-threshold model. Epidemiological data collected from radiation workers and atomic bomb survivors confirms that exposure to low dose radiation can contribute to increased cancer risk and also that the risk might correlate with the age at exposure.

Conclusions. Understanding the molecular mechanisms of response to low dose radiation is crucial for the proper evaluation of risks and benefits that stem from these exposures and should be considered in the radiotherapy treatment planning and in determining the allowed occupational exposures.

Key words: low-dose radiation; carcinogenesis; DNA; radiation induced bystander effect

Introduction

Ionizing radiation is widely used in medical procedures, including cancer radiotherapy and the use in diagnosis.¹ For over a century the biological effects of medium- and high-dose radiation (over 0.5 Gy) on human health have been investigated. Induction of cancer is one of the most severe long-term effects of radiotherapy. While the relationship between radiation effects and dose is well defined at higher doses, the effects of doses below 0.5 Gy are still unclear. Even though the use of radiotherapy resulted in a significant increase in cancer survivors², it is important to investigate the potential

negative long-term effects of radiation, considering that further advancements in therapy result in increased length of patients life after therapy. Table 1 presents the classification of radiation doses according to Kadhim *et al.*³ paired with examples of exposures.

The damage to DNA is induced by radiation through two mechanisms: the direct and indirect effect.⁹ Directly induced damage results from the deposition of radiation energy in the DNA molecule creating a break. Damage induced indirectly is a result of an attack of the reactive species, which might be produced from ionization of water, on DNA molecule. These processes induced by radia-

TABLE 1. Dose ranges and sources of radiation exposure

	Dose range	Examples of exposure
Very low doses	< 0.05 Gy	Mammography ⁴ , chest X-ray ⁴
Low doses	0.05–0.5 Gy	Cardiac CT angiogram ⁴
Medium doses	0.5–5 Gy	One fraction dose in standard fractionated radiotherapy ⁵ , dose absorbed by workers during Fukushima accident ⁶
High doses	5–15 Gy	Intraoperative radiotherapy (as boost) ⁷
Very high doses	> 15 Gy	Intraoperative radiotherapy ⁸ , cumulative dose delivered during fractionated radiotherapy ⁵

tion result in creation of single-strand breaks (SSB) and double-strand breaks (DSB) in DNA molecule.¹⁰ DSBs are prime lesions induced by ionizing radiation, and are responsible for its deleterious effect. Densely ionizing radiation has the ability to induce more damage per cell, making it possible for two or more lesions to be induced in proximity. These groups of breaks are called clustered DNA lesions, and are harder to repair than single DSBs and SSBs.¹¹ Density of radiation correlates with reparability of DNA lesions, with densely ionizing radiation being harder to repair. Radiation stimulates DNA damage repair through non-homologous end-joining (NHEJ)¹², an error prone pathway that can lead to induction of chromosome aberrations, which in turn may cause genomic instability.¹³ Genomic instability has been connected to induction of most of the human cancers, however currently the exact mechanism of radiation-induced carcinogenesis is not clear.

The dose-rate of radiation plays a major role in how much damage an exposed cell receives. High

dose-rate irradiation, like radiation created by atomic bomb, results in deployment of energy in very short time to every irradiated cell. However if radiation is protracted over long periods of time, like the dose-rates considered in calculations of occupational and environmental radiation risks, the cell turnover influences how many 'hits' a cell will receive. Low-dose rates also influence how cell reacts regarding the repair of DNA damage, since low-dose rates allow more time for damage to be repaired which makes it more favorable for cells than high-dose rate radiation.¹⁴

This review contains a description of biological consequences of low-dose radiation and possible induction of cancer (Figure 1).

DNA damage

Damage to DNA is one of the most important factors in radiation induced cancer transformation. Even though ionizing radiation induces one DSB per 20 SSBs, research indicates that DSBs are much more impactful effect of irradiation (IR).¹⁵ This difference might be caused by the fact that SSBs are repaired by error-free mechanisms and are not sustained, while DSBs induced by radiation are repaired by mechanisms prone to mis-repair and repair failure, making DSBs a main cause of radiation induced cell death.¹⁶ Recently many authors pointed towards important differences between DNA damage response exerted by high and low doses of radiation.^{17,18} Research of low dose effect on normal tissues is especially significant considering side effects of radiotherapy treatment.

Induction of DSBs is considered to be one of the main mechanisms by which radiation exerts its deleterious effect. One of the earliest events appearing in response to DSB induction is phosphorylation of histone H2AX by protein kinases: DNA-dependent protein kinase catalytic subunit (DNA-PKcs), ataxia telangiectasia and Rad3-related (ATR) and ataxia telangiectasia mutated (ATM).¹⁹ Phosphorylated H2AX (γ H2AX) foci appears around the DNA break as a part of DSB repair mechanism²⁰ and it corresponds directly with the number of DSBs.²¹ The correlation between the radiation dose and the initial number of γ H2AX foci it induces has already been thoroughly described.^{21,22} Rothkamm *et al.*²³ have shown that this linear correlation holds true also for the X-ray doses as low as 1 mGy (at dose rate of 6–60 mGy/min) for nondividing human fibroblasts cultured *in vitro*. Interestingly, authors came to the conclu-

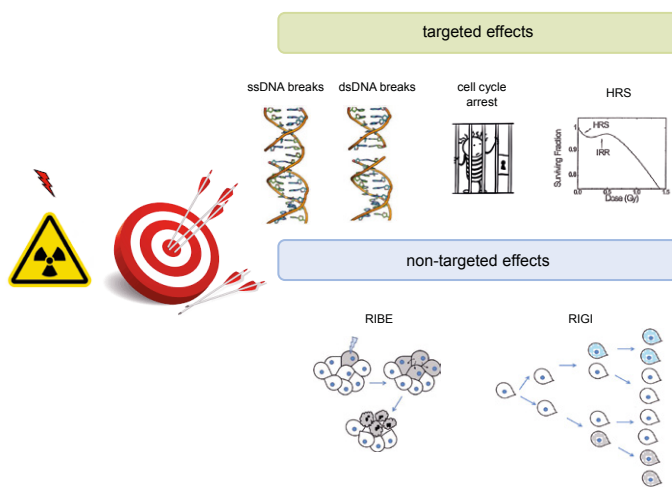


FIGURE 1. Diagram illustrating targeted and non-targeted effect induced by radiation (all described in the main text).

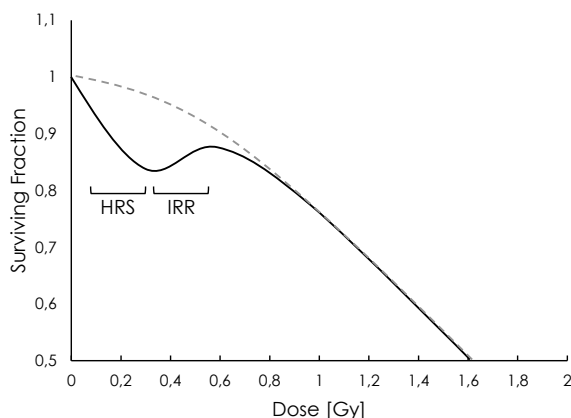


FIGURE 2. Schematic diagram illustrating cell survival curve for cells exhibiting low dose hyper radiosensitivity (HRS). Solid line shows survival curve with evidence of HRS and increased radioresistance (IRR). Dashed line shows survival curve with no evidence of HRS and IRR. Image adapted from.²⁹

sion that the damage induced by these very low doses remains unrepaired and evidence suggests that the cells with unrepaired DSBs are eliminated. Similar results were observed recently by Osipov *et al.* in research conducted on human MSCs isolated from oral mucosa.²⁴ Authors measured kinetics of γ H2AX and pATM foci formation after irradiation with X-rays at doses ranging from 20 mGy to 250 mGy and a dose rate of 40 mGy/min. Linear correlation between the number of γ H2AX foci and radiation dose was observed at all time-points after irradiation. For the intermediate doses (160 and 250 mGy) the highest number of foci was observed at 60 min followed by a significant decrease, which is typical for γ H2AX kinetics observed at higher doses. However for the lower doses (20, 40 and 80 mGy) after initial rise in γ H2AX foci number no decrease was observed. Considering the fact that pATM foci did not co-localize with γ H2AX foci at low doses and the fact that low dose radiation stimulates the MSC proliferation²⁵, authors propose that the persistence of γ H2AX foci after irradiation with low dose X-rays might be a consequence of new DSBs appearing as a result of replication stress rather than resulting from inefficient repair of DSBs. It is important to note that doses used in these experiments are in range of doses used in diagnostic procedures like CT scan.²⁶ However high linear energy transfer (LET) radiation has also been shown to induce ATM-dependent responses at low doses.²⁷ Fibroblasts isolated from patients with ataxia telangiectasia and healthy persons were irradiated with carbon ion beams (LET = 70 keV/ μ m) or with X-rays at doses between 0.1 to 2 Gy. Results

have shown that mutation frequency and cell survival after low dose carbon ion irradiation were dependent on ATM status. Authors also compared the number of γ H2AX foci in cells with different activity of ATM irradiated with 0.2 Gy of carbon ion radiation. Results indicate that ATM plays an important role in early DSB recognition and can be responsible for inefficient DSB repair, which is in line with conclusions reached by Osipov *et al.*²⁴ Authors also observed that doses higher than 0.5 Gy of carbon ion radiation caused an early G2/M arrest dependent on ATM. Some authors suggest that occurrence of this arrest might support DNA DSB repair, while a failure to induce early G2 arrest can be one of the factors responsible for low dose hyper-radiosensitivity (HRS).²⁸

Low-dose hyper radiosensitivity (HRS)

HRS is described as an increase in radiosensitivity in cells exposed to low-dose radiation, usually below 0.2–0.3 Gy for low LET radiation. When cells are exposed to doses higher than 0.3 Gy an increase in radioresistance is observed and the transition towards it on dose response curve is described as increased radioresistance (IRR).²⁹ Figure 2 presents the dose-response curves with and without the evidence of HRS and IRR. Occurrence of HRS and IRR in cells was first described using an *in vitro* culture of V79 Chinese hamster cells.³⁰ Cells were exposed to X-ray radiation doses ranging between 0.01 and 10 Gy. Using clonogenic assay authors have shown increased effectiveness of X-ray doses below 0.2 Gy. Cells exposed to doses higher than 0.4 Gy experienced a rise in radioresistance. Authors hypothesized that only X-ray doses above certain threshold can induce enough damage to activate DNA damage repair mechanisms. The dependence of HRS occurrence on cell cycle phase was also firstly noted in this research. Since then, research of HRS on different cell lines reported that HRS is increased in G2-phase cells.^{31,32} To prove this concept Short *et al.*³¹ used two glioma cell lines – T98G exhibiting HRS and U373 that did not exhibit HRS. Using cell counting authors have shown that G2 population of T98G cells irradiated with low dose X-rays demonstrated more pronounced HRS than cells in asynchronous population. Interestingly the G2 population of U373 cells also exhibited HRS indicating that in the asynchronous population the response of G1 and S-phase cells dominates. These results show that actively proliferating cells might

be more sensitive to low doses of radiation. It is important to note, that HRS can potentially be used to therapeutic advantage. Using ultra-fractionation with doses in HRS range it is possible to achieve more cytotoxic effects than after administration of same total dose at once.³³

Cell cycle arrest

In order to repair the damaged DNA, irradiated cells utilize cell cycle arrest to allow sufficient time for the DNA repair. The most important checkpoint pathways that initiate the radiation-induced arrest inhibit the cell cycle progression from G2 phase to mitosis. Two checkpoints are utilized for the repair of DNA damage induced by radiation. The classic G2/M checkpoint is activated after high doses of radiation and its role is to arrest the cells damaged in S or G1 cell cycle phase.³⁴ The early G2/M checkpoint is activated shortly after exposure to radiation and it exclusively protects cells in G2 phase of cell cycle from radiation effects.³⁵ This checkpoint is especially relevant to assessment of low-dose radiation risks because induction of this checkpoint occurs after irradiation with doses up to 10 Gy of low LET radiation³⁵ and a threshold for its activation is observed at radiation doses of 0.3 Gy.³⁶ This threshold dose coincides with radiation doses at which a transition between HRS and IRR is observed, suggesting a correlation between the two phenomenon, which was first suggested by Marples *et al.*³⁶ The activation of early G2/M checkpoint is mediated by radiation-induced, DSB-dependent phosphorylation of ATM.³⁷ It has been hypothesized that ATM acts by an interplay with Chk1 and Chk2.³² Inhibition of these factors in fibroblast cells results in an enhanced HRS response, however it also causes an increase in IRR. It is important to note that the response varied depending on the HRS status of the cell lines used.

While even very low doses of radiation are capable of inducing DSBs, there is evidence suggesting a threshold number of 10–20 DSBs for the triggering of ATM dependent G2/M checkpoint.³⁸ This can mean that low doses of radiation inducing few DSBs may not trigger G2/M arrest in irradiated cells, making it possible for cells with unrepaired DSBs to enter mitosis, which in turn might result in loss of genetic material.³⁹ Deckbar *et al.*⁴⁰ investigated induction of G2 arrest by X-ray radiation on immortalized fibroblasts and on primary human cells. γ H2AX foci count confirms, that cells irradiated with X-ray doses inducing fewer than ~20

DSBs (below 0.6 Gy for immortalized fibroblasts and below 0.2 Gy for primary human cells) did not enter G2 arrest. In cells irradiated with doses above the threshold dose, cells that exited the G2 checkpoint still had ~20 unrepaired DSBs and 1–2 chromosome breaks. These results indicate that a certain threshold of DSBs and chromosome aberrations is necessary for both activating and maintaining the G2 checkpoint arrest. The threshold dose at which G2 arrest is induced can play a role in low-dose radiosensitivity of a cell. Different cell lines show variability in this threshold dose. Although this threshold usually varies between 0.2 Gy and 0.6 Gy, in some cell lines the cell cycle arrest is induced without threshold.⁴¹ Currently the mechanism behind this difference in threshold dose is not known, however a hypothesis has been proposed stating that cell lines which show early G2 checkpoint after exposure to very low doses might have higher base level of DSBs, making it much easier to reach the number of DSBs needed for G2 arrest induction.⁴¹

Mutation in ATM gene observed in Ataxia telangiectasia, has been connected with increased chromosomal radiosensitivity and increased susceptibility to cancer.⁴² Since both DNA damage repair and G2 checkpoint induction depend on ATM kinase, Ataxia telangiectasia (AT) cells are often used to investigate the mechanisms of these processes. Using AT cells researchers were able to show for the first time that G2 checkpoint facilitates not only the repair of DSBs, but also the repair of chromosomal breaks, after irradiation with 1 Gy ionizing radiation.⁴³ Failure to activate the G2 checkpoint might be one of the reasons for increased cancer rates in patients with Ataxia telangiectasia, since unrepaired damage to DNA might alter cells genome leading to malignant transformation.⁴²

Non-targeted effects

Radiation induced genomic instability (RIGI)

Radiation induced DNA damage, specifically DSBs, are very important in occurrence of chromosomal instability, which may involve aneuploidy, deletions, and aberrations, which in turn might contribute to carcinogenesis.⁴⁴ The non-targeted effects, including bystander effects and genomic instability, contribute to the induction of cancer in a less clear way.⁴⁵ The progeny of exposed cell might exhibit phenotypes such as chromosomal aberrations and rearrangements, gene mutations and en-

hanced cell death rate.⁴⁶ Acquisition of alterations in the genome of progeny of irradiated cells is described as genomic instability (GI) and it has been accepted as the hallmark of cancer cells and one of the most important factors involved in the development of some cancers.⁴⁴ RIGI was firstly observed in one-cell mouse embryos irradiated with X-rays and with neutrons.⁴⁷ The results suggested that chromosomal aberrations might appear de novo two or three mitoses after initial exposure and also that radiation of a different quality (different LET) induces aberrations at different frequencies.

In the context of RIGI the effect on genome is mediated via the accumulation of genetic changes in the progeny of surviving irradiated cells through many generations.⁴⁸ The capacity to induce genomic instability depends on both dose and quality of radiation, with high LET radiation generally inducing chromosome- and chromatid-type aberrations more effectively.⁴⁹ This effect was observed in murine bone marrow cells irradiated with 0.25 Gy, 0.5 Gy and 1 Gy of densely ionizing α -radiation.⁵⁰ Colonies arising from irradiated cells exhibited high frequency of non-clonally induced chromatid aberrations consistent with them arising de novo and not directly from irradiation. Early studies using human lymphocytes irradiated *in vitro* show the ability of low dose X-rays to induce chromosomal aberrations.⁵¹ Linearity of chromosomal aberration yield was observed above doses of 20 mGy while doses below 20 mGy resulted in yields lower than background. Many researchers have tried to elucidate the mechanisms behind RIGI, especially induced by low dose radiation. Maxwell *et al.* observed that in HMEC cells irradiated with X-ray doses ranging from 10 to 200 cGy frequency of chromosomal aberrations increased with dose.⁵² In cells irradiated with 50 cGy the frequency of chromosome aberrations increased with time after irradiation up to 72 h. Interestingly, administration of TGF- β , a growth factor whose activity is induced by radiation, resulted in elimination of cells with chromosome aberrations. The elimination was mediated by induction of p53-dependent apoptosis in genomically unstable cells. Authors also concluded that chromosomal aberrations induced in this experiment are a targeted effect, as induction of chromosomal aberrations above 10 cGy was proportional to dose.

TGF- β signaling can be induced in nontransformed cells irradiated with very low doses of radiation. It has been shown that TGF- β signaling selectively induces reactive oxygen species (ROS) production in transformed cells leading to their

apoptosis.⁵³ This signaling pathway could be a part of surveillance network protecting cells from malignant transformation. It is important to note, that radiation induced EMT phenotype can be mediated by TGF- β , making it a "two-edged sword" in need of further investigation.⁵⁴ Authors suggest that while TGF- β might play a role in elimination of irradiated, genomically unstable cells, the chronic exposition to radiation and TGF- β signaling can induce EMT in remaining cells.⁵³

Dicentric chromosomes are an established marker used to assess IR induced chromosomal aberrations.⁵⁵ Using the measurement of dicentric frequency in human fibroblasts after irradiation, researchers were able to investigate the role of dose-rate effect in induction of chromosome aberrations.¹³¹ In cells irradiated with a single X-ray dose the frequency of dicentrics correlated exponentially with doses higher than 0.2 Gy. Irradiation of cells with a single 1 Gy dose of X-rays resulted in similar rise of frequency of dicentrics as irradiation with fractionated 1 Gy dose (fractionation: 10 x 0.1 Gy; 5 x 0.2 Gy; 2 x 0.5 Gy) given with intervals of 1 min between fractions. When intervals between fractions were increased above 5 min, the frequency of dicentric chromosomes was significantly lower, which suggests that the maximum of DNA damage repair, in relation to chromosome dicentrics, is reached after 5 min. These results show that high dose rate irradiation is more harmful to the genome than low dose rate. The measurement of frequency of dicentrics in patients lymphocytes could be utilized in examination of radiosensitivity. Linear dose response of dicentric frequency was observed in human lymphocytes after irradiation with X-ray doses above 20 mGy.⁵¹ Frequency of dicentrics was also used to evaluate human lymphocytes response to low LET γ -rays. While for doses above 20 mGy a linear increase in dicentric frequency was observed, authors were not able to detect statistically significant changes in dicentric frequencies below 20 mGy doses, despite counting over 5000 metaphases.⁵⁶ This means that dicentric frequency count might not be a precise enough method for assessment of response to very low doses.

Aneuploidy is a phenotype very often observed in tumors and it arises from incorrect chromosome segregation during mitosis.⁵⁷ Delayed appearance of aneuploid cells induced by low-dose radiation has been observed *in vitro* in human fibroblasts.⁵⁸ Fibroblasts were irradiated with X-ray doses of 20, 50 or 100 cGy and cultured for five passages. As an end point authors picked assessment of mi-

micronuclei (MN) formation with special probes for analysis of structural and numerical aberrations⁵⁹, with chromosomes 1 and 4 picked for aneuploidy analysis. Micronuclei are generated in the progeny of irradiated cells as a result of *de novo* generation of chromosome aberrations.⁴⁹ After X-ray irradiation with doses of 50 and 100 cGy frequencies of centromere-positive and negative MNs increased significantly. Frequency of aneuploidy increased with dose in a dose-dependent manner and after irradiation with 50 and 100 cGy the increase in aneuploidy with time was observed. The data show that after irradiation with low doses, chromosomal aberrations appear *de novo* up to five population doublings, which as authors suggest, might be connected with variability in the number of centrosomes.⁶⁰

One of the radiation induced phenotypes used to investigate genetic effects of low-dose radiation is loss of heterozygosity (LOH). LOH is conventionally associated with cancer as a mechanism inactivating tumor suppressor genes, however it is also found in regions of genome responsible for cancer induction.⁶¹ For research on induction of mutations *in vitro*, TK6 cells are often used, as this cell line contains heterozygosity at the thymidine kinase (TK) locus. In one of the experiments irradiation of TK6 cells with 10 cGy X-rays caused a significant increase in hemizygous LOH.⁶¹ Hemizygous type of LOH is a result of homologous end joining, a repair pathway observed after irradiation. Umabayashi *et al.* analyzed induction of LOH in TK6 cells after irradiation with low-dose, low dose-rate γ -irradiation.⁶² Even irradiation with the dose as low as 30 mGy increased the frequency of early mutations in TK gene almost 2-fold. Authors claim that detection of LOH is an efficient system for estimation of genetic effects induced by low-dose radiation.

Radiation induced bystander effect

Another non-targeted effect playing a role in carcinogenesis is radiation induced bystander effect (RIBE). This effect together with other non-targeted effects, is often described as most relevant to low-dose radiation⁶³ and is mediated through two mechanisms: secretion of soluble factors by irradiated cells⁶⁴ and also by signaling through cell-to-cell junctions.⁶⁵ One of the early works in which this effect was described used Chinese hamster ovary (CHO) cells irradiated with low doses of α -radiation.⁶⁶ The authors chose very low radiation dose (0.31 mGy), so that less than 1% of cells

were traversed through by the radiation. After irradiation close to 30% cells exhibited presence of sister chromatid exchanges which suggests, that the genetic damage was induced even in the cells whose nuclei was not traversed through by radiation. Authors speculated that this effect might have been mediated through the production of ROS by the cells which were irradiated directly. The occurrence of RIBE was also confirmed for very low doses of X-ray radiation in human fibroblasts.⁶⁷ After irradiation with doses ranging from 1.2 to 200 mGy the induction of DSBs, measured by ATM phosphorylation, followed a supralinear relationship. While cells were treated with an inhibitor of gap junction intercellular communication, the number of DSBs induced by radiation was smaller than in untreated cells. The largest differences between treated and untreated cells were observed at doses between 1.2 to 5 mGy, meaning that RIBE has the most influence on DSB induction at doses up to 10 mGy. RIBE has also been shown to induce mutations in bystander cells and the mechanism of these mutations is different than in the cells irradiated directly.⁶⁸ In bystander CHO cells, the frequency of deletions was higher after using 10 cGy α -radiation and after using 0.5 cGy α -radiation the frequency of point mutations was higher. Very low doses of α -radiation also have the ability to induce ROS production in irradiated cells⁶⁹ and ROS has been shown to induce point mutations⁷⁰ making it the likely mechanism for induction of mutations in bystander cells. However it is not clear whether the effect is mediated through ROS produced by irradiated cells and transferred to unirradiated cells, or the irradiated cells produce factors inducing ROS production in unirradiated cells.

The role of factors secreted by irradiated cells has also been confirmed for low-dose induced RIBE. Seymour and colleagues⁷¹ irradiated human keratinocytes with doses ranging from 0.01 to 0.5 Gy of γ -radiation. Then the medium from irradiated cells was collected and transferred to unirradiated cell culture. The results of clonogenic assays measuring clonogenic death of cells show that RIBE mediated by the secreted substances is most predominant in doses below 0.5 Gy. RIBE has also been confirmed to occur *in vivo* and cause chromosomal instabilities. To first demonstrate this effect *in vivo*, Watson *et al.*⁷² transplanted a mixture of irradiated (0.5 Gy, neutrons) and unirradiated bone marrow cells into unirradiated recipient. After transplantation some of the progeny of the unirradiated donor cells showed chromosomal aberrations induced through the bystander effect.

Evidence has also been presented for oncogenic effect of RIBE in *in vivo* mouse model, however the effect was observed only after irradiation with 3 Gy of X-rays.⁷³ Currently no research was able to confirm with confidence the oncogenic effect of low-dose RIBE, and even the exact mechanism of RIBE *in vivo* is not clear.⁷⁴ Presented results suggest that bystander effect plays an important role in induction of mutations after low dose irradiation, making it a potential oncogenic factor.

Conclusions

Radiation to which humans are exposed comprises mainly of low-dose and low-dose rate radiation from both natural and man-made sources. In recent years the biological effects of low-dose radiation became a point of interest due to the increase in popularity of radiation therapy and diagnostic radiology. Even though many studies point toward a link between carcinogenesis and exposure to radiation, the exact mechanism is still not clear. Induction of genomic instability is suspected to play a major role in malignant transformation after high-dose irradiation, and it might be responsible for carcinogenesis after exposure to lower doses. Latest research suggests that phenomena characteristic for low-dose exposures like HRS and RIBE might be the factors contributing to induction of genomic instability after exposure. Better understanding of these processes is crucial for the proper estimation of low-dose exposure risks for radiation workers, patients and people exposed to high background radiation.

Acknowledgement

This work was supported by the National Science Centre [grant number: 2015/19/B/NZ7/03811].

References

- Ron E. Ionizing radiation and cancer risk: evidence from epidemiology. *Pediatr Radiol* 2002; **32**: 232-7. doi: 42-410.1007/s00247-002-0672-0
- Rowland JH, Kent EE, Forsythe LP, Loge JH, Hjorth L, Glaser A, et al. Cancer survivorship research in Europe and the United States: where have we been, where are we going, and what can we learn from each other? *Cancer* 2013; **119**(Suppl 11): 2094-10810. doi: 1002/cncr.28060
- Kadhim M, Salomaa S, Wright E, Hildebrandt G, Belyakov OV, Prise KM, et al. Non-targeted effects of ionising radiation—implications for low dose risk. *Mutat Res* 2013; **752**: 84-98. doi: 10.1016/j.mrrrev.2012.12.001
- United Nations Scientific Committee on the Effects of Atomic Radiation. Radiation UNSCotEA. Sources and effects of ionizing radiation, Annex A. UNSCEAR 2008 report; 2008
- Veronesi U, Luini A, Del Vecchio M, Greco M, Galimberti V, Merson M, et al. Radiotherapy after breast-preserving surgery in women with localized cancer of the breast. *N Engl J Med* 1993; **328**: 1587-91. doi: 10.1056/NEJM199306033282202.
- Radiation UNSCotEA. Developments since the 2013 UNSCEAR report on the levels and effects of radiation exposure due to the nuclear accident following the great East-Japan earthquake and tsunami. 2016
- Ciocca M, Pedroli G, Orecchia R, Guido A, Cattani F, Cambria R, et al. Radiation survey around a Liac mobile electron linear accelerator for intraoperative radiation therapy. *J Appl Clin Med Phys* 2009; **10**: 2950.
- Veronesi U, Gatti G, Luini A, Intra M, Orecchia R, Borgen P, et al. Intraoperative radiation therapy for breast cancer: technical notes. *Breast J* 2003; **9**: 106-12.
- Ward JF. DNA damage produced by ionizing radiation in mammalian cells: identities, mechanisms of formation, and reparability. *Prog Nucleic Acid Res Mol Biol* 1988; **35**: 95-125.
- Dianov GL, O'Neill P, Goodhead DT. Securing genome stability by orchestrating DNA repair: removal of radiation-induced clustered lesions in DNA. *Bioessays* 2001; **23**: 745-9. doi: 10.1002/bies.1104
- Lorat Y, Timm S, Jakob B, Taucher-Scholz G, Rube CE. Clustered double-strand breaks in heterochromatin perturb DNA repair after high linear energy transfer irradiation. *Radiother Oncol* 2016; **121**: 154-61. doi: 10.1016/j.radonc.2016.08.028
- Takata M, Sasaki MS, Sonoda E, Morrison C, Hashimoto M, Utsumi H, et al. Homologous recombination and non-homologous end-joining pathways of DNA double-strand break repair have overlapping roles in the maintenance of chromosomal integrity in vertebrate cells. *EMBO J* 1998; **17**: 5497-508. doi: 10.1093/emboj/17.18.5497
- Ojima M, Ito M, Suzuki K, Kai M. Unstable chromosome aberrations do not accumulate in normal human fibroblast after fractionated x-irradiation. *PLoS One* 2015; **10**: e0116645. doi: 10.1371/journal.pone.0116645
- Hei TK. Response of biological systems to low doses of ionizing radiation. *Health Phys* 2016; **110**: 281. doi: 10.1097/HP.0000000000000452
- Lomax ME, Folkes LK, O'Neill P. Biological consequences of radiation-induced DNA damage: relevance to radiotherapy. *Clin Oncol* 2013; **25**: 578-85. doi: 10.1016/j.clon.2013.06.007
- Jeggo PA. DNA breakage and repair. *Adv Genet* 1998; **38**: 185-218.
- Short SC, Bourne S, Martindale C, Woodcock M, Jackson SP. DNA damage responses at low radiation doses. *Radiat Res* 2005; **164**: 292-302.
- Moore S, Stanley FK, Goodarzi AA. The repair of environmentally relevant DNA double strand breaks caused by high linear energy transfer irradiation—no simple task. *DNA Repair* 2014; **17**: 64-73. doi: 10.1016/j.dnarep.2014.01.014
- Kinner A, Wu W, Staudt C, Iliakis G. Gamma-H2AX in recognition and signaling of DNA double-strand breaks in the context of chromatin. *Nucleic Acids Res* 2008; **36**: 5678-94. doi: 10.1093/nar/gkn550
- Stucki M, Jackson SP. gammaH2AX and MDC1: anchoring the DNA-damage-response machinery to broken chromosomes. *DNA Repair* 2006; **5**: 534-43. doi: 10.1016/j.dnarep.2006.01.012
- Tommasino F, Friedrich T, Jakob B, Meyer B, Durante M, Scholz M. Induction and processing of the radiation-induced gamma-H2AX signal and its link to the underlying pattern of DSB: A combined experimental and modelling study. *PLoS One* 2015; **10**: e0129416. doi: 10.1371/journal.pone.0129416
- Kegel P, Riballo E, Kuhne M, Jeggo PA, Lobrich M. X-irradiation of cells on glass slides has a dose doubling impact. *DNA Repair* 2007; **6**: 1692-7. doi: 10.1016/j.dnarep.2007.05.013
- Rothkamm K, Lobrich M. Evidence for a lack of DNA double-strand break repair in human cells exposed to very low x-ray doses. *Proc Natl Acad Sci U S A* 2003; **100**: 5057-62. doi: 10.1073/pnas.0830918100
- Osipov AN, Pustovalova M, Grekhova A, Eremin P, Vorobyova N, Pulin A, et al. Low doses of X-rays induce prolonged and ATM-independent persistence of gammaH2AX foci in human gingival mesenchymal stem cells. *Oncotarget* 2015; **6**: 27275-87. doi: 10.18632/oncotarget.4739
- Liang X, So YH, Cui J, Ma K, Xu X, Zhao Y, et al. The low-dose ionizing radiation stimulates cell proliferation via activation of the MAPK/ERK pathway in rat cultured mesenchymal stem cells. *J Radiat Res* 2011; **52**: 380-6.

26. Brenner DJ, Hall EJ. Computed tomography - an increasing source of radiation exposure. *N Engl J Med* 2007; **357**: 2277-84. doi: 10.1056/NEJMra072149
27. Xue L, Yu D, Furusawa Y, Cao J, Okayasu R, Fan S. ATM-dependent hyper-radiosensitivity in mammalian cells irradiated by heavy ions. *Int J Radiat Oncol Biol Phys* 2009; **75**: 235-43. doi: 10.1016/j.ijrobp.2009.04.088
28. Slonina D, Gasinska A, Biesaga B, Janecka A, Kabat D. An association between low-dose hyper-radiosensitivity and the early G2-phase checkpoint in normal fibroblasts of cancer patients. *DNA Repair* 2016; **39**: 41-5. doi: 10.1016/j.dnarep.2015.12.001
29. Marples B, Collis SJ. Low-dose hyper-radiosensitivity: past, present, and future. *Int J Radiat Oncol Biol Phys* 2008; **70**: 1310-8. doi: 10.1016/j.ijrobp.2007.11.071
30. Marples B, Joiner MC. The response of Chinese hamster V79 cells to low radiation doses: evidence of enhanced sensitivity of the whole cell population. *Radiat Res* 1993; **133**: 41-51.
31. Short SC, Woodcock M, Marples B, Joiner MC. Effects of cell cycle phase on low-dose hyper-radiosensitivity. *Int J Radiat Biol* 2003; **79**: 99-105.
32. Krueger SA, Wilson GD, Piasentin E, Joiner MC, Marples B. The effects of G2-phase enrichment and checkpoint abrogation on low-dose hyper-radiosensitivity. *Int J Radiat Oncol Biol Phys* 2010; **77**: 1509-17. doi: 10.1016/j.ijrobp.2010.01.028
33. Schoenherr D, Krueger SA, Martin L, Marignol L, Wilson GD, Marples B. Determining if low dose hyper-radiosensitivity (HRS) can be exploited to provide a therapeutic advantage: a cell line study in four glioblastoma multiforme (GBM) cell lines. *Int J Radiat Biol* 2013; **89**: 1009-16. doi: 10.3109/09553002.2013.825061
34. Sinclair WK. Cyclic X-ray responses in mammalian cells in vitro. *Radiat Res* 2012; **178**: AV112-24.
35. Xu B, Kim ST, Lim DS, Kastan MB. Two molecularly distinct G(2)/M checkpoints are induced by ionizing irradiation. *Mol Cell Biol* 2002; **22**: 1049-59.
36. Marples B, Wouters BG, Joiner MC. An association between the radiation-induced arrest of G2-phase cells and low-dose hyper-radiosensitivity: a plausible underlying mechanism? *Radiat Res* 2003; **160**: 38-45.
37. Pandita TK, Lieberman HB, Lim DS, Dhar S, Zheng W, Taya Y, et al. Ionizing radiation activates the ATM kinase throughout the cell cycle. *Oncogene* 2000; **19**: 1386-91. doi: 10.1038/sj.onc.1203444
38. Lobrich M, Jeggo PA. The impact of a negligent G2/M checkpoint on genomic instability and cancer induction. *Nat Rev Cancer* 2007; **7**: 861-9. doi: 10.1038/nrc2248
39. Deckbar D, Jeggo PA, Lobrich M. Understanding the limitations of radiation-induced cell cycle checkpoints. *Crit Rev Biochem Mol Biol* 2011; **46**: 271-83. doi: 10.3109/10409238.2011.575764
40. Deckbar D, Birraux J, Krempler A, Tchouandong L, Beucher A, Walker S, et al. Chromosome breakage after G2 checkpoint release. *J Cell Biol* 2007; **176**: 749-55. doi: 10.1083/jcb.200612047
41. Fernet M, Megnin-Chanet F, Hall J, Favaudon V. Control of the G2/M checkpoints after exposure to low doses of ionising radiation: implications for hyper-radiosensitivity. *DNA Repair* 2010; **9**: 48-57. doi: 10.1016/j.dnarep.2009.10.006
42. Scott D. Chromosomal radiosensitivity, cancer predisposition and response to radiotherapy. *Strahlenther Onkol* 2000; **176**: 229-34.
43. Terzoudi GI, Manola KN, Pantelias GE, Iliakis G. Checkpoint abrogation in G2 compromises repair of chromosomal breaks in ataxia telangiectasia cells. *Cancer Res* 2005; **65**: 11292-6. doi: 10.1158/0008-5472.CAN-05-2148
44. Morgan WF, Day JP, Kaplan MI, McGhee EM, Limoli CL. Genomic instability induced by ionizing radiation. *Radiat Res* 1996; **146**: 247-58.
45. Little JB. Genomic instability and bystander effects: a historical perspective. *Oncogene* 2003; **22**: 6978-87. doi: 10.1038/sj.onc.1206988
46. Kadhim MA, Moore SR, Goodwin EH. Interrelationships amongst radiation-induced genomic instability, bystander effects, and the adaptive response. *Mutat Res* 2004; **568**: 21-32. doi: 10.1016/j.mrfmmm.2004.06.043
47. Weissenborn U, Streffer C. Analysis of structural and numerical chromosomal anomalies at the first, second, and third mitosis after irradiation of one-cell mouse embryos with X-rays or neutrons. *Int J Radiat Biol* 1988; **54**: 381-94.
48. Lorimore SA, Wright EG. Radiation-induced genomic instability and bystander effects: related inflammatory-type responses to radiation-induced stress and injury? A review. *Int J Radiat Biol* 2003; **79**: 15-25.
49. Smith LE, Nagar S, Kim GJ, Morgan WF. Radiation-induced genomic instability: radiation quality and dose response. *Health Phys* 2003; **85**: 23-9.
50. Kadhim MA, Macdonald DA, Goodhead DT, Lorimore SA, Marsden SJ, Wright EG. Transmission of chromosomal instability after plutonium alpha-particle irradiation. *Nature* 1992; **355**: 738-40. doi: 10.1038/355738a0
51. Lloyd DC, Edwards AA, Leonard A, Deknuddt GL, Verschaeve L, Natarajan AT, et al. Chromosomal aberrations in human lymphocytes induced in vitro by very low doses of X-rays. *Int J Radiat Biol* 1992; **61**: 335-43.
52. Maxwell CA, Fleisch MC, Costes SV, Erickson AC, Boissiere A, Gupta R, et al. Targeted and nontargeted effects of ionizing radiation that impact genomic instability. *Cancer Res* 2008; **68**: 8304-11. doi: 10.1158/0008-5472.CAN-08-1212
53. Portess DI, Bauer G, Hill MA, O'Neill P. Low-dose irradiation of nontransformed cells stimulates the selective removal of precancerous cells via intercellular induction of apoptosis. *Cancer Res* 2007; **67**: 1246-53. doi: 10.1158/0008-5472.CAN-06-2985
54. Andarawewa KL, Erickson AC, Chou WS, Costes SV, Gascard P, Mott JD, et al. Ionizing radiation predisposes nonmalignant human mammary epithelial cells to undergo transforming growth factor beta induced epithelial to mesenchymal transition. *Cancer Res* 2007; **67**: 8662-70. doi: 10.1158/0008-5472.CAN-07-1294
55. Bauchinger M, Schmid E, Dresch J. Calculation of the dose-rate dependence of the deceleration yield after Co gamma-irradiation of human lymphocytes. *Int J Radiat Biol Relat Stud Phys Chem Med* 1979; **35**: 229-33.
56. Iwasaki T, Takashima Y, Suzuki T, Yoshida MA, Hayata I. The dose response of chromosome aberrations in human lymphocytes induced in vitro by very low-dose gamma rays. *Radiat Res* 2011; **175**: 208-13.
57. Bakhomou SF, Swanton C. Chromosomal instability, aneuploidy, and cancer. *Front Oncol* 2014; **4**: 161. doi: 10.3389/fonc.2014.00161
58. Cho YH, Kim SY, Woo HD, Kim YJ, Ha SW, Chung HW. Delayed numerical chromosome aberrations in human fibroblasts by low dose of radiation. *Int J Environ Res Public Health* 2015; **12**: 15162-72. doi: 10.3390/ijerph121214979
59. Lucas JN, Tenjin T, Straume T, Pinkel D, Moore D, 2nd, Litt M, et al. Rapid human chromosome aberration analysis using fluorescence in situ hybridization. *Int J Radiat Biol* 1989; **56**: 35-44.
60. Dahle J, Kvam E. Induction of delayed mutations and chromosomal instability in fibroblasts after UVA-, UVB-, and X-radiation. *Cancer Res* 2003; **63**: 1464-9.
61. Cresti N, Lee J, Rourke E, Televantou D, Jamieson D, Verrill M, et al. Genetic variants in the HER2 gene: Influence on HER2 overexpression and loss of heterozygosity in breast cancer. *Eur J Cancer* 2016; **55**: 27-37. doi: 10.1016/j.ejca.2015.10.066
62. Umabayashi Y, Honma M, Suzuki M, Suzuki H, Shimazu T, Ishioka N, et al. Mutation induction in cultured human cells after low-dose and low-dose-rate gamma-ray irradiation: detection by LOH analysis. *J Radiat Res* 2007; **48**: 7-11.
63. Prise KM, Folkard M, Michael BD. A review of the bystander effect and its implications for low-dose exposure. *Radiat Prot Dosimetry* 2003; **104**: 347-55.
64. Sowa Resat MB, Morgan WF. Radiation-induced genomic instability: a role for secreted soluble factors in communicating the radiation response to non-irradiated cells. *J Cell Biochem* 2004; **92**: 1013-9. doi: 10.1002/jcb.20149
65. Azzam EI, de Toledo SM, Little JB. Oxidative metabolism, gap junctions and the ionizing radiation-induced bystander effect. *Oncogene* 2003; **22**: 7050-7. doi: 10.1038/sj.onc.1206961
66. Nagasawa H, Little JB. Induction of sister chromatid exchanges by extremely low doses of alpha-particles. *Cancer Res* 1992; **52**: 6394-6.
67. Ojima M, Ban N, Kai M. DNA double-strand breaks induced by very low X-ray doses are largely due to bystander effects. *Radiat Res* 2008; **170**: 365-71. doi: 10.1667/RR1255.1

68. Huo L, Nagasawa H, Little JB. HPRT mutants induced in bystander cells by very low fluences of alpha particles result primarily from point mutations. *Radiat Res* 2001; **156**: 521-5.
69. Narayanan PK, Goodwin EH, Lehnert BE. Alpha particles initiate biological production of superoxide anions and hydrogen peroxide in human cells. *Cancer Res* 1997; **57**: 3963-71.
70. Oller AR, Thilly WG. Mutational spectra in human B-cells. Spontaneous, oxygen and hydrogen peroxide-induced mutations at the hprt gene. *J Mol Biol* 1992; **228**: 813-26.
71. Seymour CB, Mothersill C. Relative contribution of bystander and targeted cell killing to the low-dose region of the radiation dose-response curve. *Radiat Res* 2000; **153**: 508-11.
72. Watson GE, Lorimore SA, Macdonald DA, Wright EG. Chromosomal instability in unirradiated cells induced in vivo by a bystander effect of ionizing radiation. *Cancer Res* 2000; **60**: 5608-11.
73. Mancuso M, Pasquali E, Leonardi S, Tanori M, Rebessi S, Di Majo V, et al. Oncogenic bystander radiation effects in Patched heterozygous mouse cerebellum. *Proc Natl Acad Sci U S A* 2008; **105**: 12445-50. doi: 10.1073/pnas.0804186105
74. Chai Y, Hei TK. Radiation induced bystander effect in vivo. *Acta Med Nagasaki* 2008; **53**: S65-S9.

Clinical significance of fluorine-18-fluorodeoxyglucose positron emission tomography/computed tomography in the follow-up of colorectal cancer: searching off approaches increasing specificity for detection of recurrence

Semra Ince¹, Kursat Okuyucu¹, Oguz Hancerliogullari², Engin Alagoz¹, Huseyin San¹, Nuri Arslan¹

¹ Department of Nuclear Medicine, University of Health Sciences, Gulhane Training and Research Hospital, Ankara, Turkey

² Department of General Surgery, University of Health Sciences, Gulhane Training and Research Hospital, Ankara, Turkey

Radiol Oncol 2017; 51(4): 378-385.

Received 19 July 2017

Accepted 10 September 2017

Correspondence to: Semra Ince M.D., University of Health Sciences, Gulhane Training and Research Hospital, Department of Nuclear Medicine, 06010 Etilik-Ankara, Turkey. Phone: +90 312 304 48 28; E-mail: drsemra@gmail.com

Disclosure: No potential conflicts of interest were disclosed.

Background. Nearly 40% of colorectal cancer (CRC) recurs within 2 years after resection of primary tumor. Imaging with fluorine-18-fluorodeoxyglucose (¹⁸F-FDG) positron emission tomography/computed tomography (PET/CT) is the most recent modality and often applied for the evaluation of metastatic spread during the follow-up period. Our goal was to study the diagnostic importance of ¹⁸F-FDG-PET/CT data of maximum standardized uptake value (SUVmax), total lesion glycolysis (TLG) and the difference of SUVmax on dual-time imaging in CRC.

Patients and methods. We examined the SUVmax value of lesions on control or restaging ¹⁸F-FDG-PET/CT of 53 CRC patients. All lesions with increased SUVmax values were confirmed by colonoscopy or histopathology. We compared PET/CT results with conventional imaging modalities (CT, MRI) and tumor markers [carbohydrate antigen 19-9 [Ca 19-9], carcinoembryonic antigen [CEA]].

Results. Mean SUVmax was 6.9 ± 5.6 in benign group, 12.7 ± 6.1 in malignant group. Mean TLG values of malignant group and benign group were 401 and 148, respectively. ¹⁸F-FDG-PET/CT was truly positive in 48% of patients with normal Ca 19-9 or CEA levels and truly negative in 10% of cases with elevated Ca 19-9 or CEA. CT or MRI detected suspicious malignancy in 32% of the patients and ¹⁸F-FDG-PET/CT was truly negative in 35% of these cases. We found the most important and striking statistical difference of TLG value between the groups with benign and recurrent disease.

Conclusions. Although SUVmax is a strong metabolic parameter ($p = 0.008$), TLG seems to be the best predictor in recurrence of CRC ($p = 0.001$); both are increasing the specificity of ¹⁸F-FDG-PET/CT.

Key words: metabolic tumor markers; recurrent colorectal cancer; 18F-fluorodeoxyglucose positron emission tomography; computed tomography

Introduction

Colorectal cancer (CRC) ranks in the third line amongst the most common cancers all over the world. Roundly 40% of patients recur within 2

years after resection of primary tumor by surgery.¹ In the follow-up, most guidelines recommend thoracoabdominal CT usually at 12th, 36th months after surgery or any time in case of clinical doubt as well as routine serial carcinoembryonic antigen

(CEA) and carbohydrate antigen 19-9 (Ca 19-9) assays.² Imaging has the main role for the evaluation of metastatic spread during the follow-up. Molecular imaging with 18F-fluorodeoxyglucose positron emission tomography combined with computed tomography (¹⁸F-FDG-PET/CT) is the most recent modality for this purpose.³ ¹⁸F-FDG-PET/CT has been used for baseline staging, assessment of treatment response and restaging of CRC as in many other cancers and is concerned to be more sensitive and specific imaging method than routine tools in cases of dubious recurrence and/or metastasis.^{2,3}

CEA is expressed by a lot of epithelial tumors and its serum levels may increase in non-malignant conditions such as inflammatory bowel diseases.⁴ Approximately 70% CRC patients exhibit an elevated CEA level at the time of diagnosis and this fact made it a routine monitoring marker for the disease recurrence.^{5,6} Nevertheless, recent studies of meta-analyses revealed controversies about its utility for the detection of recurrence with a sensitivity of 64% and a specificity of 90% which might be considered poor as a biomarker on its own goal.⁷ Ca 19-9 assays have also a poor performance. It has been reported that Ca 19-9 was positive only in 20-40% of metastatic CRCs.⁸

¹⁸F-FDG-PET has the ability to detect recurrent CRC (as in many other cancers), through pathologically increased tissue metabolism, which precedes the appearance of morphological changes.^{3,9,10} ¹⁸F-FDG-PET, however has some intrinsic limitations and its use in the monitoring of CRC is vexed.^{11,12} Latest data offer no indication except the cases with inconclusive CT with suspicion of distant metastasis or in the existence of negative CT and serial CEA rises.¹³ Some current interventions on ¹⁸F-FDG-PET/CT such as dual-time or voxel-based dual-time parametric imaging and use of metabolic tumor parameters have been suggested to improve its diagnostic accuracy in several cancers.¹⁴ Previously, quantitative analyses based on volume-of-interest FDG uptake were introduced. Maximum standardized uptake value (SUVmax) is the vanguard of them. Determination of a cutoff level of SUVmax which differentiates between benign conditions and recurrence of CRC would certainly be helpful. The goal of this paper is to appraise clinical significance of 18F-fluorodeoxyglucose uptake on FDG-PET/CT in the aftermath of primary curative surgery and/or chemoradiotherapy with respect to recurrence in patients with CRC. We also aimed to research the diagnostic power of ¹⁸F-FDG-PET in recurrent CRC over total lesion glycolysis

(TLG), the difference of SUVmax on dual-time imaging, calculation of a cutoff point of SUVmax discriminating metastasis/recurrence from benign conditions on restaging ¹⁸F-FDG-PET/CT.

Patients and methods

This retrospective cohort study was carried out between 2011 and 2016. It was conducted at nuclear medicine department of a tertiary health care hospital. Inclusion criteria were: histopathologically proven CRC by surgical specimen after primary curative surgery, pathologic FDG uptake on control (evaluation of treatment response) ¹⁸F-FDG-PET/CT or restaging ¹⁸F-FDG-PET/CT performed for the existence of suspicious recurrence or metastasis by routine conventional screening methods in the follow-up, confirmation of all these abnormal uptakes by colonoscopy or histopathologic examination. All cases were treated by surgery and/or chemoradiotherapy. The files of the patients were retrieved from the archive and looked over retrospectively.

We evaluated the lesions on ¹⁸F-FDG-PET/CT in 53 patients. Indications for ¹⁸F-FDG-PET/CT were suspicion of recurrence/metastasis (27 patients) and treatment response monitoring (26 patients). Elevated CEA and/or Ca 19-9 levels raised the suspicion of recurrence in 10 cases, conventional imaging (CT or MRI) in 17 cases. All foci of FDG uptake were confirmed by colonoscopic findings and/or histopathologically. Normal range of Ca 19-9 is 0-35 U/mL, CEA < 2.5 ng/ml for nonsmokers and < 5 ng/ml for smokers.

¹⁸F-FDG-PET/CT imaging protocol

370-555 MBq of ¹⁸F-FDG, calculated according to body weight, was administered to patients by intravenous injection. They fasted for 6 hours prior to the examination and their blood glucose level needed to be below 150 mg/dl before the injection. Image acquisition was performed 1 hour after the injection with an integrated PET/CT scanner (Discovery 690-GE Healthcare, WI, USA). A low-dose unenhanced CT was performed. CT data were obtained with the automated dose modulation technique of 120 kVp (maximal 100 mA), collimated by 64×0.625 mm, measured field of view (FOV) of 50 cm, noise index of 20% and reconstructed to images of 0.625 mm transverse pixel size and 3.75 mm slice thickness. PET emission data were obtained from the middle of thigh up to vertex of the

skull while the patient was in supine position with the arms raised over head. Acquired PET data were in 3D mode with scanning time of 2 min per bed position and an axial FOV of 153 mm. A standardized way (random, scatter and attenuation) and iterative reconstruction (matrix size 256×256, Fourier rebinning, VUE Point FX [3D]) with 3 iterations, 18 subsets) were used for correction of emission data. Dual-time ¹⁸F-FDG-PET/CT was performed in 28 patients. 105 ± 10 minutes post-injection after the completion of standard protocol, delayed imaging for the whole abdomen with the CT scan and repositioning was performed.

Visual and quantitative interpretation

¹⁸F-FDG-PET/CT images were interpreted visually by two nuclear medicine specialists aware of patient history. Focally or heterogeneously increased FDG uptake, diffuse or heterogeneously increased FDG uptake and/or soft tissue mass on CT component, hypodense or nodular lesion on CT (with or without FDG uptake), diffuse uptake accompanied by wall thickening, consolidation or ambiguous lesions on CT (with or without uptake) were accepted pathologic. SUVmax was calculated for all patients. Other quantitative parameters of average standardized uptake value (SUVmean), metabolic tumor volume (MTV) and TLG were calculated in 20 cases on ¹⁸F-FDG-PET/CT. We calculated TLG values by multiplying MTV and SUV mean. The corresponding CT scans of lesions were used as a guideline to demarcate them if their boundaries were difficult to define for the calculation of SUVmax.

Quantitative PET/CT parameters were calculated from a routine protocol used on a sophisticated workstation (Volumetrix for PET-CT and AW volume share 4.5, GE Healthcare, Waukesha, WI, USA). Standard methods computed SUVmax and SUVmean, corrected for body weight, from the voxel having the most intense activity in three-dimensional tumor region on transaxial whole-body images of attenuation-corrected PET/CT images. MTV (cm³) was measured with a half-automatic PET analysis computer program, having an automatic isocontour threshold method based on a notion of being greater than 42% of the SUV max value within the tumor.

Statistical analysis

The whole data were analysed by IBM Corp. Released 2013. IBM SPSS Statistics for Windows,

TABLE 1. Locations of pathologic FDG uptake

Sites of abnormal FDG uptake	n
Anastomosis line (area)	7
Rectum	9
Rectosigmoid region	11
Liver	9
Caecum	1
Kidney	1
Abdominal mass	4
Presacral mass	5
Sigmoid region	3
Descending colon	2
Lung	1

Version 22.0. Armonk, NY: IBM Corp. Number and percentage values were used for the description of categorical data. Mean, median, standard deviation (SD), minimum and maximum values described continuous data. Intergroup (benign conditions versus malignant group) comparisons were carried out by Mann-Whitney U test for SUVmax, TLG and the difference between SUVmax values of dual-time imaging. Wilcoxon test was used for ingroup comparison between SUVmax values of early and delayed imaging for benign and malignant group. The variables having a value of $p < 0.05$ were accepted as statistically meaningful. ROC curve analysis was plotted to see the diagnostic value of SUVmax on recurrent disease. Informed consent was supposed as a retrospective study which permitted to use records, documents and data of patients applied on our clinic for the test. The study was ratified by our Institutional Review Ethics Committee (approval number 80/2016). This study conforms to the Declaration of Helsinki.

Results

Mean age was 58.6 ± 10.9 years (30–89). 24 of the patients were male (45%), 29 of them were female (55%). Primary tumor sites were rectum (n = 23), sigmoid colon (n = 5) and other colonic segments (n = 25). The most common localization of FDG uptake was rectosigmoid region (43.3%). Locations of pathologic FDG uptake were demonstrated in Table 1. Sensitivity, specificity, positive predictive value (PPV) and negative predictive value (NPV) of ¹⁸F-FDG-PET/CT in the detection of recurrence

TABLE 2. ¹⁸F-FDG-PET/CT results, sensitivity, specificity, positive predictive value (PPV) and negative predictive value (NPV) according to final histopathologic diagnosis

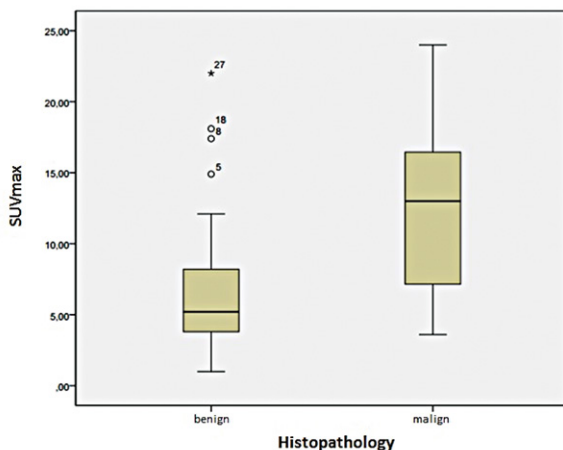
Histopathologic diagnosis	¹⁸ F-FDG-PET/CT Results						Total (n)
	Positive	Negative	Sensitivity	Specificity	PPV	NPV	
Malignant	TP = 24	FN = 0					24
Benign	FP = 14	TN = 15					29
Total (n)	38	15	100%	51.7%	63.1%	100%	53

FN = False negative; FP = False positive; TN = True negative; TP = True positive

and/or metastasis were 100%, 51.7%, 63.1% and 100%, respectively. ¹⁸F-FDG-PET/CT results and final histopathologic diagnosis were represented in Table 2.

¹⁸F-FDG-PET/CT was truly positive in 48% of patients with normal Ca 19-9 and/or CEA levels and truly negative in 10% of cases with elevated Ca 19-9 and/or CEA levels according to histopathological confirmation or colonoscopy findings. In the follow-up, conventional imaging tests (CT or MRI) detected suspicious malignancy in 32% of the patients (17/53) and further examination with ¹⁸F-FDG-PET/CT was truly negative in 35% of these cases (6/17) according to histopathology. ¹⁸F-FDG-PET/CT findings in histopathologically proven recurrence according to tumor markers (Ca 19-9 and/or CEA) and conventional imaging modalities (CT-MRI) were described in Table 3,4.

Mean SUVmax was 6.9 ± 5.6 (1–22) in benign group and 12.7 ± 6.1 (3.6–24) in malignant group. There is a statistically significant difference ($p = 0.008$) between them according to SUVmax. A box-plot graph illustrates the distribution of SUVmax in benign conditions versus disease recurrence

**FIGURE 1.** Box-plot graph illustrating the distribution of SUVmax through benign conditions and disease recurrence.

(Figure 1). ROC curve of SUVmax was plotted for the differentiation between benign conditions and malignant group (Area Under Curve: 0.755) (Figure 2). Nevertheless, sensitivity and specificity couldn't be calculated due to undersampling and inconvenient SUVmax data not suggesting a determinant cutoff value. There is also a statistically significant difference between early and delayed SUVmax values of both groups separately in them ($p = 0.013$ for benign group, $p = 0.012$ for malignant group). However, we don't see a significant difference between them according to early and delayed SUVmax values ($p = 0.238$). Mean TLG of malignant group was 401 ± 226 . Mean TLG of benign group was 148 ± 126 (median value: 44). The most important and striking statistical difference between them was found for TLG ($p = 0.001$).

Discussion

Recurrent disease is seen in 30–50% of patients with CRC after curative resection.⁶ The recurrence rate

TABLE 3. FDG-PET/CT findings according to serum Ca 19-9 or CEA levels for histopathologically proven recurrence

Ca 19-9 or CEA levels	¹⁸ F-FDG-PET/CT results		Total (n)
	True positive	True negative	
Elevated	9	1	10
Normal	13	14	27
Total (n)	22	15	37

TABLE 4. Overlap between ¹⁸F-FDG-PET/CT findings and conventional imaging modalities (CT or MRI) in histopathologically proven recurrence

CT/MRI	¹⁸ F-FDG-PET/CT results		Total (n)
	True positive	True negative	
Malign	11	6	17

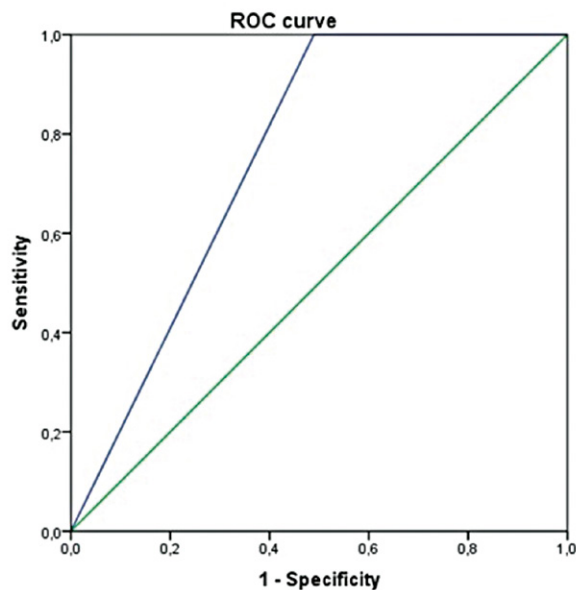


FIGURE 2. ROC curve drawn to indicate the detection and diagnostic accuracy of SUVmax in recurrence/metastasis.

in our study was 45% and it is accordant with literature. The main goal of follow-up surveillance is to reveal recurrences as soon as possible at an early stage for an immediate cure.⁵ Most of the relapsed cases are not operable at the time of diagnosis and 1/3 of the patients with isolated locoregional or distant metastases survive 5 years.¹⁵

Several studies have proven that ¹⁸F-FDG-PET/CT is very sensitive, but not that much specific for detection of recurrence in CRC and affects patient management.³ Sobhani *et al.*¹⁶ included 130 patients with recurrent CRC in their study and compared ¹⁸F-FDG-PET/CT and conventional follow-up. They found no difference in recurrence rate, but recurrences were detected earlier by ¹⁸F-FDG-PET/CT. Scott *et al.*¹⁷ showed that ¹⁸F-FDG-PET/CT detected 45 additional lesions in a multicenter prospective trial of 93 patients. Lu *et al.*¹⁸ studied sensitivity and specificity of diagnostic CT in a meta-analysis and found 51% and 90%, respectively. The sensitivity and specificity of conventional imaging tests (CT or MRI) and ¹⁸F-FDG-PET/CT were 71%, 87% and 100%, 52%, respectively in our study. In Figure 3, example of a true positive recurrent lesion suspected on MRI and confirmed by ¹⁸F-FDG-PET/CT is shown. Maas *et al.*¹⁹, in a meta-analysis of 14 studies, investigated which imaging modality has the highest accuracy in CRC recurrence/metastasis suspected clinically or because of the elevated tumor marker levels. They reached the conclusion that ¹⁸F-FDG-PET/CT is absolutely more accurate (areas under curves were 0.94 for PET, 0.94 for PET/CT, 0.83 for CT). We found true positivity on ¹⁸F-FDG-PET/CT in 48% of patients with normal Ca 19-9 and/or CEA levels, although there was true negativity in 10% of cases with elevated Ca 19-9

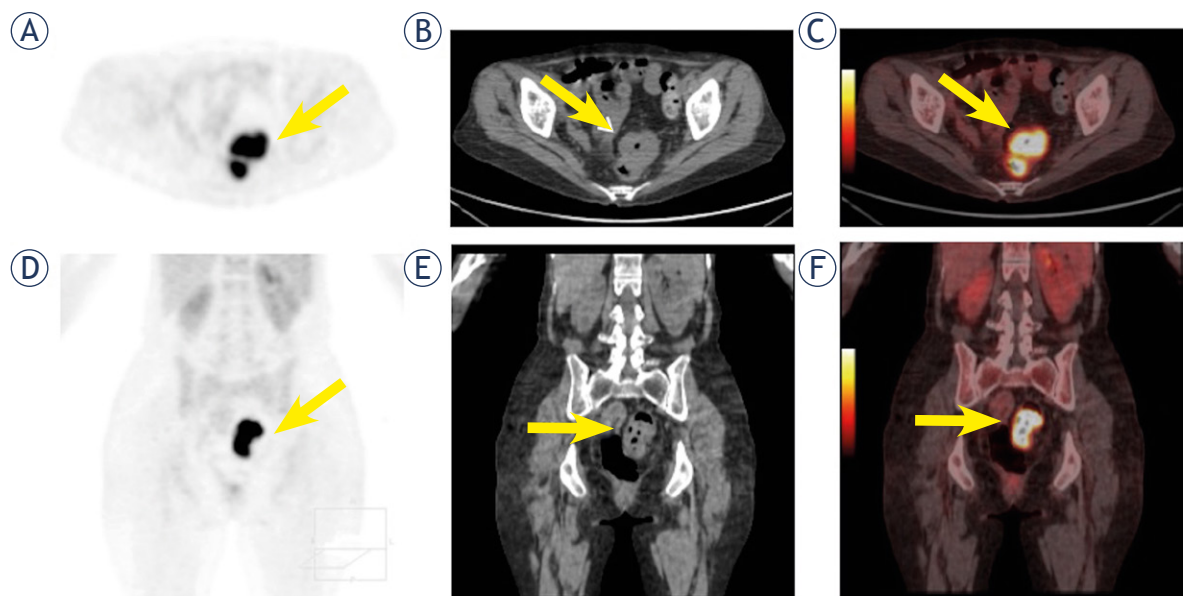


FIGURE 3. A female patient aged 51 years with rectum cancer was operated and treated by chemoradiotherapy. MRI findings revealed suspected metastasis with serum CEA and Ca 19-9 in normal range during the follow-up. Her axial PET (A), CT (B), fusion (C) and coronal PET (D), CT (E), fusion (F) images on ¹⁸F-FDG-PET/CT showed a focal uptake in sigmoid colon with a SUVmax of 13.7 and TLG of 272 accompanied by wall thickening causing a mass lesion on CT component (arrows). Histopathology established the diagnosis as recurrence.

and/or CEA levels. All our findings are in line with data from literature.

Although functional imaging with ^{18}F -FDG PET is a useful technique for evaluating treatment response, it has some limitations. ^{18}F -FDG is taken up at a relatively higher rate in cancer cells and accumulates during glucose metabolism. However, cancer cells are not the only cells that are metabolically hyperactive. Inflammation, infection and other non-neoplastic conditions such as hyperplastic colorectal polyps may have increased FDG accumulation.^{20,21} Depending upon this, PET scans have a high sensitivity but a low specificity for CRC²¹ as it was also the case in our study. Compared to PET alone, combination of PET and CT, having the advantage of detecting metabolic abnormality with anatomic localization, is superior in localizing lesions and differentiating between physiologic and malignant uptake of FDG. The benign pathologies diagnosed in our study were granulation tissue, fibrin and inflammation, fibrosis, pyelonephritis, ulceration of colonic mucosa, fibrosis and inflammation, polip, as well as changes secondary to radiotherapy or operation.

Some manipulative registration or intervention methods on ^{18}F -FDG-PET/CT imaging have been suggested to increase the specificity. Recently, Prieto *et al.*²² suggested voxel-based dual-time ^{18}F -FDG-PET images for brain tumors and demonstrated that parametric images provided enhanced tumor identification. Voxel-based analysis is different from VOI-based one in that it is an attempt enabling calculation of real increase in delayed scan of the same voxel. Choi *et al.*¹² investigated voxel-based dual-time ^{18}F -FDG-PET parametric imaging in the evaluation of residual tumor for rectal cancer and found promising results. Dual-time ^{18}F -FDG-PET has also been reported to improve diagnostic accuracy for several cancers.¹⁴

This is based on the different pattern of FDG uptake in malignant tumors displaying a slow increment, whereas benign lesions show an earlier peak and then a decline.²³ Lots of benign conditions and physiologic FDG uptakes displaying focal or diffuse FDG accumulations in gastrointestinal tract can be seen in patients with CRC during the follow-up and may be confused with true pathologic lesions. When such a pattern is observed on ^{18}F -FDG-PET/CT, invasive interventions (colonoscopy, biopsy) are recommended. So it is essential to distinguish them. An example of false positivity is shown in Figure 4.

Miyake *et al.*²⁴ showed that delayed scans increased correct differentiation of physiologic FDG uptakes causing false positivities from foci of pathologic uptake in CRC. Yoon *et al.*²⁵ reported that dual-time ^{18}F -FDG-PET/CT had better accuracy in diagnosing tumor response and recurrence. We researched the difference of SUVmax on early and delayed images of dual-time ^{18}F -FDG-PET between

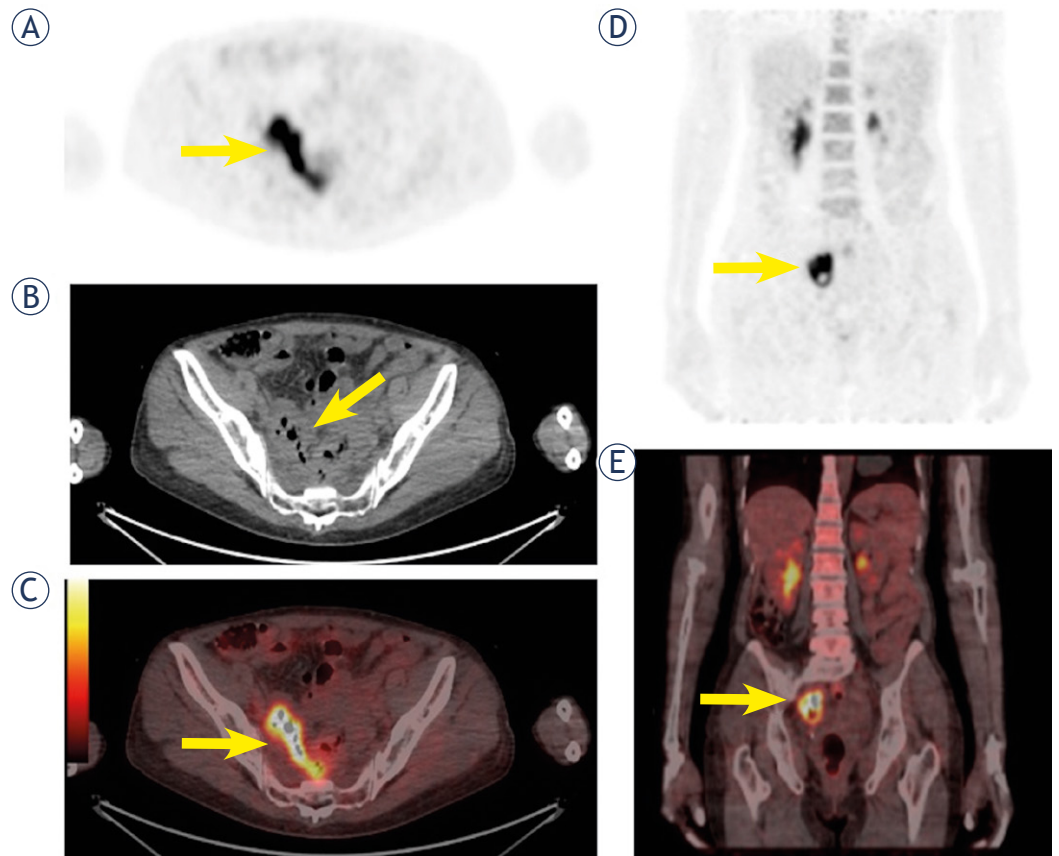


FIGURE 4. A female patient aged 73 years with sigmoid colon cancer was operated and treated by chemoradiotherapy. Her serum CEA level was 3.2 ng/ml, and Ca 19-9 was 7.3 U/ml. In the evaluation of treatment response; axial PET (A), CT (B), fusion (C) and coronal PET (D), fusion (E) images on ^{18}F -FDG-PET/CT exhibited a diffuse uptake in sigmoid colon with a SUVmax of 10.1 and TLG of 154 accompanied by wall thickening on CT component (arrows). This uptake raised the suspicion of a probable recurrence, but histopathology confirmed it as benign.

benign and malignant group. We didn't find a meaningful statistics and discriminative power for this parameter.

We investigated the value of SUVmax and TLG too. Most of the studies including SUVmax and TLG evaluation in CRC are related to prognosis estimation. Marcus *et al.*²⁶ declared SUVmax and TLG to be higher in patients having bad prognosis. Gade *et al.*² found a lower mean SUVmax of 8.6, Marcus *et al.*²⁶ 7.3 in recurrent CRC when compared to ours (12.7). Shamim *et al.*²⁷ found a significant increase according to mean SUVmax in recurrence (11.8 for recurrence versus 3.7 for benign conditions) in a study of 32 patients with CRC. They were 12.7 for recurrence against 6.9 for benign group in our study and there was a significant difference ($p = 0.008$). Giacomobono *et al.*²⁸ assessed SUVmax in CRC patients with increased CEA levels and found a worse overall survival for SUVmax values greater than 5.7. Inflammatory pathologies, fibrosis or edema following irradiation and/or surgery can also be FDG-avid and their SUVmax values can be as high as malignant ones due to the degree of cellular metabolism reflected by ¹⁸F-FDG uptake.^{11,12} Therefore, big overlaps in SUVmax values of both benign conditions and recurrent/metastatic disease may be seen just like in our study. However, we found SUVmax was very helpful for the differentiation of recurrent disease from benign conditions. As our results trended towards improved diagnostic accuracy, a determinative cutoff value for SUVmax was not obtained. Undersampling and inconvenient SUVmax data didn't let an estimated cutoff value on ROC curve for related sensitivity and specificity calculation.

Quantitative PET parameters have been used in prognosis estimation and evaluation of treatment response for several cancers. There is not a specific study in literature which investigated metabolic tumor parameters for the differentiation of benign conditions from recurrence. As far as we know, our study is the first one in literature. Higher metabolic activity and glucose consumption of tumor cells are measured by these parameters. SUVmax is the first one and represents the highest FDG uptake within the tumor. More lately volume-based metabolic parameters emerged out. TLG is a volume-based metabolic tumor parameter having widespread use and increasing recognition in many cancers as a predictor. Arslan *et al.*²⁹ reported it has a role in prediction of survival for patients with small cell lung cancer. Caglar *et al.*³⁰ investigated metabolic tumor markers in recurrent CRC and found moderate correlation. Marcus *et al.*²⁶ found mean TLG

280, Caglar *et al.*³⁰ 55 in recurrent CRC. It was 401 in our study. There was significant difference between benign conditions and recurrence according to mean TLG and TLG was the most striking factor for this purpose in the study ($p = 0.001$). Again, we didn't intentionally calculate a cutoff value which could be misleading due to insufficient sampling. But first impressions imply determinative cutoff values for SUVmax and TLG increasing the specificity may be obtained from studies with larger patient numbers. Higher SUVmax and TLG values in suspected cases would favour in recurrence/metastasis and support the necessary invasive interventions.

Absence of an estimated cutoff value on ROC curve for related sensitivity, specificity calculations due to undersampling and inconvenient SUVmax data was a limitation in the study. The number of subjects were small. Evaluation with larger populations is required for definitive results. Study design was also a limitation. Ideally, prospective studies are needed. The other limitation was that TLG calculations and dual-time imaging could not be performed for all the patients.

Conclusions

FDG uptake on PET/CT imaging is quite sensitive for both benign and malignant lesions in patients with CRC. ¹⁸F-FDG-PET/CT appears to be very beneficial in revealing especially true-negative lesions suspected of recurrence or metastasis and may prevent unnecessary treatments. Although SUVmax is a strong metabolic parameter ($p = 0.008$), TLG seems to be the best predictor in recurrence of colorectal cancers ($p = 0.001$). Both are increasing the specificity of ¹⁸F-FDG-PET/CT.

References

1. Hammond K, Margolin DA. The role of postoperative surveillance in colorectal cancer. *Clin Colon Rectal Surg* 2007; **20**: 249-54. doi: 10.1055/s-2007-984869
2. Gade M, Kubik M, Fisker RV, Thorlacius-Ussing O, Petersen LJ. Diagnostic value of (18)F-FDG PET/CT as first choice in the detection of recurrent colorectal cancer due to rising CEA. *Cancer Imaging* 2015; **15**: 11. doi: 10.1186/s40644-015-0048-y
3. Laurens ST, Oyen WJ. Impact of fluorodeoxyglucose PET/Computed Tomography on the management of patients with colorectal cancer. *PET Clin* 2015; **10**: 345-60. doi: 10.1016/j.cpet.2015.03.007
4. Chen CH, Hsieh MC, Lai CC, Yeh CY, Chen JS, Hsieh PS, et al. Lead time of carcinoembryonic antigen elevation in the postoperative follow-up of colorectal cancer did not affect the survival rate after recurrence. *Int J Colorectal Dis* 2010; **25**: 567-71. doi: 10.1007/s00384-010-0889-6

5. Chiaravalloti A, Fiorentini A, Palombo E, Rinino D, Lacanfora A, Danieli R, et al. Evaluation of recurrent disease in the re-staging of colorectal cancer by 18F-FDG PET/CT: Use of CEA and CA 19-9 in patient selection. *Oncol Lett* 2016; **12**: 4209-13. doi: 10.3892/ol.2016.5143
6. Van de Velde CJ, Boelens PG, Borrás JM, Coebergh JW, Cervantes A, Blomqvist L, et al. EURECCA colorectal: Multidisciplinary management: European consensus conference colon & rectum. *Eur J Cancer* 2014; **50**: 1.e1-34. doi: 10.1016/j.ejca.2013.06.048
7. Tan E, Gouvas N, Nicholls RJ, Ziprin P, Xynos E, Tekkis PP. Diagnostic precision of carcinoembryonic antigen in the detection of recurrence of colorectal cancer. *Surg Oncol* 2009; **18**: 15-24. doi: 10.1016/j.suronc.2008.05.008
8. Filella X, Molina R, Piqué JM, Garcia-Valdecasas JC, Grau JJ, Novell F, et al. Use of CA 19-9 in the early detection of recurrences in colorectal cancer: Comparison with CEA. *Tumour Biol* 1994; **15**: 1-6.
9. Panagiotidis E, Datsis IE, Rondogianni P, Vrontzou E, Skilakaki M, Exarhos D, et al. Does CEA and CA 19-9 combined increase the likelihood of 18F-FDG in detecting recurrence in colorectal patients with negative CeCT? *Nucl Med Commun* 2014; **35**: 598-605. doi: 10.1097/MNM.000000000000107
10. Sanli Y, Kuyumcu S, Ozkan ZG, Kilic L, Balik E, Turkmen C, et al. The utility of FDG-PET/CT as an effective tool for detecting recurrent colorectal cancer regardless of serum CEA levels. *Ann Nucl Med* 2012; **26**: 551-8. doi: 10.1007/s12149-012-0609-0
11. Zhuang H, Alavi A. 18-Fluorodeoxyglucose positron emission tomographic imaging in the detection and monitoring of infection and inflammation. *Semin Nucl Med* 2002; **32**: 47-59. doi: 10.1053/snuc.2002.29278
12. Choi H, Yoon HJ, Kim TS, Oh JH, Kim DY, Kim SK. Voxel-based dual-time 18F-FDG parametric imaging for rectal cancer: differentiation of residual tumor from postchemoradiotherapy changes. *Nucl Med Commun* 2013; **34**: 1166-73. doi: 10.1097/MNM.0000000000000002
13. Chan K, Welch S, Walker-Dilks C, Raifu A. Ontario provincial Gastrointestinal Disease Site Group. Evidence-based guideline recommendations on the use of positron emission tomography imaging in colorectal cancer. *Clin Oncol (R Coll Radiol)* 2012; **24**: 232-49. doi: 10.1016/j.clon.2011.11.008
14. Basu S, Alavi A. Partial volume correction of standardized uptake values and the dual time point in FDG-PET imaging: should these be routinely employed in assessing patients with cancer? *Eur J Nucl Med Mol Imaging* 2007; **34**: 1527-9. doi: 10.1007/s00259-007-0467-5
15. Bowne WB, Lee B, Wong WD, Ben-Porat L, Shia J, Cohen AM, et al. Operative salvage for locoregional recurrent colon cancer after curative resection: An analysis of 100 cases. *Dis Colon Rectum* 2005; **48**: 897-909. doi: 10.1007/s10350-004-0881-8
16. Sobhani I, Tiret E, Lebtahi R, Aparicio T, Itti E, Montravers F, et al. Early detection of recurrence by 18FDG-PET in the follow-up of patients with colorectal cancer. *Br J Cancer* 2008; **98**: 875-80. doi: 10.1038/sj.bjc.6604263
17. Scott AM, Gunawardana DH, Kelley B, Stuckey JG, Byrne AJ, Ramshaw JE, et al. PET changes management and improves prognostic stratification in patients with recurrent colorectal cancer: results of a multicenter prospective study. *J Nucl Med* 2008; **49**: 1451-7. doi: 10.2967/jnumed.108.051615
18. Lu YY, Chen JH, Chien CR, Chen WT, Tsai SC, Lin WY, et al. Use of FDG-PET or PET/CT to detect recurrent colorectal cancer in patients with elevated CEA: a systematic review and meta-analysis. *Int J Colorectal Dis* 2013; **28**: 1039-47. doi: 10.1007/s00384-013-1659-z
19. Maas M, Rutten IJ, Nelemans PJ, Lambregts DM, Cappendijk VC, Beets GL, et al. What is the most accurate whole-body imaging modality for assessment of local and distant recurrent disease in colorectal cancer? A meta-analysis: imaging for recurrent colorectal cancer. *Eur J Nucl Med Mol Imaging* 2011; **38**: 1560-71. doi: 10.1007/s00259-011-1785-1
20. Schmidt E, Nehra V, Lowe V, Oxentenko AS. Clinical significance of incidental [18F]FDG uptake in the gastrointestinal tract on PET/CT imaging: a retrospective cohort study. *BMC Gastroenterol* 2016; **16**: 125. doi: 10.1186/s12876-016-0545-x
21. Abdel-Nabi H, Doerr RJ, Lamonica DM, Cronin VR, Galantowicz PJ, Carbone GM, et al. Staging of primary colorectal carcinomas with fluorine-18 fluorodeoxyglucose whole-body PET: correlation with histopathologic and CT findings. *Radiology* 1998; **206**: 755-60. doi: 10.1148/radiology.206.3.9494497
22. Prieto E, Marti-Climent JM, Dominguez-Prado I, Garrastachu P, Díez-Valle R, Tejada S, et al. Voxel-based analysis of dual-time-point 18F-FDG PET images for brain tumor identification and delineation. *J Nucl Med* 2011; **52**: 865-72. doi: 10.2967/jnumed.110.085324
23. Schillaci O. Use of dual-point fluorodeoxyglucose imaging to enhance sensitivity and specificity. *Semin Nucl Med* 2012; **42**: 267-80. doi: 10.1053/j.semnuclmed.2012.02.003
24. Miyake KK, Nakamoto Y, Togashi K. Dual-time-point 18F-FDG PET/CT in patients with colorectal cancer: clinical value of early delayed scanning. *Ann Nucl Med* 2012; **26**: 492-500. doi: 10.1007/s12149-012-0599-y
25. Yoon HJ, Kim SK, Kim TS, et al. New application of dual time point 18F-FDG PET/CT in the evaluation of neoadjuvant chemoradiation response of locally advanced rectal cancer. *Clin Nucl Med* 2013; **38**: 7-12. doi: 10.1097/RLU.0b013e3182639a58
26. Marcus C, Wray R, Taghipour M, Marashdeh W, Ahn SJ, Mena E, et al. Journal club: Value of quantitative FDG PET/CT volumetric biomarkers in recurrent colorectal cancer patient survival. *AJR Am J Roentgenol* 2016; **207**: 257-65. doi: 10.2214/AJR.15.15806
27. Shamim SA, Kumar R, Halanaik D, Shandal V, Reddy RM, Bal CS, et al. Role of FDG-PET/CT in detection of recurrent disease in colorectal cancer. *Nucl Med Commun* 2010; **31**: 590-6. doi: 10.1097/MNM.0b013e328338a120
28. Giacomobono S, Gallicchio R, Capacchione D, Nardelli A, Gattozzi D, Lettini G, et al. F-18 FDG PET/CT in the assessment of patients with unexplained CEA rise after surgical curative resection for colorectal cancer. *Int J Colorectal Dis* 2013; **28**: 1699-705. doi: 10.1007/s00384-013-1747-0.
29. Arslan N, Tuncel M, Kuzhan O, Alagoz E, Budakoglu B, Ozet A, et al. Evaluation of outcome prediction and disease extension by quantitative 2-deoxy-2-[18F] fluoro-D-glucose with positron emission tomography in patients with small cell lung cancer. *Ann Nucl Med* 2011; **25**: 406-13. doi: 10.1007/s12149-011-0478-y
30. Caglar M, Yener C, Karabulut E. Value of CT, FDG PET-CT and serum tumor markers in staging recurrent colorectal cancer. *Int J Comput Assist Radiol Surg* 2015; **10**: 993-1002. doi: 10.1007/s11548-014-1115-8

Is there a role for contrast-enhanced ultrasound in the detection and biopsy of MRI only visible breast lesions?

Aki Nykänen^{1,2}, Otso Arponen¹, Anna Sutela¹, Ritva Vanninen^{1,2,3}, Mazen Sudah¹

¹ Kuopio University Hospital, Diagnostic Imaging Center, Department of Clinical Radiology, Kuopio, Finland

² University of Eastern Finland, Institute of Clinical Medicine, School of Medicine, Kuopio, Finland

³ University of Eastern Finland, Cancer Center of Eastern Finland, Kuopio, Finland

Radiol Oncol 2017; 51(4): 386-392.

Received 17 August 2017

Accepted 2 October 2017

Correspondence to: Aki Nykänen, BM, Department of Clinical Radiology, Kuopio University Hospital, Puijonlaaksontie 2, P.O. Box 100, FI-70029 Kuopio, Finland. Phone: +358 40 532 0129; E-mail: akinyk@uef.fi

Disclosure: No potential conflicts of interest were disclosed.

Background. This study aimed to evaluate the feasibility of contrast-enhanced ultrasound (CEUS) and CEUS-guided interventions in the diagnostics of MRI visible targeted US occult breast lesions.

Patients and methods. This retrospective study examined 10 females with 10 occult, MRI only detected breast lesions between July 2014 and April 2017. Targeted second look US followed by CEUS with 2.4 ml of SonoVue® were performed for all of the lesions. After positive CEUS localization the same dose was repeated for confirmation and CEUS-guided interventions were performed.

Results. MRI revealed 8 mass lesions with a mean size of 9 mm (range 5–16 mm) and 2 non-mass enhancing lesions of 10 and 20 mm in largest diameters. Targeted US revealed no morphological correlate for the lesions. Five out of 10 lesions (50%) were visible on CEUS. CEUS-guided core biopsy was performed on 4 lesions and 1 was marked with a clip for later surgical removal. Histopathological analysis confirmed 4 of them to be malignant. Three out of 5 nonvisible lesions on CEUS underwent MRI-guided interventions, 1 lesion was scheduled for follow-up as it was non-amenable for MRI biopsy, and 1 lesion was biopsied under US-guidance. Three of these nonvisible lesions on CEUS were confirmed to be malignant.

Conclusions. Based on our preliminary results, CEUS is a feasible tool for detecting many MRI only visible breast lesions, resulting in a more cost effective and less time-consuming practice. It is a more convenient alternative than MRI guided biopsy and has the potential to be included in the diagnostic algorithm which evaluates MRI only visible breast lesions.

Key words: additional lesions; MRI; MRI-guided interventions; contrast-enhanced ultrasound; CEUS; CEUS-guided interventions

Introduction

Breast magnetic resonance imaging (MRI) has emerged as the most sensitive imaging modality in the detection and evaluation of breast lesions. One of the major indications for breast MRI is the preoperative local staging of breast cancer and despite controversies about its benefits, the number of preoperatively imaged women has increased.^{1,2}

MRI detects additional lesions in 16% (range 11%–24%) of patients in the ipsilateral breast and 9.3% (95% confidence interval, 5.8%–14.7%) in the contralateral breast, depending on the patient population and the definition criteria.³⁻⁵ MRI-detected primarily mammographically and sonographically (US) occult lesions have been shown to rarely display features that are suggestive of malignancy.⁶ Therefore, it is important to characterize and man-

age these breast lesions correctly, because if these additional lesions are malignant, this can alter the surgical treatment protocol.²

Additional MRI-detected lesions are characterized and evaluated using the BI-RADS[®] lexicon. Lesions categorized as suspicious for malignancy (e.g. BI-RADS[®] 4 or 5) need to undergo a second look targeted ultrasound⁷, and when visible, their nature should be verified histologically with core biopsy (CB) under US guidance whenever possible. A recent meta-analysis of 17 articles that included benign and malignant lesions revealed that the second look ultrasound had a pooled detection rate of 57.5% (range 22.6–82.1%) in the MRI suspicious additional lesions.⁷ The second look ultrasound is able to observe mass lesions and malignant lesions better than non-mass-enhancing (NME) or benign lesions.^{8,9} The additional lesions that have no morphological correlate on targeted ultrasound should then undergo further MRI-guided vacuum assisted biopsy (VAB). Nevertheless, MRI-guided biopsy is a time consuming, expensive and occasionally, challenging procedure. Furthermore, not all MRI only detected lesions are accessible for MRI biopsy.¹⁰ Therefore, other, more practical, methods to aid in the evaluation of additional MRI-detected lesions are needed.

Contrast-enhanced ultrasound (CEUS) is a non-invasive non-nephrotoxic technique that does not subject the patient to ionizing radiation. The method utilizes microbubble contrast agents, blood flow and tissue perfusion specific imaging.¹¹ Tissue perfusion is correlated to microvascular density (MVD)^{12,13} and angiogenic factor expression¹⁴ are analogous in CEUS and contrast-enhanced MRI (CE-MRI).¹¹ MRI contrast agents additionally extravasate to the extracellular matrix due to the increased permeability of the microvessels.^{15,16} However, the microbubbles in CEUS contrast agent do not extravasate; thus it is the contrast agent accumulating in the intravascular, not in the extracellular space, that is detected in the angiogenetic lesions.¹⁷ CEUS can be administered intravenously to differentiate benign and malignant breast lesions¹⁸, to assess the disease extent¹⁹ and to monitor the tumour response to neoadjuvant chemotherapy.^{20,21}

The utility of CEUS to detect MRI only visible lesions has not been previously reported, yet it is an attractive additional tool to be incorporated into the routine clinical practise, because when the targeted US fails, the patients are already in the US investigation position while rescheduling for MRI-guided biopsy will inevitably delay treatment decisions. In our institution, CEUS is a routine practice

for various indications; in breast diagnostics it is occasionally applied to characterize breast lesions or to identify the sentinel axillary lymph nodes in appropriate situations.²² The aim of this retrospective study is to report the feasibility of CEUS and CEUS-guided interventions in the detection of US occult MRI visible breast lesions.

Patients and methods

Study design and patients

Patients with malignant or suspicious breast findings are referred to our tertiary hospital (catchment area 260,000 inhabitants) for consultation and further management. All patients undergo a full mammography as well as a clinical and bilateral breast US evaluation upon referral. Patients are referred to breast MRI according to national guidelines which are in concordance with those issued by the European Society of Breast Cancer Specialists working group (EUSOMA).²³ Annually, approximately 200 breast MRI examinations are performed for various indications. For the purposes of the present study patients with MRI-detected additional lesions that were investigated with CEUS were retrospectively retrieved from the local picture archiving and communication system. The local chair of the hospital district waived the need for written informed consent from the patients.

Between July 2014 and April 2017, a total of 10 patients fulfilling the following inclusion criteria were evaluated: 1) bilateral mammograms and breast US performed by a breast radiologist; 2) breast MRI according to a structured protocol; 3) an occult, MRI only detected lesion found on MRI that might alter the surgical plan; the lesion had not been evident initially in mammography, US or clinical examination, 4) no morphological correlate of the lesion found during the targeted US performed by a breast radiologist.

Breast MRI protocol and image analysis

MRI examinations in 8 patients were performed at our institution in the prone position with a seven element, phased-array coil dedicated to breast imaging (Philips Achieva 3.0 T TX, Philips N.V., Eindhoven, The Netherlands). The structural breast MRI protocol consisted of five sequences as seen in Table 1.

Breast radiologists (with > 20 years of experience in breast radiology) primarily evaluated the morphological and kinetic features of MRI findings

TABLE 1. Breast MRI protocol

Sequence	TR/TE (ms)	in-plane resolution mm	Slice thickness (mm)	Scanning time
T1-FFE	4.57/2.3	0.48×0.48	0.7	6 min 11 s
T2-TSE	5000/120	0.6×0.6	2	3 min 20 s
STIR	5000 /60	1×1	2	5 min 40 s
T1 dynamic*	4.67/ 2.31	0.96×0.96	1	58.5 s
DWI#	7168 /95	1.15×1.15	4	min 8 s

#DWI = Diffusion weighted echo planar imaging with five respective b factors (0, 200, 400, 600 and 800 s/mm²); *eTHRIVE spectrally adiabatic inversion recovery (SPAIR) fat suppression; pre-contrast and six phases after the gadoterate meglumine (0.2 ml/kg, 3 ml/s) injection followed by a saline chaser; FFE = fast field echo; STIR = Short tau inversion recovery; TSE = turbo spin echo

together with mammograms and US examinations guided by the BI-RADS[®] lexicon. Two patients were referred to our university hospital from two central hospitals for MRI-guided interventions because of MRI only visible lesions. These patients were scanned with 1.5 T scanners yet with a similar structured MRI protocol. MRI-guided interventions were performed with automated 10 gauge (G) vacuum assisted biopsy device (EnCore Enspire Breast Biopsy System, C.R. Bard Inc., Tempe, AZ, USA).

Second look targeted US examination

Patients were meticulously scanned with both grey scale and Doppler US. For MRI lesions detected in the lateral part of the breast, patients were scanned in the opposite lateral decubitus position and consequently in the ipsilateral oblique position for medial lesions in an attempt to simulate the MRI position of the breast. If no morphologically concordant lesions were detected in targeted US, then a CEUS examination was considered.

CEUS procedures

The purpose and nature of the CEUS procedure was discussed with the patient and all patients provided verbal consent. Nonlinear harmonic imaging using an Esaote MyLabClassC ultrasound scanner (Esaote S.p.A., Genova, Italy) equipped with a 7–13 MHz linear array transducer was performed at baseline with a low mechanical index (MI) of 0.08 in three patients. The remaining examinations were performed using Logiq E9 class US scanner (GE, Wauwatosa, Wisconsin, USA) with a low MI of 0.11. A microbubble contrast agent (SonoVue[®], Bracco S.p.A., Milan, Italy) was used for localizing occult lesions. The contrast agent was adminis-

tered according to the guidelines of the manufacturer: microbubble dispersion was prepared before use by injecting through the septum the contents of the vial a total of 5 ml of sodium chloride 9 mg/ml (0.9%) solution for injection. The vial was then shaken vigorously for a few seconds until the lyophilisate was completely dissolved. A standard dose of 2.4 ml of dispersion was drawn into a syringe and administered intravenously via an 18-G cannula placed in a cubital vein. Injections were flushed with 5 ml of sodium chloride 9 mg/ml (0.9%) solution.

After contrast agent administration, the suspected area was scanned to detect enhancements morphologically concordant with the MRI finding. If the lesion was identified, then the skin area was ink-marked and sterilized. The marked area was confirmed with another SonoVue injection and thereafter, without moving the US probe, the breast area was anesthetized and an incision was made to collect the biopsy. Histopathological CB samples were obtained using 14-G core needle targeted at the area of interest. After the CB, the targeted area was marked with a coil. Both gray scale targeted US and CEUS breast examination were performed in all cases by or under the direct supervision of a breast radiologist with over 20 years of experience in multimodality breast imaging. All interventions were performed by the same senior breast radiologist.

Histopathological analysis

CB specimens were placed into 10% formalin and embedded in paraffin after fixation. The samples were cut into 5 µm slices at four different levels and stained with haematoxylin and eosin. Biopsy samples were evaluated by two pathologists, first at the time of diagnosis, and then at a multidisciplinary meeting. Diagnosis was confirmed from final surgical specimens when indicated. Both non-invasive and invasive carcinomas were considered malignant.

Results

MRI detected 8 mass lesions with a mean size of 9 mm (range 5–16 mm) and 2 non-mass enhancement of 10 and 20 mm in largest diameters. Five of these lesions were CEUS positive, of which 4 underwent CEUS-guided CB (Figure 1) and one was primarily marked with a clip for later surgical removal. Of these 5 lesions, 4 proved to be malignant.

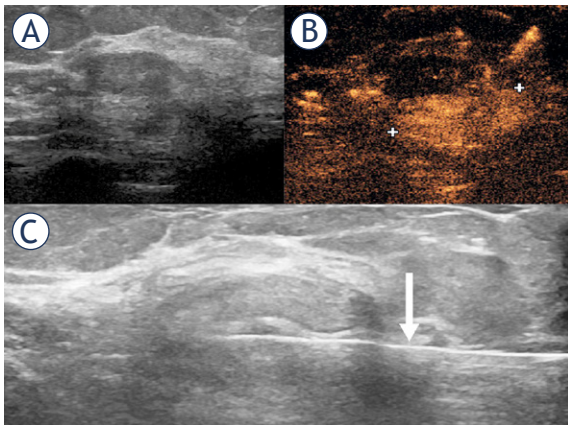


FIGURE 1. 53 year old female patient with invasive carcinoma of the right breast. MRI detected an occult, BI-RADS 5, oval, 20x16 mm irregular mass lesion in the lower medial quadrant of the left breast (not shown). Targeted US (A) was negative. Contrast-enhanced ultrasound (B) revealed a 21 mm enhancement. Core biopsies were obtained from the enhancement area (C, ARROW) showing the core biopsy needle's position). Both core biopsy and final histology showed high grade invasive carcinoma.

In one of these patients, CEUS showed a round 5 mm lesion which was evaluated to be low grade ductal carcinoma in situ (DCIS) at CB. At final histology, a low grade invasive carcinoma was found in the continuation of the DCIS. It is presumed that the CEUS showed only the DCIS component which was also carefully targeted (Figure 2).

Of the 5 CEUS negative patients, 2 underwent MRI-guided vacuum assisted biopsy and 1 was subjected to MRI-guided coil localization. One patient had a non-mass lesion close to the chest wall deemed non-amenable to MRI-guided biopsy. The patient's preference was follow-up with MRI and mammography. The lesion remained stable after 2 rounds of breast MRI at 6 and 14 months. In one CEUS negative patient, targeted US had revealed only a slight nonspecific architectural distortion at the site of MRI enhancement not deemed to be morphologically concordant with confidence. Nonetheless, it was biopsied and coil marked after the negative CEUS and subsequently proved to be malignant. More detailed patient and lesion characteristics are presented in Table 2.

After coiling, a mammogram was acquired in two orthogonal views to confirm the localization of the coil. Seven coil-marked lesions were surgically removed after stereotactic or US-guidance wire localization of the coil. One patient with negative CEUS and malignant MRI-guided vacuum biopsy is treated in another hospital and her

medical records on final treatment decisions are not available.

Discussion

MRI-detected primarily occult additional lesions are small, have few specific suspicious features, and are therefore challenging to characterize.⁶ When imaged by US, these lesions are usually subtle and appear as nonspecific findings.²⁴ Searching for such lesions can therefore be challenging and time consuming even in the hands of experienced breast radiologists. Our findings indicate that CEUS and CEUS-guided interventions are feasible in the evaluation of half of the MRI only visible lesions and represent a practicable alternative for MRI-guided biopsy in these situations.

In general, CEUS is known to be a safe, rapid, cost-effective and less time-consuming procedure for both the clinician and the patient.²⁵ In our study, half of the CEUS studies were, however, negative, meaning that there were some additional contrast agent costs. Nevertheless, these costs are less than the savings made when MRI-guidance is avoided. In our institution, the basic list price of CEUS and CEUS-guided biopsy and coil placement is 313 € compared to 1167 € for MRI-guided biopsy. Furthermore, patients can be evaluated and managed immediately in positive cases, thus eliminating the need for rescheduling for MRI-guided intervention.

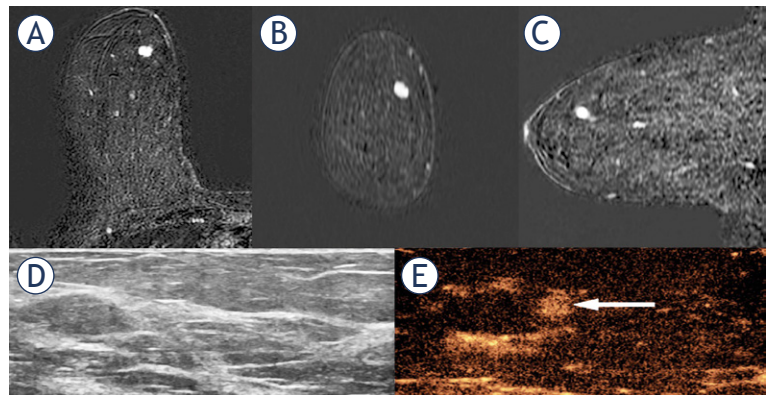


FIGURE 2. 60 year old female patient with invasive carcinoma of no specific type (NST) of the left breast (not shown). MRI detected an occult BI-RADS 4 oval, 7x5 mm mass lesion in the upper medial quadrant of the right breast (A-C thin slice multiplanar reconstruction in axial, coronal and sagittal orientations). Targeted US was negative (D). Contrast-enhanced ultrasound (E, ARROW) revealed a 5 mm round enhancement. Low grade ductal carcinoma in situ (DCIS) was diagnosed in the core biopsy of the enhanced lesion. The final histology was both DCIS (6x4 mm) and low grade invasive carcinoma NST (6x5 mm) in close vicinity.

TABLE 2. Patients, indications for MRI and MRI-only detected lesions' characteristics, interventions and histopathological diagnosis

Case	Age yrs	Indication for MRI	Occult-lesion characteristics on MRI	Occult lesion size	CEUS visualization	Intervention	CB and final histopathological diagnosis and size of lesion
1	71	Preoperative local staging	Mass, round, circumscribed, washout kinetic curve	6 mm	Positive	CEUS-guided CB	CB: Low grade DCIS Final: Low grade DCIS. 3 mm
2	78	Problem solving	Mass, oval, circumscribed, washout kinetic curve	7 mm	Negative	MRI-guided localization	Final: Papilloma. 5 mm
3	64	Incidental breast lesion on CT	NME, focal, heterogeneous	20 mm	Negative	US-guided CB	CB: high grade DCIS. Final: high grade DCIS. 16 mm
4	54	Preoperative local staging	Mass, round, circumscribed, heterogeneous, washout kinetic curve	7 mm	Positive	CEUS-guided clip placement	Final: Intermediate grade IC NST. 5 mm
5	54	Axillary metastasis from an occult breast cancer	Mass, irregular, not circumscribed, plateau kinetic curve	12 mm	Negative	MRI-guided CB	VAB: Carcinoma with medullary feature Final: Carcinoma with medullary feature and high grade DCIS. 10 mm
6	66	Problem solving	Mass, round, circumscribed, ring like enhancement, persistent kinetic curve	5 mm	Positive	CEUS-guided CB. Follow-up	CB: Fibrocystic lesion, liponecrosis
7	30	Problem solving	NME, focal, heterogeneous	10 mm	Negative	Follow-up	--
8	61	Preoperative local staging	Mass, oval, irregular, washout kinetic curve	10 mm	Positive	CEUS-guided CB	CB: Low grade DCIS Final: low grade IC NST 6 mm and Low grade DCIS 5mm
9	53	Preoperative local staging	Mass, oval, irregular, washout kinetic curve	16 mm	Positive	CEUS-guided CB	CB: High grade IC NST Final: High grade IC NST. 13 mm
10	65	Axillary recurrence	Mass, oval, circumscribed, homogeneous, persistent kinetic curve	9 mm	Negative	MRI-guided VAB	VAB: High grade DCIS + suspected microinvasion

CB = Core biopsy; CEUS = Contrast-enhanced ultrasound; CT = Computed tomography; DCIS = Ductal carcinoma in situ; IC NST = Invasive carcinoma no special type; MRI = Magnetic resonance imaging; NME = Non-mass-enhancing; US = Ultrasound; VAB = Vacuum assisted biopsy

Tumor-induced angiogenesis results in immature and dysfunctional vessels with different levels of vascular permeabilities and these are also visualized in dynamic gadolinium enhanced breast MRI. Microvascular density is linked to tumor growth and prognosis. As MRI contrast readily leaks out of the vasculature especially in malignant tumors, it obscures the structures of possible microvessels and complicates the assessment of their density.²⁶ Nevertheless, it is believed permissible to link the morphology of MRI enhancement to the microvascularity pattern.²⁷ Furthermore, according to an animal model study conducted by Jansen *et al.*, it has been speculated that gadolinium penetrates and collects inside the dilated DCIS ducts *i.e.* gadolinium accumulation was observed within the intraductal neoplastic space 2 minutes after the administration of the contrast agent. In contrast, CEUS specifically reveals only the microvascular structures without any interfering leakage. Intuitively, it can be assumed that invasive cancers have a denser microvascular network and are thus more

amenable to CEUS visualization. Interestingly, in our study, we were not able to visualize some of the more aggressive DCIS and invasive lesions, indicating that the vascular density of a malignant lesion is not necessarily related to either lesion morphology or histopathology. Therefore, a negative CEUS cannot be used to rule out malignancy and further evaluation with MRI-guided interventions should be deemed necessary. This observation will need to be confirmed in a larger patient population.

The use of CEUS also requires experience and state of the art US scanners with contrast applications. Biopsy and clip-marking of CEUS visualized lesions, although feasible as demonstrated in our study, can prove to be a challenging procedure. It could therefore be speculated that in cases of negative second look targeted US, MRI-guided biopsy would be a straightforward next step procedure. Nevertheless, non-visualization after contrast agent administration does occur also on MRI-guided biopsy in about 8–13% cases requiring

short term follow-up.²⁸ Furthermore, the technical aspects of MRI-guidance have additional weaknesses including the use of a compression grid system which limits access to areas between grid holes and makes it difficult to localize lesions in the retromamillary region, near the chest wall and in axillary tail. Even though compression grid freehand MRI biopsy technique is not subject to localization limitations, it might prolong examination time due to repeated imaging to confirm proper needle placement.²⁹ Nonetheless, regardless of all the previously mentioned difficulties, we believe that CEUS confers considerable added value in the immediate evaluation of occult lesions and therefore more investigations into its applicability are warranted.

The small number of patients in this study is a major limitation and therefore no definitive solid conclusions can be made about the diagnostic performance and cost-effectiveness of CEUS in this indication. Nevertheless, our study can be considered as a pilot report, clearly showing that some small US occult lesions do enhance with CEUS and therefore this procedure is feasible and further investigations on this issue are well-founded.

In conclusion, CEUS is a feasible and more convenient alternative to MRI-guided biopsy for some MRI only visible lesions, resulting in a more cost-effective and less time-consuming practice. CEUS has the potential to be included in the diagnostic algorithm for the evaluation of MRI only visible breast lesions. Based on our initial experience, further studies are warranted to confirm our findings and possibly to define which lesions benefit most from this technique.

Acknowledgements

This study was supported in part (AN) by Kuopio University Hospital (VTR grant: 5063542) and Cancer Society of Finland. The funders had no role in study design, data collection and analysis, decision to publish, or preparation of the manuscript.

References

- Breslin TM, Banerjee M, Gust C, Birkmeyer NJ. Trends in advanced imaging use for women undergoing breast cancer surgery. *Cancer* 2013; **119**: 1251-6. doi: 10.1002/cncr.27838
- Houssami N, Hayes DF. Review of preoperative magnetic resonance imaging (MRI) in breast cancer: should MRI be performed on all women with newly diagnosed, early stage breast cancer? *CA Cancer J Clin* 2009; **59**: 290-302. doi: 10.3322/caac.20028
- Teifke A, Lehr HA, Vomweg TW, Hlawatsch A, Thelen M. Outcome analysis and rational management of enhancing lesions incidentally detected on contrast-enhanced MRI of the breast. *AJR Am J Roentgenol* 2003; **181**: 655-62. doi: 10.2214/ajr.181.3.1810655
- Brennan ME, Houssami N, Lord S, Macaskill P, Irwig L, Dixon JM, et al. Magnetic resonance imaging screening of the contralateral breast in women with newly diagnosed breast cancer: systematic review and meta-analysis of incremental cancer detection and impact on surgical management. *J Clin Oncol* 2009; **27**: 5640-9. doi: 10.1200/JCO.2008.21.5756
- Houssami N, Turner R, Morrow M. Preoperative magnetic resonance imaging in breast cancer: meta-analysis of surgical outcomes. *Ann Surg* 2013; **257**: 249-55. doi: 10.1097/SLA.0b013e31827a8d17
- Arponen O, Masarwah A, Sutela A, Taina M, Könönen M, Sironen R, et al. Incidentally detected enhancing lesions found in breast MRI: analysis of apparent diffusion coefficient and T2 signal intensity significantly improves specificity. *Eur Radiol* 2016; **26**: 4361-70. doi: 10.1007/s0033-016-4326-2
- Spick C, Baltzer PA. Diagnostic utility of second-look US for breast lesions identified at MR imaging: systematic review and meta-analysis. *Radiology* 2014; **273**: 401-9. doi: 10.1148/radiol.14140474
- Hollowell L, Price E, Arasu V, Wisner D, Hylton N, Joe B. Lesion morphology on breast MRI affects targeted ultrasound correlation rate. *Eur Radiol* 2015; **25**: 1279-84. doi: 10.1007/s00330-014-3517-y
- Newburg AR, Chhor CM, Young Lin LL, Heller SL, Gillman J, Toth HK, et al. Magnetic resonance imaging-directed ultrasound imaging of non-mass enhancement in the breast: Outcomes and frequency of malignancy. *J Ultrasound Med* 2017; **36**: 493-504. doi: 10.7863/ultra.16.03001
- Gao Y, Bagadiya NR, Jardon ML, Heller SL, Melsaether AN, Toth HB, et al. Outcomes of preoperative MRI-guided needle localization of nonpalpable mammographically occult breast lesions. *AJR Am J Roentgenol* 2016; **207**: 676-84. doi: 10.2214/AJR.15.15913
- Wilson SR, Greenbaum LD, Goldberg BB. Contrast-enhanced ultrasound: what is the evidence and what are the obstacles? *AJR Am J Roentgenol* 2009; **193**: 55-60. doi: 10.2214/AJR.09.2553
- Buckley DL, Drew PJ, Mussurakis S, Monson JR, Horsman A. Microvessel density of invasive breast cancer assessed by dynamic Gd-DTPA enhanced MRI. *J Magn Reson Imaging* 1997; **7**: 461-4.
- Giesel FL, Choyke PL, Mehndiratta A, Zechmann CM, von Tengg-Kobligk H, Kayser K. Pharmacokinetic analysis of malignant pleural mesothelioma-initial results of tumor microcirculation and its correlation to microvessel density (CD-34). *Acad Radiol* 2008; **15**: 563-70. doi: 10.1016/j.acra.2007.12.014
- Knopp MV, Weiss E, Sinn HP, Mattern J, Junkermann H, Radeleff J, et al. Pathophysiologic basis of contrast enhancement in breast tumors. *J Magn Reson Imaging* 1999; **10**: 260-6.
- Hayes C, Padhani AR, Leach MO. Assessing changes in tumour vascular function using dynamic contrast-enhanced magnetic resonance imaging. *NMR Biomed* 2002; **15**: 154-63.
- Jansen SA, Paunesku T, Fan X, Woloschak GE, Vogt S, Conzen SD, et al. Ductal carcinoma in situ: X-ray fluorescence microscopy and dynamic contrast-enhanced MR imaging reveals gadolinium uptake within neoplastic mammary ducts in a murine model. *Radiology* 2009; **253**: 399-406. doi: 10.1148/radiol.2533082026
- Giorgio R, Roberta C. *Enhancing the role of ultrasound with contrast agents*. Milan: Springer; 2006.
- Du J, Wang L, Wam CF, Hua J, Fang H, Chen J, et al. Differentiating benign from malignant solid breast lesions: combined utility of conventional ultrasound and contrast-enhanced ultrasound in comparison with magnetic resonance imaging. *Eur J Radiol* 2012; **81**: 3890-9. doi: 10.1016/j.ejrad.2012.09.004
- Jiang YX, Liu H, Liu JB, Zhu QL, Sun Q, Chang XY. Breast tumor size assessment: comparison of conventional ultrasound and contrast-enhanced ultrasound. *Ultrasound Med Biol* 2007; **33**: 1873-81. doi: 10.1016/j.ultras-medbio.2007.06.002
- Corcioni B, Santilli L, Quercia S, Zamagni C, Santini D, Taffurelli M, et al. Contrast-enhanced US and MRI for assessing the response of breast cancer to neoadjuvant chemotherapy. *J Ultrasound* 2008; **11**: 143-50. doi: 10.1016/j.jus.2008.09.007
- Fujisawa T, Hirakata T, Yanagita Y, Iijima M, Horikoshi H, Takeuchi K, et al. The detection of pCR after PST by contrast-enhanced ultrasonography for breast cancer. *Breast Cancer* 2013; **20**: 75-82. doi: 10.1007/s12282-011-0311-4

22. Rautiainen S, Sudah M, Joukainen S, Sironen R, Vanninen R, Sutela A. Contrast-enhanced ultrasound -guided axillary lymph node core biopsy: Diagnostic accuracy in preoperative staging of invasive breast cancer. *Eur J Radiol* 2015; **84**: 2130-6. doi: 10.1016/j.ejrad.2015.08.006
23. Sardanelli F, Boetes C, Borisch B, Decker T, Federico M, Gilbert FJ, et al. Magnetic resonance imaging of the breast: recommendations from the EUSOMA working group. *Eur J Cancer* 2010; **46**: 1296-316. doi: 10.1016/j.ejca.2010.02.015
24. Abe H, Schmidt RA, Shah RN, Shimauchi A, Kulkarni K, Sennett CA, et al. MR-directed ("Second-Look") ultrasound examination for breast lesions detected initially on MRI: MR and sonographic findings. *AJR Am J Roentgenol* 2010; **194**: 370-7. doi: 10.2214/AJR.09.2707
25. Westwood M, Joore M, Grutters J, Redekop K, Armstrong N, Lee K, et al. Contrast-enhanced ultrasound using SonoVue(R) (sulphur hexafluoride microbubbles) compared with contrast-enhanced computed tomography and contrast-enhanced magnetic resonance imaging for the characterisation of focal liver lesions and detection of liver metastases: a systematic review and cost-effectiveness analysis. *Health Technol Assess* 2013; **17**: 1-243. doi: 10.3310/hta17160
26. Heijblom M, Klaase JM, van den Engh FM, van Leeuwen TG, Steenberg W, Manohar S. Imaging tumor vascularization for detection and diagnosis of breast cancer. *Technol Cancer Res Treat* 2011; **10**: 607-23. doi: 10.7785/rt.2012.500227
27. Santamaria G, Velasco M, Farrús B, Caparrós FX, Fernández PL. Dynamic contrast-enhanced MRI reveals the extent and the microvascular pattern of breast ductal carcinoma in situ. *Breast J* 2013; **19**: 402-10. doi: 10.1111/tbj.12135
28. Chevrier MC, David J, Khoury ME, Lalonde L, Labelle M, Trop I. Breast biopsies under magnetic resonance imaging guidance: Challenges of an essential but imperfect technique. *Curr Probl Diagn Radiol* 2016; **45**: 193-204. doi: 10.1067/j.cpradiol.2015.07.002
29. Choi HY, Kim SM, Jang M, Yun BL, Kim SW, Kang E, et al. MRI-guided intervention for breast lesions using the freehand technique in a 3.0-T closed-bore MRI scanner: feasibility and initial results. *Korean J Radiol* 2013; **14**: 171-8. doi: 10.3348/kjr.2013.14.2.171

Baseline tumor Lipiodol uptake after transarterial chemoembolization for hepatocellular carcinoma: identification of a threshold value predicting tumor recurrence

Yusuke Matsui^{1,2}, Masahiro Horikawa¹, Younes Jahangiri Noudeh¹, John A. Kaufman¹, Kenneth J. Kolbeck¹, Khashayar Farsad¹

¹ Dotter Interventional Institute, Oregon Health and Science University, 3181 SW Sam Jackson Park Rd, Portland, USA

² Department of Radiology, Okayama University Medical School, 2-5-1 Sikata-cho, Kita-ku, Okayama 700-8558, Japan

Radiol Oncol 2017; 51(4): 393-400.

Received 16 April 2017
Accepted 30 June 2017

Correspondence to: Yusuke Matsui, Department of Radiology, Okayama University Medical School, 2-5-1 Sikata-cho, Kita-ku, Okayama 700-8558, Japan. Phone: +81 86 235 7313; Fax: +81 86 235 7316; E-mail: y-matsui@okayama-u.ac.jp

Disclosure: Financial activities related to the present article: Khashayar Farsad received a grant from Guerbet for this study. Financial activities not related to the present article: Yusuke Matsui reports a grant from Japan Radiological Society supported by Bayer Yakuin, a consultancy fee from Stryker Japan, a lecturer's fee from Terumo Corporation; John A. Kaufman reports grants from NIH, WL Gore, and BTG, personal fees from VIVA Physicians, Delcath, MarrowStim and COOK Medical, book royalties and journal editor stipend from Elsevier, section editor stipend from ARRS/AJR, stock ownership in Hatch Medical, Vu Medi, Endoshape, and Veniti, stock options in Javelin Medical, AV Medical, and BIO2 Medical; Kenneth J. Kolbeck reports a grant from Guerbet. A summary of this work was presented at the Society of Interventional Radiology (SIR) 2016 annual meeting (<http://dx.doi.org/10.1016/j.jvir.2015.12.227>).

Background. The aim of the study was to evaluate the association between baseline Lipiodol uptake in hepatocellular carcinoma (HCC) after transarterial chemoembolization (TACE) with early tumor recurrence, and to identify a threshold baseline uptake value predicting tumor response.

Patients and methods. A single-institution retrospective database of HCC treated with Lipiodol-TACE was reviewed. Forty-six tumors in 30 patients treated with a Lipiodol-chemotherapy emulsion and no additional particle embolization were included. Baseline Lipiodol uptake was measured as the mean Hounsfield units (HU) on a CT within one week after TACE. Washout rate was calculated dividing the difference in HU between the baseline CT and follow-up CT by time (HU/month). Cox proportional hazard models were used to correlate baseline Lipiodol uptake and other variables with tumor response. A receiver operating characteristic (ROC) curve was used to identify the optimal threshold for baseline Lipiodol uptake predicting tumor response.

Results. During the follow-up period (mean 5.6 months), 19 (41.3%) tumors recurred (mean time to recurrence = 3.6 months). In a multivariate model, low baseline Lipiodol uptake and higher washout rate were significant predictors of early tumor recurrence ($P = 0.001$ and < 0.0001 , respectively). On ROC analysis, a threshold Lipiodol uptake of 270.2 HU was significantly associated with tumor response (95% sensitivity, 93% specificity).

Conclusions. Baseline Lipiodol uptake and washout rate on follow-up were independent predictors of early tumor recurrence. A threshold value of baseline Lipiodol uptake > 270.2 HU was highly sensitive and specific for tumor response. These findings may prove useful for determining subsequent treatment strategies after Lipiodol TACE.

Key words: transarterial chemoembolization; hepatocellular carcinoma; Lipiodol, tumor response, threshold

Introduction

Transarterial chemoembolization (TACE) has been proven effective for treatment of intermediate stage hepatocellular carcinoma (HCC).^{1,2} Lipiodol, a di-

iodinated ethyl ester derivative of poppy seed oil, has been widely used in the standard TACE procedure.³ When administered selectively via the hepatic artery, Lipiodol accumulates preferentially in HCC and is retained for a longer period than in the

background liver parenchyma.⁴⁻⁶ Because Lipiodol demonstrates trans-sinusoidal penetration, arterial injection of Lipiodol can temporarily achieve dual arterial and portal embolization, unlike other particulate embolic materials such as microspheres.^{3,7} An association between intratumoral Lipiodol accumulation, pathological tumor necrosis⁸⁻¹² and local recurrence rate¹³⁻¹⁵ has been shown in retrospective analyses; however, no study has investigated a specific value of baseline Lipiodol uptake, i.e., the Lipiodol uptake immediately after TACE, predicting tumor recurrence. If a specific baseline Lipiodol uptake value proves useful to predict tumor recurrence, it should have significant meaning for subsequent clinical management of HCC patients. This study examined whether baseline Lipiodol uptake in HCC was associated with tumor response, and whether a cutoff value of Lipiodol uptake could be identified predicting tumor recurrence.

Patients and methods

Study population

Retrospective single institution database review was performed of patients with primary HCC who underwent Lipiodol-TACE from April 2007 to August 2013. Institutional review board approval was obtained. Inclusion criteria were i) documented non-contrast computed tomography (CT) of the liver within one week after TACE, ii) at least one documented triphasic contrast CT including non-contrast, arterial and delayed phase imaging on follow-up for evaluation of tumor recurrence, iii) lesion diameter ≥ 10 mm, and iv) lesions stained entirely and homogeneously with Lipiodol after TACE. Exclusion criteria were i) patients with more than 6 lesions, ii) lesions stained partially or heterogeneously with Lipiodol; those lesions were not suitable for the Lipiodol uptake measurement because of the nonuniform Lipiodol concentration and possibility of incomplete treatment, iii) lesions treated with additional particulate embolic materials, iv) lesions for which a second TACE or any additional treatment including surgery, radiofrequency ablation (RFA), radiation therapy, or systemic therapy (e.g., sorafenib) was performed before the initiation of follow up. Forty-six tumors in 30 patients meeting criteria were evaluated.

TACE procedure

Selective catheterization of lobar, segmental or subsegmental hepatic arteries supplying tumor was

performed under standard fluoroscopic guidance using 5–6 Fr base catheters in the first order aortic branch (celiac or superior mesenteric artery) followed by microcatheter selection of higher order branches as appropriate. A Lipiodol-chemotherapy emulsion (doxorubicin or epirubicin, 50mg) was prepared by admixture in a 1:1 or 2:1 ratio using a three-way stopcock and injected into selected hepatic arteries through the microcatheter. The endpoint of injection was stasis of blood flow in the feeding artery or visualization of trans-sinusoidal portal branches. The volume of Lipiodol injected ranged from 1 to 10 mL per lesion. Lipiodol was used as the sole embolic material; no additional embolization with other particulate embolic materials was performed. Although this method corresponds to “chemo-lipiodolization” in European guidelines¹⁶ or “Lip-TAI (transcatheter arterial infusion)” in Japanese guidelines¹⁷, “TACE” was employed as a unified term in this study. The embolic particles were not routinely used in our institutional practice because our institutional data (not shown) demonstrated patients’ survival outcome was not significantly different using particulate embolization.

Data collection and image evaluation

Patient data including age, sex, etiology of liver disease, Child-Pugh classification, and Barcelona Clinic Liver Cancer (BCLC) staging were collected from the electronic medical record. Procedural details recorded included selectivity of treatment (lobar vs. subsegmental/segmental), volume of Lipiodol delivered and amount of chemotherapeutic delivered. Image evaluation was performed using a Digital Imaging and Communication in Medicine (DICOM) viewer (IMPAX; Agfa, Mortsel, Belgium). Lipiodol uptake was measured using the Hounsfield units (HU) of the target lesion on a non-contrast CT taken within one week after TACE and on every follow-up CT. The HUs on the CT within one week after TACE represented the baseline Lipiodol uptake. The follow-up interval varied case by case. The HUs were measured by hand drawing a region of interest (ROI) along the lesion periphery at the axial slice with the tumor maximum diameter, using the contrast-enhanced pre-procedure diagnostic scan as a reference. ROI analysis was performed with consistent contrast window level (WL) and width (WW) (WL/WW = 50/350). The diameter of the ROI on the baseline CT was used as the lesion size, since only lesions demonstrating entire and homogeneous uptake were included in the analysis. Lipiodol washout was defined as de-

creased density of Lipiodol in a part of the tumor or uniformly within the entire tumor, and evaluated using HU analysis on every available follow-up CT. The degree of washout was quantitatively evaluated by calculating the HU difference between the baseline CT and the follow-up CT at which washout was initially detected. If the HUs within the tumor on the last follow-up CT were greater than at baseline CT, as was occasionally seen with contracting tumors after treatment, the quantitative washout was recorded as 1.0 HU. The washout rate was calculated by dividing the quantitative washout by the follow up time period (HU/month). Tumor recurrence was defined as the appearance of new arterial enhancement within or along the margins of a completely treated lesion on the follow-up triphasic contrast CT. Evaluation was terminated when additional treatment was performed or when recurrence was identified. Two board-certified radiologists independently performed all image evaluation, with discrepancies decided by consensus with a third radiologist. Mean values of two measurements were used in all analyses.

Statistical analysis

Numerical data were summarized as mean \pm standard deviation (SD) and the categorical variables were shown as frequency (percentage). Inter-observer reliability of measurements was assessed by Cronbach's alpha¹⁸, and standard error of the measurement was calculated using the formula: $SEM = SD \times \sqrt{1 - r_{xx}}$, where SEM is standard error of measurement, SD is standard deviation and r_{xx} demonstrates the reliability of the test represented by Cronbach's alpha¹⁹. Analyses for predictors of tumor response and estimation of the cutoff lipiodol uptake value predicting tumor response were performed on lesion-by-lesion basis. Uni- and multivariate Cox proportional hazard models were created to evaluate the predictability of baseline Lipiodol uptake for tumor response. In addition to the baseline Lipiodol uptake, other variables such as lesion size, treatment selectivity and washout rate were subjected to the univariate model. Variables with a *P* value < 0.200 were entered in the multivariable model. Independent samples t-test was used to compare the mean baseline Lipiodol uptake between the tumors with and without recurrence, as well as between the degrees of treatment selectivity. The median recurrence-free interval was defined, and tumor recurrence before the median recurrence-free interval was defined as early recurrence. Baseline Lipiodol up-

TABLE 1. Summary of the study population

Characteristics		
Patients		
Age (years)		59.9 \pm 7.9
Gender	Female	12 (40.0%)
	Male	18 (60.0%)
Liver disease etiology	HCV	13 (43.3%)
	HCV + Alcohol	7 (23.3%)
	Alcohol	4 (13.3%)
	HBV	1 (3.3%)
	Other	5 (16.7%)
Child-Pugh class	A	10 (33.3%)
	B	20 (66.7%)
BCLC stage	A	17 (56.7%)
	B	13 (43.3%)
Tumors		
Baseline tumor size (mm)		20.3 \pm 10.1
Treatment selectivity	Lobar	16 (34.8%)
	Segmental	22 (47.8%)
	Sub-segmental	8 (17.4%)
Baseline Lipiodol uptake (HU)		328.3 \pm 185.2
Lipiodol uptake at final evaluation (HU)		205.0 \pm 219.5
Washout (HU)		136.9 \pm 127.6
Follow-up time (months)		5.6 \pm 6.2
Tumor recurrence	Yes	19 (41.3%)
	No	27 (58.7%)

The numerical data were summarized as mean \pm standard deviation and the categorical data were shown as frequency (percentage). BCLC = Barcelona clinic liver cancer; HBV = hepatitis B virus; HCV = hepatitis C virus; HU = Hounsfield unit

take and washout rates were compared between tumors with and without early recurrence using the independent samples t-test. Receiver operating characteristic (ROC) curve analysis was used to determine the optimal cutoff point for baseline Lipiodol uptake predicting tumor recurrence, and for Lipiodol washout rates predicting early tumor recurrence. Natural logarithm values of the numerical exposure variables were used in Cox regression models, and *P* values < 0.05 were considered statistically significant. All statistical analyses were done using Stata IC version 13.1 for Windows.

Results

The study population is summarized in Table 1. The mean follow-up period was 5.6 months (range,

TABLE 2. Results of cox regression analysis to predict factors for tumor recurrence

Predicting factor	Univariate model		Multivariate model*	
	Hazard ratio (CI)	p Value	Hazard ratio (CI)	p Value
Lesion size (mm)	0.70 (0.24–2.09)	0.527	-	-
Treatment selectivity (Segmental or subsegmental vs. lobar)	0.19 (0.07–0.51)	0.001	3.05 (0.62–15.05)	0.171
Baseline Lipiodol uptake (HU)	0.37 (0.19–0.70)	0.002	0.002 (0.0–0.087)	0.001
Presence of Lipiodol washout	NA**	NA	-	-
Washout rate (HU/month)	3.37 (1.78–6.36)	< 0.0001	149.03 (11.20–1983.54)	< 0.0001

* Variables with a p value less than 0.200 were entered in the multivariate model. ** Not calculated because no tumors without Lipiodol washout recurred while 65.5% (19/29) of the tumors with Lipiodol washout recurred. CI = confidence interval; HU = Hounsfield unit

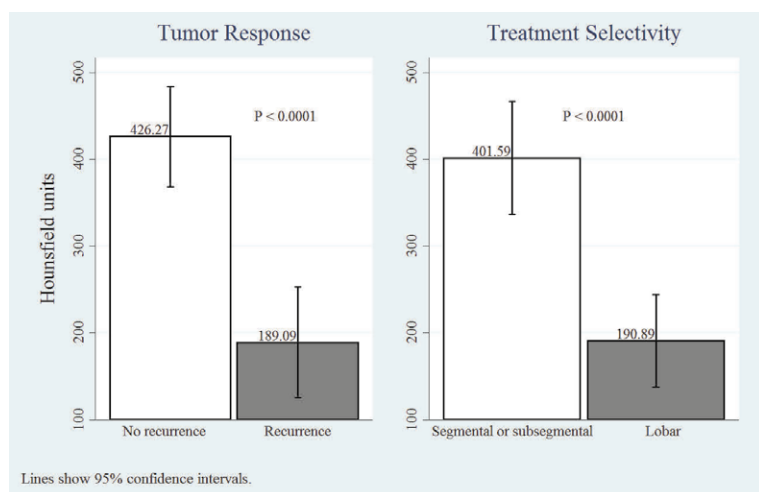


FIGURE 1. Baseline Lipiodol uptake after TACE for HCC. Significantly higher Lipiodol uptake was noted in tumors without recurrence and in tumors treated selectively with TACE.

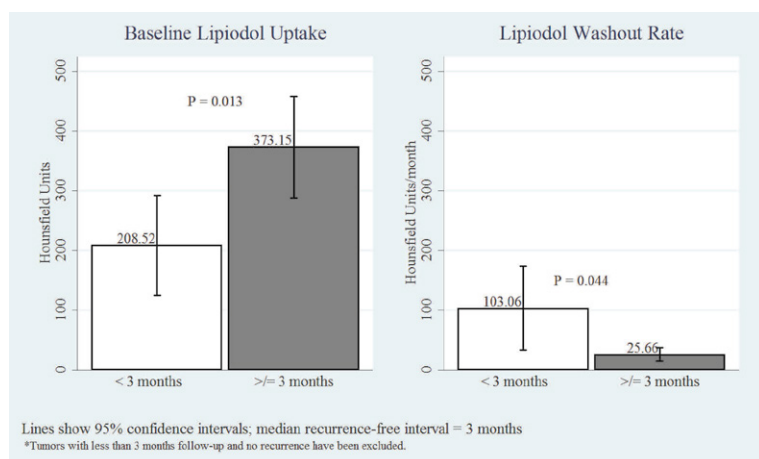


FIGURE 2. Baseline Lipiodol uptake and washout rate in relation to early tumor recurrence. Early recurring tumors demonstrated significantly lower baseline Lipiodol uptake and higher Lipiodol washout rates relative to tumors recurring after the median recurrence free interval (= 3 months) and tumors with no recurrence.

1.1–37.6). Nineteen (41.3%) lesions recurred, with a mean time to recurrence of 3.6 months (range, 1.1–15.1) and a median recurrence-free interval of 3.0 months. The mean baseline Lipiodol uptake was 328.3 ± 185.2 HU. The mean quantitative washout of Lipiodol during the entire follow-up period was 136.9 ± 127.6 HU (58.4 ± 89.5 HU per month). Inter-observer reliability was high amongst the two independent radiologists for measuring Lipiodol uptake (Cronbach's alpha = 0.994), with a standard error of measurement of 14.3 HU.

Predictors of tumor response

No recurrences were seen in tumors with uniformly retained Lipiodol at follow up imaging. Of the 29 tumors with visible washout on follow-up imaging, 19 (65.5%) demonstrated recurrence. In univariate analysis, lower baseline Lipiodol uptake and greater Lipiodol washout rate were statistically significant predictors of earlier time to tumor recurrence (Table 2, $P = 0.002$ and < 0.0001 , respectively). Performing a non-selective (lobar) TACE was also significantly associated with earlier time to recurrence compared to selective (segmental/subsegmental) TACE (Table 2, $P = 0.001$). In multivariate Cox regression analysis, lower baseline Lipiodol uptake and greater Lipiodol washout rate were both significant predictors of earlier time to tumor recurrence (Table 2, $P = 0.001$ and < 0.0001 , respectively).

The mean baseline Lipiodol uptake of tumors without recurrence was significantly higher than in tumors demonstrating recurrence (Figure 1; 426.3 ± 148.8 HU vs. 189.1 ± 137.5 HU, $P < 0.0001$). Tumors treated with selective TACE demonstrated significantly higher baseline Lipiodol uptake compared with tumors treated with lobar TACE (Figure 1; 401.6 ± 32.4 HU vs. 190.9 ± 26.4 HU, $P < 0.0001$). Baseline Lipiodol uptake was significantly lower in

tumors recurring before the median recurrence-free interval (e.g., early tumor recurrence) compared to tumors recurring after the median recurrence-free interval and tumors without recurrence (Figure 2; 208.5 ± 154.8 HU vs. 373.2 ± 200.3 HU, $P = 0.013$). By comparison, the rate of Lipiodol washout at follow up was significantly greater in early tumor recurrence compared to tumors recurring after the median recurrence-free interval and tumors without recurrence (Figure 2; 103.1 ± 129.1 HU/month vs. 25.7 ± 26.6 HU/month, $P = 0.044$).

Estimating the cutoff Lipiodol uptake value predicting tumor recurrence

Using the area under the ROC curve for post-TACE baseline Lipiodol uptake, an estimated threshold Lipiodol uptake value of 270.2 HU was identified below which there was a high probability of tumor recurrence and above which there was a high probability of tumor response over the mean follow-up time of 5.6 months with a sensitivity of 95% and specificity of 93% (Figure 3). Comparison of the cumulative hazards of tumor recurrence over the follow-up period also showed significantly higher hazards of recurrence in tumors with Lipiodol uptake < 270.2 HU after TACE (Figure 4; $P < 0.0001$). ROC curve analysis for follow up Lipiodol washout rate revealed a value of 37.8 HU per month above which there was a high probability of early tumor recurrence with a sensitivity of 78% and specificity of 74% (Figure 5). The cumulative hazards for tumor recurrence were significantly higher in tumors with a washout rate > 37.8 HU per month (Figure 6; $P = 0.001$).

Discussion

In this study, we found a strong correlation between baseline Lipiodol uptake after TACE for HCC and tumor response. The baseline uptake was that defined by the density of Lipiodol tumor stain on non-contrast CT imaging within the first week after TACE. The critical threshold value for baseline Lipiodol uptake predicting tumor recurrence vs. response in this cohort was 270.2 HU with a high degree of sensitivity and specificity (95% and 93%, respectively) over the roughly 6 months mean follow up interval. Post-TACE Lipiodol uptake has been shown to predict necrosis in HCC lesions.⁸⁻¹² Moreover, low or incomplete Lipiodol uptake has been shown to predict tumor recurrence.¹³⁻¹⁵ The present study contributes to this body of knowl-

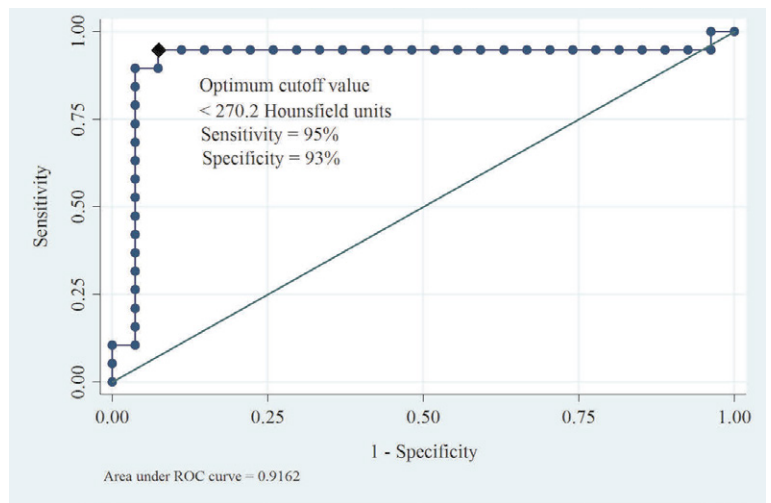


FIGURE 3. ROC curve showing the area under curve and optimal cutoff value of baseline Lipiodol uptake after TACE to predict tumor recurrence.

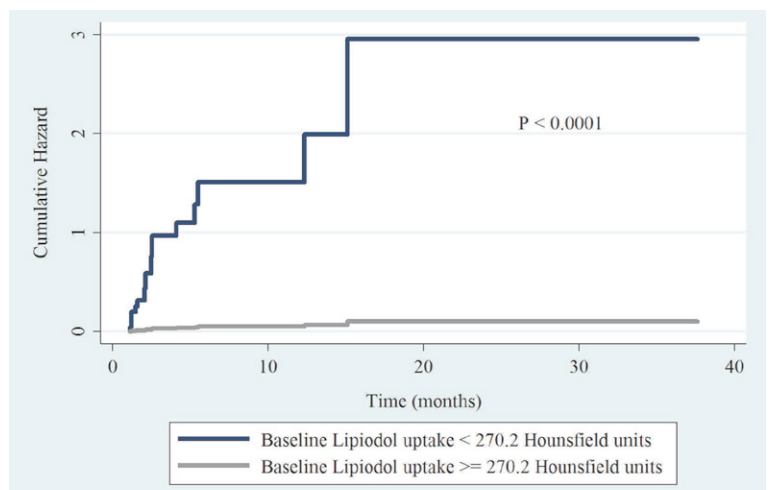


FIGURE 4. Comparison of the cumulative hazards of tumor recurrence over the follow-up period between baseline Lipiodol uptake above and below the identified threshold. Tumors with Lipiodol uptake < 270.2 HU demonstrated significantly higher hazards of recurrence after TACE.

edge by focusing on the baseline uptake at the time of TACE, and identifies a threshold value of 270.2 HU on baseline post-TACE non-contrast CT imaging as a predictor of tumor recurrence. Moreover, our cohort involved TACE using Lipiodol as the sole embolic agent, therefore demonstrating the effect of Lipiodol accumulation independently from additional embolic agent effects.

We found only one previous study discussing a critical cutoff point of post-TACE Lipiodol uptake

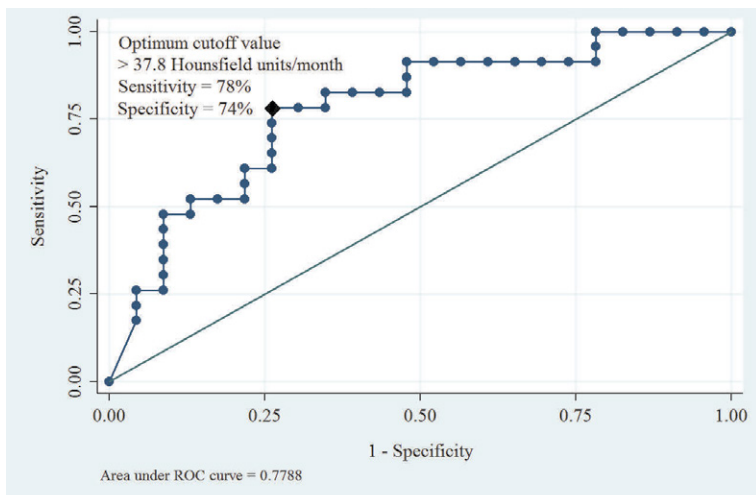


FIGURE 5. ROC curve showing the area under curve and optimal cutoff value of Lipiodol washout rate after TACE to predict early tumor recurrence.

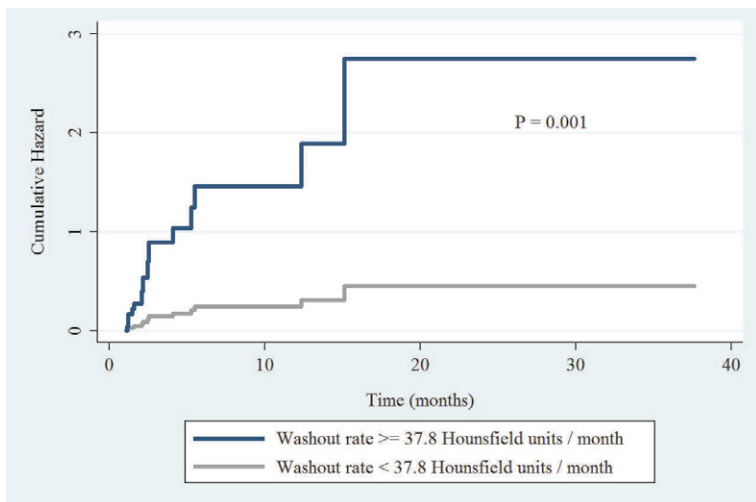


FIGURE 6. Comparison of the cumulative hazards of tumor recurrence over the follow-up period between Lipiodol washout rates above and below the identified threshold. Tumors with Lipiodol washout rates \geq 37.8 HU/month demonstrated significantly higher hazards of recurrence after TACE.

associated with tumor necrosis.¹² Imaeda *et al.*¹² evaluated the histological necrosis level in 12 autopsies and 23 surgical resection specimens from patients with HCC who had undergone TACE. They reported that uniform dense retention of Lipiodol was observed on CT 3–4 weeks after TACE in 12 out of 15 cases with massive (\geq 97%) histological necrosis and in only one out of 20 cases with non-massive necrosis ($P < 0.01$), showing a Lipiodol uptake value of 365 HU as a cutoff value for massive necrosis with 89% sensitivity and 73% specificity.¹²

The cutoff value identified in our study is less than that found in this study, which may be related to the differences in TACE technique, study methods and outcomes. For example, we used the baseline Lipiodol uptake (within one week of treatment) as the input variable, and tumor recurrence by CT as the main outcome variable. Furthermore, we used follow-up data from larger number of lesions (46 tumors in 30 patients). We have observed that lesion contraction over time can create a greater density of Lipiodol stain compared to baseline values in tumors responding to therapy, which may partially explain the higher threshold value observed by Imaeda *et al.* when evaluating scans obtained approximately one month after TACE.

We found the Lipiodol washout rate, defined as loss of HU per month, was also a strong and independent predictor of early tumor recurrence. A similar finding has been observed in another study after evaluation of 42 HCC patients who were scheduled for liver transplantation.²⁰ The authors subjectively classified Lipiodol washout on CT into complete, strong, moderate, and poor, and found that a moderate or strong Lipiodol washout was correlated with lower degrees (\leq 75%) of tumor necrosis.²⁰ In the present study, we identified a washout rate of 37.8 HU above which there was a high risk of early tumor recurrence over the follow up period in our cohort.

Lipiodol can pass through arterio-portal communications such as the peribiliary plexus, terminal arterial-sinusoidal branches, portal vaso vatori, and direct arterioportal anastomoses.^{3,7} Consequently, transarterial delivery of Lipiodol results in embolization of feeding vessels from both the arterial and portal sides of the tumor.^{3,7} Another role of Lipiodol is that of a carrier of the chemotherapeutic agent.⁷ In this regard, higher Lipiodol uptake may represent enhanced embolization of tumor blood supply and also contribute to a higher local concentration of chemotherapeutic agents in the tumor.

Cone-beam CT (CBCT) has been shown to demonstrate tumor Lipiodol accumulation with TACE, and HUs measured on CBCT have been shown to be comparable to multidetector CT.²¹ The use of intraprocedural CBCT and the threshold Lipiodol uptake value shown in our study may enable intraprocedural assessment of TACE endpoints. This may prove beneficial in deciding when additional therapy is needed and to facilitate a treatment strategy following TACE, such as early repeat intervention or treatment using a different modality (i.e. ablation or Y90 radioembolization).

There are a few limitations in this study. Because of the retrospective nature and strict inclusion/exclusion criteria of this study to rigorously detect a baseline Lipiodol threshold uptake value, the size of study population was limited and the follow-up period was relatively short. Although the baseline Lipiodol uptake was defined as HUs on the CT within one week after TACE, the HUs might vary by the timing of CT even during one week; e.g., the HUs on the 1st and the 7th day after TACE might be different. The concentration of the chemotherapeutic agents and the volume of Lipiodol injected was different by the case, which might potentially affect the treatment outcome, although the purpose of this study was simply to evaluate the association of the baseline Lipiodol uptake, which was obtained as the results of our practice, with the tumor recurrence. In addition, we excluded lesions treated with additional embolic materials. As mentioned above, we do not use the embolic particles routinely because we did not find a survival advantage with the use of particulate embolization (data not shown). This practice would be different from so-called conventional TACE, in which chemo-Lipiodol injection is usually followed by injection of additional embolic particles such as gelatin sponge. A recent randomized trial by Shi *et al.* showed no difference in survival outcomes between TACE with and without additional embolic materials following chemo-Lipiodol injection.²² On the contrary, a large cohort study by Takayasu *et al.* showed that TACE with gelatin sponge embolization was associated with a higher survival rate than was a therapy without the particulate embolization.²³ Thus, the significance of the particulate embolization in TACE seems still controversial and needs further investigation. Nevertheless, in the present study, the cohort of Lipiodol only TACE without embolic particles allowed us to analyze significance of Lipiodol uptake without being influenced by the embolic effect of other materials. This practice and our findings, however, may not extrapolate to a population treated with TACE followed by additional particulate embolization.

Conclusions

In conclusion, we demonstrated that Lipiodol uptake at baseline and Lipiodol washout rates at follow-up independently predicted tumor response after TACE for HCC. The critical threshold for baseline Lipiodol uptake predicting tumor recurrence was 270.2 HU. The association between

baseline Lipiodol uptake and tumor response may prove useful for determining subsequent treatment strategies after Lipiodol TACE.

Acknowledgments

Khashayar Farsad received a grant from Guerbet for this study.

References

1. Bruix J, Sherman M. Management of hepatocellular carcinoma: an update. *Hepatology* 2011; **53**: 1020-22. doi: 10.1002/hep.24199
2. Llovet JM, Bruix J. Systematic review of randomized trials for unresectable hepatocellular carcinoma: Chemoembolization improves survival. *Hepatology* 2003; **37**: 429-42. doi: 10.1053/jhep.2003.50047
3. Idee JM, Guiu B. Use of Lipiodol as a drug-delivery system for transcatheter arterial chemoembolization of hepatocellular carcinoma: a review. *Crit Rev Oncol Hematol* 2013; **88**: 530-49. doi: 10.1016/j.critrevonc.2013.07.003
4. Nakakuma K, Tashiro S, Hiraoka T, Uemura K, Konno T, Miyauchi Y, et al. Studies on anticancer treatment with an oily anticancer drug injected into the ligated feeding hepatic artery for liver cancer. *Cancer* 1983; **52**: 2193-200.
5. Iwai K, Maeda H, Konno T. Use of oily contrast medium for selective drug targeting to tumor: enhanced therapeutic effect and X-ray image. *Cancer Res* 1984; **44**: 2115-21.
6. Ohishi H, Uchida H, Yoshimura H, Ohue S, Ueda J, Katsuragi M, et al. Hepatocellular carcinoma detected by iodized oil. Use of anticancer agents. *Radiology* 1985; **154**: 25-9. doi: 10.1148/radiology.154.1.2981114
7. Kan Z, Madoff DC. Liver anatomy: microcirculation of the liver. *Semin Intervent Radiol* 2008; **25**: 77-85. doi: 10.1055/s-2008-1076685
8. Jinno K, Moriwaki S, Tanada M, Wada T, Mandai K, Okada Y. Clinicopathological study on combination therapy consisting of arterial infusion of Lipiodol-dissolved SMANCS and transcatheter arterial embolization for hepatocellular carcinoma. *Cancer Chemother Pharmacol* 1992; **31**(Suppl): S7-12.
9. Choi BI, Kim HC, Han JK, Park JH, Kim YI, Kim ST, et al. Therapeutic effect of transcatheter oily chemoembolization therapy for encapsulated nodular hepatocellular carcinoma: CT and pathologic findings. *Radiology* 1992; **182**: 709-13. doi: 10.1148/radiology.182.3.1311116
10. Takayasu K, Arii S, Matsuo N, Ryu M, Takasaki K, Sato M, et al. Comparison of CT findings with resected specimens after chemoembolization with iodized oil for hepatocellular carcinoma. *AJR Am J Roentgenol* 2000; **175**: 699-704. doi: 10.2214/ajr.175.3.1750699
11. Kwan SW, Fidelman N, Ma E, Kerlan RK, Jr., Yao FY. Imaging predictors of the response to transarterial chemoembolization in patients with hepatocellular carcinoma: a radiological-pathological correlation. *Liver Transpl* 2012; **18**: 727-36. doi: 10.1002/lt.23413
12. Imaeda T, Yamawaki Y, Seki M, Goto H, Iinuma G, Kanematsu M, et al. Lipiodol retention and massive necrosis after Lipiodol-chemoembolization of hepatocellular carcinoma: correlation between computed tomography and histopathology. *Cardiovasc Intervent Radiol* 1993; **16**: 209-13.
13. Takayasu K, Muramatsu Y, Maeda T, Iwata R, Furukawa H, Muramatsu Y, et al. Targeted transarterial oily chemoembolization for small foci of hepatocellular carcinoma using a unified helical CT and angiography system: analysis of factors affecting local recurrence and survival rates. *AJR Am J Roentgenol* 2001; **176**: 681-8. doi: 10.2214/ajr.176.3.1760681
14. Rou WS, Lee BS, Moon HS, Lee ES, Kim SH, Lee HY. Risk factors and therapeutic results of early local recurrence after transcatheter arterial chemoembolization. *World J Gastroenterol* 2014; **20**: 6995-7004. doi: 10.3748/wjg.v20.i22.6995

15. Kinugasa H, Nouse K, Takeuchi Y, Yasunaka T, Onishi H, Nakamura S, et al. Risk factors for recurrence after transarterial chemoembolization for early-stage hepatocellular carcinoma. *J Gastroenterol* 2012; **47**: 421-6. doi: 10.1007/s00535-011-0492-9
16. European Association for the Study of The Liver, European Organisation for Research and Treatment of Cancer. EASL-EORTC clinical practice guidelines: management of hepatocellular carcinoma. *J Hepatol* 2012; **56**: 908-43. doi: 10.1016/j.jhep.2011.12.001
17. The Japan Society of Hepatology. Clinical Practice Guidelines for Hepatocellular Carcinoma 2013. [cited 2015 Sep 04]. Available at: http://www.jsh.or.jp/English/guidelines_en/Guidelines_for_hepatocellular_carcinoma_2013.
18. Becker G. Creating comparability among reliability coefficients: the case of Cronbach alpha and Cohen kappa. *Psychol Rep* 2000; **87**: 1171-82. doi: 10.2466/pr0.2000.87.3f.1171
19. Harvill LM. Standard error of measurement. *Educational measurement: Issues and practice* 1991; **10**: 33-41. doi: 10.1111/j.1745-3992.1991.tb00195.x
20. Herber S, Biesterfeld S, Franz U, Schneider J, Thies J, Schuchmann M, et al. Correlation of multislice CT and histomorphology in HCC following TACE: predictors of outcome. *Cardiovasc Intervent Radiol* 2008; **31**: 768-77. doi: 10.1007/s00270-007-9270-8
21. Wang Z, Lin M, Lesage D, Chen R, Chapiro J, Gu T, et al. Three-dimensional evaluation of Lipiodol retention in HCC after chemoembolization: a quantitative comparison between CBCT and MDCT. *Acad Radiol* 2014; **21**: 393-9. doi: 10.1016/j.acra.2013.11.006
22. Shi M, Lu LG, Fang WQ, Guo RP, Chen MS, Li Y, et al. Roles played by chemolipiodolization and embolization in chemoembolization for hepatocellular carcinoma: single-blind, randomized trial. *J Natl Cancer Inst* 2013; **105**: 59-68. doi: 10.1093/jnci/djs464
23. Takayasu K, Arai S, Ikai I, Kudo M, Matsuyama Y, Kojiro M, et al. Overall survival after transarterial lipiodol infusion chemotherapy with or without embolization for unresectable hepatocellular carcinoma: propensity score analysis. *AJR Am J Roentgenol* 2010; **194**: 830-7. doi: 10.2214/AJR.09.3308

The relationship between chondromalacia patella, medial meniscal tear and medial periarticular bursitis in patients with osteoarthritis

Mustafa Resorlu¹, Davut Doner², Ozan Karatag¹, Canan Akgun Toprak¹

¹ Department of Radiology, Canakkale Onsekiz Mart University, Faculty of Medicine, Canakkale, Turkey

² Department of Physical Medicine and Rehabilitation, Canakkale Onsekiz Mart University, Faculty of Medicine, Canakkale, Turkey

Radiol Oncol 2017; 51(4): 401-406.

Received 9 May 2017

Accepted 26 September 2017

Correspondence to: Mustafa Resorlu, M.D., Canakkale Onsekiz Mart University, Terzioğlu Yerleşkesi, Barbaros Mh, 17100, Canakkale, Turkey. Phone: +90 505 454 8722; Fax: +90 286 2180393; E-mail: mustafaresorlu77@gmail.com

Disclosure: No potential conflicts of interest were disclosed.

Background. This study investigated the presence of bursitis in the medial compartment of the knee (pes anserine, semimembranosus-tibial collateral ligament, and medial collateral ligament bursa) in osteoarthritis, chondromalacia patella and medial meniscal tears.

Patients and methods. Radiological findings of 100 patients undergoing magnetic resonance imaging with a preliminary diagnosis of knee pain were retrospectively evaluated by two radiologists. The first radiologist assessed all patients in terms of osteoarthritis, chondromalacia patella and medial meniscal tear. The second radiologist was blinded to these results and assessed the presence of bursitis in all patients.

Results. Mild osteoarthritis (grade I and II) was determined in 55 patients and severe osteoarthritis (grade III and IV) in 45 cases. At retropatellar cartilage evaluation, 25 patients were assessed as normal, while 29 patients were diagnosed with mild chondromalacia patella (grade I and II) and 46 with severe chondromalacia patella (grade III and IV). Medial meniscus tear was determined in 51 patients. Severe osteoarthritis and chondromalacia patella were positively correlated with meniscal tear ($p < 0.001$ and $p = 0.018$, respectively). Significant correlation was observed between medial meniscal tear and bursitis in the medial compartment ($p = 0.038$). Presence of medial periarticular bursitis was positively correlated with severity of osteoarthritis but exhibited no correlation with chondromalacia patella ($p = 0.023$ and $p = 0.479$, respectively). Evaluation of lateral compartment bursae revealed lateral collateral ligament bursitis in 2 patients and iliotibial bursitis in 5 patients.

Conclusions. We observed a greater prevalence of bursitis in the medial compartment of the knee in patients with severe osteoarthritis and medial meniscus tear.

Key words: medial periarticular bursitis; medial meniscal tear; osteoarthritis

Introduction

Although osteoarthritis (OA), a common joint disease, is not fatal it compromises quality of life. It has become more important in terms of public health with the increase in the average life span associated with advances in the medical sphere. The process

begins with progressive loss of joint cartilage and gradually causes meniscal, muscle, bone tissue, ligament and bursa pathologies.¹ Various factors are implicated in the link between aging and OA. The most important of these are decreased cartilage perfusion, impaired joint morphology, increased ligament laxity, decreased anabolic response and

thinning in the cartilage plate.² Female gender and obesity are other important risk factors in addition to aging. Hormonal changes in particular occurring in women in the postmenopausal period are also a significant predisposing factor.³ Obesity also leads to osteoarthritis, not only through its mechanical effect but also due to its metabolic consequences, and has an adverse effect on clinical findings.^{1,3} Since it results in a mechanical disadvantage for lower extremity functions, pain is more frequent and more severe.⁴ Another clinical condition frequently encountered together with aging is chondromalacia patella (CP). Vascular insufficiency, patellar variations, trauma, dislocation, fracture, rheumatological diseases and impairment of mechanical stress balance on the joint are implicated in the etiology.⁵ The principal changes in cartilage tissue are softening, swelling, fissuring or ulceration.⁵ There are several superficially or deeply located bursae in the knee joint, their principal function being to reduce friction between the surfaces. Pes anserine (PA) bursa, semimembranosus-tibial collateral ligament (SM-TCL) bursa and medial collateral ligament (MCL) bursa inflammations may cause to medial knee pain. Similarly, inflammation in the iliotibial or lateral collateral ligament (LCL) bursae in the lateral of knee also lead to knee pain. Etiological factors such as recurring trauma, impaired joint stability and joint overloading play a role in the development of bursitis.⁶ Magnetic resonance imaging (MRI) is the gold standard radiological technique in the assessment of pathologies of the ligament, meniscus, cartilage, bursa and bone marrow in the knee joint.⁷ This study investigated the relationship between pathologies, such as meniscal tear, OA and CP, affecting knee mechanics and bursitis in medial compartment of knee

Patients and methods

Patients

MR images from 100 patients with OA of the knee were evaluated retrospectively. The patients included in our study group were selected from among individuals presenting to our hospital in 2014–2016. Individuals aged 65 or over were included in the study group, irrespective of gender. Patient selection was based on the order of patients on the work station. Patients with OA determined with conventional radiography were included. Exclusion criteria included presence of acute trauma or fracture, inadequate image quality, rheumatological disease or history of knee surgery.

Imaging protocol

All patients were evaluated with a routine knee imaging protocol on a 1.5 Tesla MRI unit (Signa Excite; GE Medical Systems, Wisconsin, USA). Section thicknesses were 3.5 mm in sagittal images and 4 mm in axial and coronal images. The fluid-sensitive sequences were performed with fat suppression. The imaging protocol consisted of a sagittal T1 weighted spin-echo sequence (540 ms/11.3 ms, repetition time [TR]/echo time [TE], 320x224 matrix, number of excitations [NEX] 1.0), sagittal T2 weighted spin-echo (4480 ms/85 ms, TR/TE; 256x256 matrix; NEX,1.0) axial proton density (3300 ms/34.7 ms, [TR]/ [TE]; [NEX], 1.0; 320x224 matrix), sagittal proton density sequence (4480 ms/45 ms, TR/TE; NEX,1.0; 320x224 matrix) and a coronal proton density sequence (3620 ms/31.8 ms, TR/TE; 320x224 matrix; NEX,1.0).

Image assessment

The radiological findings of 100 patients with OA of the knee undergoing MRI with a preliminary diagnosis of knee pain were retrospectively evaluated by two radiologists. The first radiologist assessed all patients in terms of OA, CP, medial meniscal damage and anterior and posterior cruciate ligament pathologies. The second radiologist, blinded to the results, investigated the presence of bursitis in all patients. An approval was obtained from Canakkale Onsekiz Mart University Ethics Committee and written informed consent was waived because of the retrospective nature of the study. Presence of osteophytes, narrowing in the articular space and sclerotic changes were assessed with radiography. OA grading was based on radiography and the Kellgren-Lawrence system grading scale.⁸ Grades I and II were regarded as mild and grades III and IV as severe.

The Noyes Chondral Injury Classification system was used to classify CP. Grade 0 was regarded as normal, grade I as focal signal increase in cartilage, grade II as fissure or ulcer in cartilage of up to 50%, grade III as greater than 50% loss in cartilage thickness and grade IV as full thickness cartilage defect and subchondral edema. Grade I and II were regarded as mild and grade III and IV as severe. Meniscal damage was classified under three groups - Group 1; normal, Group 2; degenerative signal increase without tear, and Group 3; tear opening onto at least one articular surface. Enlargement in the bursa, fluid deposition, wall thickening and accompanying edema in close proximity were in-

terpreted in favor of bursitis.⁹ Hypointense signal changes on T1W images and hyperintense signal changes on T2W images reflecting increased concentration of compounds containing H⁺ ions in the bone medulla were interpreted in favor of bone marrow edema.¹⁰

Statistical analysis

Statistical analysis was performed on SPSS 20.0 (SPSS Inc., Chicago, IL, USA) software. The Kolmogorov-Smirnov/Shapiro-Wilk tests were used to assess normal distribution of variables. Descriptive data were expressed as mean, standard deviation and minimum and maximum values, frequency and percentage values. The t test was used to compare means in independent groups and the chi square test in the analysis of categorical variables. Relations between constant variables were investigated using Kendall's correlation analysis. $P < 0.05$ was regarded as statistically significant.

Results

Gender distribution was 54 female (54%) and 46 male (46%), and the mean age was 70.47 ± 5.35 years (min 65, max 84). Mild OA (grade I and II) was determined in 55 patients and severe OA (grade III and grade IV) in 45. There was no difference between male and female patients in terms of severity of OA ($p = 0.170$). At evaluation of the retropatellar cartilage, 25 patients were normal, while mild CP (grade I and II) was determined in 25 and severe CP (grade III-IV) in 46.

Since lateral meniscal tear was determined in only six patients, this could not be subjected to statistical analysis. At radiological examination of the medial meniscus, 4 patients were normal, while degenerative signal increase was present in 45 patients and meniscal tear in 51. Meniscal tear was present in 36 of the 45 patients with severe OA and in 15 of the 55 patients with mild OA, and the correlation between severity of OA and meniscal tear was statistically significant ($p < 0.001$). Similarly, significant correlation was determined between CP and meniscal tear ($p = 0.018$). Bursitis in the medial compartment was present in 26 of the 51 patients with medial meniscal tear, and in 15 of the 49 patients with no tear ($p = 0.038$). Bone marrow edema in the tibia or femur was determined in 45 patients. Presence of bone marrow edema was positively correlated with severity of OA, but not with CP ($p < 0.001$ and $p = 0.93$, respectively). Patients' demo-

TABLE 1. Patients' demographic characteristics and radiological findings

Mean age, years	70.47±5.5
Gender, no.	
Female	54
Male	46
Osteoarthritis, n	
Mild (Grade I and II)	55
Severe (Grade III and IV)	45
Chondromalacia patella, n	
Normal	25
Mild (Grade I and II)	29
Severe (Grade III and IV)	46
Medial meniscal tear, no	
Normal	4
Degeneration	45
Tear	51
Bone marrow edema, no	45
Others	
Enchondroma	4
Synovial chondromatosis	4
Osteochondroma	1

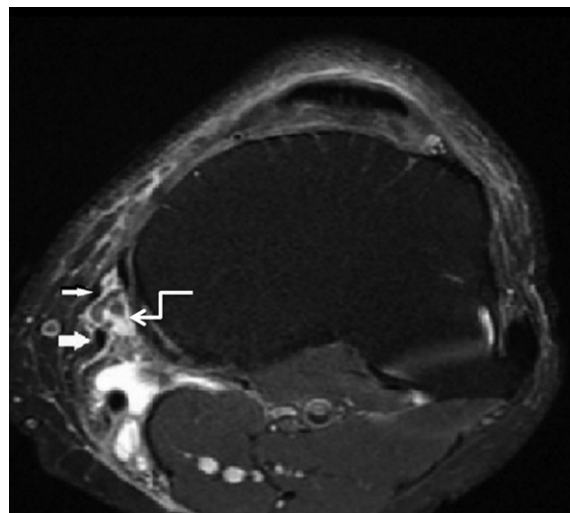


FIGURE 1. A 70 year-old patient presented with knee pain. Axial MR image shows sartorius (thin arrow) and gracilis tendon (thick arrow) in the patient with pes anserine bursitis (curved arrow).

graphic characteristics and radiological findings are shown in Table 1.

Bursitis was determined in at least one of the medial periarticular bursae in 41 patients, the most common form being PA bursitis (Figure 1). Bursitis cases determined at MRI are shown in Table 2.

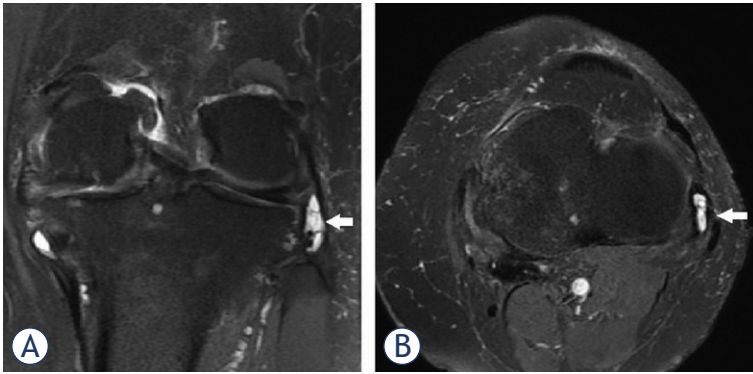


FIGURE 2. Coronal (A) and axial (B) proton-density fat-suppressed images of knee show LCL bursitis in a 70 years old patient.

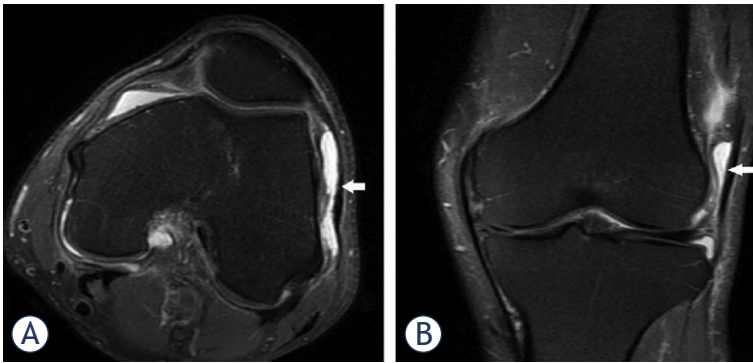


FIGURE 3. A 80 year-old patient presented with pain and tenderness in knee joint. Axial (A) and coronal (B) images demonstrate a fluid collection in the dilated iliotibial bursa.

TABLE 2. Locations of bursitis determined in the knee joint

Bursae	No.
PA bursitis	26
MCL bursitis	13
SM-TCL bursitis	12
Iliotibial bursitis	5
LCL bursitis	2
Prepatellar bursitis	4
Infrapatellar bursitis	4
Suprapatellar bursitis	3
Baker's cyst	36

LCL = lateral collateral ligament; MCL = medial collateral ligament; PA = Pes Anserine; SM-TCL = semimembranosus-tibial collateral ligament

Presence of bursitis in the medial compartment was positively correlated with severity of OA, but was not correlated with CP ($p = 0.023$ and $p = 0.479$, respectively). The relation between medial meniscal tear, OA and CP and bursitis in the medial com-

partment is shown in Table 3. Baker's cyst was determined in 36 patients, the prevalence increasing with severity of OA but was not correlated with CP ($p = 0.044$ and $p = 0.264$, respectively).

Positive correlation was present between severity of OA and CP ($p = 0.03$). Evaluation of lateral compartment bursae revealed lateral collateral bursitis in two patients and iliotibial bursitis in five (Figure 2 and 3). Prepatellar bursitis in the anterior compartment was determined in four patients, infrapatellar bursitis in four and suprapatellar bursitis in three. Additionally, synovial enchondromatosis was present in four patients, enchondroma in four and osteochondroma in one.

Discussion

The knee joint is frequently subjected to trauma, and degenerative changes occur with aging. Trauma, degenerative changes, morphological variations, mechanical stress impairments and aging are factors involved in the etiology of OA, CP, bursitis and medial meniscal tear.^{3,11} Common risk factors are one of the reasons why pathologies in the knee joint affect more than one anatomical structure, rather than remaining local. Moreover, pathologies that begin locally induce morphological and functional changes in other anatomical structures by compromising biomechanics.^{11,12} Burger *et al.* investigated the development of OA as a result of inadequate meniscal tear repair in an animal study.¹² They reported that OA developed in the medial tibiofemoral and patellofemoral joint due to insufficient meniscal tear repair. Cicuttini *et al.* showed gradual loss of cartilage in patients under-

TABLE 3. The relation between osteoarthritis, chondromalacia patella, meniscal tear and medial periarticular bursitis

	Medial compartment bursitis		
	Yes	No	p
Osteoarthritis			
Mild (n = 55)	17	38	0.023
Severe (n = 45)	24	21	
Chondromalacia Patella			
Normal (n = 25)	8	17	
Mild (n = 29)	14	15	0.479
Severe (n = 46)	19	27	
Meniscal Tear			
No (n = 49)	15	34	0.038
Yes (n = 51)	26	25	

going partial meniscectomy.¹³ The significant correlation observed in our study between both OA and CP with meniscal tear ($p < 0.001$ and $p = 0.018$) was compatible with these findings. Additionally, the correlation between severity of OA and CP ($p = 0.030$) also supports the previous literature.^{12,14} These findings all suggest that these pathologies induce one another as a result of changes in knee biomechanics and morphology. Furthermore, common risk factors such as advanced age and degeneration reinforce this association.

Inflammation occurring in the PA, SM-TCL (Figure 4) and MCL bursa in the medial of knee is an important cause of pain. Obesity, degenerative joint disease, valgus deformity, trauma, impaired joint stability, excessive loading on the joint and sporting activity are important causes of inflammation in the bursae.¹⁵ Some authors have suggested that the structure of the female pelvis creates a predisposition to bursitis.¹⁶ We determined no relation between gender and the prevalence of bursitis ($p = 0.954$). Toktas *et al.* investigated the prevalence of pes anserine bursitis in patients with OA.¹⁷ They determined a greater pes anserine thickness not only in OA patients with bursitis, but also in OA patients without bursitis compared to the control group. We selected all our cases from OA patients and took the OA grade (mild and severe) as our reference points. We also investigated the presence of SM-TCL and MCL bursitis in addition to PA bursitis. We observed higher prevalence of medial periarticular bursitis in patients with severe OA compared to those with mild OA ($p = 0.023$). Our results are compatible with recent studies revealing an association between OA and pes anserine bursitis.¹⁶

Another important finding of this study was a positive correlation between medial meniscal tear and medial compartment bursitis. Bursitis was present in 26 of the 51 patients in whom medial meniscal tear was determined, and in 15 of the 49 patients with no tear. The difference was statistically significant ($p = 0.038$). Various factors affect the positive relation between prevalence of bursitis and severity of OA and medial meniscal tear. The first are similar etiological factors. Second are structural changes associated with OA and meniscal tear and impairment of joint stability.¹⁶ Despite the common etiological factors and the effect on joint biomechanics, we determined no relation between CP and medial compartment bursitis. We think that this finding was affected by patellar and trochlear morphology. Variations such as patella alta and baja influence the development of

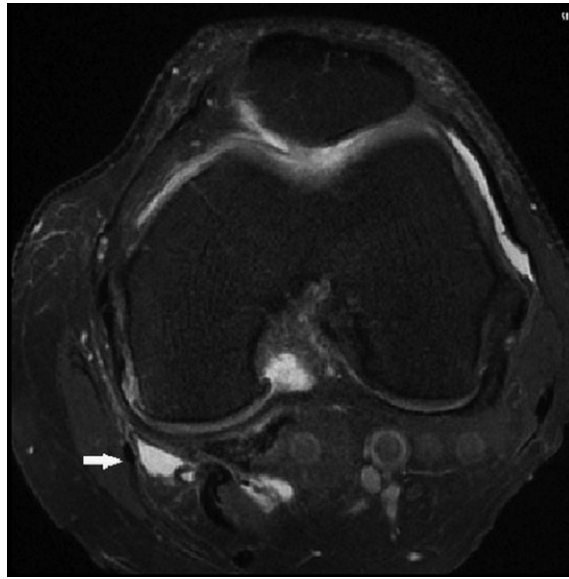


FIGURE 4. The axial fat saturated proton density weighted image demonstrates a fluid collection in the SM-TCL bursa.

CP. Additionally, it has been suggested that a short medial facet increases mechanical stress on cartilage and causes CP.^{5,18} One recent study proposed the sulcus angle/trochlear depth ratio as a powerful predictor.¹¹ One limitation of our study is that patellar and trochlear morphology were not evaluated. Another limitation is that due to its retrospective nature patients were not assessed in terms of diabetes during the study.

The prevalence of Baker's cyst was 36%, iliotibial bursitis 5% and LCL bursitis 2%. In their study of 163 patients, Hayashi *et al.* reported prevalences of popliteal cyst of 40% and of iliotibial bursitis of 1%.¹⁹ Baker's cyst was the most common lesion in both studies, and the results were compatible. A relation was determined between Baker's cyst and severity of OA in our study, but there was no correlation between bursitis in the medial compartment and Baker's cyst ($p = 0.044$ and $p = 0.954$, respectively). The positive correlation between Baker's cyst and OA is compatible with the previous literature.²⁰ Increased joint effusion and intra-articular pressure in OA may be involved in this relationship. We observed prepatellar (4%), infrapatellar (4%) and suprapatellar bursitis (3%) in the anterior of joint. Hayashi *et al.* reported the prevalence of prepatellar and infrapatellar bursitis at 2%. The mean age of their study population was 52 ± 6 years, and patients without OA constituted 32% of their cases.¹⁹ The higher mean age in our study and all our patients having OA may explain the difference in the findings.

In conclusion, we observed a correlation between the prevalence of bursitis in the medial compartment and the severity of OA and medial meniscal tear. We determined no relation between severity of CP and bursitis.

References

1. Ayral X, Pickering EH, Woodworth TG, Mackillop N, Dougados M. Synovitis: A potential predictive factor of structural progression of medial tibiofemoral knee osteoarthritis: results of a 1 year longitudinal arthroscopic study in 422 patients. *Osteoarthr Cartil* 2005; **13**: 361-7. doi: 10.1016/j.joca.2005.01.005
2. Arden N, Nevitt MC. Osteoarthritis: epidemiology. *Best Pract Res Clin Rheumatol* 2006; **20**: 3-25. doi: 10.1016/j.berh.2005.09.007
3. Creamer P, Lethbridge-Cejku M, Hochberg MC. Factors associated with functional impairment in symptomatic knee osteoarthritis. *Rheumatology (Oxford)* 2000; **39**: 490-6.
4. de Miguel Mendieta E, Cobo Ibáñez T, Usón Jaeger J, Bonilla Hernan G, Martín Mola E. Clinical and ultrasonographic findings related to knee pain in osteoarthritis. *Osteoarthritis Cartilage* 2006; **14**: 540. doi: 10.1016/j.joca.2005.12.012
5. Tanamas SK, Teichtahl AJ, Wluka AE, Wang Y, Davies-Tuck M, Urquhart DM, et al. The associations between indices of patellofemoral geometry and knee pain and patella cartilage volume: a cross-sectional study. *BMC Musculoskelet Disord* 2010; **11**: 87. doi: 10.1186/1471-2474-11-87
6. Alvarez-Nemegyei J. Risk factors for pes anserinus tendinitis/bursitis syndrome: a case control study. *J Clin Rheumatol* 2007; **13**: 63-5. doi: 10.1097/01.rhu.0000262082.84624.37
7. Nenezic D, Kocijancic I. The value of the sagittal-oblique MRI technique for injuries of the anterior cruciate ligament in the knee. *Radiol Oncol* 2013; **47**: 19-25. doi: 10.2478/raon-2013-0006
8. Kellgren JH, Lawrence JS. Radiological assessment of osteoarthritis. *Ann Rheum Dis* 1957; **16**: 499-502.
9. Hirji Z, Hunjun JS, Choudur HN. *Imaging of the bursae. J Clin Imaging Sci* 2011; **1**: 22. doi: 10.4103/2156-7514.80374
10. Oztekin O, Calli C, Kitis O, Adibelli ZH, Eren CS, Apaydin M, et al. Reliability of diffusion weighted MR imaging in differentiating degenerative and infectious end plate changes. *Radiol Oncol* 2010; **44**: 97-102. doi: 10.2478/v10019-010-0006-z
11. Resorlu H, Zateri C, Nusran G, Goksel F, Aylanc N. The relation between chondromalacia patella and meniscal tear and the sulcus angle/trochlear depth ratio as a powerful predictor. *J Back Musculoskelet Rehabil* 2017; **30**: 603-8. doi: 10.3233/BMR-160536.
12. Burger C, Kabir K, Mueller M, Rangger C, Minor T, Tolba RH. Reropatellar chondromalacia associated with medial osteoarthritis after meniscus injury. One year of observations in sheep. *Eur Surg Res* 2006; **38**: 102-8. doi: 10.1159/000093281
13. Cicuttini FM, Forbes A, Yuanyuan W, Rush G, Stuckey SL. Rate of knee cartilage loss after partial meniscectomy. *J Rheumatol* 2002; **29**: 1954-6.
14. Kalichman L, Zhang Y, Niu J, Goggins J, Gale D, Felson DT, et al. The association between patellar alignment and patellofemoral joint osteoarthritis features-an MRI study. *Rheumatology (Oxford)* 2007; **46**: 1303-8. doi: 10.1093/rheumatology/kem095
15. Saggini R, Di Stefano A, Dodaj I, Scarcello L, Bellomo RG. Pes anserine bursitis in symptomatic osteoarthritis patients: A mesotherapy Treatment study. *J Altern Complement Med* 2015; **21**: 480-4. doi: 10.1089/acm.2015.0007
16. Helfenstein M Jr, Kuromoto J. Anserine syndrome. *Rev Bras Reumatol* 2010; **50**: 313-27. doi: 10.1590/S0482-50042010000300011
17. Toktas H, Dundar U, Adar S, Solak O, Ulasli AM. Ultrasonographic assessment of pes anserinus tendon and pes anserinus tendinitis bursitis syndrome in patients with knee osteoarthritis. *Mod Rheumatol* 2015; **25**: 128-33. doi: 10.3109/14397595.2014.931909
18. Endo Y, Schweitzer ME, Bordalo-Rodrigues M, Rokito AS, Babb JS. MRI quantitative morphologic analysis of patellofemoral region: lack of correlation with chondromalacia patella surgery. *AJR Am J Roentgenol* 2007; **189**: 1165-8. doi: 10.2214/AJR.07.2236
19. Hayashi D, Roemer FW, Dhina Z, Kwok CK, Hannon MJ, Moore C, et al. Longitudinal assessment of cyst-like lesions of the knee and their relation to radiographic osteoarthritis and MRI-detected effusion and synovitis in patients with knee pain. *Arthritis Res Ther* 2010; **12**: R172. doi: 10.1186/ar3132
20. Hill CL, Gale DG, Chaisson CE, Skinner K, Kazis L, Gale ME, et al. Knee effusions, popliteal cysts, and synovial thickening: association with knee pain in osteoarthritis. *J Rheumatol* 2001; **28**: 1330-7.

Phytotherapeutics oridonin and ponicedin show additive effects combined with irradiation in pancreatic cancer *in vitro*

Jakob Liermann¹, Patrick Naumann¹, Franco Fortunato², Thomas E. Schmid³, Klaus-Josef Weber¹, Jürgen Debus³, Stephanie E. Combs^{3,4}

¹ Department of Radiation Oncology, Heidelberg University Hospital, Heidelberg, Germany

² Heidelberg University Hospital, Section Surgical Research, Heidelberg, Germany

³ Department of Radiation Oncology, Klinikum rechts der Isar, Technische Universität München, Munich, Germany

⁴ Institute of Innovative Radiotherapy (iRT), Department of Radiation Sciences (DRS), Helmholtz Zentrum München, Neuherberg, Germany

Radiol Oncol 2017; 51(4): 407-414.

Received 28 June 2017

Accepted 13 October 2017

Correspondence to: Dr. Jakob Liermann, Department of Radiation Oncology, Heidelberg University Hospital, INF 400, 69120 Heidelberg, Germany. E-mail: jakob.liermann@med.uni-heidelberg.de

Disclosure: No potential conflicts of interest were disclosed.

*J Liermann and P Naumann contributed equally to this work.

Background. Chemoradiation of locally advanced non-metastatic pancreatic cancer can lead to secondary operability by tumor mass reduction. Here, we analyzed radiomodulating effects of oridonin and ponicedin in pancreatic cancer *in vitro*. Both agents are ent-kaurane diterpenoids, extracted from *Isodon rubescens*, a plant that is well known in Traditional Chinese Medicine. Cytotoxic effects have recently been shown in different tumor entities for both agents.

Materials and methods. Pancreatic cancer cell lines AsPC-1, BxPC-3, Panc-1 and MIA PaCa-2 were pretreated with oridonin or ponicedin and irradiated with 2 Gy to 6 Gy. Long-term survival was determined by clonogenic assay. Cell cycle effects and intensity of γ H2AX as indicator for DNA double-strand breaks were investigated by flow cytometry. Western blotting was used to study the DNA double-strand break repair proteins Ku70, Ku80 and XRCC4.

Results. Oridonin and ponicedin lead to a dose-dependent reduction of clonogenic survival and an increase in γ H2AX. Combined with irradiation we observed additive effects and a prolonged G2/M-arrest. No relevant changes in the levels of the DNA double-strand break repair proteins were detected.

Conclusions. Pretreatment with oridonin or ponicedin followed by irradiation lead to an additional reduction in survival of pancreatic cancer cells *in vitro*, presumably explained by an induced prolonged G2/M-arrest. Both agents seem to induce DNA double-strand breaks but do not interact with the non-homologous end joining (NHEJ) pathway.

Key words: oridonin; ponicedin; irradiation; pancreatic cancer; γ H2AX; radiosensitivity

Introduction

Pancreatic cancer is the fourth leading cause of cancer related deaths in the United States.¹ Surgical resection is still the most important treatment modality and prognostic factor, but in the late stage of the disease, only 10–20% of all primary tumours are still operable.² Beside primary metastasized and thus palliative stage IV disease 30-40% of all cases

are locally advanced but non-metastasized tumors that could benefit from neoadjuvant treatment.³ We recently reported that approximately one third of these locally advanced tumors become resectable by a neoadjuvant combined chemoradiation and thus regain a curative therapy option.⁴ To further increase the efficacy of radiotherapy in pancreatic cancer, new chemotherapeutics, that can sensitize pancreatic cancer tissue to radiation, are needed.

The diterpenoids oridonin and ponicipidin are both extracts from *Isodon rubescens*, a plant used in Traditional Chinese Medicine that is known for its anti-inflammatory and antitumor properties in the treatment of esophageal and cardiac cancer.⁵ Recently, antineoplastic properties of oridonin and ponicipidin have been published.⁶⁻⁸ In pancreatic cancer oridonin induces apoptosis and leads to an arrest in the G2/M-phase of the cell cycle.⁹⁻¹² Further, oridonin inhibits nuclear factor- κ B.¹³ Ponicipidin is also known to induce apoptosis¹⁴⁻¹⁷ but to our knowledge, there is no data for ponicipidin in pancreatic cancer.

Potential radiosensitization could be observed in chinese-hamster-V79 cells by oridonin.¹⁸ Apart from this study we found no publication concerning oridonin or ponicipidin induced radiomodulation.

As natural occurring products for both substances no serious side effects in humans are known which qualifies them as potential new chemotherapeutic drugs. Data of an *in vivo* trial for oridonin used in acute leukemia seems to confirm this hypothesis.¹⁹ Here, we analyzed radiomodulating effects of oridonin and ponicipidin in pancreatic cancer cells *in vitro* by clonogenic assay, cell cycle analysis, γ H2AX expression and DNA repair proteins expression analysis.

Material and methods

Cell culture and irradiation

The pancreatic cancer cell lines AsPC-1, BxPC-3 and MIA PaCa-2 were cultured in RPMI-1640 medium, the cell line Panc-1 in Dulbecco's modified Eagle's Medium (DMEM). Media included 10% FBS and 1% Penicillin/Streptomycin. The cells were cultured at 37°C in 5% CO₂. AsPC-1 and Panc-1 cell lines were purchased from CLS cell line service GmbH, Germany and BxPC-3 as well as MIA PaCa-2 cells from LGC Standards GmbH (ATCC), Germany. Oridonin was obtained from Sigma-Aldrich Corporation, USA and ponicipidin from Shanghai Zhanshu Chemical Technology Co., Ltd., China. Both reagents were dissolved in DMSO and stored at -80°C.

Cells were X-irradiated (X-RAD 320, Precision X-Ray, Inc., USA) operated at 320 kV and 12.5 mA. The average dose rate was 1.1 Gy/min. The used filter consisted of 1.5 mm Al, 0.25 mm Cu and 0.75 mm Sn. The tissue culture flasks, in which the cells were cultured, were placed on a PMMA-plate of 1 cm height.

Clonogenic assay

To assess long-term cell survival, a defined number of cells were seeded in 25 cm² tissue culture flasks and incubated for 24 hours. Cell counts were adjusted for the different treatment schemes. Cell lines AsPC-1, BxPC-3 and Panc-1 were treated with oridonin, ponicipidin or DMSO (control) for 24 hours as indicated and irradiated afterwards once with 2 Gy or 6 Gy. The dose of each substance and the intensity of irradiation were established through pre-experiments to achieve a survival rate of 20-70% after single treatment alone. MIA PaCa-2 cells were pretreated with lower doses of oridonin and ponicipidin due to higher sensitivity to the reagents. 8-9 days (time differs among cell lines) after the treatment cells were fixed in 70% ethanol and stained with 0.2% methylenblue. Colonies, defined as containing at least 50 cells, were counted manually under a light microscope and the plating efficiency, defined as the quotient of counted colonies to plated cells, was determined. The surviving fraction was defined as the ratio of each experiment's plating efficiency to its control. Cells were plated in triplets to compensate for pipetting errors and at least three independent experiments were performed.

Determination of radiosensitivity

To analyze combined treatments, surviving fractions were normalized to the values of corresponding single reagent treatment using a ratio of the combined treatment's plating efficiency to the single reagent treatment one's. Dose-response curves were created using the linear-quadratic model.²⁰

Combination effects were analyzed defining additivity according to Steel and Peckham.²¹ For this purpose a dose-response curve was calculated that represents the course of the measured control curve at a pre-effect similar to the single reagent treatment's effect („theoretical control-curve“). Additive effects were defined as area between the measured control curve and the theoretical one. Supraadditive effects were defined as beneath the theoretical control curve and radioprotective effects as above the measured control curve. Independent toxicity was defined as identical curve to the measured control curve (for further information see Suppl. Figure 1).

Cell cycle analysis

Since impact on cell cycle distribution was regressing 24 hours after pretreatment a shorter exposi-

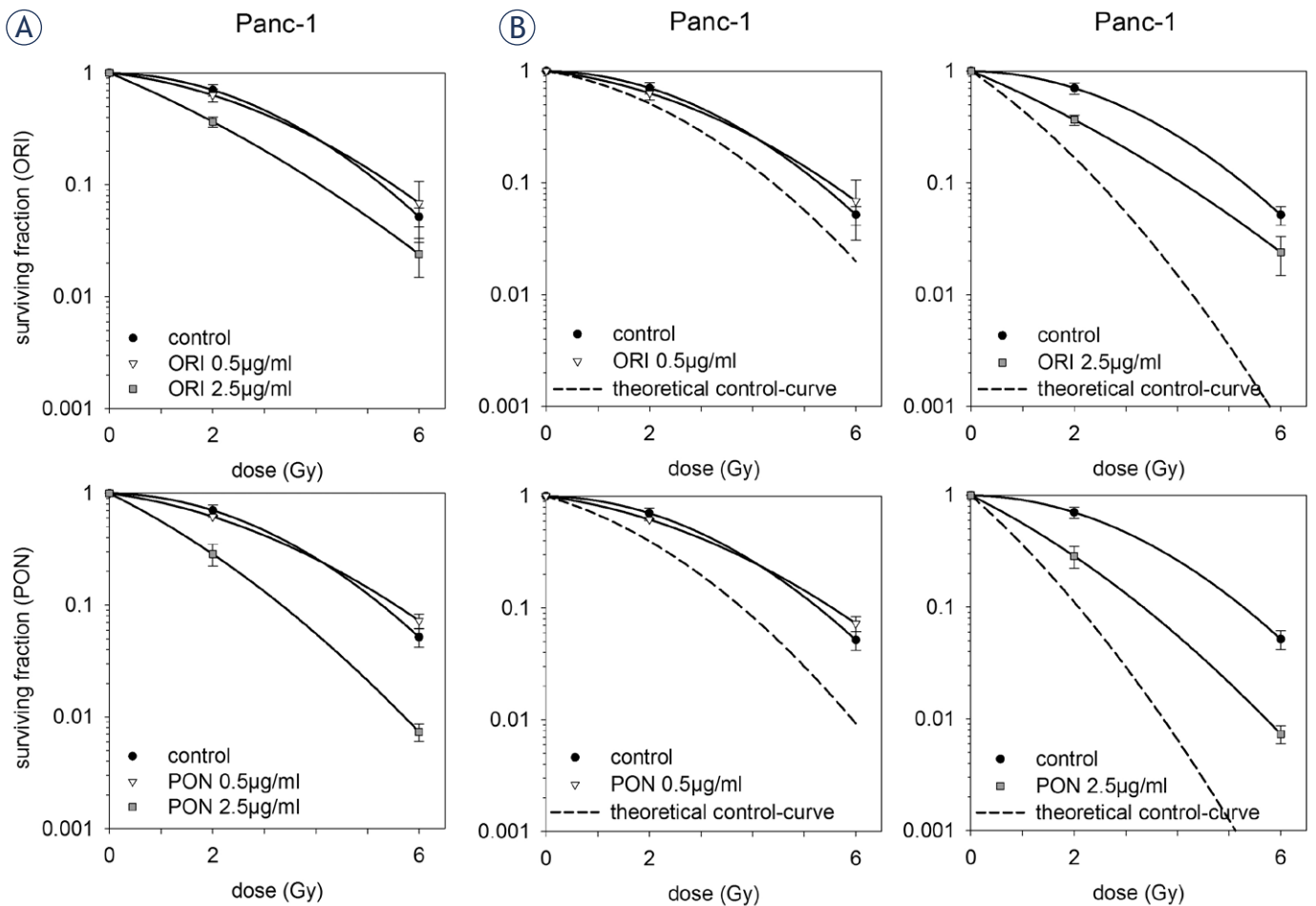


FIGURE 1. Clonogenic survival of Panc-1 cells treated with either irradiation and/or oridonin (ORI) and ponocidin (PON) as indicated. **(A)** survival curves and **(B)** radiosensitivity to different dosages with measured and theoretical control curve, according to Steel and Peckham for Panc-1 cells. Results are presented as mean values +/- standard deviation. At least three independent experiments were performed.

tion time to oridonin and ponocidin compared to the other experiments was chosen. Simultaneously the dosage was augmented to compensate for shortage in exposition time. Cell lines Panc-1 and MIA PaCa-2 were pretreated for two hours with oridonin, ponocidin or DMSO (control) and irradiated as indicated. To induce a less lethal damage than one would expect of 6 Gy, an irradiation dose of 4 Gy was chosen. Cells were then fixed in ice-cold ethanol and RNA-strands were cleaved by RNase A (AppliChem GmbH, Germany) at the following time points: beginning of the treatment, before irradiation, 12 and 24 hours after irradiation. Then cells were stained with propidium iodide (Sigma-Aldrich Corporation, USA) and the amount of propidium iodide per cell was quantified in a flow cytometer (FACScan, Becton Dickinson and Company, USA). At least 10^4 ungated cells were analyzed by BD CellQuest Pro 4.0.2 (Becton

Dickinson and Company, USA) and the different phases of the cell cycle were determined using the software ModFit LT 3.0 (Verity Software House, Inc., USA). At least two independent experiments were performed.

γ H2AX-quantification

Since clonogenic assays revealed different sensitivity between AsPC-1, BxPC-3 and Panc-1 cells on the one hand and MIA PaCa-2 cells on the other hand further experiments were done with the cell lines Panc-1 and MIA PaCa-2. To quantify the induction of DNA double-strand breaks Panc-1 and MIA PaCa-2 cells were pretreated with oridonin, ponocidin or DMSO (control) for 24 hours and were irradiated once as indicated. At different time points after irradiation MIA PaCa-2 and Panc-1 cells were fixed using 1% PFA and ice-cold ethanol. Cells

were then stained with a γ H2AX-antibody (art. no. 16-202A, Merck KGaA, Darmstadt, Germany) and pan-nuclear intensity was measured using a flow cytometer. Results were normalized by creating a ratio of the measured intensity to the intensity of the control probes. At least three independent experiments were performed.

Western Blot

Cell lines Panc-1 and MIA PaCa-2 were treated with oridonin, ponidicin or DMSO (control) for 24 hours. Then lysates of the cells were gained using lysis buffer (10 mM HEPES pH 7.4, 5 mM CHAPS, 5 mM DTT) and inhibitors (PMSF, Pepstatin, Leupeptin, Aprotinin). The protein concentration was determined in a Bradford protein assay and 20 μ g to 30 μ g Protein were used for Western Blots. A SDS-polyacrylamide-gel-electrophoresis was run using 12% polyacrylamide-gels with a voltage of 160 V and amperage of 250 mA. A wet transfer was performed (80 V, 60 mA) to transfer the proteins on a polyvinylidene fluoride membrane. The membrane was blocked using Roti-Block (Carl Roth. GmbH & Co. KG, Germany). b-Actin (art. no. 4967), GAPDH (art. no. 2118), Ku70 (art. no. 4588) and Ku80 (art. no. 2753) primary antibodies were purchased from Cell signaling Technology Inc., USA. XRCC4 (art. no. sc-271087) and secondary antibodies (art. no. sc-2380, sc-2379) were obtained from Santa Cruz Biotechnology, Inc., USA. Dilution was done according to manufacturer's instructions. X-Ray films were scanned and the density of the protein bands were determined with the software Image J 1.47V (National Institute of Health, USA). Density was normalized by creating a ratio of protein band to house-keeping protein's one to avoid minimal differences in the amount of protein load. Then another ratio of the treatment's value to its control was calculated and allowed to quantify densities and treatment differences. At least two independent experiments were performed.

Statistical analysis

The results of each experiment were generated as described above. Statistical analysis of the results was done with an unpaired two-tailed t-test using Microsoft® Excel® 2008 for Mac 12.3.6 (Microsoft Corporation, USA). The dose control curves and the figures were calculated and generated with SigmaPlot 12.0 (Systat Software Inc., USA). Results are presented as mean values \pm standard deviation. $P < 0.05$ was considered as a significant differ-

ence between the compared results. * $P < 0.05$, ** $P < 0.005$, *** $P < 0.001$.

Results

Oridonin and ponidicin reduce clonogenic survival and show additive effects when combined with irradiation

To investigate long-term survival cells were treated with oridonin or ponidicin in a low dosage of 0.5 μ g/ml and high dosage of 2.5 μ g/ml (Figure 1A). Since MIA PaCa-2 cells exposed a higher sensitivity to both oridonin and ponidicin, we used 0.1 μ g/ml and 0.5 μ g/ml as the low and the high dosage in these cells, respectively. MIA PaCa-2 cells showed a significant reduction in clonogenic survival to a fraction of 51% when treated with the lower dosage of oridonin and thus were much more sensitive than the other cell lines, with a mean surviving fraction of 88% in AsPC-1, BxPC-3 and Panc-1 cells (Suppl. Figure 2). Interestingly, ponidicin was more effective than oridonin: 2.5 μ g/ml of ponidicin lead to a mean surviving fraction of 12%. The same amount of oridonin showed an almost three-fold higher surviving fraction of 32% in AsPC-1-, BxPC-3- and Panc-1 cells (Suppl. Figure 3).

A further dose-dependent reduction in survival could be observed by combination with irradiation. The mean surviving fraction of 88% after single treatment with low dosage of oridonin could be further attenuated by additional irradiation with 2 Gy or 6 Gy to mean 63% and 13%, respectively.

Using these results we investigated the radiosensitivity according to the model of Steel and Peckham as described in the methods section.²¹ The higher dose of oridonin and ponidicin lead to additive effects in almost all investigated cell lines when combined with 2 Gy or 6 Gy irradiation, whereas the lower dose just showed independent toxicity (Figure 1B and Suppl. Figure 4). Radioprotectivity as well as supraadditivity could not be observed.

G2/M-arrest after combined treatment of radiation and oridonin or ponidicin

To determine changes in cell cycle, the four pancreatic cancer cell lines were treated with oridonin or ponidicin alone as well as in combination with irradiation. Cell cycle phases were analyzed 12 and 24 hours after irradiation. Pretreatment with oridonin (Figure 2A) or ponidicin (Figure 2B) induced a clear G2/M-arrest of the cell lines AsPC-1 and Panc-1 after 12 hours with up to 36% (Figure 2 and Suppl.

Figure 5). The G2/M- fraction of combined treatments was not as high as the one observed after irradiation alone but was augmented in time leading to the fact that 24 hours after irradiation there still was a clear G2/M-arrest in the cell lines AsPC-1, BcPC-3 and Panc-1 when treated with the combined therapy. MIA PaCa-2 cells showed a clear G2/M-arrest 24 hours after combined treatment with ponicedin but not with oridonin (Suppl. Figure 5). We did not observe a sub-G1 fraction as surrogate of apoptosis.

Oridonin and ponicedin induce an increased pan-nuclear γ H2AX-intensity

The potential influence of oridonin or ponicedin on the DNA double-strand break repair was analyzed by measuring the pan-nuclear γ H2AX-intensity of pretreated cells via flow cytometry. Both oridonin (Figure 3A) and ponicedin (Figure 3B) lead to an approximately 2.5-fold increase of the γ H2AX-intensity shortly after treatment, independent of the particular dose level (7.5 μ g/mL vs. 15 μ g/mL). There was an increase of γ H2AX after irradiation alone but highest γ H2AX-intensities could be observed in combined treatments. The Intensity of γ H2AX already declined 10 hours posttreatment. We could not observe a difference in the relative reduction of the γ H2AX-intensity between irradiation alone and combined treatments.

Oridonin and ponicedin do not influence the expression of DNA repair proteins related to the non-homologous end joining (NHEJ) pathway

To determine the influence of oridonin or ponicedin on the repair of DNA double-strand breaks, Panc-1- and MIA PaCa-2-cells were treated with either agent and three main proteins of the NHEJ pathway, namely XRCC4, Ku70 and Ku80 were detected by Western Blots. Pretreatment with oridonin or ponicedin lead to a slight reduction of XRCC4-expression but there was no considerable change in Ku70 and Ku80 protein expression in MIA PaCa-2 cells. Panc-1 cells showed no stringent effect in XRCC4 protein expression but a dose-dependent increase of Ku70 and Ku80 after pretreatment with oridonin or ponicedin (Figure 4).

Discussion

The aim of this study was to investigate the two phytotherapeutics oridonin and ponicedin for their

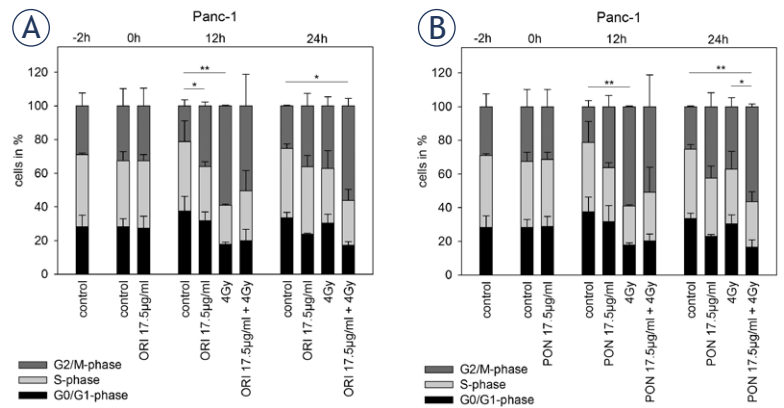


FIGURE 2. Cell cycle assay of Panc-1 cells treated with irradiation and/or (A) oridonin (ORI) and (B) ponicedin (PON) as indicated. Results are presented as mean values \pm standard deviation. * $P < 0.05$, ** $P < 0.005$, asterisk referring to the amount of cells in G2/M-phase. At least two independent experiments were performed.

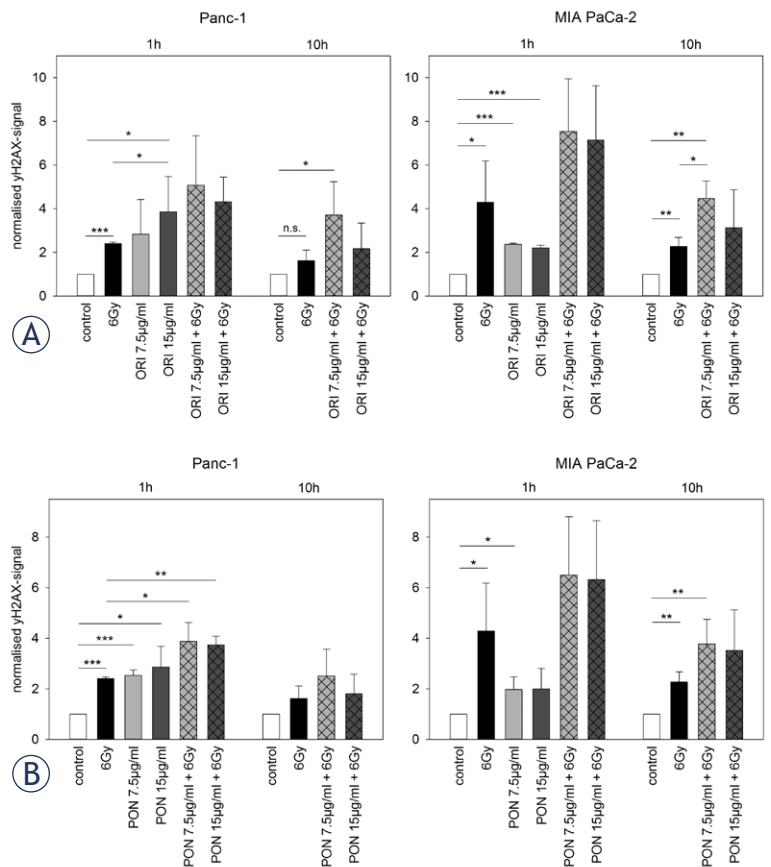


FIGURE 3. γ H2AX-intensity of Panc-1 and MIA PaCa-2 cells treated with irradiation and/or (A) oridonin (ORI) and (B) ponicedin (PON) as indicated. Results are presented as mean values \pm standard deviation. * $P < 0.05$, ** $P < 0.005$, *** $P < 0.001$, n.s.=not significant. At least three independent experiments were performed.

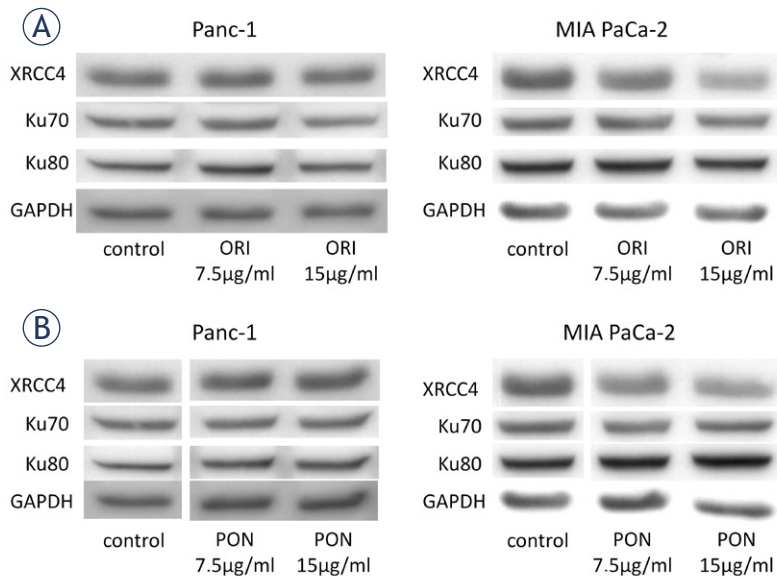


FIGURE 4. Western Blots of Panc-1 and MIA PaCa-2 cells treated with either (A) oridonin (ORI) and (B) ponicedin (PON) as indicated. One representative Western Blot is shown. At least two independent experiments were performed. NHEJ = non-homologous end-joining.

capability to enhance effects of irradiation in pancreatic cancer cells. Compared to other tumor entities pancreatic cancer cells are more resistant to chemo- and radiotherapy and thus radiosensitizing agents are highly clinically relevant.

To investigate treatment efficacy long-term survival was determined by clonogenic assays. Changes in cell cycle distribution and intensity of γ H2AX as indicator for DNA double-strand breaks were investigated by flow cytometry, since effects of radiotherapy base predominantly on induction of DNA double-strand breaks.²² Western blotting was used to study key proteins of the NHEJ pathway of the DNA double-strand break repair. To our knowledge we are the first who tested ponicedin in combination with irradiation whereas potential radiosensitizing effects of oridonin could already be observed in chinese-hamster-V79 cells.¹⁸

After treatment with either oridonin or ponicedin we observed a dose-dependent reduction of clonogenic survival in all tested pancreatic cancer cell lines AsPC-1, BxPC-3, MIA PaCa-2 and Panc-1 after treatment with either oridonin or ponicedin. Compared to oridonin, equal doses of ponicedin were more effective in reducing clonogenic survival. Similar results were observed by Hsieh *et al.* in clonogenic survival assays of the breast cancer cell line MCF-7, who also tested both agents in proliferation assays with comparable results of oridonin and ponicedin.²³ Based on these data we infer that

ponicedin might be a more potent cytostatic agent than oridonin.

After combined treatment with irradiation and different concentrations of oridonin or ponicedin we observed an increased reduction of clonogenic survival. The analysis of potential interactions revealed a trend towards additive effects for the higher concentration of oridonin as well as ponicedin. Supraadditive effects that provide evidence for actual radiosensitization could not be observed.

Cell cycle assays of the present study showed that both oridonin and ponicedin lead to an accumulation of cells in the G2/M-phase of the cell cycle. The combination of irradiation and oridonin or ponicedin leads to an even prolonged G2/M-arrest. Cells that are stuck in this phase usually present DNA-lesions, such as DNA double-strand breaks or blocked DNA replication forks, which have to be repaired before passing the G2/M-checkpoint.²⁴ An oridonin-induced G2/M-arrest was previously reported by Qi *et al.* for the pancreatic cancer cell line Panc-1 along with a suppression of cell cycle regulating cyclin B1 and cdc2.¹⁰ In our study, we focused on DNA double-strand breaks as underlying mechanism especially after combination with irradiation. Therefore we did not investigate any changes in proteins of the cell cycle regulation but further experiments should pinpoint the precise mode G2/M-phase arrest induced by oridonin and ponicedin. Since induction of apoptosis was reported for both oridonin and ponicedin^{9-12,14-17}, we expected a sub-G1 peak in cell cycle analysis but could not observe any peak in the sub-G1 noise. Interestingly, the cell cycle assays of Qi *et al.* for PANC-1 cells treated with oridonin also did not show any sub-G1 peak.¹⁰

The analyzed pan-nuclear γ H2AX-quantification revealed a two-fold higher γ H2AX-intensity after treatment with oridonin or ponicedin. This increase in γ H2AX level was independent of the particular dose level of oridonin and ponicedin. Combined with irradiation both oridonin and ponicedin lead to an even higher amount of γ H2AX. Pan-nuclear determination of γ H2AX is just an indirect indicator of DNA double-strand break induction, but it is comparable to the quantification of γ H2AX-foci²⁵ which is known to be highly suspect for an induction of DNA double-strand breaks.²⁶ Accordingly, oridonin and ponicedin as well as irradiation seem to induce DNA double-strand breaks. Beside possible effects on cell cycle phase proteins as suggested by Qi *et al.*¹⁰ the induction of DNA double-strand breaks are a good explanation for the observed G2/M-arrest. An already described augmentation

of γ H2AX in oridonin-treated BxPC-3 cells and an increased γ H2AX-concentration in breast cancer cells exposed to irradiation are in line with our present data.^{9,27}

By comparison of γ H2AX-intensities at different time points the level of γ H2AX of the combined treatment schemes decreased quite similar to that of the irradiation treatment alone. We therefore have to conclude that oridonin and ponidicin do not significantly lower the DNA double-strand break repair capacity. To verify this, proteins of the DNA double-strand break repair were detected by Western Blot. Since pancreatic cancer cells are known to show only weak activity of the homologous recombination pathway²⁸, we concentrated on the key proteins of the NHEJ. There were no relevant changes in the amount of Ku70, Ku80 or XRCC4 in oridonin- or ponidicin-treated cells supporting the hypothesis that oridonin and ponidicin do not reduce the DNA double-strand break repair mechanisms. Further studies should investigate if oridonin or ponidicin interfere with proteins of the homologous recombination pathway of DNA double-strand break repair, such as RAD51 or MRE11/RAD50/NBS1 complex.

Recently, Wang *et al.* could show synergistic effects of an oridonin derivative and paclitaxel through increased reactive oxygen species (ROS) levels and subsequent apoptosis induction.²⁹ Cao *et al.* observed a synergistic effect of cetuximab and oridonin through increased ROS levels and epidermal growth factor receptor (EGFR) inhibition.³⁰ Activation of ROS is known to be one of the main effects of irradiation in cancer treatment. These findings strengthen the idea of combined treatment schemes with oridonin and irradiation.

In the next step, both substances should be tested in combination with the recent standard chemotherapies such as gemcitabine or FOLFIRINOX. Finally, *in vivo* data are needed to reveal if efficacy of irradiation in pancreatic cancer patients can be improved by oridonin and ponidicin.

Conclusions

The current data demonstrate new aspects of the two interesting phytotherapeutics oridonin and ponidicin. *In vitro* both substances are highly effective against pancreatic cancer cells especially when combined with irradiation. Therefore both oridonin and ponidicin are promising agents in pancreatic cancer therapy. Our data warrant further *in vivo* investigations especially in combination

with irradiation or standard chemotherapy such as FOLFIRINOX or gemcitabine and nab-paclitaxel.

Acknowledgements

We thank Lena Orschiedt, Sigrid Daffinger, Sylvia Trinh and Ludmilla Frick for the excellent technical assistance with the experiments.

The datasets used and/or analysed during the current study are available from the corresponding author on reasonable request.

JL and PN designed and performed the experiments. JL and PN wrote the manuscript. TES performed the γ H2AX-quantification. FF, SEC, KJW and JD helped finalizing the manuscript. All authors read and approved the final manuscript.

We acknowledge financial support by Deutsche Forschungsgemeinschaft and Ruprecht-Karls-Universität Heidelberg within the funding programme Open Access Publishing.

References

1. Siegel RL, Miller KD, Jemal A. Cancer statistics, 2015. *CA Cancer J Clin* 2015; **65**: 5-29. doi: 10.3322/caac.21254
2. Kleeff J, Friess H, Buchler MW. Neoadjuvant therapy for pancreatic cancer. *Br J Surg* 2007; **94**: 261-2. doi: 10.1002/bjs.5737
3. Gillen S, Schuster T, Meyer Zum Buschenfelde C, Friess H, Kleeff J. Preoperative/neoadjuvant therapy in pancreatic cancer: a systematic review and meta-analysis of response and resection percentages. *PLoS Med* 2010; **7**: e1000267. doi: 10.1371/journal.pmed.1000267
4. Naumann P, Habermehl D, Welzel T, Debus J, Combs SE. Outcome after neoadjuvant chemoradiation and correlation with nutritional status in patients with locally advanced pancreatic cancer. *Strahlenther Onkol* 2013; **189**: 745-52. doi: 10.1007/s00066-013-0393-3
5. Han QB, Li ML, Li SH, Mou YK, Lin ZW, Sun HD. Ent-kaurane diterpenoids from *Isodon rubescens* var. *lushanensis*. *Chem Pharm Bull (Tokyo)* 2003; **51**: 790-3.
6. Owona BA, Schluessener HJ. Molecular insight in the multifunctional effects of oridonin. *Drugs R D* 2015; **15**: 233-44. doi: 10.1007/s40268-015-0102-z
7. Tian W, Chen SY. Recent advances in the molecular basis of anti-neoplastic mechanisms of oridonin. *Chin J Integr Med* 2013; **19**: 315-20. doi: 10.1007/s11655-013-1437-3
8. Bai N, He K, Zhou Z, Tsai ML, Zhang L, Quan Z, et al. Ent-kaurane diterpenoids from *Rabdosia rubescens* and their cytotoxic effects on human cancer cell lines. *Planta Med* 2010; **76**: 140-5. doi: 10.1055/s-0029-1186002
9. Xu B, Shen W, Liu X, Zhang T, Ren J, Fan Y, et al. Oridonin inhibits BxPC-3 cell growth through cell apoptosis. *Acta Biochim Biophys Sin (Shanghai)* 2015; **47**: 164-73. doi: 10.1093/abbs/gmu134
10. Qi X, Zhang D, Xu X, Feng F, Ren G, Chu Q, et al. Oridonin nanosuspension was more effective than free oridonin on G2/M cell cycle arrest and apoptosis in the human pancreatic cancer PANC-1 cell line. *Int J Nanomedicine* 2012; **7**: 1793-804. doi: 10.2147/IJN.S29483
11. Bu HQ, Liu DL, Wei WT, Chen L, Huang H, Li Y, et al. Oridonin induces apoptosis in SW1990 pancreatic cancer cells via p53- and caspase-dependent induction of p38 MAPK. *Oncol Rep* 2014; **31**: 975-82. doi: 10.3892/or.2013.2888

12. Bu HQ, Luo J, Chen H, Zhang JH, Li HH, Guo HC, et al. Oridonin enhances antitumor activity of gemcitabine in pancreatic cancer through MAPK-p38 signaling pathway. *Int J Oncol* 2012; **41**: 949-58. doi: 10.3892/ijo.2012.1519
13. Ikezoe T, Yang Y, Bandobashi K, Saito T, Takemoto S, Machida H, et al. Oridonin, a diterpenoid purified from *Rabdosia rubescens*, inhibits the proliferation of cells from lymphoid malignancies in association with blockade of the NF-kappa B signal pathways. *Mol Cancer Ther* 2005; **4**: 578-86. doi: 10.1158/1535-7163.MCT-04-0277
14. Liu JJ, Huang RW, Lin DJ, Peng J, Zhang M, Pan X, et al. Ponicedin, an ent-kaurane diterpenoid derived from a constituent of the herbal supplement PC-SPES, *Rabdosia rubescens*, induces apoptosis by activation of caspase-3 and mitochondrial events in lung cancer cells in vitro. *Cancer Invest* 2006; **24**: 136-48. doi: 10.1080/07357900500524371
15. Liu JJ, Zhang Y, Guang WB, Yang HZ, Lin DJ, Xiao RZ. Ponicedin inhibits monocytic leukemia cell growth by induction of apoptosis. *Int J Mol Sci* 2008; **9**: 2265-77. doi: 10.3390/ijms9112265
16. Zhang JF, Liu PQ, Chen GH, Lu MQ, Cai CJ, Yang Y, et al. Ponicedin inhibits cell growth on hepatocellular carcinoma cells by induction of apoptosis. *Dig Liver Dis* 2007; **39**: 160-6. doi: 10.1016/j.dld.2006.09.011
17. Liu YF, Lu YM, Qu GQ, Liu Y, Chen WX, Liao XH, et al. Ponicedin induces apoptosis via JAK2 and STAT3 signaling pathways in gastric carcinoma. *Int J Mol Sci* 2015; **16**: 1576-89. doi: 10.3390/ijms16011576
18. Murayama C, Nagao Y, Sano S, Ochiai M, Fuji K, Fujita E, et al. Effect of oridonin, a *Rabdosia* diterpenoid, on radiosensitization with misonidazole. *Experientia* 1987; **43**: 1221-3.
19. Zhou GB, Kang H, Wang L, Gao L, Liu P, Xie J, et al. Oridonin, a diterpenoid extracted from medicinal herbs, targets AML1-ETO fusion protein and shows potent antitumor activity with low adverse effects on t(8;21) leukemia in vitro and in vivo. *Blood* 2007; **109**: 3441-50. doi: 10.1182/blood-2006-06-032250
20. Denekamp J, Waites T, Fowler JF. Predicting realistic RBE values for clinically relevant radiotherapy schedules. *Int J Radiat Biol* 1997; **71**: 681-94.
21. Steel GG, Peckham MJ. Exploitable mechanisms in combined radiotherapy-chemotherapy: the concept of additivity. *Int J Radiat Oncol Biol Phys* 1979; **5**: 85-91.
22. Morgan MA, Lawrence TS. Molecular pathways: overcoming radiation resistance by targeting DNA damage response pathways. *Clin Cancer Res* 2015; **21**: 2898-904. doi: 10.1158/1078-0432.CCR-13-3229
23. Hsieh TC, Wijeratne EK, Liang JY, Gunatilaka AL, Wu JM. Differential control of growth, cell cycle progression, and expression of NF-kappaB in human breast cancer cells MCF-7, MCF-10A, and MDA-MB-231 by ponicedin and oridonin, diterpenoids from the chinese herb *Rabdosia rubescens*. *Biochem Biophys Res Commun* 2005; **337**: 224-31. doi: 10.1016/j.bbrc.2005.09.040
24. Roos WP, Kaina B. DNA damage-induced cell death: from specific DNA lesions to the DNA damage response and apoptosis. *Cancer Lett* 2013; **332**: 237-48. doi: 10.1016/j.canlet.2012.01.007
25. MacPhail SH, Banath JP, Yu TY, Chu EH, Lambur H, Olive PL. Expression of phosphorylated histone H2AX in cultured cell lines following exposure to X-rays. *Int J Radiat Biol* 2003; **79**: 351-8.
26. Sedelnikova OA, Rogakou EP, Panyutin IG, Bonner WM. Quantitative detection of (125)IdU-induced DNA double-strand breaks with gamma-H2AX antibody. *Radiat Res* 2002; **158**: 486-92.
27. Zhang T, Tan Y, Zhao R, Liu Z. DNA damage induced by oridonin involves cell cycle arrest at G2/M phase in human MCF-7 cells. *Contemp Oncol (Pozn)* 2013; **17**: 38-44. doi: 10.5114/wo.2013.33772
28. Li YH, Wang X, Pan Y, Lee DH, Chowdhury D, Kimmelman AC. Inhibition of non-homologous end joining repair impairs pancreatic cancer growth and enhances radiation response. *PLoS One* 2012; **7**: e39588. doi: 10.1371/journal.pone.0039588
29. Wang SQ, Wang C, Chang LM, Zhou KR, Wang JW, Ke Y, et al. Geridonin and paclitaxel act synergistically to inhibit the proliferation of gastric cancer cells through ROS-mediated regulation of the PTEN/PI3K/Akt pathway. *Oncotarget* 2016; **7**: 72990-3002. doi: 10.18632/oncotarget.12166
30. Cao S, Xia M, Mao Y, Zhang Q, Donkor PO, Qiu F, et al. Combined oridonin with cetuximab treatment shows synergistic anticancer effects on laryngeal squamous cell carcinoma: involvement of inhibition of EGFR and activation of reactive oxygen species-mediated JNK pathway. *Int J Oncol* 2016; **49**: 2075-87. doi: 10.3892/ijo.2016.3696

Focused transhepatic electroporation mediated by hypersaline infusion through the portal vein in rat model. Preliminary results on differential conductivity

Clara Pañella¹, Quim Castellví², Xavier Moll³, Rita Quesada¹, Alberto Villanueva⁴, Mar Iglesias⁵, Dolores Naranjo⁵, Patricia Sánchez-Velázquez¹, Anna Andaluz³, Luís Grande¹, Antoni Ivorra² and Fernando Burdío¹

¹ General Surgery Department, Hospital del Mar Medical Research Institute (IMIM), Universitat Pompeu Fabra, Barcelona, Spain

² Department of Informatics and Communication Technologies, Universitat Pompeu Fabra, Barcelona, Spain

³ Department of Pathological Anatomy, Hospital del Mar Medical Research Institute (IMIM), Universitat Pompeu Fabra, Barcelona, Spain

⁴ Chemoresistance and Predictive Factors Group, Program Against Cancer Therapeutic Resistance (ProCURE), Catalan Institute of Oncology (ICO), Bellvitge Biomedical Research Institute (IDIBELL), Hospitalet de Llobregat, Barcelona, Spain

⁵ Medical and Surgery Animal Department, Faculty of Veterinary, Universitat Autònoma de Barcelona³, Cerdanyola del Vallès, Barcelona, Spain

Radiol Oncol 2017; 51(4): 415-421.

Received 2 July 2017

Accepted 22 October 2017

Correspondence to: Fernando Burdío M.D., Clara Pañella M.D., Unidad de Cirugía Hepática. Servicio de Cirugía General y Digestiva, Hospital del Mar de Barcelona, Passeig Marítim 25-29, 08003 Barcelona, Spain. E-mail: fburdio@hotmail.com, cpvilamu@gmail.com

Disclosure: No potential conflicts of interest were disclosed.

Background. Spread hepatic tumours are not suitable for treatment either by surgery or conventional ablation methods. The aim of this study was to evaluate feasibility and safety of selectively increasing the healthy hepatic conductivity by the hypersaline infusion (HI) through the portal vein. We hypothesize this will allow simultaneous safe treatment of all nodules by irreversible electroporation (IRE) when applied in a transhepatic fashion.

Material and methods. Sprague Dawley (Group A, n = 10) and Athymic rats with implanted hepatic tumour (Group B, n = 8) were employed. HI was performed (NaCl 20%, 3.8 mL/Kg) by trans-splenic puncture. Deionized serum (40 mL/Kg) and furosemide (2 mL/Kg) were simultaneously infused through the jugular vein to compensate hypernatremia. Changes in conductivity were monitored in the hepatic and tumour tissue. The period in which hepatic conductivity was higher than tumour conductivity was defined as the therapeutic window (TW). Animals were monitored during 1-month follow-up. The animals were sacrificed and selective samples were used for histological analysis.

Results. The overall survival rate was 82.4% after the HI protocol. The mean maximum hepatic conductivity after HI was 2.7 and 3.5 times higher than the baseline value, in group A and B, respectively. The mean maximum hepatic conductivity after HI was 1.4 times higher than tumour tissue in group B creating a TW to implement selective IRE.

Conclusions. HI through the portal vein is safe when the hypersaline overload is compensated with deionized serum and it may provide a TW for focused IRE treatment on tumour nodules.

Key words: irreversible electroporation; liver tumour; electrical conductivity

Introduction

Electroporation (EP) is the phenomenon by which the cell membrane permeability is increased when

the cell is subjected to high electric fields. Such increase in membrane permeability can irreversibly alter cell homeostasis and lead to cell death, either by necrosis or apoptosis. In this case the term irre-

versible electroporation (IRE) is used.¹⁻⁵ IRE is typically performed by inserting thin needle electrodes into the targeted tissue and delivering a number (8-100) of short (10-100 μ s) high-voltages pulses across the electrodes, thereby producing field magnitudes in the tissue in the order of 1000 V/cm or more.³

The ideal ablation system for multiple hepatic nodules should treat the tumoural tissue while preserving the remaining healthy hepatic tissue. Unfortunately, the IRE as it is used today, does not allow the preservation of the surrounding healthy tissue. Although, it is a non-thermal technique and is credited with sparing the extracellular matrix, IRE leads to the apoptosis of either healthy or tumoural hepatic tissue where the electric field is applied.⁵⁻¹⁰ In fact, this technique is highly dependent on tissue conductivity¹¹⁻¹³ and tumours have higher dielectric properties (and higher conductivities) than normal healthy tissue because of the higher sodium and water content of cancer cells.¹⁴ This higher conductivity may lead to a lower electric field in the tumoural tissue than in the surrounding healthy tissue.¹²

Our group recently studied the long-term effectiveness of treating a large amount of healthy hepatic tissue harbouring an implanted tumour with parallel transhepatic electrodes.¹⁵ In this study we showed that even with high electrical fields (up to 2000 V/cm) complete eradication of the tumour was infrequent even when massive destruction of nearby healthy hepatic tissue was present (expressed by life-threatening ionic imbalances).¹⁶

In this context, we recently used a mathematical model aiming to assess the electrical conductivity of the liver after introducing hypertonic solution (20% NaCl) through the portal vasculature (Figure 1). This model was further validated with an *in vivo* pilot safety study on pigs, which demonstrated that this infusion could increase the mean basal conductivity by up to 4 times.¹⁷ Interestingly, the tumour nodules lack of sinusoids means they are only supplied with blood from the hepatic artery.¹⁸⁻²⁰ In fact, this characteristic is currently used for identifying tumours by injecting contrast agents with CT or MRI. Hypersaline infusion through the portal vein would therefore raise the electrical conductivity of the healthy hepatic tissue, so that, when a potential difference is applied between the opposite sides of the liver, the electrical field magnitude in the tumours would be significantly larger than in the rest of the healthy tissue. Thus it would make possible to produce electroporation in tumour cells and without affecting healthy hepatic tissue (Figure 1).¹⁸

The aim of this study was to evaluate feasibility and safety of selectively increasing of healthy hepatic conductivity by HI through the portal vein as a means to increase the electric field in scattered tumoural nodules with transhepatic IRE.

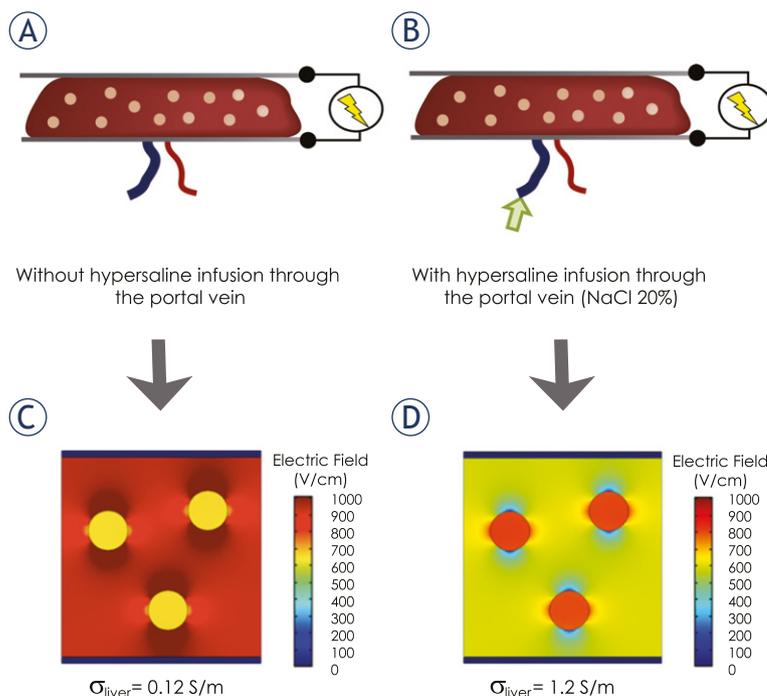


FIGURE 1. IRE application model with plate electrodes, in scattered tumoural liver without (A) or with (B) hypersaline infusion through the portal vein and its corresponding numerical simulation (C and D) obtained from the received electric field in healthy and tumoural tissue – own results obtained from our previous research (17, 18). (C) Without hypersaline infusion through the portal vein, there is not selective effect on scattered tumoural nodules. Nevertheless, in (D) with hypersaline infusion through the portal vein, there is an increase on the electric field on scattered tumours (meaning a preferential ablative IRE effect on these nodules) because of the increase in healthy tissue conductivity (σ).

Materials and methods

All aspects of this study had the approval of the Ethics Committee on Animal Research of the Government of Catalonia (FBP-13-1474P2 procedure, DAAM: 7016). This animal experimental study was conducted following directives 2010/63/EU of the European Parliament and Council of 22 September 2010, for the protection of animals for experimental and scientific purposes.

Animal model

Two animal models were considered in the study: Group A (n = 10) Sprague Dawley rats (Charles River Laboratories, Kingston, NY, USA) and Group

B (n = 8) Athymic nude rats Hsd:RH-Foxn1^{nu} (Harlan laboratories, Indianapolis, IN, USA). Eighteen six-week-old males were used and all of them were maintained under standard conditions with a laboratory animals diet and water *ad libitum*. We supervised all the animals following Morton and Griffiths' guidelines on the recognition of pain, distress and discomfort in experimental animals.²¹

Group A was used to develop the HI protocol and show that it had no influence on survival rate; and group B was conceived for tumour implantation and conductivity test on changes between hepatic and tumour tissue.

Tumour implantation technique

Primary colorectal metastases were obtained from Bellvitge Hospital (HUB) and the Catalan Institute of Oncology (ICO) with approval by the Ethical Committee, and ethical and legal protection guidelines of human subjects, including informed consent, were followed. Primary metastasis was implanted orthotopically in the liver of Crl:NU-FOXn1 nu mice, and when the orthoxenograft or patient derived orthotopic xenograft (PDOX) growth, the mice were sacrificed. Then, the tumour was minced and re-implanted in the left hepatic lobe of group B, after a quarantine period at the

age of six weeks, by midline laparotomy under general anaesthesia (mixture of isoflurane and inhaled oxygen). Tumour pieces of measuring 5-8 mm² were sutured with non-reabsorbable prolene 6/0 on the surface of the left hepatic lobe. The midline laparotomy closure was made up of a running suture within the muscle layer with reabsorbable monocryl 5/0 and skin with simple silk 5/0 stitches. The tumour grew for a mean of 20 days to allow adequate hepatic implantation. All the animals developed a tumour on the left hepatic lobe, appropriate for conductivity measurement after HI through the portal vein.

Hypersaline infusion protocol

HI was applied by means of a hypersaline infusion at 20% (NaCl), which is an aqueous solution with high conductivity (204 S/m).^{22,23}

Once anaesthetised by inhalation anaesthesia (isoflurane 4% for induction and 2.5% for maintenance with O₂ 0.8 L/minute), subcutaneous analgesia was administered (buprenorphine 0.05 mg/Kg). The abdomen and anterior cervical area were shaved and prepared aseptically with iodine. The liver was exposed by iterative abdominal incision and dressing pad underneath, after 7 days after the tumour implantation in group A and after mean of

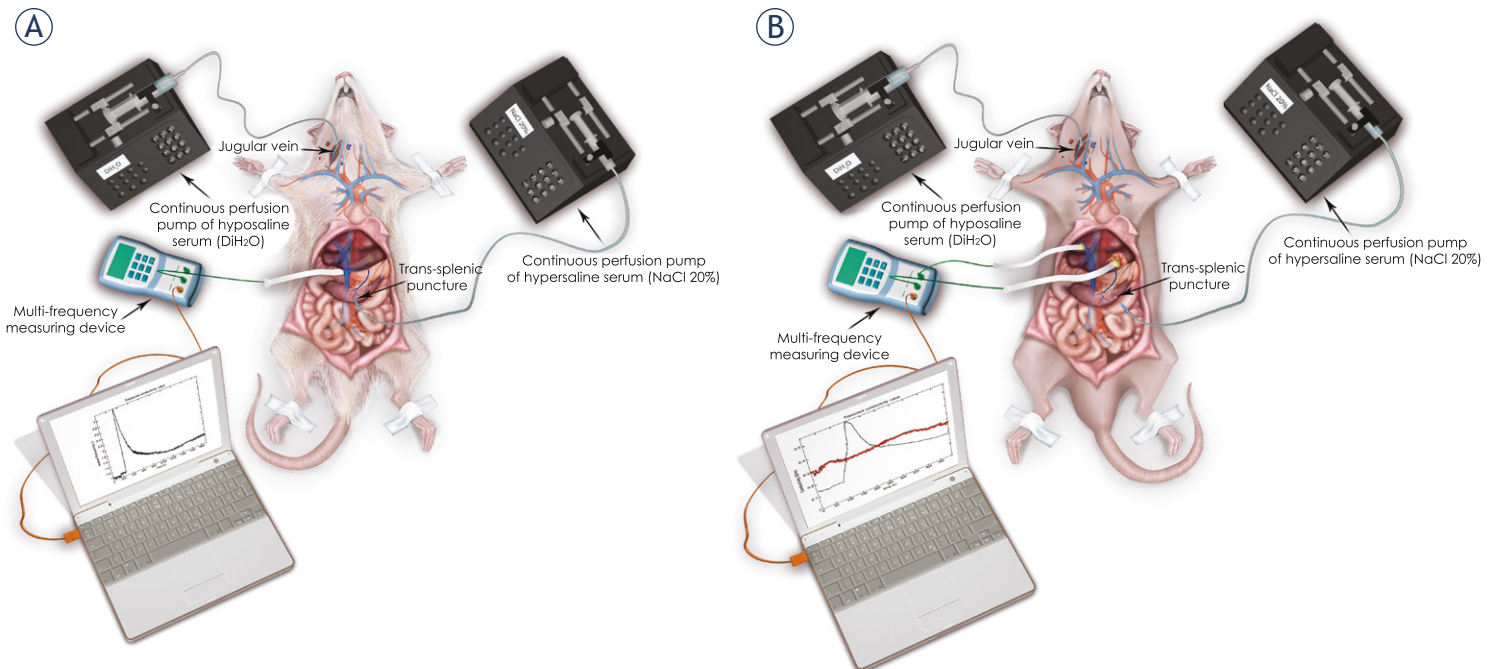


FIGURE 2. General setting of the hypersaline infusion protocol through the portal vein in Sprague Dawley rats (A) and in Athymic rats with implanted tumour (B). After exposing spleen at abdominal midline, hypersaline infusion was performed by trans-splenic puncture with a pump. Hypersaline infusion through the jugular vein was performed to compensate the systemic hypernatremia. Two tetrapolar setup electrodes measured tumour and healthy hepatic conductivity and data were collected with a multi-frequency device and gathered in a computer.

20 days of tumour growth in group B. The anterior vertical cervicotomy approach allowed anterior jugular vein dissection and catheterization with a flexible plastic tube (Tygon® ND 100-80 tubing, USP corporation, USA) for deionised serum infusion (DiH₂O). The infusion of hyposaline serum, DiH₂O, (40 mL/Kg)¹⁸, through the anterior jugular vein, avoids the HI side effects, such as systemic hypernatremia. Prior to the HI protocol, the animals were pre-hydrated with a quarter of the total hyposaline serum (DiH₂O), calculated by weight, at the same infusion rate as the HI. NaCl 20% (3.8 mL/Kg) was then injected into the portal vein by trans-splenic puncture (27G needle)¹⁸, during hyposaline infusion. The HI rate was set up to administer the dose in 1 minute. Trans-splenic puncture was used for the HI protocol, since splenic vein is a part of the portomesenteric system and infusion is more feasible than dissection of the portal vein (Figure 2).

Intravenous infusion of furosemide (2 mL/Kg) was administered before and after HI protocol in order to compensate the fluid overload after intravenous administration of hyposaline serum (via jugular) and hypersaline serum (via trans-splenic).¹⁸

Electrical conductivity measurement

Hepatic and tumour conductivity were measured using the tetrapolar method following the setup employed in²⁴. This consists of four stainless steel needles (0.25 mm of diameter and 3.5 mm of exposure) placed in a straight line with 0.5 mm between the centres of the needles. Tumour electrode was inserted at the centre of the tumour, with four-needle shape, in a way that it favoured its stability.

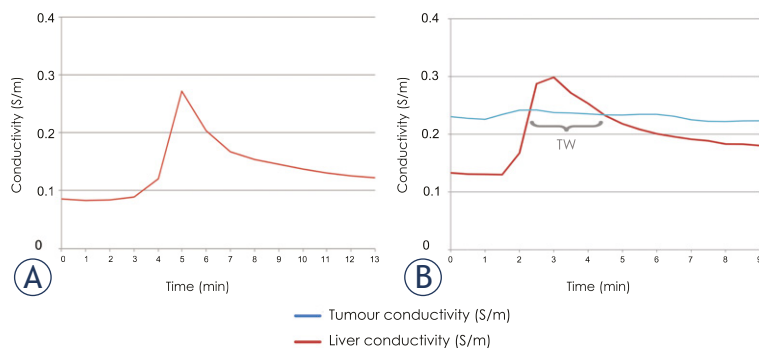


FIGURE 3. Conductivity changes after hypersaline infusion protocol in a representative case of group A (Sprague Dawley) and B (Athimic rats with implanted tumour). In both groups, a sharp increase and a posterior slowing decrease of conductivity in healthy hepatic tissue was observed. On the contrary, conductivity of the tumoural tissue (Group B) was stable. Thus, it created a therapeutic window (TW), the safety period where IRE it would be applied.

Measurements were performed at ten-excitation frequencies from 5 kHz to 1 MHz at a rate of one sweep per second. Signal generation and the acquisition of both current and voltage across the sample were performed by a Red Pitaya board and a front-end.²⁵

Post-surgical management

During the surgical procedure and during the immediate postoperative period, a heat lamp or heat pad controlled the risk of hypothermia. Administered analgesia was buprenorphine 0.05 mg/Kg s.c. and meloxicam 1 mg/Kg s.c., both every 24 hours for 3 days. An oral prophylactic antibiotic was also supplied: enrofloxacin in drinking water, 500 mg/Kg, for the first 3 days. Weight was monitored periodically as an objective sign of positive outcome after catheterization and the HI protocol.

Histopathological samples

Animals were sacrificed according to modified Morton and Griffiths criteria²¹ if signs of suffering or distress were observed. Animals of group A were sacrificed 1 month after the procedure while animals of group B were sacrificed in case of clinical evidence of tumour dissemination (for instance, subcutaneous tumour implants). At necropsy, liver and spleen were collected from both groups. Tissue samples were fixed on formaldehyde and kept in paraffin blocks. Sections of 3 µm were prepared for routine haematoxylin-eosin staining (HEOS) slides.

Statistical analyses

All the statistics were processed by the SPSS statistical software package (SPSS, version 21, IBM, Armonk, NY, USA) and expressed as mean ± standard deviation. Since the sample was small, the Wilcoxon test was used for non-parametric data to make pairwise comparisons of weight and conductivity of healthy tissue before and after HI, in both groups. A P-value of < 0.05 was considered statistically significant.

Results

Hypersaline infusion through the portal vein is safe when compensated

The HI protocol was reproduced in 94.4% (17/18) of cases in group A and B. One animal died from anaesthetic problems before the HI protocol. Overall

TABLE 1. Comparison between two groups A (Sprague Dawley) and B (Athimic). *PO: Postoperative

	GROUP A	p-value	GROUP B	p-value
Administration of HI protocol		n= 9		n=8
Weight increase during PO* (grams)	100±30.57	0.012	-1.94±37.81	0.386
Baseline Conductivity in healthy tissue (S/m)	0.10±0.02	0.008	0.13±0.02	0.008
Conductivity after HI in healthy tissue (S/m)	0.27±0.75		0.49±0.17	
Baseline Conductivity in tumour tissue (S/m)	NA		0.24±0.03	
Therapeutic window (sec)	NA		175±115	

technical-related survival rate was 82.4% (14/17) after the HI protocol for both groups and there were 3 technical-related deaths (one animal in group A and 2 in group B). In all of these technical-related deaths, extra HI was administered after observing recurrent reflux of the HI through the transplenic puncture and no correct compensation of the HI overload was possible in these cases. Two died shortly after the HI protocol and the other was sacrificed two days after when it was seen to be lethargic (see comments on this animal in histology section). During the postoperative period of the animals with HI protocol, a mean increase of weight of 100 grams was observed in the other animals in group A (from 366.5±51.6 grams to 466.5±71.9 grams at the necropsy date).

Implantation and tumour development

The polyclonal human colon adenocarcinoma tumour model was well implanted with a correct growth after 60-90 days and with no evidence of peritoneal carcinomatosis at necropsy in all cases. Mean tumour volume, at implantation, was 122.5±84.3 mm³ and it remained stable at the time of the HI protocol, being 121±65.11 mm³. Mean tumour volume at the necropsy was 692.8±347.3 mm³.

As expected in this tumoural model, the mean weight of the animals in group B initially increased after tumour implantation (from 158±7.33 grams to a mean maximum weight of 217.34±9.19 grams), but then decreased (156.06±39.68 grams, at necropsy) (Table 1).

Hypersaline infusion increases conductivity in healthy hepatic parenchyma

In all animals increased hepatic tissue conductivity was observed after the HI protocol. In group A,

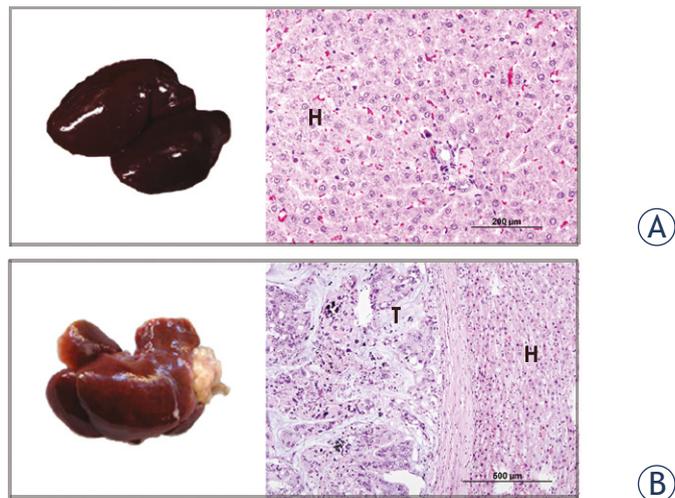


FIGURE 4. These were representative livers from group A (Sprague Dawley) and group B (Athimic rats with implanted tumour) after HI protocol at the 4th week of postoperative. Histological analysis revealed the indemnity of the architecture and morphology of healthy hepatocytes (H) of both groups A and B. In group B, histological samples showed that HI protocol did not interfere in tumour (T) evolution.

the mean baseline conductivity before administering HI was 0.10±0.02 S/m and the mean maximum conductivity peaked at 0.27±0.75 S/m. Likewise, in group B, the mean baseline hepatic conductivity was 0.11±0.02 S/m and the mean maximum hepatic conductivity after HI was 0.38±0.16 S/m (range 0.19-0.66 S/m), which was around 3.5 times higher than the baseline value (Figure 3).

Hypersaline infusion through the portal vein does not change tumoural conductivity

As expected, tumoural conductivity in group B was not influenced by HI (mean value: 0.24±0.03 S/m). The higher conductivity in healthy hepatic tissue created a mean TW of 175±115.23 seconds (Figure 3B), where the mean maximum hepatic

conductivity after HI was 1.4 times higher (range 1.04-1.76) than tumour tissue. In this TW, electroporation could therefore be advantageously applied.

Histopathological evaluation

In group A, hepatic parenchyma exhibited normal architecture, with polygonal hepatocytes and preserved porta triads (Figure 4A). Congestion in vessels was seldom scattered throughout healthy hepatic tissue. No changes were present in cellular component or architecture after HI.

Similar results to group A were found in group B, with no architectural or morphological damage after the HI protocol. However, the animal that was sacrificed two days after two extra doses of HI showed patchy areas of coagulation necrosis in the liver especially around the central veins of acini. No damage in neoplastic tissue was observed (Figure 4B).

Discussion

The preliminary results show that the HI employed in this study selectively increases the conductivity of healthy tissue, so that when the electric pulses are applied to a whole hepatic section, the magnitude of the electric field in the tumours would be significantly higher than in the rest of the healthy tissue. The results also show that this infusion could be safe when it is correctly compensated as we previously demonstrated in the pilot study on pigs.¹⁷

Concerning the safety of the protocol, it should be remembered that hypersaline solutions has been extensively used to resuscitate patients with traumatic brain injury.²⁶ It is currently assumed that the maximum dosage at 20% is 1.8 ml/Kg. Twice this dose was used in the present study (3.8 ml/Kg) combined with measures to compensate the corresponding hypernatremia (doses of hyposaline serum through the anterior jugular vein and furosemide). With this protocol all the animals survived the HI protocol, with the appropriate increase in their body weight and no histological damage being found at necropsy. The three animal deaths were related to extra HI doses (administered after observing recurrent reflux of the infusion through the trans-splenic puncture) without correct compensation for the overload.

As regards the potential translation of these conductivity results, the basal hepatic and tu-

moural conductivity observed are similar to those described in the literature for humans and in the tumour itself can vary up to 20%.²⁷ For example, Laufer *et al.* found 0.12 S/m and 0.27 S/m for normal and tumoural liver tissue, respectively.²⁴ Although little data is available in the literature on increasing conductivity by administering HI through the portal vein, in our previous study on pigs, with the same HI protocol, similar peak conductivity results were obtained (range 0.21-0.37 S/m)¹⁷, which further supports the consistency of the present data despite the small sample size. Finally, our actual TW (175±115.2 sec) appears to be enough to implement a conventional IRE protocol. Although the application protocols are varied, most studies use between 70 and 90 pulses for duration of 70-100 µs.²⁸⁻³⁰ For instance, our previous IRE protocol with plate electrodes lasted for 100 seconds (90-100 pulses at a frequency of 1 Hz).^{16,31} Our protocol IRE lasted 100 seconds, without pauses. However, pauses can be reduced in case the TW values obtained in this preliminary study are set in this range of time, in future essays with bigger sample size. In other words, the IRE protocol can be adjusted according to the average TW obtained.

In conclusion, the presented preliminary results provide evidence in favour of safety of administering HI through the portal vein when compensated and show that it may provide a therapeutic window for focused IRE treatment on tumour nodules. Further studies should be carried out to confirm these results, giving that this study is a preliminary research.

Acknowledgements

This work received financial support from the Spanish Government (Ministry of Economy and Competitiveness) under Grant TEC2014-52383-C3. The authors disclose no conflicts of interests.

References

1. Appelbaum L, Ben-David E, Faroja M, Nissenbaum Y, Sosna J, Goldberg SN. Irreversible electroporation ablation: creation of large-volume ablation zones in in vivo porcine liver with four-electrode arrays. *Radiology* 2014; **270**: 416-24. doi: 10.1148/radiol.13130349
2. Charpentier KP, Wolf F, Noble L, Winn B, Resnick M, Dupuy DE. Irreversible electroporation of the liver and liver hilum in swine. *HPB (Oxford)* 2011; **13**: 168-73. doi: 10.1111/j.1477-2574.2010.00261.x
3. Davalos RV, Mir IL, Rubinsky B. Tissue ablation with irreversible electroporation. *Ann Biomed Eng* 2005; **33**: 223-31. doi: 10.1111/j.1477-2574.2010.00261.x

4. Bower M, Sherwood L, Li Y, Martin R. Irreversible electroporation of the pancreas: definitive local therapy without systemic effects. *J Surg Oncol* 2011; **104**: 22-8. doi: 10.1002/jso.21899
5. Daniels C, Rubinsky B. Electrical field and temperature model of nonthermal irreversible electroporation in heterogeneous tissues. *J Biomech Eng* 2009; **131**: 071006. doi: 10.1115/1.3156808
6. Al-Sakere B, Bernat C, Andre F, Connault E, Opolon P, Davalos RV, et al. A study of the immunological response to tumor ablation with irreversible electroporation. *Technol Cancer Res Treat* 2007; **6**: 301-6. doi: 10.1177/153303460700600406
7. Bellard E, Markelc B, Pelofy S, Le Guerrou F, Sersa G, Teissie J, et al. Intravital microscopy at the single vessel level brings new insights of vascular modification mechanisms induced by electroporation. *J Control Release* 2012; **163**: 396-403. doi: 10.1016/j.jconrel.2012.09.010
8. Dollinger M, Zeman F, Niessen C, Lang SA, Beyer LP, Muller M, et al. Bile duct injury after irreversible electroporation of hepatic malignancies: evaluation of MR imaging findings and laboratory values. *J Vasc Interv Radiol* 2016; **27**: 96-103. doi: 10.1016/j.jvir.2015.10.002
9. Kanthou C, Kranjc S, Sersa G, Tozer G, Zupanic A, Cemazar M. The endothelial cytoskeleton as a target of electroporation-based therapies. *Mol Cancer Ther* 2006; **5**: 3145-52. doi: 10.1158/1535-7163.MCT-06-0410
10. Maor E, Rubinsky B. Endovascular nonthermal irreversible electroporation: a finite element analysis. *J Biomech Eng* 2010; **132**: 031008. doi: 10.1115/1.4001035
11. Ben-David E, Ahmed M, Faroja M, Moussa M, Wandel A, Sosna J, et al. Irreversible electroporation: treatment effect is susceptible to local environment and tissue properties. *Radiology* 2013; **269**: 738-47. doi: 10.1148/radiol.13122590
12. Ivorra A, Villemejane J, Mir LM. Electrical modeling of the influence of medium conductivity on electroporation. *Phys Chem Chem Phys* 2010; **12**: 10055-64. doi: 10.1089/c004419a
13. Qasrawi R, Silve L, Burdío F, Abdeen Z, Ivorra A. Anatomically realistic simulations of liver ablation by irreversible electroporation. *Technol Cancer Res Treat* 2017. doi: 10.1177/1533034616687477. [Epub ahead of print]
14. Peyman A, Kos B, Djokic M, Trotoevsek B, Limbaeck-Stokin C, Sersa G, et al. Variation in dielectric properties due to pathological changes in human liver. *Bioelectromagnetics* 2015; **36**: 603-12. doi: 10.1002/bem.21939
15. Sanchez-Velazquez P, Castellvi Q, Villanueva A, Iglesias M, Quesada R, Panella C, et al. Long-term effectiveness of irreversible electroporation in a murine model of colorectal liver metastasis. *Sci Rep* 2017; **7**: 44821. doi: 10.1038/srep44821
16. Sanchez-Velazquez P, Castellvi Q, Villanueva A, Quesada R, Panella C, Caceres M, et al. Irreversible electroporation of the liver: is there a safe limit to the ablation volume? *Sci Rep* 2016; **6**: 23781. doi: 10.1038/srep23781
17. Castellvi Q, Sanchez-Velazquez P, Moll X, Berjano E, Andaluz A, Burdío F, et al. Modeling liver electrical conductivity during hypertonic injection. *Int J Numer Meth Bio* 2017. doi: 10.1002/cnm.2904. [Epub ahead of print]
18. Castellví Q, Sánchez-Velázquez P, Berjano E, Burdío F, Ivorra A. Selective electroporation of liver tumor nodules by means of hypersaline infusion: A feasibility study. In: Lacković I, Vasic D, editors. 6th European Conference of the International Federation for Medical and Biological Engineering: MBEC 2014, 7-11 September 2014, Dubrovnik, Croatia. Cham: Springer International Publishing; 2015. p. 821-4. doi: 10.1007/978-3-319-11128-5_204
19. Dezzo K, Bugyik E, Papp V, Laszlo V, Dome B, Tovari J, et al. Development of arterial blood supply in experimental liver metastases. *Am J Pathol* 2009; **175**: 835-43. doi: 10.2353/ajpath.2009.090095
20. Liu Y, Matsui O. Changes of intratumoral microvessels and blood perfusion during establishment of hepatic metastases in mice. *Radiology* 2007; **243**: 386-95. doi: 10.1148/radiol.2432060341
21. Morton DB, Griffiths PH. Guidelines on the recognition of pain, distress and discomfort in experimental animals and an hypothesis for assessment. *Vet Rec* 1985; **116**: 431-6.
22. Sala J, Guardia E, Marti J. Effects of concentration on structure, dielectric, and dynamic properties of aqueous NaCl solutions using a polarizable model. *J Chem Phys* 2010; **132**: 214505. doi: 10.1063/1.3429253
23. Yamaguchi T, Matsuoka T, Koda S. A theoretical study on the frequency-dependent electric conductivity of electrolyte solutions. II. Effect of hydrodynamic interaction. *J Chem Phys* 2009; **130**: 094506. doi: 10.1063/1.3085717
24. Laufer S, Ivorra A, Reuter VE, Rubinsky B, Solomon SB. Electrical impedance characterization of normal and cancerous human hepatic tissue. *Physiol Meas* 2010; **31**: 995-1009. doi: 10.1088/0967-3334/31/7/009
25. Ruiz-Vargas A, Arkwright JW, Ivorra A, editors. A portable bioimpedance measurement system based on Red Pitaya for monitoring and detecting abnormalities in the gastrointestinal tract. 2016 IEEE EMBS Conference on Biomedical Engineering and Sciences (IECBES); 2016 4-8 Dec. 2016. doi: 10.1016/j.hpb.2016.03.609
26. Tyagi R, Donaldson K, Loftus CM, Jallo J. Hypertonic saline: a clinical review. *Neurosurg Rev* 2007; **30**: 277-89; discussion 89-90. doi: 10.1007/s10143-007-0091-7
27. Muftuler LT, Hamamura MJ, Birgul O, Nalcioglu O. In vivo MRI electrical impedance tomography (MREIT) of tumors. *Technol Cancer Res Treat* 2006; **5**: 381-7.
28. Valerio M, Dickinson L, Ali A, Ramachandran N, Donaldson I, Freeman A, et al. A prospective development study investigating focal irreversible electroporation in men with localised prostate cancer: Nanoknife Electroporation Ablation Trial (NEAT). *Contemp Clin Trials* 2014; **39**: 57-65. doi: 10.1016/j.cct.2014.07.006
29. van den Bos W, de Bruin DM, Muller BG, Varkarakis IM, Karagiannis AA, Zondervan PJ, et al. The safety and efficacy of irreversible electroporation for the ablation of prostate cancer: a multicentre prospective human in vivo pilot study protocol. *BMJ open* 2014; **4**: e006382. doi: 10.1136/bmjopen-2014-006382
30. Wendler JJ, Porsch M, Nitschke S, Kollermann J, Siedentopf S, Pech M, et al. A prospective Phase 2a pilot study investigating focal percutaneous irreversible electroporation (IRE) ablation by NanoKnife in patients with localised renal cell carcinoma (RCC) with delayed interval tumour resection (IRENE trial). *Contemp Clin Trials* 2015; **43**: 10-9. doi: 10.1016/j.cct.2015.05.002
31. Sahakian AV, Al-Angari HM, Adeyanju OO. Electrode activation sequencing employing conductivity changes in irreversible electroporation tissue ablation. *IEEE Trans Biomed Eng* 2012; **59**: 604-7. doi: 10.1109/TBME.2011.2180722

Minimally invasive electrochemotherapy procedure for treating nasal duct tumors in dogs using a single needle electrode

Felipe Maglietti^{1,2,4}, Matías Tellado³, Nahuel Olaiz^{1,2,4}, Sebastian Michinski^{1,2,4}, Guillermo Marshall^{*1,2,4}

¹ Universidad de Buenos Aires, Facultad de Ciencias Exactas y Naturales, Departamento de Física, Buenos Aires, Argentina

² CONICET-Universidad de Buenos Aires, Instituto de Física del Plasma (INFIP), Buenos Aires, Argentina

³ Universidad de Buenos Aires, Facultad de Ciencias Veterinarias, Buenos Aires, Argentina

⁴ CONICET-Universidad de Buenos Aires, Facultad de Ciencias Exactas y Naturales, Departamento de Computación, Laboratorio de Sistemas Complejos, Buenos Aires, Argentina

Radiol Oncol 2017; 51(4): 422-430.

Received 1 August 2017

Accepted 2 October 2017

Correspondence to: Prof. Guillermo Marshall, Universidad de Buenos Aires, Facultad de Ciencias Exactas y Naturales, Departamento de Física, Buenos Aires, Argentina. E-mail: marshall.guillermo@gmail.com

Disclosure: No potential conflicts of interest were disclosed.

Background. Nasal cavity tumors are usually diagnosed late, when they already have infiltrated adjacent tissues thus requiring very aggressive treatments with serious side effects. Here we use electrochemotherapy (ECT), a well demonstrated treatment modality for superficial tumors.

Materials and methods. In the case of deep-seated tumors, the main limitation of ECT is reaching the tumor with an appropriate electric field. To overcome this limitation we introduce the single needle electrode (SiNE), a minimally invasive device that can deliver an appropriate electric field with a simple procedure. Twenty-one canine patients with spontaneous tumors were selected, eleven were treated using the SiNE with ECT, and ten with surgery plus adjuvant chemotherapy as a control group.

Results. In the SiNE group, 27% achieved a complete response, 64% had a partial response, and 9% had a stable disease. This means that 91% of objective responses were obtained. The mean overall survival was 16.86 months (4–32 months, median 16.5 months), with a survival rate significantly higher ($p = 0.0008$) when compared with control group. The only side effect observed was the inflammation of the treated nasal passage, which was controlled with corticosteroid therapy for one week. One year after the treatment, 60% of the canine of the SiNE group vs. 10% of the control group remained alive, and after the 32 months follow-up, the survival rate were 30% and 0%, respectively.

Conclusions. ECT with the SiNE can be safely used in canine to treat nasal tumors with encouraging results.

Key words: electrochemotherapy; nasal cavity; canine; cancer; electrochemotherapy

Introduction

Spontaneous tumors of the nasal cavity and paranasal sinuses in canine patients account for 1% of all neoplasms. Their etiology is unknown, but animals living in urban areas are at an increased risk, due to the nasal filtering of pollutants. Also, exposure to tobacco smoke and fossil fuel combustion products increase the risk of this type of cancer. The average age of dogs with nasal cancer is around 10

years, predominantly in medium and large breeds. Common clinical signs include epistaxis, mucopurulent nasal discharge, facial deformity, sneezing, dyspnea, local pain, stertorous breathing, exophthalmos, and ocular discharge.¹

The diagnostic procedures are the same as in human patients and involve high-resolution imaging procedures such as Computed Tomography (CT) scans or Magnetic Resonance Imaging (MRI) to determine the extension of the tumor and evaluating

the involvement of neighboring structures such as the palate, the retro-orbital area, the sinuses, and the cranial vault.¹ The most common histologies are adenocarcinoma, squamous cell carcinoma and sarcomas.^{1,2} Metastases are rare at the time of presentation, yet they are present at the time of death in around 40–50% of the cases. Lungs and lymph nodes are common metastatic sites.¹

Electrochemotherapy (ECT) is a new treatment modality which has been gaining territory in oncology since the Standard Operating Procedures were published in 2006.^{3,4,5} ECT consists of the application of an electric field to a tumor in order to increase the uptake of bleomycin that was previously administered (locally or intravenously) at a very low dose⁶; alternatively, cisplatin can be used locally with equally good results.⁷ ECT is mainly indicated for cutaneous and subcutaneous tumors of any histology. As cell membrane permeabilization is produced by a physical phenomenon known as electroporation, it affects all cells, regardless of the histology of the tumor. Recently, a meta-analysis of ECT clinical studies in human oncology showed that the overall objective response (OR) rate vary from 62.6% to 82.2% depending also on the route of administration of the drug, being either intravenous or intratumoural.⁸ Great efforts are being made to extend ECT to non-cutaneous locations such as the liver⁹, the brain¹⁰ and the bones.¹¹ Moreover, an endoscopic electrode was developed to treat the colon.¹² For deep-seated tumors, ECT is performed in an intraoperative manner, thus requiring the patient to be exposed to the risks and complications of an open surgery. Here we explore ECT for treating nasal cavity tumors by means of the Single Needle Electrode (SiNE).

The aim of this work is to perform a validation study of the treatment of nasal cavity tumors using the SiNE with ECT in dogs and compare the overall survival with the standard treatment available in our setting, *i.e.*: surgery plus adjuvant chemotherapy.

Materials and methods

Consent was obtained from the dog's owner to perform the treatment and for using the dog's image in this scientific work. In all cases, all recommendations from the Consejo Profesional de Médicos Veterinarios de Buenos Aires (Buenos Aires Veterinary Council) were observed, as well as the relevant local legislation in Argentina, Act No. 14072 which governs Veterinary Medicine prac-

tice. Recommendations from Campana *et al.*¹³ for reporting clinical studies on ECT were followed.

The SiNE pictured in Figure 1 is an electrode specifically designed in our lab for deep-seated tumor treatment with ECT. It consists of an insulated needle with an anode in one side and a cathode in the other. This design provides an electric field of cylindrical shape around it, strong enough to produce the electroporation of the cells.

Twenty-one patients were selected, eleven for the SiNE group and ten for the control group. The patients for the SiNE group were selected according to the following inclusion criteria:

- Canine patient with confirmed diagnosis of nasal duct tumor.
- Life expectancy of more than 1 month.
- Surgery refusal by the owner.

The control group was formed with ten patients whose owners accepted surgery plus adjuvant chemotherapy.

In the SiNE group, rhinoscopy was performed using a flexible or a rigid endoscope of variable diameters according to patient size; nasal neoplasia was diagnosed on the basis of histological findings. A complete blood count, serum biochemical profile, coagulation profile, abdominal ultrasound, and 3-view thoracic radiographs were performed. A CT/MRI was performed to determine the size and extension of the tumor. The patients were staged using Adam's staging system (Table 1).

TABLE 1. Adam's modified staging system

Stage	Tumor characteristics
T1	Confined to one nasal passage, paranasal sinus, or frontal sinus with no bony involvement.
T2	Any bony involvement, but no evidence of orbital, subcutaneous, or submucosal mass.
T3	Involvement of orbit or subcutaneous or submucosal mass.
T4	Tumor extension into nasopharynx or cribriform plate.

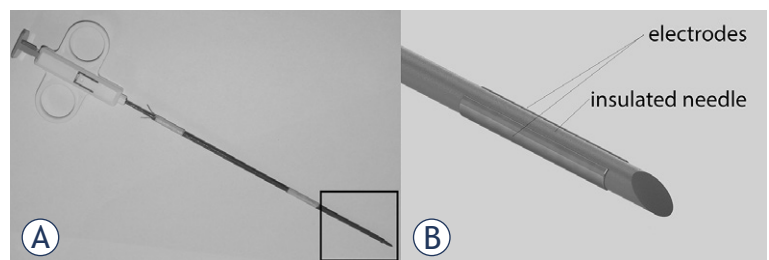


FIGURE 1. The SiNE. In (A) the prototype, in (B) the scheme of the tip, zoomed from the squared area in A. The electrode consists of a needle isolated surrounded by two parallel plaques at each side.

TABLE 2. SiNE group patient details and treatment outcome

Patient	Breed	Histology	Adam's stage	Response	Clinical Evaluation
1	Golden Retriever	Adenocarcinoma grade 3	T2	PR	Partial reduction of clinical signs, with a persistent minimum nasal discharge.
2	Miniature Pinscher	Adenocarcinoma grade 2	T2	CR	Complete resolution of clinical signs.
3	Labrador Retriever	Solid carcinoma grade 3	T3	PR	Partial reduction of clinical signs, with persistence of ocular discharge. Death by euthanasia due to distal radius metastasis.
4	Old English Mastiff	Adenocarcinoma grade 2	T4	PR	Complete Resolution of clinical signs.
5	Crossbreed	Squamous cell carcinoma	T2	PR	Partial reduction of clinical signs with persistence of minimum nasal discharge.
6	Labrador Retriever	Round cell sarcoma	T3	PR	Complete resolution of clinical signs.
7	Collie	Sticker sarcoma	T1	CR	Complete resolution of clinical signs.
8	Golden Retriever	Squamous cell carcinoma	T2	PR	Partial reduction of clinical signs, sneezing remains every day with occasional nasal discharge. Death by euthanasia based on the owner's decision.
9	Spanish Breton	Adenocarcinoma grade 2	T4	SD	No reduction of clinical signs was observed, sneezing remained every day with continuous nasal discharge and persistent inflammation of the subcutaneous tissue and paranasal sinuses. Death by euthanasia based on poor quality of life.
10	Labrador Retriever	Squamous cell carcinoma	T2	PR	Partial reduction of clinical symptoms with occasional sneezing.
11	Golden Retriever	Fibrosarcoma	T2	CR	Complete resolution of clinical signs.

In this set of patients (Table 2), 7 were males and 4 females. Four of the males were neutered, and 3 of the females were spayed. The median age of the dogs starting ECT treatment was 9 years (range of 6–13 years). The mean weight was 26 kg (range of 3.5–48 kg). Labrador Retriever (n = 3) and Golden Retriever (n = 3) were the most common breeds in this study. The other breeds were Collie, Old English Mastiff, Miniature Pincher, Spanish Breton, and a crossbreed dog. The clinical findings revealed sneezing in 11 dogs (100%), nasal discharge in 9 dogs (81%), epistaxis in 6 dogs (55%), exophthalmos in 2 dogs (18%), neurological symptoms in 2 dogs (18%) and facial deformity in 1 dog (9%). Regarding clinical Adam's staging, there was 1 dog with T1 disease (9%), 6 dogs with T2 disease (55%), 2 dogs with T3 disease (18%) and 2 dogs with T4 disease (18%). No dogs had regional lymph nodes or distant metastasis at initial presentation. None of the patients had previous treatments.

The treatment was performed under general anesthesia with premedication with intramuscular administration of xylazine (Xylazine 100®, Richmond, Buenos Aires, Argentina) 0.5 mg/kg and tramadol (Tramadol®, John Martin, Buenos Aires, Argentina) 2 mg/kg. The induction was made with intravenous administration of propofol (Propofol Gemepe®, Gemepe, Buenos

Aires, Argentina) 3 mg/kg. The maintenance was performed with inhaled isoflurane (Zuflax®, Richmond, Buenos Aires, Argentina) 2–3% and intravenous fentanyl (Fentanyl Gemepe®, Gemepe, Buenos Aires, Argentina) 2 mcg/kg. This anesthesia scheme provided adequate comfort during the treatment. Prophylactic antibiotics and meloxicam (Meloxivet®, John Martin, Buenos Aires, Argentina) 0.2 mg/kg were administered orally for analgesia after the treatment according to the needs of each patient.

The ECT procedure consisted of an intravenous bolus of bleomycin (Blocamicina®, Gador, Buenos Aires, Argentina) at a dose of 15 U/m² of body surface area in 30–45 seconds, followed by the delivery of the electric pulses eight minutes later to allow drug distribution according to the Standard Operating Procedures published by Mir et al. [14].

The SiNE was inserted deep into the nasal fossa and a train of pulses was delivered, see Figure 2. For that purpose, a BTX ECM 830 Harvard Apparatus (Holliston, MA, USA) was used. The electric pulses consisted of thirty-two square pulses of 300V, 100 µs long at 1 Hz. The electrode was rotated 90 degrees clockwise and the pulses were repeated. After the rotation, the electrode was removed 2 cm and the whole procedure was repeated until complete coverage of the nasal duct. It was not possible

to treat safety margins due to the location of the tumors.

In order to prevent the SiNE from inadvertently passing through the cribriform plate during the insertion, it was marked to show the maximum insertion depth (following CT/MRI measurements performed before the treatment).

A single ECT treatment session was performed, and no other oncological treatment was indicated previously, concomitantly or afterward.

For the assessment of treatment results, follow-up was performed within 7, 15 and 30 days; during each visit, a complete clinical examination was performed. A second CT/MRI was obtained 60 days after the treatment to determine results. The patients were followed up for 32 months and responses reported according to WHO's Criteria.¹⁵

The control group consisted of 10 cases, 5 males, and 5 females, whose owners accepted surgery as treatment (Table 3). One of the males and three of the females were neutered. The median age of the dogs was 10 years (range of 6–14 years). The mean weight was 22.7 kg (range of 5.6–34 kg). Crossbreed (n = 4) was the most common breed, other breeds were Puddle, Akita Inu, Boxer, Labrador Retriever, Fox Terrier and Cocker Spaniel. The clinical findings revealed sneezing in 10 dogs (100%), weight loss in 7 dogs (70%), epistaxis in 6 dogs (60%), hyporexia in 6 dogs (60%), facial deformity in 4 dogs (40%) and neurological symptoms in 1 dog (10%). Regarding Adam's staging, there was 1 dog with T1 disease (10%), 5 dogs with T2 disease (50%), 3 dogs with T3 disease (30%) and 1 dog with T4 disease (10%). No dog had regional lymph nodes or distant metastases.

Surgery plus adjuvant chemotherapy was performed since it is the standard treatment available



FIGURE 2. Picture of patient 9 during the treatment. The SiNE is inserted in the nasal fossa.

in our setting. The surgical procedure consisted of a dorsal/ventral uni/bilateral rhinotomy depending on the surgeon's decision, and according to tumor localization and extension. The anesthesia procedure was identical to the one mentioned above. The patients remained in observation for 24 hours with intravenous butorphanol (Torbutrol Plus®, Alpha Farma, Buenos Aires, Argentina) 0.1 mg/kg every 4 hours for one day and oral meloxicam (Meloxivet®, John Martin, Buenos Aires, Argentina) 0.2 mg/kg every 24 hours for 10 days for analgesia. The adjuvant chemotherapy consisted of intravenous carbo-

TABLE 3. Control group patient details

Patient	Breed	Histology	Adam's stage	Cause of death
1	Puddle	Tubulopapillary carcinoma	T1	Euthanasia due to local progression.
2	Crossbreed	Carcinoma	T2	Euthanasia due to local progression.
3	Akita Inu	Chondrosarcoma	T2	Euthanasia due to local progression to central nervous system
4	Crossbreed	Adenocarcinoma	T3	Death due to local progression.
5	Boxer	Carcinoma	T4	Death due to lung metastasis.
6	Crossbreed	Squamous cell carcinoma	T2	Euthanasia due to breathing difficulty.
7	Crossbreed	Carcinoma	T2	Euthanasia.
8	Labrador Retriever	Carcinoma	T3	Euthanasia due to uncontrollable pain.
9	Fox Terrier	Solid carcinoma	T2	Euthanasia.
10	Cocker Spaniel	Adenocarcinoma	T3	Euthanasia due to local progression and pain.

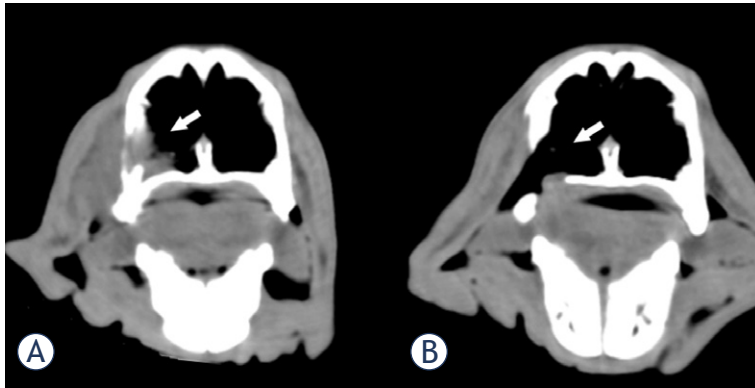


FIGURE 3. CT image of patient 11 before and after the treatment. (A) The tumor can be seen occupying the lateral inferior part of the left nasal passage (white arrow). (B) Two months after a single treatment a CR was obtained; as readily observed, the tumor tissue is absent leaving a defect in the nasal wall (white arrow).

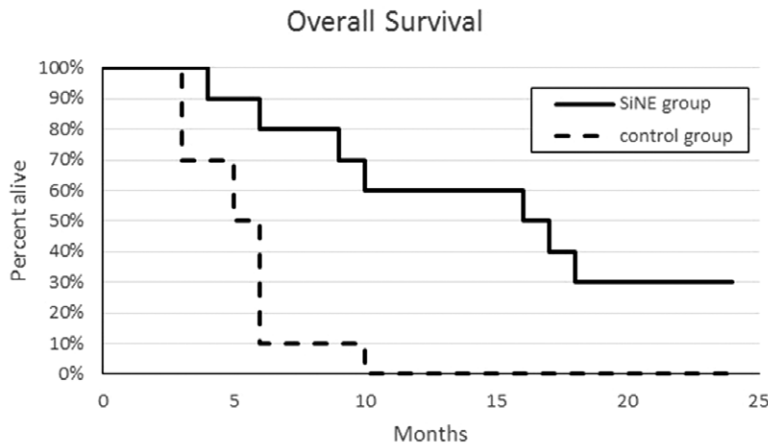


FIGURE 4. Kaplan-Meier graph of the outcome of dogs with nasal tumors treated using the SiNE with ECT procedure (SiNE group) versus the dogs treated with surgery plus adjuvant chemotherapy (control group).

platin (Carboplatino Delta Farma®, Sidus, Buenos Aires, Argentina) 300 mg/m² of body surface area every 21 days.

Regarding the statistical analysis, Kaplan–Meier curves for survival were compared by the log-rank test with an alpha of 0.05. Age and body weight were compared between groups with the Mann-Whitney U test, with an alpha of 0.05.

Results

From the 21 patients selected, 11 were treated using the SiNE with ECT (SiNE group), and 10 were treated with surgery plus adjuvant chemotherapy (control group). The SiNE and control groups did

not show significant differences in age or body-weight ($p = 0.46$ and $p = 0.13$, respectively).

In the SiNE group, out of the 11 patients: 27% (3/11) achieved a complete response (CR), 64% (7/11) had a partial response (PR), and 9% (1/11) had a stable disease (SD). In the nasal duct treated, tumor reduction remained stable and the lesions did not grow again during the follow-up period. In the first two patients only one nasal duct was treated, in the non-treated duct, the tumor continued growing according to its natural history. For this reason and because of the highly satisfactory results obtained in the treated duct, both nasal passages were treated from patient number 3 onwards. The only side effect observed was the inflammation of the treated nasal passage, which was very well controlled with corticosteroid therapy for one week. The bleeding through the nasal fossa ceased immediately after the procedure.

The patients remained in follow-up for 32 months, with no relapses in the treated area. This means that 91% objective responses (OR) were obtained. Figure 3, pictures the CT scan of patient 11 showing a complete response obtained with the treatment.

The Kaplan-Meier graph for overall survival in both groups can be seen in Figure 4. The overall survival of the SiNE group was significantly higher ($p = 0.0008$) than in the control group, with a mean survival time of 16.86 months (4–32 months, median 16.5 months). In the control group, a mean survival time of 5.3 months (3–10 months, median 5.5 months) was obtained. One year after the treatment, 60% of the patients of the SiNE group *vs.* 10% of the control group remained alive, and after the 32 months follow-up, the survival rate for the SiNE group is 30% *vs.* 0% for the control group.

Discussion

In an effort to provide a satisfactory treatment modality to canine patients with nasal tumors, and advance in the area of deep-seated tumor treatment using ECT, we developed the SiNE and a protocol for its implementation. We compared the results of this new treatment modality with the standard treatment modality in our setting: surgery plus chemotherapy.

When treating deep-seated tumors, the standard ECT procedure consists of inserting multiple needles to cover the whole tumor with an appropriate electric field. This procedure is very complex and prone to fail because the misplacement of the

needles leaves areas of the tumor untreated. In some cases, open surgery is needed for placing the needles correctly¹⁶, such as in the case reported by Suzuki et al.¹⁷, where the results were very good though the procedure required open surgery and the filling of the nasal cavity with gel to improve conductivity. These was not needed in our case since the electrode is inserted through the nasal orifice and, secretions and blood present in the nasal duct replaced conductive gel. The most important advantage of the SiNE against standard electrodes is that only a single needle is inserted, thus reducing tissue intrusion and simplifying treatment planning and its guidance by imaging procedures. The disadvantage is that it is restricted to small tumors when compared with multiple needles.

A high percentage of objective responses was obtained. Most of them were partial responses (64%), mainly because these tumors are highly infiltrative, making them very difficult to treat. In these cases, tumor tissue was still seen in CT/MRI scans. This could be due to the fact that the electric field was not enough to cover all the tumor, leaving it untreated, or more likely because those tumor cells are quiescent. In the latter case, bleomycin already acted on those cells by cleaving the DNA strands, and they will die when cell division is attempted. If the electric field would not have been strong enough, we would have seen a rapid growth of the residual tumoral tissue, at least, comparable to the non-treated passage, which did not happen. Although a fraction of the tumor remained, a considerable improvement in the quality of life was achieved due to the reduction in the clinical symptoms. The patients who achieved a complete response (27%), had a complete palliation of the symptoms as was expected.

Regarding short-term side effects, the inflammation and pain of the treated nasal passage proved to be non-problematic and easily manageable with medication. Regarding the bleeding during the procedure it ceased immediately after the treatment was completed, probably because of the "vascular lock" phenomenon, which consists of the sudden stop of blood flow in the area exposed to the electric field used in ECT procedures.³ We observed no long-term side effects.

The gold standard treatment is surgery plus adjuvant radiotherapy.¹⁸ Although surgery is usually rejected by the owner due to mutilating results, frequently it is impossible to perform, and even procedures such as rhinotomy, can result in acute and chronic morbidity. Hypofractionated or orthovoltage radiation therapy have many side effects such

as oral mucositis, rhinitis, moist desquamation, keratoconjunctivitis, and blepharitis. These symptoms can last for up to 8 weeks after therapy, even with medication, but if they persist, esophagostomy or gastrostomy tubes may be needed in the short term for an adequate nourishment of the animal. Long-term side effects include cataracts, keratoconjunctivitis, anterior uvea hemorrhage, brain necrosis, seizures, optic nerve degeneration, osteonecrosis, and fibrosis. Some of these complications are generally non-treatable.^{19,20}

Our results show that mean survival with SiNE group was 16.86 months (4–32 months) with 60% of survival at 1 year and a 30% at 2 years. This is very encouraging since it is better when compared with the standard treatment option in our setting (surgery plus chemotherapy). Also, it is similar to the best treatments described in the literature. As mentioned before, the treatment of choice for nasal tumors is surgery plus radiotherapy. Unfortunately, due to the facilities and resources required, this option is not locally available for veterinary patients. In fact, this situation is replicated in the vast majority of centers around the world. In relation to the data available for this treatment in the literature we found that for radiotherapy alone in its different modalities, the median survival reported is around 8 months.^{21,22} The combination of radiation therapy followed by surgery when it is possible seems to have better results in the overall median survival (47.7 months).²³ The new modalities like intensity-modulated radiation therapy (IMRT) report a median survival of 446 d (14.9 months) with 50% of survival at 1 year and a 25% at 2 years.²⁴

The prolonged survival in our study may be partially due to the lack of need for euthanasia as the general condition of the patients greatly improved. Further research is needed to confirm this hypothesis. It remains to be seen whether the combination of treatments can improve outcomes. The combination of ECT using the SiNE with radiotherapy or systemic chemotherapy may enable the reduction of the dose in later treatments, reducing their side effects.^{25,26}

Canine patients with spontaneous tumors are excellent models for preclinical validation. In particular, nasal tumors in dogs behave in a similar way to nasal tumors in humans.²⁷ Dogs are exposed to similar environmental carcinogens. They develop tumors with the same histologies having the same interactions between tumor and stroma to those found in human patients; thus, the tumor grows in the context of an intact immune system

that has been developed during its lifetime and exposed to different antigens. They show spontaneous metastasis and resistance to different forms of therapy. They have similar druggable targets, angiogenic pathways, and mechanisms of apoptosis. This enables a more accurate assessment of therapeutic approaches compared to rodent models. Other advantages of dogs, particularly for the purpose of this work, is that their size allows the use of the typical imaging procedures performed in humans; there is no need for miniaturization of the electrodes, and it is possible to repeat tissue and fluid sampling over time with more tissue for analysis than that available in rodent models. Also, typical forms of treatment used in humans can be performed in dogs to compare the results of the treatment.^{27,28}

In human patients the situation is similar to canine patients, nasal tumors are a complex pathology in which current treatments do not often provide satisfactory results. The variety of tumor types, its proximity to critical anatomical structures and the late development of symptoms make malignant tumors of the paranasal sinuses and nasal cavity a complex problem. Diagnostic procedures and treatment modalities are also very similar to canine patients.²⁹ Therefore, new therapeutic approaches that improve outcomes and minimize adverse effects are required. These tumors are rare and patients are often asymptomatic until late in the course of the disease. In the United States, nasal tumors account for only 0.2–0.8% of all cancers diagnosed annually. The incidence reported is 0.3–1 per 100,000 populations. They occur most commonly in the fifth decade of life, although they can occur at any age.²⁹ These tumors are usually diagnosed when airway obstruction symptoms are present and the disease is at an advanced stage. Early and late symptoms are similar to those in canine patients.³⁰ These regions are affected by a wide variety of tumor types³¹, with very similar histologies.^{32,33,34}

In a study conducted by Dulguerov *et al.* the 5-year survival rate was 40%, and the local control rate was 59%. The prognosis depends on tumor histology, localization, tumor stage, and treatment modality.³⁵ There is a consensus that complete surgical resection should be performed if possible. Surgery and postoperative radiation therapy may result in improved local control, absolute survival and complications when compared with radiation therapy alone.³⁶ Chen *et al.* have not found improvements in disease control or overall survival for patients treated with radiotherapy in the last

five decades.³⁷ Nevertheless, new forms of radiotherapy reduce complications³⁸, and intensity-modulated radiation therapy particularly promises better outcomes when compared to conventional radiotherapy.³⁹ The role of chemotherapy in the neoadjuvant setting and/or postoperatively with irradiation is not clearly defined, but it is generally used for the most advanced cases and requires further investigation.^{34,40}

In such a sensitive region, the proximity of critical normal anatomical structures restricts in many cases the possibility to adequately perform surgery and apply effective radiotherapy.³⁸ Sometimes a tumor is resectable, but the patient's clinical status may preclude surgery or, very often, patients reject it.⁴¹ For these reasons, also in human patients, new approaches for treating nasal tumors are needed.

Besides obvious differences between canine and human nasal tumors, this work shows that nasal tumors can be effectively treated with ECT and further studies should be conducted to validate this treatment in human patients.

Treating nasal tumors in human or canine patients using the ECT with the SiNE could be useful in selected cases where first-line treatments are not possible. It can be especially used to palliate symptoms in patients with short life expectancy, or a poor clinical condition. In any case, it can be performed as a cytoreductive treatment to simplify surgery and does not preclude other treatments.^{42,43,44} Therefore, it remains to be seen whether the use of the SiNE followed by surgery will improve survival, as happens with radiotherapy.

In conclusion, deep nasal tumors in canine patients can be successfully treated by ECT, and it can be safely and effectively performed using the SiNE, especially in tumors that are difficult or impossible to reach with conventional electrodes.

Acknowledgements

F Maglietti holds a scholarship from CONICET, N Olaiz and G Marshall are researchers from CONICET, S Michinski is a CPA-CONICET. This work is supported by grants from Consejo Nacional de Investigaciones Científicas y Técnicas, www.conicet.gov.ar, (PIP 379/2012/2016 and STAN 599/12) and Universidad de Buenos Aires, www.uba.ar, (UBACyT 2014/2017). The funders had no role in study design, data collection and analysis, decision to publish, or preparation of the manuscript. This was proofread by YasminTranslations.com.

Author contributions

FM developed the electrode, worked on the production of the prototype, treated the patients and worked in the preparation of this manuscript. MT selected and treated the patients and collaborated on the preparation of the manuscript. NO was in charge of provision of study material and equipment setup. SM collaborated on the treatment of the patients and the preparation of the manuscript. GM coordinated the group and collaborated on the preparation of the manuscript.

References

1. Withrow SJ, Vail DM, Page R. *Withrow and MacEwen's small animal clinical oncology*. Elsevier Health Sciences; 2013. doi: 10.1111/avj.12086
2. Madewell B, Priestner W, Gillette E, Snyder S. Neoplasms of the nasal passages and paranasal sinuses in domesticated animals as reported by 13 veterinary colleges. *Am J Vet Res* 1976; **37**: 851-6.
3. Marty M, Sersa G, Garbay JR, Gehl J, Collins CG, Snoj M, et al. Electrochemotherapy –An easy, highly effective and safe treatment of cutaneous and subcutaneous metastases: Results of ESOP (European Standard Operating Procedures of Electrochemotherapy) study. *Eur J Cancer Suppl* 2006; **4**: 3-13. doi: 10.1016/j.ejcsup.2006.08.002
4. Cemazar M, Tamzali Y, Sersa G, Tozon N, Mir LM, Miklavcic D, et al. Electrochemotherapy in veterinary oncology. *J Vet Int Med* 2008; **22**: 826-31. doi: 10.1111/j.1939-1676.2008.0117.x
5. Impellizzeri J, Aurisicchio L, Forde P, Soden D. Electroporation in veterinary oncology. *Vet J* 2016; **217**: 18-25. doi: 10.1016/j.tvjl.2016.05.015
6. Kotnik T, Kramar P, Pucihar G, Miklavcic D, Tarek M. Cell membrane electroporation-Part 1: The phenomenon. *Electrical Insulation Magazine, IEEE*. 2012; **28**: 14-23. doi: 10.1109/MEI.2012.6268438
7. Tamzali Y, Borde L, Rols M, Golzio M, Lyazrhi F, Teissie J. Successful treatment of equine sarcoids with cisplatin electrochemotherapy: a retrospective study of 48 cases. *Equine Vet J* 2012; **44**: 214-20. doi: 10.1111/j.2042-3306.2011.00425.x
8. Mali B, Jarm T, Snoj M, Sersa G, Miklavcic D. Antitumor effectiveness of electrochemotherapy: a systematic review and meta-analysis. *EJSO* 2013; **39**: 4-16. doi: https://doi.org/10.1016/j.ejso.2012.08.016.
9. Edhemovic I, Breclj E, Gasljevic G, Marolt Music M, Gorjup V, Mali B, et al. Intraoperative electrochemotherapy of colorectal liver metastases. *J Surg Oncol* 2014; **110**: 320-7. doi: 10.1002/jso.23625
10. Linnert M, Agerholm-Larsen B, Mahmood F, Iversen HK, Gehl J. Treatment of brain tumors: Electrochemotherapy. In: *Tumors of the Central Nervous System*, Volume 12. Springer; 2014. p. 247-59. doi: 10.1007/978-94-007-7217-5_22
11. Fini M, Salamanna F, Parrilli A, Martini L, Cadossi M, Maglio M, et al. Electrochemotherapy is effective in the treatment of rat bone metastases. *Clin Exp Met* 2013; **30**: 1033-45. doi: 10.1007/s10585-013-9601-x
12. Soden DM, Larkin JO, Collins CG, Tangney M, Aarons S, Piggott J, et al. Successful application of targeted electrochemotherapy using novel flexible electrodes and low dose bleomycin to solid tumours. *Cancer Lett* 2006; **232**: 300-10. doi: 10.1016/j.canlet.2005.03.057
13. Campana LG, Clover AJP, Valpione S, Quaglino P, Gehl J, Kunte C, et al. Recommendations for improving the quality of reporting clinical electrochemotherapy studies based on qualitative systematic review. *Radiol Oncol* 2016; **50**: 1-13. doi: 10.1515/raon-2016-0006
14. Mir LM, Gehl J, Sersa G, Collins CG, Garbay JR, Billard V, et al. Standard operating procedures of the electrochemotherapy: instructions for the use of bleomycin or cisplatin administered either systemically or locally and electric pulses delivered by the Cliniporator TM by means of invasive or non-invasive electrodes. *Eur J Cancer Suppl* 2006; **4**: 14-25. doi: 10.1016/j.ejcsup.2006.08.003
15. World Health Organization. *WHO handbook for reporting results of cancer treatment*. Geneva: WHO; 1979.
16. Miklavcic D, Mali B, Kos B, Heller R, Sersa G. Electrochemotherapy: from the drawing board into medical practice. *BioMed Engineering OnLine* 2014; **13**: 29. doi: 10.1186/1475-925X-13-29
17. Suzuki DO, Berkenbrock JA, de Oliveira KD, Freytag JO, Rangel MM. Novel application for electrochemotherapy: Immersion of nasal cavity in dog. *Artif Organs* 2017; **41**: 767-73. doi: 10.1111/aor.12858
18. Adams W, Withrow S, Walshaw R, Turrell J, Evans S, Walker M, et al. Radiotherapy of malignant nasal tumors in 67 dogs. *J Am Vet Med Assoc* 1987; **191**: 311-5.
19. Maruo T, Shida T, Fukuyama Y, Hosaka S, Noda M, Ito T, et al. Retrospective study of canine nasal tumor treated with hypofractionated radiotherapy. *J Vet Med Sci* 2011; **73**: 193-197. doi: 10.1292/jvms.10-0194
20. Dah-Renn F, Daiki K, Ai Watabe YE, Endo Y, Kadosawa T. Prognostic utility of apoptosis index, Ki-67 and survivin expression in dogs with nasal carcinoma treated with orthovoltage radiation therapy. *J Vet Med Sci* 2014; **76**: 1505. doi: 10.1292/jvms.14-0245
21. Northrup NC, Etue SM, Ruslander DM, Rassnick KM, Hutto DL, Bengtson A, et al. Retrospective study of orthovoltage radiation therapy for nasal tumors in 42 dogs. *J Vet Int Med* 2001; **15**: 183-9. doi: 10.1111/j.1939-1676.2001.tb02309.x
22. Kubicek L, Milner R, An Q, Kow K, Chang M, Cooke K, et al. Outcomes and prognostic factors associated with canine sinonasal tumors treated with curative intent cone-based stereotactic radiosurgery (1999-2013). *Vet Radiol Ultrasound* 2016; **57**: 331-40. doi: 10.1111/vru.12349
23. Adams WM, Bjorling DE, McNulty JF, Green EM, Forrest LJ, Vail DM. Outcome of accelerated radiotherapy alone or accelerated radiotherapy followed by exenteration of the nasal cavity in dogs with intranasal neoplasia: 53 cases (1990-2002). *J Am Vet Med Assoc* 2005; **227**: 936-41. doi: 10.2460/javma.2005.227.936
24. Hunley DW, Mauldin GN, Shiomitsu K, Mauldin GE. Clinical outcome in dogs with nasal tumors treated with intensity-modulated radiation therapy. *Can Vet J* 2010; **51**: 293.
25. Domanico R, Trapasso S, Santoro M, Pingitore D, Allegra E. Electrochemotherapy in combination with chemoradiotherapy in the treatment of oral carcinomas in advanced stages of disease: efficacy, safety, and clinical outcomes in a small number of selected cases. *Drug Design Development and Therapy* 2015; **9**: 1185. doi: 10.2147/DDDT.S75752
26. Raeisi E, Aghamiri S, Bandi A, Rahmatpour N, Firoozabadi S, Kafi-Abad S, et al. The antitumor efficiency of combined electrochemotherapy and single dose irradiation on a breast cancer tumor model. *Radiol Oncol* 2012; **46**: 226-32. doi: 10.2478/v10019-012-0035-x
27. Spugnini EP, Fanciulli M, Citro G, Baldi A. Preclinical models in electrochemotherapy: the role of veterinary patients. *Future Oncology* 2012; **8**: 829-37. doi: 10.2217/fon.12.64
28. London CA. Abstract SY28-01: Spontaneous cancer in dogs: opportunities for preclinical evaluation of novel therapies. *Cancer Res* 2011; **71** (8 Suppl): SY28-01. doi: 10.1158/1538-7445.AM2011-SY28-01
29. Holland JF, Hong WK. *Holland-Frei cancer medicine 8*. Hong WK, Bast R, Hait WN, Kufe DW, Pollock RE, Weichselbaum RR, et al, editors. Shelton: People's Medical Publishing House; 2010.
30. Edge SB, Byrd DR, Compton CC, Fritz AG, Greene FL, Trotti A, et al. *AJCC cancer staging manual*. Vol. 649. New York: Springer; 2010. doi: 10.1001/jama.2010.1525
31. Iezzoni JC, Mills SE. "Undifferentiated" small round cell tumors of the sinonasal tract: differential diagnosis update. *Am J Clin Pathol* 2005; **124**(Suppl 1): S110-21. doi: 10.1309/59RBT2RK6LQE4YHB
32. Marcus DM, Marcus RP, Prabhu RS, Owonikoko TK, Lawson DH, Switchenko J, et al. Rising incidence of mucosal melanoma of the head and neck in the United States. *J Skin Cancer* 2012; **2012**: 231693. doi: 10.1155/2012/231693.S
33. Smith SR, Som P, Fahmy A, Lawson W, Sacks S, Brandwein M. A clinicopathological study of sinonasal neuroendocrine carcinoma and sinonasal undifferentiated carcinoma. *Laryngoscope* 2000; **110**: 1617-22. doi: 10.1097/00005537-200010000-00007

34. Mourad WF, Hauerstock D, Shourbaji RA, Hu KS, Culliney B, Li Z, et al. Trimodality management of sinonasal undifferentiated carcinoma and review of the literature. *Am J Clin Oncol* 2013; **36**: 584-8. doi: 10.1097/COC.0b013e31825eb3a5
35. Dulguerov P, Jacobsen MS, Allal AS, Lehmann W, Calcaterra T. Nasal and paranasal sinus carcinoma: are we making progress? *Cancer* 2001; **92**: 3012-29. doi: 10.1002/1097-0142(20011215)92:12
36. Katz TS, Mendenhall WM, Morris CG, Amdur RJ, Hinerman RW, Villaret DB. Malignant tumors of the nasal cavity and paranasal sinuses. *Head & Neck* 2002; **24**: 821-9. doi: 10.1002/hed.10143
37. Chen AM, Daly ME, Buccì MK, Xia P, Akazawa C, Quivey JM, et al. Carcinomas of the paranasal sinuses and nasal cavity treated with radiotherapy at a single institution over five decades: are we making improvement? *Int J Rad Oncol Biol Phys* 2007; **9**: 141-7. doi: 10.1016/j.ijrobp.2007.02.031
38. Porceddu S, Martin J, Shanker G, Weih L, Russell C, Rischin D, et al. Paranasal sinus tumors: Peter MacCallum Cancer Institute experience. *Head Neck* 2004; **26**: 322-30. doi: 10.1002/hed.10388
39. Dirix P, Vanstraelen B, Jorissen M, Vander Poorten V, Nuyts S. Intensity-modulated radiotherapy for sinonasal cancer: improved outcome compared to conventional radiotherapy. *Int J Radiat Oncol Biol Phys* 2010; **78**: 998-1004. doi: 10.1016/j.ijrobp.2009.09.067
40. Sohrabi S, Drabick JJ, Crist H, Goldenberg D, Sheehan JM, Mackley HB. Neoadjuvant concurrent chemoradiation for advanced esthesioneuroblastoma: a case series and review of the literature. *J Clin Oncol* 2011; **29**: e358-61. doi: 10.1200/JCO.2010.30.9278
41. Pfister DG, Ang KK, Brizel DM, Burtneß BA, Busse PM, Caudell JJ, et al. Head and neck cancers, version 2. 2013. *J Natl Compr Canc Netw* 2013; **11**: 917-23. doi: 10.6004/jnccn.2013.0113
42. Spugnini EP, Citro G, Baldi A. Adjuvant electrochemotherapy in veterinary patients: a model for the planning of future therapies in humans. *J Exp Clin Cancer Res* 2009; **28**: 1. doi: 10.1186/1756-9966-28-114
43. Lowe R, Gavazza A, Impellizeri J, Soden D, Lubas G. The treatment of canine mast cell tumours with electrochemotherapy with or without surgical excision. *Vet Comp Oncol* 2017; **15**: 775-84. doi: 10.1111/vco.12217
44. Spugnini E, Vincenzi B, Citro G, Dotsinsky I, Mudrov T, Baldi A. Evaluation of Cisplatin as an electrochemotherapy agent for the treatment of incompletely excised mast cell tumors in dogs. *J Vet Int Med* 2011; **25**: 407-411. doi: 10.1111/j.1939-1676.2011.0678.x

Metformin enhanced *in vitro* radiosensitivity associates with G2/M cell cycle arrest and elevated adenosine-5'-monophosphate-activated protein kinase levels in glioblastoma

Sebastian Adeberg^{1,4}, Denise Bernhardt^{1,3,4}, Semi B. Harrabi^{1,3,4}, Nils H. Nicolay^{1,4}, Juliane Hörner-Rieber^{1,3,4}, Laila König^{1,3,4}, Michael Repka⁵, Angela Mohr^{1,3,4}, Amir Abdollahi^{1,3,4,6}, Klaus-Josef Weber^{1,4}, Juergen Debus^{1,4}, Stefan Rieken^{1,3,4}

¹ University Hospital of Heidelberg, Department of Radiation Oncology, Heidelberg, Germany

² Clinical Cooperation Unit Radiation Oncology, German Cancer Research Center (DKFZ), Heidelberg, Germany

³ Heidelberg Ion-Beam Therapy Center (HIT), Heidelberg, Germany

⁴ Heidelberg Institute for Radiation Oncology, University Hospital of Heidelberg, Heidelberg, Germany

⁵ Department of Radiation Medicine, Georgetown University Hospital, Washington DC, USA

⁶ Translational Radiation Oncology, German Cancer Consortium (DKTK), National Center for Tumor Diseases German Cancer Research Center (DKFZ), Heidelberg, Germany

Radiol Oncol 2017; 51(4): 431-437.

Received 12 February 2017
Accepted 30 September 2017

Presented in part at the Annual Meeting of the German Society of Radiation Oncology (DEGRO), 15th - 18th June 2017, Berlin, Germany

Correspondence to: Sebastian Adeberg, M.D., University Hospital of Heidelberg, Department of Radiation Oncology, Im Neuenheimer Feld 400, 69120 Heidelberg, Germany. Phone: +49 6221 5635654; Fax: +49 6221 56565353; Email: sebastian.adeberg@med.uni-heidelberg.de

Disclosure: No potential conflicts of interest were disclosed.

Background. It is hypothesized that metabolism plays a strong role in cancer cell regulation. We have recently demonstrated improved progression-free survival in patients with glioblastoma who received metformin as an antidiabetic substance during chemoradiation. Although metformin is well-established in clinical use the influence of metformin in glioblastoma is far from being understood especially in combination with other treatment modalities such as radiation and temozolomide.

Materials and methods. In this study, we examined the influence of metformin in combinations with radiation and temozolomide on cell survival (clonogenic survival), cell cycle (routine flow cytometric analysis, FACScan), and phosphorylated Adenosine-5'-monophosphate-activated protein kinase (AMPK) (Phospho-AMPKalpha1 - ELISA) levels in glioblastoma cell lines LN18 and LN229.

Results. Metformin and temozolomide enhanced the effectiveness of photon irradiation in glioblastoma cells. Cell toxicity was more pronounced in O⁶-methylguanine DNA methyltransferase (MGMT) promoter non-methylated LN18 cells. Induction of a G2/M phase cell cycle block through metformin and combined treatments was observed up to 72 h. These findings were associated with elevated levels of activated AMPK levels in LN229 cells but not in LN18 cells after irradiation, metformin, and temozolomide treatment.

Conclusions. Radiosensitizing effects of metformin on glioblastoma cells treated with irradiation and temozolomide *in vitro* coincided with G2/M arrest and changes in pAMPK levels.

Key words: metformin; glycolysis; metabolism; gliomas; proliferation; cell cycle

Introduction

The relationship of tumorigenesis, and tumor cell metabolism by an increased glycolysis was

first described in the early 20th century by Otto Warburg.^{1,2} Multiple modifications in cancer cell metabolism have subsequently been detected, but the influence on alterations in signaling path-

ways, cell growth, and therapy response is not yet understood. Nonetheless, tumor cell metabolism represents an intriguing potential target in the multidisciplinary treatment of cancer. The addition of metabolically active substances, particularly those with limited toxicity, with chemotherapy and radiation is an area of active research. In this context, the antidiabetic medication metformin is of particular interest as it demonstrated prolonged progression-free survival in a retrospective study in diabetic patients with glioblastoma (GBM).³ The primary glucoregulatory effects of metformin are predominantly explained through reduced hepatic glucose production and increased glucose uptake in the periphery.⁴ These effects lead to decreased mitochondrial-dependent ATP production and cell proliferation, increased glycolytic ATP production, induction of cell cycle arrest, autophagy, and apoptotic processes through activation of adenosine-5'-monophosphate-activated protein kinase (AMPK)⁵ and inhibition of the mTOR (mammalian target of rapamycin) pathway in glioblastoma cells.^{6,7}

AMPK is a serine/threonine kinase that functions as a cellular energy sensor. AMPK is an obligate heterotrimer, consisting of one catalytic subunit (α) and two regulatory subunits (β and γ).⁸ Under cellular stress conditions, AMPK is activated by increased AMP-to-ATP ratios to promote catabolism and inhibit anabolism.⁸ High cellular activated AMPK levels, particularly by phosphorylation (pAMPK), seems to be associated with tumor cell growth and cell survival.^{9,10} Furthermore, increased AMPK phosphorylation has been observed in cells following radiation-induced DNA damage in several studies.^{7,11,12} The activation of AMPK is hypothesized to regulate irradiation-induced metabolism changes and might be a key determinant of cell survival after exposure to ionizing radiation.⁷ The AMPK pathway is therefore a potential objective for targeted therapies. Although the concomitant application of metformin with temozolomide (TMZ) and this effect is not well understood. In this study, we investigated the effects of metformin effect in combination with current standard of care therapy in glioblastoma cell lines.

Materials and methods

Cell lines and culture conditions

Two representative human GBM cell lines (ATCC; Manassas, VA, USA) were utilized in this study. LN18 is a GBM cell line with a mutant tumor sup-

pressor protein 53 (p53mut) and an un-methylated O⁶-methylguanine DNA methyltransferase (MGMT) promoter. LN229 is a GBM cell line with both mutant and wild type p53 (p53 mut/WT) and a methylated MGMT promoter. Both cell lines were cultured in Dulbeccos's modified Eagle medium (Biochrom, Berlin, Germany) supplemented with 10% Fetal Calf Serum (FCS) superior (Biochrom AG) and 1% penicillin/streptomycin (Gibco, Darmstadt, Germany). Cultures were maintained in exponential monolayer at incubator conditions with 37°C, 5% CO₂, and 95% humidity.

Drug treatment and irradiation

We performed clonogenic assays to evaluate treatment effects on cell survival. Low passage cells were plated in T25 flasks (Becton, Dickinson, Heidelberg, Germany) with 5 ml medium as described previously.¹³ TMZ was obtained by Schering-Plough (Kenilworth, NJ, USA) and dissolved in dimethyl sulfoxide (DMSO) (Sigma-Aldrich, Deisenhofen, Germany) at concentrations < 0.5%. Cell samples were incubated with 10 μ M or 50 μ M TMZ for 4 hours prior to irradiation. 1,1-Dimethylbiguanide hydrochloride (metformin; 97%) was provided by Sigma-Aldrich Chemie GmbH (Steinheim, Germany) and applied in concentrations of 1 mM or 20 mM for 24 hours prior to irradiation. Immediately prior to irradiation, all samples were rinsed twice with phosphate buffered saline and fresh medium was added. Adherent cells were irradiated using a 6MV photon linear accelerator (XRAD 320 Precision X-ray Inc., N.Bradford, USA) with single photon doses up to 6 Gy. Cells were fixed with 70% ethanol and stained with methylene blue. Colonies of > 50 were counted. Experiments were repeated in triplicate at least three times.

Cell cycle analyses

To evaluate cell cycle distributions, cells were harvested, washed and fixed in ice-cold 70% ethanol after 24, 48 or 72 hours and stained with propidium iodide (Sigma-Aldrich). 10.000 events were counted for each experimental setup with routine flow cytometric analysis (FACScan, Becton-Dickinson, Heidelberg, Germany). Histograms were created and analyzed using ModFit software (Verity Software House, Topsham, ME, USA). Each experiment was repeated at least three times on different days for validation.

Phospho-AMPK α 1 - ELISA

ELISA for pAMPK levels in LN229 and LN18 cell lysates was performed by commercially available DuoSet ELISA development kits (R&D Systems, Minneapolis, USA) according to the manufacturer's instruction using goat anti-human AMPK α 1 (T183) as primary antibody and biotinylated rabbit anti-human phospho-AMPK α 1 (T183) as secondary antibody. Recombinant human phospho-AMPK α 1 (T183) was utilized as standard. The results were presented as relative values to the control value, which was set as 1. Data analysis was carried out using the Infinite® F50/Robotic ELISA plate reader (absorbance at 450 nm, correction wavelength at 570 nm) and Magellan for F50 software (Tecan Group Ltd, Crailsheim, Germany). Measurements were repeated at least three times on three different days.

Statistical analysis

Clonogenic survival was calculated from the measured plating efficiencies. With the data of the combined treatment approaches survival curves were generated with the linear quadratic (LQ) - model as described earlier.¹⁴ Sigma Plot's (Systat Software GmbH, Erkrath, Germany) non-linear least-squares regression option was used to fit the calculated survival curves. Clonogenic survival was calculated using the sensitizer enhancement ratio (SER), comparing the radiation dose at 20% cell survival, due to the high efficiency of TMZ and metformin on cellular killing.

$$SER = \frac{\text{radiation dose without sensitizer}}{\text{radiation dose with sensitizer}}$$

The Student's two-sided t-test was used for comparison of cell survival curves, differences in cell cycle analysis distribution and pAMPK levels. Data are shown as mean values \pm standard deviation. Statistical significance was set at $p < 0.05$.

Results

Metformin enhances the effectiveness of irradiation in glioblastoma cells

Metformin sensitivity of glioblastoma cell lines LN18 and LN229 was investigated by clonogenic survival assays. Increasing concentrations of metformin (1 mM and 20 mM) and TMZ (10 μ M and 50 μ M) were chosen for all baseline experiments. Representative concentrations (20 mM metformin

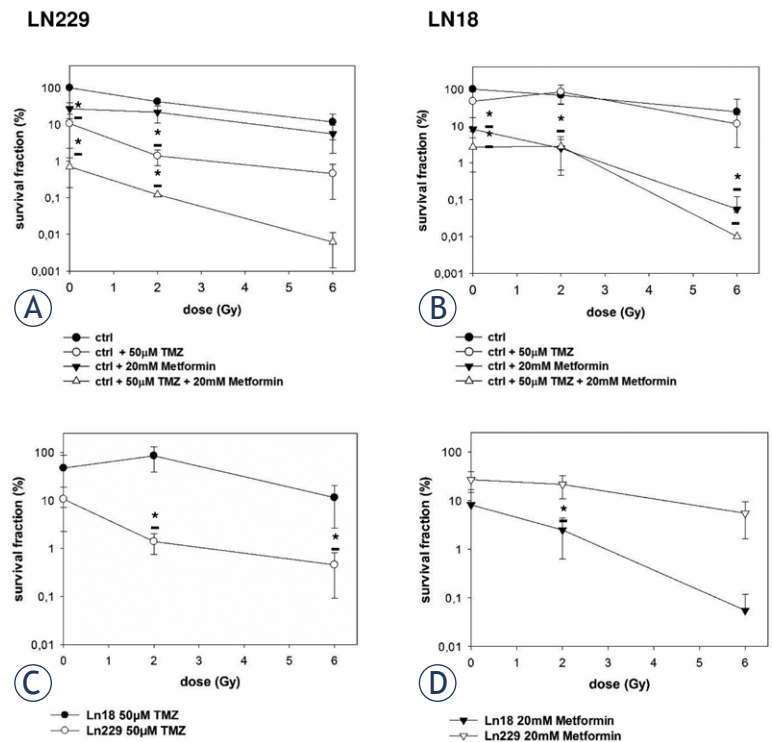


FIGURE 1. (A,B) Clonogenic survival assays of LN229 and LN18 glioblastoma cell lines after treatment with photon irradiation. (C,D) Clonogenic survival assays after comparing LN229 and LN18 cell lines after combined treatment with TMZ (C) or metformin (D). Error bars represent standard deviations. * shows a statistical significance ($P < 0.05$). In LN229 enhanced cell kill was observed by TMZ and in LN18 cells lines metformin treatment resulted in increased cell toxicity compared to the control, as well as the combination of both agents itself. Combined bimodal and trimodal treatment results in superior cell toxicity.

in and 50 μ M TMZ) were chosen for subsequent combined experiments. Clonogenic survival of the MGMT promoter methylated LN229 cell line was significantly reduced after treatment with TMZ compared to the untreated control and LN18 cell lines. Combined treatment approaches with irradiation

TABLE 1. Sensitizer enhancement ratio (SER 20%) for LN229 and LN18 cells after treatment with metformin, temozolomide (TMZ) and combined treatment with 2Gy irradiation

SER (20% survival) / 2 Gy		
Cell line	LN18	LN229
50 μ M TMZ	1.11	2.15
1 mM Metformin	0.67	0.74
20 mM Metformin	3.13	0.61
50 μ M TMZ + 20 mM Metformin	2.57	2.69

SER values (ranging from 0.67–3.13) depending on cell line, chemotherapeutic agent and dose

TABLE 2. Cell cycle distribution into G1, S, and G2/M phase of LN18 and LN229 cells after various treatments. Measurements were performed after 72h. * shows a statistical significance ($P < 0.05$) of the treatment compared to the control

Ln18 24h	72h	G1 (%) ± std.dev.	S (%) ± std.dev.	G2/M (%) ± std.dev.
Ctrl		74.5 ± 8	5.6 ± 0	19.9 ± 1
50µM TMZ		66.0 ± 8	9.5 ± 1	24.6 ± 3
1mM Metformin		71.0 ± 5	6.3 ± 1	22.7 ± 0
20mM Metformin		46.9 ± 3	9.3 ± 2	43.8 ± 2*
50µM TMZ + 1mM Metformin		64.5 ± 0	8.6 ± 4	26.9 ± 4
50µM TMZ + 20mM Metformin		41.2 ± 0	19.4 ± 7	39.4 ± 2
2Gy		71.7 ± 1	7.5 ± 1	20.8 ± 4
6Gy		56.2 ± 5	8.0 ± 1	35.7 ± 1
2Gy + 50µM TMZ		62.0 ± 5	6.6 ± 5	31.4 ± 4
2Gy + 1mM Metformin		68.2 ± 7	10.3 ± 1	21.5 ± 2
2 Gy + 20mM Metformin		41.3 ± 0	16.1 ± 1	42.6 ± 4*
2Gy + 50µM TMZ + 1mM Metformin		60.1 ± 7	8.6 ± 1	31.3 ± 0
2Gy + 50µM TMZ + 20mM Metformin		33.5 ± 2	20.0 ± 3	46.5 ± 4*
6Gy + 50µM TMZ		47.1 ± 7	11.6 ± 3	41.3 ± 3*
6Gy + 1mM Metformin		51.3 ± 2	10.4 ± 0	38.2 ± 3
6Gy + 20mM Metformin		36.1 ± 3	14.2 ± 0	49.7 ± 3*
6Gy + 50µM TMZ + 1mM Metformin		46.3 ± 4	10.7 ± 1	42.9 ± 2*
6Gy + 50µM TMZ + 20mM Metformin		27.9 ± 1	14.1 ± 3	58.0 ± 2*

Ln229 24h	72h	G1 (%)	S (%)	G2/M (%)
Ctrl		86.0 ± 2	3.6 ± 2	10.4 ± 2
50µM TMZ		37.4 ± 3	8.1 ± 2	54.6 ± 5*
1mM Metformin		87.4 ± 3	3.3 ± 1	9.3 ± 0
20mM Metformin		63.9 ± 10	14.9 ± 1	21.2 ± 9
50µM TMZ + 1mM Metformin		38.9 ± 0	6.1 ± 2	55.0 ± 4*
50µM TMZ + 20mM Metformin		25.2 ± 1	25.4 ± 2	49.4 ± 2*
2Gy		83.5 ± 5	3.3 ± 2	13.2 ± 5
6Gy		67.1 ± 2	6.2 ± 1	26.7 ± 1
2Gy + 50µM TMZ		44.4 ± 1	6.9 ± 1	48.7 ± 4*
2Gy + 1mM Metformin		82.3 ± 1	3.5 ± 1	14.2 ± 2
2 Gy + 20mM Metformin		55.6 ± 2	11.8 ± 2	32.6 ± 1*
2Gy + 50µM TMZ + 1mM Metformin		46.0 ± 1	7.9 ± 1	46.1 ± 0*
2Gy + 50µM TMZ + 20mM Metformin		32.3 ± 3	28.9 ± 7	38.8 ± 5*
6Gy + 50µM TMZ		41.6 ± 2	8.9 ± 3	49.5 ± 3
6Gy + 1mM Metformin		55.5 ± 11	8.8 ± 4	35.7 ± 23
6Gy + 20mM Metformin		56.5 ± 18	7.8 ± 6	35.7 ± 16
6Gy + 50µM TMZ + 1mM Metformin		41.9 ± 2	5.9 ± 2	52.2 ± 2*
6Gy + 50µM TMZ + 20mM Metformin		18.4 ± 1	16.2 ± 3	65.4 ± 3*

diation, TMZ and metformin showed additive cell toxicity compared to the control ($P < 0.05$, Student's t-test) (Figure 1A,B and Table 1). Furthermore, clonogenic survival after metformin exposure was reduced in LN18 cells when compared to the untreated control and to LN229 cells ($P < 0.05$) (Figure 1C,D and Table 1). Additionally, additive cell toxicity could be reached in LN229 cells adding ionizing irradiation (2 Gy and 6 Gy) to TMZ and Metformin, whereas additional effects with ionizing irradiation could only be reached for metformin in LN18 cells.

Metformin induces a G2/M phase block in combination with irradiation

Cell cycle assessment of glioblastoma cell lines was carried out using FACS analyses. Exposure to metformin (20 mM) resulted in accumulation at G2/M phases after 72 hours to a higher degree in LN18 cells (G2 phase cells: ctrl vs 20mM metformin: 19.9% vs 43.8%). However, the results did not reach statistical significance. Combined treatment approaches with irradiation and metformin resulted in a more pronounced G2/M block after 72 hours ($P < 0.05$, Student's t-test) (Table 2). Accumulations in G2/M phases after 72 hours were even more marked when using higher radiation doses (6 Gy) (Table 2) and trimodal approaches with irradiation, 50 µM TMZ, and 20 mM metformin ($P < 0.05$, Student's t-test) (Table 2). Analysis of sub-G1 populations indicating apoptosis did not show any measurable results.

Irradiation, TMZ and metformin enhance activated AMPK levels in glioblastoma cells

Phosphorylated serine/threonine kinase AMPK levels induced by irradiation, TMZ, and metformin exposure were investigated as a potential mechanism for the described metformin sensitivity of glioblastoma cell lines. Increased pAMPK levels were demonstrated in LN229 cells after treatment with the following regimens: 2 Gy + 50 µM TMZ, 2 Gy + 20 mM metformin, 2 Gy + 50 µM TMZ + 20 mM metformin, 6 Gy, 6 Gy + 50 µM TMZ, 6 Gy + 20 mM metformin, and 6 Gy + 50 µM TMZ + 20 mM metformin ($P < 0.05$, Student's t-test) (Figure 2A). All other treatment approaches showed a trend towards higher pAMPK levels in LN229 cells ($P < 0.1$, Student's t-test). Higher radiation doses were associated with increased pAMPK levels ($P < 0.05$, Student's t-test) (Figure 2A). Interestingly, LN229

demonstrated a twofold higher level of pAMPK after treatment with 6 Gy compared to the untreated control ($P < 0.05$, Student's t-test). pAMPK measurements obtained from LN18 cell lines did not show a significant increase after each treatment combination (Figure 2B).

Discussion

Standard of care multidisciplinary management of GBM entails surgical resection followed by radiotherapy with concomitant and adjuvant TMZ, resulting in overall survival rates of approximately one year. Given this dismal prognosis, the need to improve the efficacy of chemoradiation for these common primary brain tumors is urgent. Recently, we demonstrated improved progression-free survival rates in diabetic patients receiving metformin³, a biguanide that is commonly used and well tolerated in patients with type II diabetes. Accordingly, combined approaches targeting cell metabolism became attractive. Metformin is known to exhibit anticancer effects via LKB1/AMPK/mTOR/S6K1 pathway blockade^{15,16}, inhibition of tumor growth^{17,18} and induction of autophagy and apoptosis^{19,20} in various cancer cell lines. Accordingly, integration of approaches targeting cell metabolism into standard therapy is an attractive area of investigation. In the present study, we examined the interaction of metformin in combination with photon irradiation and the alkylating agent TMZ. Furthermore, we demonstrated that metformin has antitumoral effects and increases sensitivity to ionizing radiation, which was particularly pronounced in a non-MGMT methylated cell line (LN18).

Of note, both the LN18 and LN229 cell lines express wildtype for PTEN, which is associated with increased sensitivity to metformin.⁶ This susceptibility may be explained by opposing PI3K signaling, thus leading to a down-regulated AKT survival pathway and decreased glucose consumption.⁶ Therefore, the higher metformin sensitivity for LN18 cannot solely be explained by the more effective deactivation of AKT in these cells. The authors believe the MGMT promoter methylation in metformin sensitive LN18 cells is rather a coincident than the cause of this finding. In fact, glioma cells are known to have a high intrinsic radiation sensitivity caused by several intrinsic factors such as high efficient radiation damage repair, a high ratio of hypoxic cell fraction and rapid repopulation following irradiation.²¹ The intrinsic sensitivity of

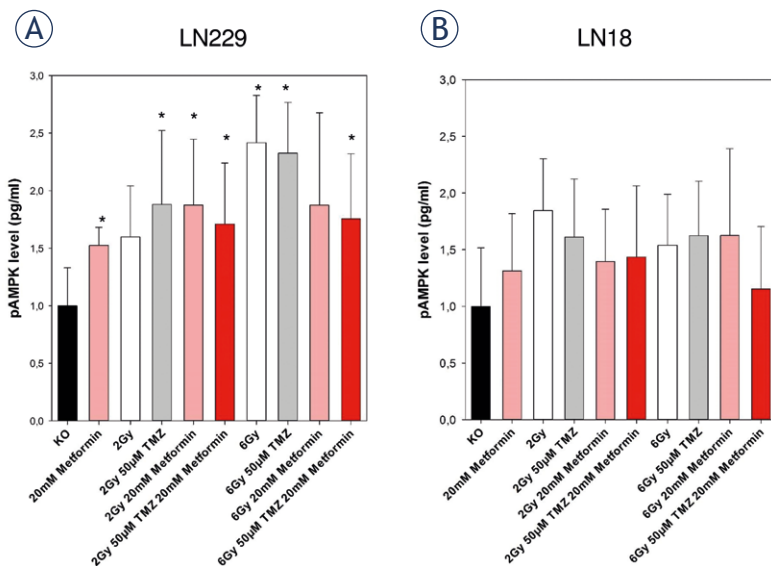


FIGURE 2. (A) In LN229 pAMPK measurements were significantly increased after treatment with Metformin, 2 Gy and temozolomide and 6 Gy combined with Metformin compared to the control if not otherwise specified (* $p < 0.05$). (B) No significant increase of pAMPK levels were observed in cell line LN18. Error bars represent standard deviation.

GBM cells is probably independent of the MGMT promoter methylation status. The mechanistic effects of these findings are beyond the scope of this manuscript and will be evaluated in future experiments. An inverse effect was shown for TMZ, where the MGMT promoter-methylated LN229 cells were more sensitive to TMZ compared to MGMT promoter non-methylated LN18 cells. This finding can be explained by the lack of the MGMT DNA-repair protein in LN229 cells which normally removes O6-MG-DNA and counteracts the anti-neoplastic effect of TMZ.²²

We performed cell cycle analyses in order to further investigate the antiproliferative effects of metformin on glioblastoma cell lines. In PTEN wild-type cells, cytotoxic effects have been described starting at 48 hours.⁶ However, in LN18 and LN229 cell lines, significant increase of G2/M block rates started delayed, chiefly 72 hours after irradiation. This effect was pronounced in combined treatment approaches with higher radiation doses and TMZ administration. These results indicate that the antiproliferative effects of metformin on glioblastoma cell lines might be mediated through cell cycle arrest starting at 72 hours post-exposure. These results are in line with results from *in vitro* data of Yu *et al.* who observed G2/M cell cycle arrests after TMZ and metformin. A combined treatment showed synergistic effects.²³ In a former study G1 arrests were described after metformin exposure,

whereas mainly G2/M phase arrests were observed in the current study. This effect might be due to the two-fold metformin dose (10 nM vs 20 nM) with varying impact. Furthermore metformin effects were mainly observed after 72 hours but the observation period of Sesen *et al.* ended after 48 hours.⁶ Nevertheless, molecular mechanisms of metformin are far from understood and further research to examine its role in tumor cell metabolism is necessary.

Previous studies have demonstrated that activation of AMPK leads to an inhibition of mTOR^{6,15,24,25} and is essential for glioma proliferation by promoting cell cycle progression *in vitro* and *in vivo*.²⁶ These findings are supported by reports indicating a major AMPK phosphorylation and activation through the tumor suppressor LKB1.²⁷⁻²⁹ Furthermore, AMPK has been associated with p53-dependent apoptosis through p53 phosphorylation³⁰, underlining the potential function of AMPK activation as an “energy checkpoint”.³¹ This proposed mechanism permits proliferation and cell growth in cells with intact AMPK signaling only in favorable metabolic cell conditions. Conversely, cancer cells with deficient AMPK signaling might be capable of receiving a metabolism-independent growth stimulus. In these cases, induction of AMPK activation could present a valuable therapeutic approach.²⁶ Although the role of AMPK as a metabolic sensor in homeostasis is well described, its function in cancer remains opaque. *In vitro* studies have shown highly efficient inhibition of tumor cell growth across multiple glioblastoma cell lines with several AMPK agonists, including 5-aminoimidazole-4-carboxamide ribonucleotide (AICAR) and activated AMPK adenovirus.³²⁻³⁵

In this study, we demonstrated a dose-dependent increase of AMPK in LN229 glioblastoma cells following radiation in combination with metformin and TMZ. Although AMPK level changes did not show statistically significant changes in the LN18 cell line, the radiosensitizing effect of metformin was more pronounced in these cells. Another reason for the absent of significant findings could be attributed to a high standard deviation masking subtle changes (Figure 4B). The authors carefully performed pAMPK level measurements with at least n=3. Even though, future in-depth analyses may help to unmask subtle changes. Interestingly, the failure of LN18 to phosphorylate AMPK compared to LN 229 cells could be a reason for the enhanced radiosensitivity in the latter, since AMPK activation might be a keyregulator for glioma cell proliferation.²⁶ On the other hand, it is likely that

metformin exhibits both AMPK dependent and AMPK-independent effects which are contingent on molecular tumor characteristics.^{6,15}

Taken together, the present finding that activated AMPK levels are elevated after treatment with radiation, TMZ, and metformin contributes to the understanding of GBM metabolism following therapeutic intervention. However, more detailed knowledge of the antitumoral effects of metformin, the role of AMPK, and tumor cell biology is necessary to establish a novel multidisciplinary approach to glioblastoma therapy. We planned to perform mechanistic *in vitro* metformin experiments in the future based on the current baseline results. Additional challenges, including the ability of AMPK activating agents such as AICAR to cross the blood brain barrier more effectively, are ongoing. Nonetheless, our results suggest that the development of an AMPK activating agent with high central nervous system bioavailability may be a promising new therapeutic avenue in the treatment of this aggressive malignancy.

Conclusions

Together with our previously published clinical findings³ and the well-established use of metformin in clinical practice, these data show that radiosensitizing effects of metformin on glioblastoma cells treated with irradiation and temozolomide *in vitro* coincided with G2/M arrest and changes in pAMPK levels.

Acknowledgement

The authors thank Mrs Lena Orschiedt and Mrs Sigrid Daffinger for excellent technical assistance.

References

1. Warburg O, Wind F, Negelein E. The metabolism of tumors in the Body. *J Gen Physiol* 1927; **8**: 519-30.
2. Warburg O. On the origin of cancer cells. *Science* 1956; **123**: 309-14.
3. Adeberg S, Bernhardt D, Harrabi SB, Bostel T, Mohr A, Koelsche C, et al. Metformin influences progression in diabetic glioblastoma patients. *Strahlentherapie Onkol* 2015; **191**: 928-35. doi: 10.1007/s00066-015-0884-5
4. Goodarzi MO, Bryer-Ash M. Metformin revisited: re-evaluation of its properties and role in the pharmacopoeia of modern antidiabetic agents. *Diabetes Obes Metab* 2005; **7**: 654-65. doi: 10.1111/j.1463-1326.2004.00448
5. Zhou G, Myers R, Li Y, Chen Y, Shen X, Fenyk-Melody J, et al. Role of AMP-activated protein kinase in mechanism of metformin action. *J Clin Invest* 2001; **108**: 1167-74. doi: 10.1172/JCI13505

6. Sesen J, Dahan P, Scotland SJ, Saland E, Dang VT, Lemarie A, et al. Metformin inhibits growth of human glioblastoma cells and enhances therapeutic response. *PLoS One* 2015; **10**: e0123721. doi: 10.1371/journal.pone.0123721
7. Zannella VE, Cojocari D, Hilgendorf S, Vellanki RN, Chung S, Wouters BG, et al. AMPK regulates metabolism and survival in response to ionizing radiation. *Radiother Oncol* 2011; **99**: 293-9. doi: 10.1016/j.radonc.2011.05.049
8. Steinberg GR, Kemp BE. AMPK in health and disease. *Physiol Review* 2009; **89**: 1025-78. doi: 10.1152/physrev.00011.2008
9. Jang T, Caloagan JM, Kwon E, Samuelsson S, Recht L, Laderoute KR. 5'-AMP-activated protein kinase activity is elevated early during primary brain tumor development in the rat. *Int J Cancer* 2011; **128**: 2230-9. doi: 10.1002/ijc.25558
10. Park HU, Suy S, Danner M, Dailey V, Zhang Y, Li H, et al. AMP-activated protein kinase promotes human prostate cancer cell growth and survival. *Mol Cancer Ther* 2009; **8**: 733-41. doi: 10.1158/1535-7163
11. Sanli T, Rashid A, Liu C, Harding S, Bristow RG, Cutz JC, et al. Ionizing radiation activates AMP-activated protein kinase (AMPK): a target for radiosensitization of human cancer cells. *Int J Radiat Oncol Biol Phys* 2010; **78**: 221-9. doi: 10.1016/j.ijrobp
12. Zhang WB, Wang Z, Shu F, Jin YH, Liu HY, Wang QJ, et al. Activation of AMP-activated protein kinase by temozolomide contributes to apoptosis in glioblastoma cells via p53 activation and mTORC1 inhibition. *J Biol Chem* 2010; **285**: 40461-71. doi: 10.1074/jbc.M110.164046
13. Bischof M, Abdollahi A, Gong P, Stoffregen C, Lipson KE, Debus JU, et al. Triple combination of irradiation, chemotherapy (pemetrexed), and VEGFR inhibition (SU5416) in human endothelial and tumor cells. *Int J Radiat Oncol Biol Phys* 2004; **60**: 1220-32. doi: 10.1016/j.ijrobp
14. Combs SE, Bohl J, Elsasser T, Weber KJ, Schulz-Ertner D, Debus J, et al. Radiobiological evaluation and correlation with the local effect model (LEM) of carbon ion radiation therapy and temozolomide in glioblastoma cell lines. *Int J Radiat Biol* 2009; **85**: 126-37. doi: 10.1080/09553000802641151
15. Liu X, Chhipa RR, Pooya S, Wortman M, Yachyshin S, Chow LM, et al. Discrete mechanisms of mTOR and cell cycle regulation by AMPK agonists independent of AMPK. *Proc Natl Acad Sci U S A* 2014; **111**: E435-44. doi: 10.1073/pnas.1311121111
16. Wurth R, Pattarozzi A, Gatti M, Bajetto A, Corsaro A, Parodi A, et al. Metformin selectively affects human glioblastoma tumor-initiating cell viability: A role for metformin-induced inhibition of Akt. *Cell Cycle* 2013; **12**: 145-56. doi: 10.4161/cc.23050
17. Janjetovic K, Harhaji-Trajkovic L, Misirkic-Marjanovic M, Vucicevic L, Stevanovic D, Zogovic N, et al. In vitro and in vivo anti-melanoma action of metformin. *Eur J Pharmacol* 2011; **668**: 373-82. doi: 10.1016/j.ejphar
18. Scotland S, Saland E, Skuli N, de Toni F, Boutzen H, Micklow E, et al. Mitochondrial energetic and AKT status mediate metabolic effects and apoptosis of metformin in human leukemic cells. *Leukemia* 2013; **27**: 2129-38. doi: 10.1038/leu
19. Feng Y, Ke C, Tang Q, Dong H, Zheng X, Lin W, et al. Metformin promotes autophagy and apoptosis in esophageal squamous cell carcinoma by down-regulating Stat3 signaling. *Cell Death Dis* 2014; **5**: e1088. doi: 10.1038/cddis
20. Tomic T, Botton T, Cerezo M, Robert G, Luciano F, Puissant A, et al. Metformin inhibits melanoma development through autophagy and apoptosis mechanisms. *Cell Death Dis* 2011; **2**: e199. doi: 10.1038/cddis
21. Taghian A, Suit H, Pardo F, Gioioso D, Tomkinson K, DuBois W, et al. In vitro intrinsic radiation sensitivity of glioblastoma multiforme. *Int J Radiat Oncol Biol Phys* 1992; **23**: 55-62.
22. Harrabi S, Combs SE, Brons S, Haberer T, Debus J, Weber KJ. Temozolomide in combination with carbon ion or photon irradiation in glioblastoma multiforme cell lines - does scheduling matter? *Int J Radiat Biol* 2013; **89**: 692-7. doi: 10.3109/09553002
23. Yu Z, Zhao G, Li P, Li Y, Zhou G, Chen Y, et al. Temozolomide in combination with metformin act synergistically to inhibit proliferation and expansion of glioma stem-like cells. *Oncol Lett* 2016; **11**: 2792-800. doi: 10.3892/ol.2016.4315
24. Shi WY, Xiao D, Wang L, Dong LH, Yan ZX, Shen ZX, et al. Therapeutic metformin/AMPK activation blocked lymphoma cell growth via inhibition of mTOR pathway and induction of autophagy. *Cell Death Dis* 2012; **3**: e275. doi: 10.1038/cddis
25. Zheng B, Jeong JH, Asara JM, Yuan YY, Granter SR, Chin L, et al. Oncogenic B-RAF negatively regulates the tumor suppressor LKB1 to promote melanoma cell proliferation. *Mol Cell* 2009; **33**: 237-47. doi: 10.1016/j.molcel.2008.12.026
26. Rios M, Foretz M, Viollet B, Prieto A, Fraga M, Costoya JA, et al. AMPK activation by oncogenesis is required to maintain cancer cell proliferation in astrocytic tumors. *Cancer Res* 2013; **73**: 2628-38. doi: 10.1158/0008-5472
27. Hawley SA, Boudeau J, Reid JL, Mustard KJ, Udd L, Makela TP, et al. Complexes between the LKB1 tumor suppressor, STRAD alpha/beta and MO25 alpha/beta are upstream kinases in the AMP-activated protein kinase cascade. *J Biol* 2003; **2**: 28. doi: 10.1186/1475-4924-2-28
28. Shaw RJ, Kosmatka M, Bardeesy N, Hurley RL, Witters LA, DePinho RA, et al. The tumor suppressor LKB1 kinase directly activates AMP-activated kinase and regulates apoptosis in response to energy stress. *Proc Natl Acad Sci U S A* 2004; **101**: 3329-35. doi: 10.1073/pnas.0308061100
29. Woods A, Johnstone SR, Dickerson K, Leiper FC, Fryer LG, Neumann D, et al. LKB1 is the upstream kinase in the AMP-activated protein kinase cascade. *Curr Biol* 2003; **13**: 2004-8.
30. Jones RG, Plas DR, Kubek S, Buzzai M, Mu J, Xu Y, et al. AMP-activated protein kinase induces a p53-dependent metabolic checkpoint. *Mol Cell* 2005; **18**: 283-93. doi: 10.1016/j.molcel
31. Fogarty S, Hardie DG. Development of protein kinase activators: AMPK as a target in metabolic disorders and cancer. *Biochim Biophys Acta* 2010; **1804**: 581-91. doi: 10.1016/j.bbapap
32. Guo D, Cloughesy TF, Radu CG, Mischel PS. AMPK: A metabolic checkpoint that regulates the growth of EGFR activated glioblastomas. *Cell Cycle* 2010; **9**: 211-2. doi: 10.4161/cc
33. Isakovic A, Harhaji L, Stevanovic D, Markovic Z, Sumarac-Dumanovic M, Starcevic V, et al. Dual anti-glioma action of metformin: cell cycle arrest and mitochondria-dependent apoptosis. *Cell Mol Life Sci* 2007; **64**: 1290-302. doi: 10.1007/s00018-007-7080-4
34. Kifalvi K, Eibl G, Sinnott-Smith J, Rozengurt E. Metformin disrupts crosstalk between G protein-coupled receptor and insulin receptor signaling systems and inhibits pancreatic cancer growth. *Cancer Res* 2009; **69**: 6539-45. doi: 10.1158/0008-5472.CAN-09-0418
35. Sato A, Sunayama J, Okada M, Watanabe E, Seino S, Shibuya K, et al. Glioma-initiating cell elimination by metformin activation of FOXO3 via AMPK. *Stem Cell Trans Med* 2012; **1**: 811-24. doi: 10.5966/sctm.2012-0058

Evaluation of deformable image registration (DIR) methods for dose accumulation in nasopharyngeal cancer patients during radiotherapy

Wannapha Nobnop^{1,2}, Imjai Chitapanarux², Hudsaleark Neamin¹, Somsak Wanwilairat², Vicharn Lorvidhaya², Taweap Sanghangthum³

¹ Department of Radiologic Technology, Faculty of Associated Medical Sciences, Chiang Mai University, Chiang Mai, Thailand

² Division of Radiation Oncology, Department of Radiology, Faculty of Medicine, Chiang Mai University, Chiang Mai, Thailand

³ Division of Radiation Oncology, Department of Radiology, Faculty of Medicine, Chulalongkorn University, Bangkok, Thailand

Radiol Oncol 2017; 51(4): 438-446.

Received 3 June 2017

Accepted 16 July 2017

Correspondence to: Imjai Chitapanarux, Division of Radiation Oncology, Department of Radiology, Faculty of Medicine, Chiang Mai University, 110 Intavaroros Rd., Sriphum 50200, Chiang Mai, Thailand. Phone: +66 539 354 56; +66 869 133 065; Fax: +66 539 354 91; E-mail: imjai@hotmail.com

Disclosure: No potential conflicts of interest were disclosed.

Introduction. Deformable image registration (DIR) is used to modify structures according to anatomical changes for observing the dosimetric effect. In this study, megavoltage computed tomography (MVCT) images were used to generate cumulative doses for nasopharyngeal cancer (NPC) patients by various DIR methods. The performance of the multiple DIR methods was analysed, and the impact of dose accumulation was assessed.

Patients and methods. The study consisted of five NPC patients treated with a helical tomotherapy unit. The weekly MVCT images at the 1st, 6th, 11th, 16th, 21st, 26th, and 31st fractions were used to assess the dose accumulation by the four DIR methods. The cumulative dose deviations from the initial treatment plan were analysed, and correlations of these variations with the anatomic changes and DIR methods were explored.

Results. The target dose received a slightly different result from the initial plan at the end of the treatment. The organ dose differences increased as the treatment progressed to 6.8% (range: 2.2 to 10.9%), 15.2% (range: -1.7 to 36.3%), and 6.4% (range: -1.6 to 13.2%) for the right parotid, the left parotid, and the spinal cord, respectively. The mean uncertainty values to estimate the accumulated doses for all the DIR methods were 0.21 ± 0.11 Gy (target dose), 1.99 ± 0.76 Gy (right parotid), 1.19 ± 0.24 Gy (left parotid), and 0.41 ± 0.04 Gy (spinal cord).

Conclusions. Accuracy of the DIR methods affects the estimation of dose accumulation on both the target dose and the organ dose. The DIR methods provide an adequate dose estimation technique for observation as a result of inter-fractional anatomic changes and are beneficial for adaptive treatment strategies.

Key words: deformable image registration; dose accumulation; nasopharyngeal cancer; MVCT; helical tomotherapy

Introduction

Modern radiation therapy has the ability to utilize multimodality imaging technologies for disease definition, patient setup, and treatment assessment.¹ Helical megavoltage CT (MVCT), which is a volumetric imaging modality, is adopted with the

primary purpose of more accurate target localization.² Moreover, with this, information about inter-fractional anatomical variations has become more accessible.³ Some head and neck cancer patients undergo significant anatomical changes, and these may result in unforeseen changes in the delivered dose.³ In ideal practice, when a patient's anatomy

changes, a new adaptive plan must be developed, in accordance with the concept of adaptive radiotherapy (ART).⁴ These procedures include modification of the initial plan according to the changes in the target volume or normal organs; manual contouring can be used to modify deformation in order to evaluate the dosimetric effect.⁵⁻⁷ However, the process of manual contouring is time-consuming. Therefore, a deformable image registration (DIR) can be used to resolve these challenges. By registering multiple daily CTs to the planned CT, the algorithm can automatically generate deformed contours on daily CTs while creating cumulative doses by tracking the dose to the tissue voxels throughout the course of the radiation therapy.²

As for the application of MVCT in deformable dose accumulation routinely, it would require accurate structure deformation even in low contrast regions⁸ because accuracy of DIR may have a significant dosimetric impact on radiation treatment planning.⁹ Nowadays, various deformable image registration algorithms have been developed³ and the accuracy of the deformable image registration naturally depends on the deformation model.¹⁰ Therefore, the choice of the deformation algorithms and the transformation in the MVCT image application are of great importance in the registration process as it entails important compromise between computational efficiency and richness of description for more accurate results.¹⁰

Deformable image registration and adaptive radiotherapy (DIRART)¹¹ is a software suite for DIR plus ART. DIRART is a large set of programs developed using MATLAB. Four DIR methods by two algorithms, Horn & Schunck optical flow and demon with the two transformation frameworks, asymmetric and symmetric transformation, have been considered. In this study, weekly MVCT images from helical tomotherapy were used to generate cumulative doses for nasopharyngeal cancer (NPC) patients. Different DIR methods from DIRART were used. The weekly cumulative doses were analysed to assess the dosimetric impact of the DIR methods on dose accumulation. The dosimetric variations from the initial plan were reported, and correlations of these variations with anatomic changes and DIR methods were explored.

Patients and methods

Patient characteristics

The study population consisted of five NPC patients treated using a helical tomotherapy unit

(Tomo-Therapy, Inc., Madison, Wisconsin). All the patients underwent intensity modulated radiotherapy (IMRT) with a planned dose of 70 Gy delivered to the gross disease at 2.12 Gy/fraction for a total of 33 fractions with a simultaneous integrated boost technique (SIB) according to the RTOG 0225¹², keeping the mean parotid dose as low as could be possibly achieved and respecting the tissue tolerance of other normal structures. Patient positioning was ensured by appropriate headrest and a personalized HN and shoulder mask. This study received ethics approval, granted by the institutional research committee.

Image acquisition

The planned kVCT images were acquired on a computerized tomography unit (Somatom, SIEMENS, Germany) by using a matrix of 512 × 512 with voxel dimension of 0.976 × 0.976 × 3mm³ for the treatment planning process. The 1st day MVCT images were also acquired on the helical tomotherapy unit as source images for deformable investigation on the same day of acquisition of the planned kVCT images.

When the radiotherapy treatment was started, the daily MVCT images were acquired on the helical tomotherapy unit prior to each treatment fraction used for patient alignment by using a matrix of 512 × 512 with voxel dimension of 0.763 × 0.763 × 4 mm³. Typically, the MVCT scan range covers the entirety of the gross tumour volume (GTV), the clinical target volume (CTV), and the parotid glands bilaterally. The weekly MVCT images on the 1st, 6th, 11th, 16th, 21st, 26th, and 31st fractions were used as the target images to assess the dose accumulation in this study.

Target localization

The regions of interest (ROIs) including the target and the organ at risks (OARs) were defined by the radiation oncologist on planned kVCT images for the treatment planning processes. The ROIs on the planned kVCT images were transferred to the first-day MVCT images as the source images for each image set. The same oncologist who localized the target and the OAR for the HT treatment planning process also contoured the GTV, CTV, the bilateral parotid glands, and the spinal cord on the weekly MVCT images as the reference images. These contours were compared to the automatic deformed structure generated by the deformable image registration software.

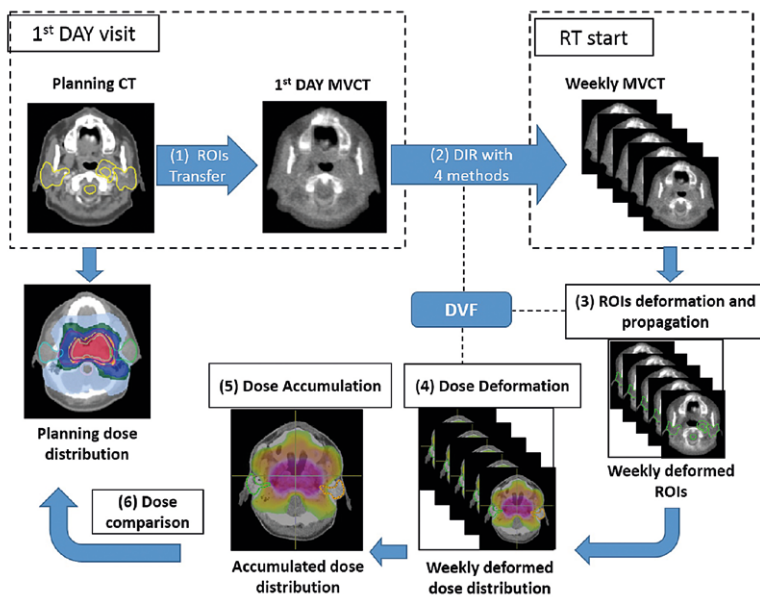


FIGURE 1. The diagram of the study workflow for dose accumulation and dose comparison.

DIR

The popular software suite for DIR and ART, DIRART version 1a developed by Yang (2009)¹¹, was used to create automatic deformed contours and dose accumulation from the MVCT images of NPC patients. DIRART works complementarily with computational environment for radiotherapy research (CERR) to offer more functions⁹ and provide the capability of selecting various deformation algorithms, transformation frameworks, and mapping directions for providing the deformation vector field (DVF) in deformable registration procedures.

In this study, the algorithms used were Horn and Schunck (HS) optical flow and demons (DM) combined with the asymmetric (Asy) and symmetric (Sym) transformation framework. Therefore, the study was carried out with four DIR methods, including the asymmetric transformation with the Horn and Schunck optical flow (AsyHS), the asymmetric transformation with the demon algorithm (AsyDM), the symmetric transformation with the Horn and Schunck optical flow (SymHS), and the symmetric transformation with the demon algorithm (SymDM).

A multi-resolution technique was used in this study. For the optimum DIR performance for each algorithm, various parameters were systematically adjusted: four multigrids were used ($n = 1, 2, 3,$ and 4) with $10n$ to $40n$ iterations per pass.⁹ The number of passes for the optical flow algorithm was 6

and the number of passes for the demon algorithm was between 2 and 6. Coarser stages were typically run with a greater number of passes to improve the agreement with the target image prior to resampling at finer resolutions.⁹

Validation of DIR

The objective of the validation technique was to evaluate the accuracy of the automatic deformed contour by four DIR methods on weekly MVCT images, including the terms of the volume-based criterion and the deformation field analysis.

Regarding the volume-based criterion, the most common overlap metric is the Dice similarity coefficient (DSC).¹³ DSC is the metric that computes the number of pixels that overlaps between two volumes. If the images have no overlap, then the DSC is 0, and as the contours become identical, the DSC approaches the value of 1.¹³ Zimring *et al.*¹⁴ suggested that the satisfactory volume matching should be 70% (DSC of 0.7) or more for adaptive radiotherapy application.

Inverse consistency error (ICE) was used to ensure that the transformations were physically invertible for the deformation field analysis. Optimal transformation is found when the ICE minimizes the distance error.¹⁵

Assessment of impact of DIR methods on dose accumulation

The dose accumulation process relied on six steps, as illustrated in Figure 1. Firstly, the ROIs from the planned kVCT images were transferred to the 1st day MVCT as source images for registration. The four DIR methods were performed between the 1st day MVCT and the weekly MVCTs (step 2). The deformation vector field was applied for creating the automatic deformed structure of the ROIs and for propagation to the weekly MVCT images (step 3), and the weekly dose distribution was deformed (step 4). The weekly dose deformation values were summed to the accumulated dose (step 5) and compared to the initial planned dose distribution (step 6).

To evaluate the effect of dose accumulation from DIR errors, the reference accumulated dose on ROIs was computed by summing the weekly doses corresponding to the weekly MVCTs defined by the radiation oncologist. Moreover, to ensure that the weekly dose summation from the DIRART software was accurate, dose accumulation from independent software, *Planned Adaptive software*

(TomoTherapy Inc., Madison, WI) was used to compare.

Regarding the evaluation of accumulated dose, for the target volume, the median absorbed dose ($D_{50\%}$), the near-minimum ($D_{98\%}$) absorbed dose, and the near-maximum ($D_{2\%}$) absorbed dose values from each DIR method were assessed, the mean absorbed dose (D_{mean}) of the bilateral parotid glands and $D_{2\%}$ of the spinal cord were compared to the original planned dose for the OARs investigation. The one-way analysis of variance (ANOVA) test and the paired sample t-test were carried out on each set of comparison metrics to determine the statistical significance, with a threshold of $p < 0.05$; SPSS statistical software version 17 was used to compare and assess the impact of each of the DIR methods.

Results

ROI volume variations

Regarding volume variations during the radiotherapy, the percent ratio to the volume at the initial treatment planning of five NPC patients is illustrated in Figure 2. The averages of the NPC patients for the volume variation in the initial plan were significantly different from the averages after the treatment in 3 weeks for GTV, with p -value = 0.025, as demonstrated in Figure 2A, and for CTV, with p -value = 0.020, as demonstrated in Figure 2B. The volume was observed to have decreased by an average of 29.8% (GTV) and 21.0% (CTV) at the end of the treatment course.

As regards the OARs, the right and the left parotid volume variations were significantly different from those of the initial plan after 5 weeks and 4 weeks of treatment, with p -values of 0.017 and 0.026, respectively. The average volume decreased by 40.3% (right) and 43.6% (left) at the end of the treatment.

DIR validation

The results of DIR accuracy were consistent between the volume-based criterion, DSC, and the deformation field analysis, ICE. Figure 3A demonstrates the histogram of the DSC values for all of the ROIs by four DIR methods. The SymDM methods showed significant difference from other methods by the one-way ANOVA analysis, with p -value = 0.00, with the worst performance in terms of volume-based criterion by mean values of DSC = 0.50 ± 0.30 , 0.56 ± 0.34 , 0.67 ± 0.19 , 0.65 ± 0.28 , and 0.69 ± 0.19 for GTV, CTV, right parotid, left parotid,

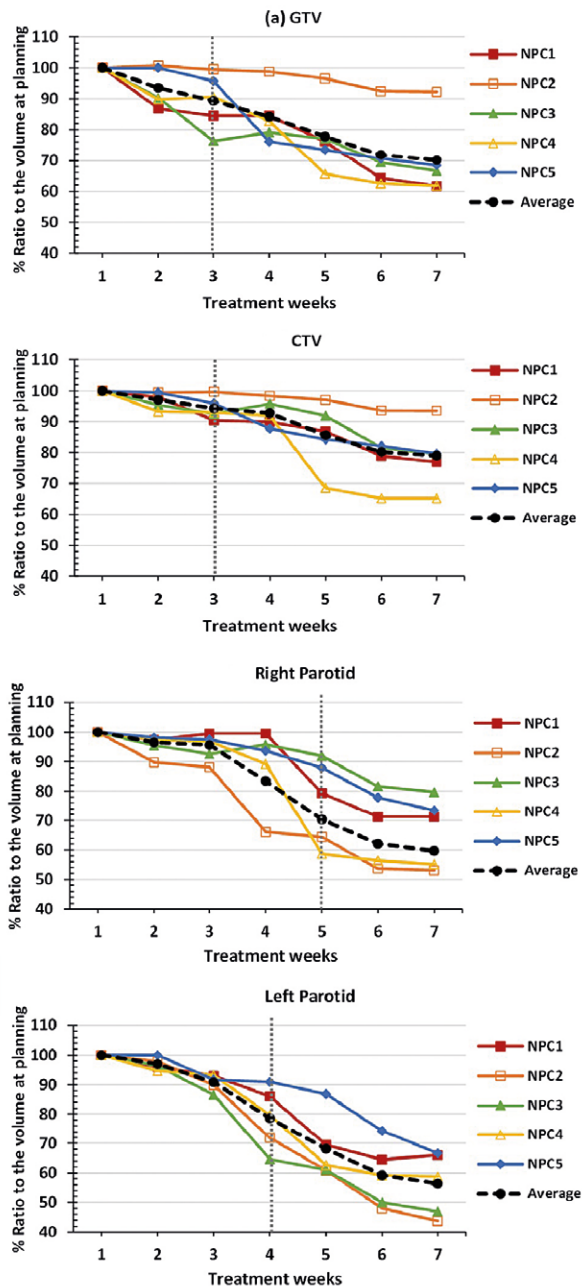


FIGURE 2. The percent ratio to the volume at the initial treatment planning of (A) gross target volume GTV, (B) clinical target volume CTV, (C) right parotid gland, and (D) left parotid gland.

and spinal cord, respectively. The average of DSC value was less than 0.7 for all the ROIs, that represented unsatisfactory volume matching for adaptive radiotherapy application.¹⁴ Regarding the ICE analysis, the results were consistent with DSC value. Figure 3B illustrates the histogram of the ICE values for all of the ROIs by the four DIR methods. The SymDM method also showed the maximum error in the deformation field analysis in terms of

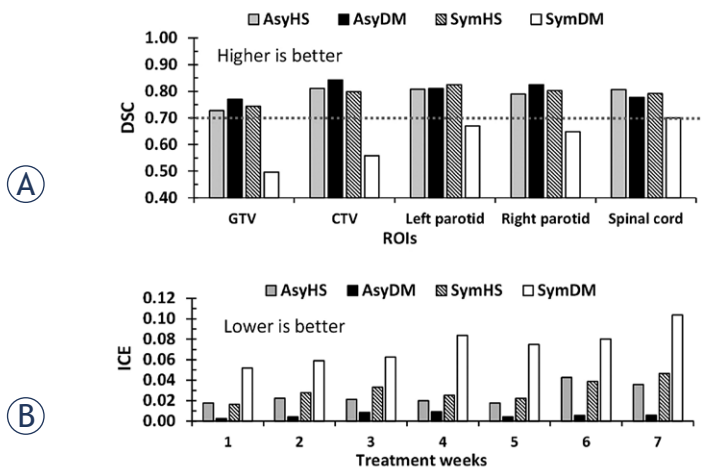


FIGURE 3. Histogram of (A) the dice similarity coefficients (DSC) for all of the targets and organs at risk and (B) the inverse consistency error (ICE) in each treatment week and by asymmetric Horn and Schunck (AsyHS), asymmetric demon (AsyDM), symmetric Horn and Schunck (SymHS), and symmetric demon (SymDM) deformable image registration (DIR) methods.

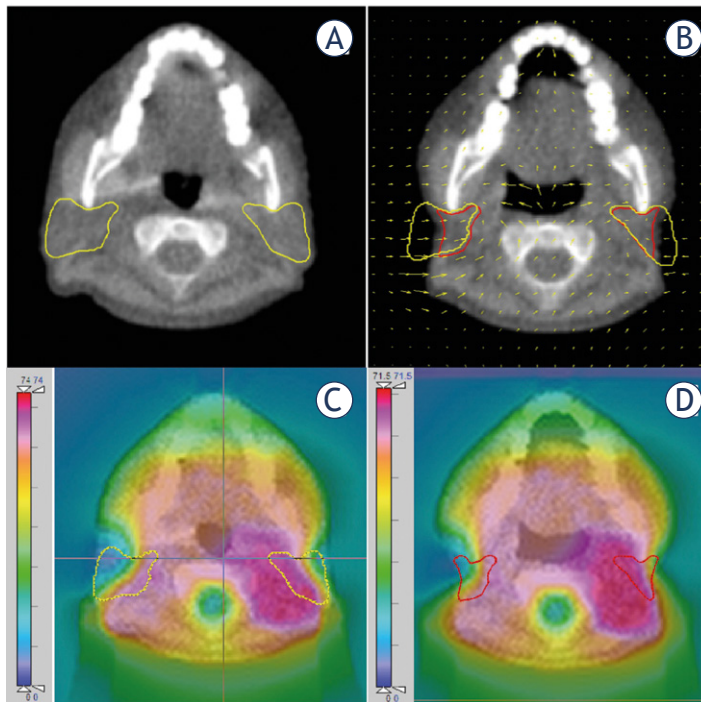


FIGURE 4. The 1st day MVCT image showing the original bilateral parotid gland (A) and the MVCT image at the 31st fraction showing the automatic deformed contour (B) from the AsyDM method. The initial planned dose distribution on the 1st day MVCT image (C) which was used to compare with the accumulated dose distribution at the end of the treatment (D).

ICE for all of the ROIs throughout the treatment. The one-way ANOVA analysis showed that the SymDM method was significantly different from other methods, with p -value = 0.00. Therefore, the SymDM failed to adequately register on weekly

MVCT for the dose accumulation application in this study. This paper focuses on the three highest performing algorithms in the AsyHS, AsyDM, and SymHS methods for dose accumulation.

Accumulated dose variation from initial planned dose

As regards target dose variation, the median GTV and CTV doses received at the end of treatment were slightly different from those in the initial plan. They were 0.11% (range: 0–0.29%) lower than the initial planned dose. The median dose variations of the GTV and CTV were significantly different from the initial planned dose after 6 weeks of treatment, with p -value = 0.016. Regarding the minimum and the maximum doses, they are represented by near-minimum dose ($D_{98\%}$) and near-maximum dose ($D_{2\%}$), respectively. As for the $D_{98\%}$, they received slightly higher doses than the initial plan deals, with an average variation less than 0.5% (range: 0.29–1.60%). However, the dose at the end of treatment received slightly decreased doses of 0.45% (GTV) and 0.28% (CTV) from the initial doses planned for the $D_{2\%}$.

Regarding organ dose variation, the dose differences tended to increase as the treatment progressed. For the bilateral parotid gland, the discrepancy between the delivered and the planned mean doses was found to have increased by 6.8% (range: 2.2 to 10.9%) for the right parotid and by 15.2% (range: -1.7 to 36.3%) for the left parotid. The average mean parotid dose increased in the ranges of 2.24 ± 0.97 Gy (right) and 5.70 ± 4.12 Gy (left) at the end of the treatment. The mean parotid dose variations were significantly different from the initial plan after 6 weeks (right) and 5 weeks (left) of the treatment, with p -value = 0.049 (right) and p -value = 0.010 (left). The spinal cord dose received increased by 6.4% (range: -1.6 to 13.2%) from the initial plan, with the average near-maximum dose increasing in the range of 1.83 ± 1.5 Gy at the end of the treatment.

Impact of DIR methods on weekly dose accumulation

For each patient, the running cumulative doses were calculated using the CERR software through the three deformable image registration methods carried out by the DIRART software. Figure 4 demonstrates the 1st day MVCT image with original bilateral parotid gland (A) and the MVCT image at the 31st fraction with the automatic deformed con-

four obtained using the AsyDM method (B). The initial planned dose distribution on the 1st day MVCT image, as illustrated in Figure 4C, was used for comparison with the accumulated dose distribution at the end of the treatment, as demonstrated in Figure 4D. The variations in the cumulative doses between the delivered dose and the initial planned dose are illustrated in Figure 5 and Figure 6.

Figure 5A illustrates the weekly GTV dose variation from the initial plan with three DIR methods. The average of the median dose difference for all methods at the end of the treatment was lower than that in the initial plan, with 0.34 Gy (0.5%), 0.04 Gy (0.1%), and 0.30 Gy (0.4%) for the AsyHS, AsyDM, and SymHS DIR methods, respectively. However, the reference dose of GTV was found to have decreased by 0.11%, with the accumulated GTV dose at 70.12 Gy (range: 69.9–70.4 Gy), at the end of treatment. The median dose variations of the GTV was significantly different from the initial planned dose after 6 weeks of treatment, with p-value = 0.016.

Regarding the near-minimum dose and the near-maximum dose, the $D_{98\%}$ of GTV in three DIR methods were found to be lower than that in the initial plan, as illustrated in Figure 5B; the average discrepancy of the three DIR methods between the planned dose and the delivered dose was 0.33 Gy (0.5%) at the end of the treatment with the high differences of 1.0% after 5 week for AsyHS method. However, the reference near-minimum dose was found to have increased by 0.3% of the initial planned dose, with 69.2 Gy (range: 68.7–70 Gy). As for the maximum GTV dose consideration, the three DIR methods of $D_{2\%}$ are presented in Figure 5C with gradually decrease in dose difference from initial plan for all methods when the time increase. The average $D_{2\%}$ from the three methods was lower than the initial $D_{2\%}$, with 0.76 Gy (1.1%), at the end of the treatment. The reference $D_{2\%}$ was found to have decreased by 0.45% of the initial planned dose, with 71.5 Gy (range: 70.9–72.5 Gy).

As regards the median CTV dose, the dose variations tended to be similar to the dose variations of GTV. Figure 5D illustrates the very small median CTV differences of various deformable registration methods from the initial planned dose. The discrepancy at the end of the treatment was lower than that in the initial planned dose, by 0.34 Gy (0.4%), 0.02 Gy (0%), and 0.26 Gy (0.4%) for AsyHS, AsyDM, and SymHS DIR methods, respectively. However, the reference median dose was found to have decreased by 0.11%, with 70.12 Gy (range: 69.9–70.4 Gy) at the end of the treatment.

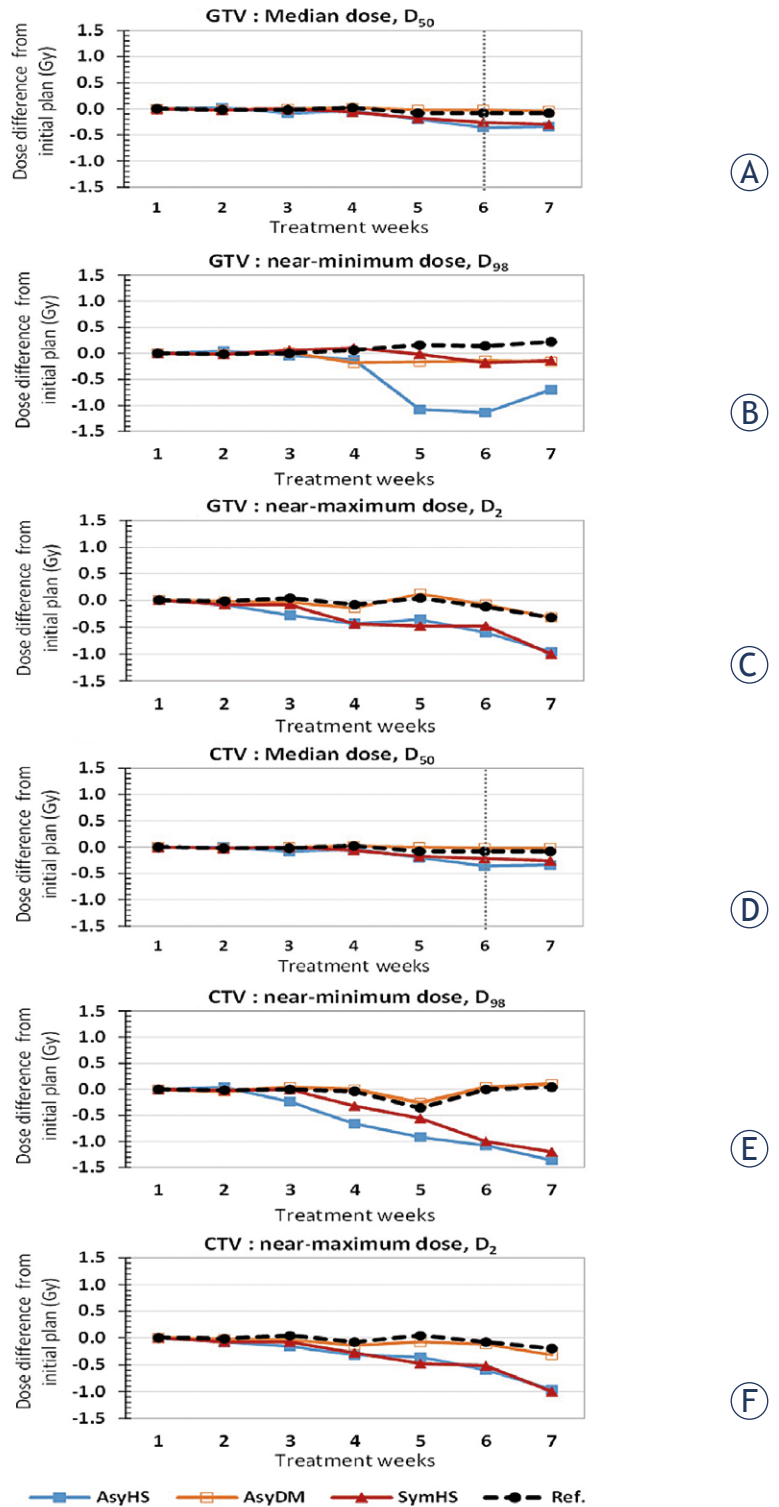


FIGURE 5. Cumulative dose comparison, calculated by the asymmetric Horn and Schunck (AsyHS), asymmetric demon (AsyDM), symmetric Horn and Schunck (SymHS), and symmetric demon (SymDM) deformable registration methods of gross tumour volume (GTV) for (A) median dose, D_{50} (B) near-minimum dose, D_{98} and (C) near-maximum dose, D_2 , and clinical tumour volume (CTV) for (D) median dose, D_{50} (E) near-minimum dose, D_{98} , and (F) near-maximum dose, D_2 . The reference (Ref) accumulated dose was computed by summing the weekly doses corresponding to the weekly MVCTs defined by the radiation oncologist.

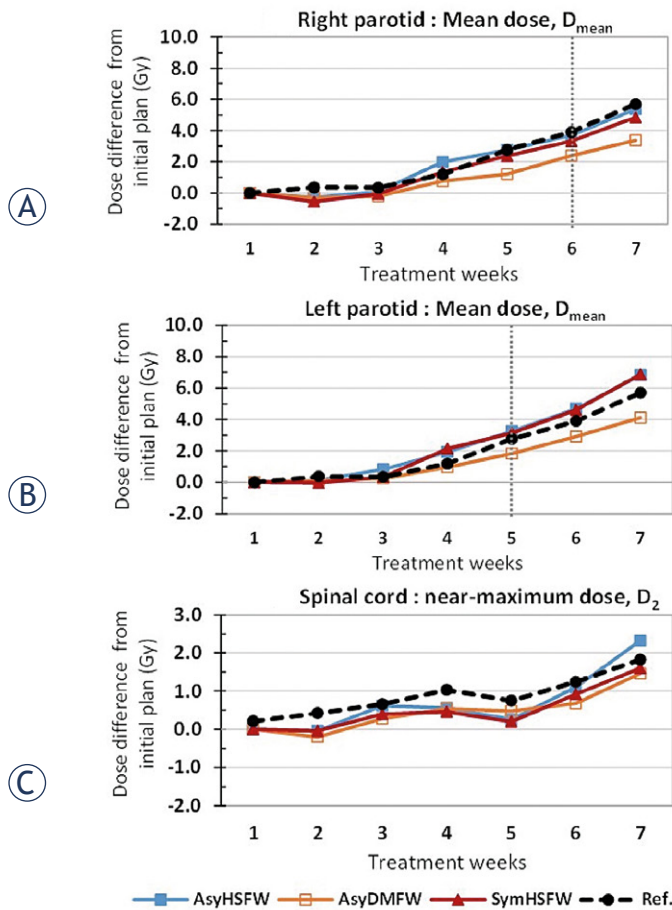


FIGURE 6. Cumulative dose comparison, calculated from the asymmetric Horn and Schunck (AsyHS), asymmetric demon (AsyDM), symmetric Horn and Schunck (SymHS), and symmetric demon (SymDM) deformable registration methods in mean dose, D_{mean} , of (A) right parotid gland and (B) left parotid gland, and near-maximum dose, D_2 , of (C) spinal cord.

The median dose variations of the CTV was significantly different from the initial planned dose after 6 weeks of treatment, with p -value = 0.016.

Regarding the D_{98} dose analysis of CTV, the discrepancy between the initial and the delivered dose of the three DIR methods are shown in Figure 5E. The average of the $D_{98\%}$ variations from the initial $D_{98\%}$ in the three DIR methods was 0.89 Gy (1.2%). Figure 5F shows the $D_{2\%}$ of CTV; the average variation from the initial $D_{2\%}$ of the three DIR methods was 0.76 Gy (1.1%).

As regards organ dose accumulation in the three DIR methods, Figure 6 illustrates the weekly dose difference from the initial plan in the three DIR methods for the bilateral parotid gland and the spinal cord. Overall, the dose differences tended to increase as the treatment progressed. Figure 6A shows the mean right parotid dose (D_{mean}) to be higher than the initial planned dose, by 5.38 Gy (16.0%), 3.38 Gy (10.1%), and 4.84 Gy (14.4%) for

the AsyHS, AsyDm, and SymHS methods, respectively. However, the reference mean dose was found to have increased by 2.24 Gy (range: 0.8–3.7 Gy), at 6.82%, at the end of the treatment.

For the left parotid mean dose, as illustrated in Figure 6B, these variations were higher after treatment than those for the initial planned dose, and the discrepancy was by 6.88 Gy (18.3%), 4.12 Gy (11.0%), and 6.82 Gy (18.1%) for the AsyHS, AsyDm, and SymHS DIR methods, respectively. However, the reference mean dose was found to have increased by 5.7 Gy (range: -0.6 to 12.4 Gy), at 15.2% at the end of the treatment. The mean parotid dose variations were significantly different from the initial plan after 6 weeks (right parotid) and 5 weeks (left parotid) of the treatment, with p -value of 0.049 and 0.010, respectively.

As regards spinal cord weekly dose accumulation, the variations tended to increase in all the three DIR methods, by 2.33 Gy (7.9%), 1.46 Gy (4.9%) and 0.60 Gy (5.4%) for AsyHS, AsyDm, and SymHS, respectively. However, the reference cord dose variation was found to have increased by 1.83 Gy (range: -0.5 to 4.0 Gy), at 6.37% at the end of the treatment.

DIRART and planned adaptive software for dose accumulation

To ensure dose summation on the DIRART software, the independent planned adaptive software on helical tomotherapy treatment planning was used to compare the dose accumulation values. The same data set of all the reference ROIs on weekly MVCTs defined by the radiation oncologist was transferred to the planned adaptive software. The comparison of the weekly accumulated doses between DIRART and planned adaptive is illustrated in Figure 7. The variations in the accumulated median parotid doses of DIRART were not significantly different according to the planned adaptive software, with p -value = 0.972 for the right parotid gland, as shown in Figure 7A, and p -value = 0.958 for the left parotid gland, as shown in Figure 7B. The consistency in the dose variations between the two independent types of software demonstrates that the dose accumulation of the DIRART software can be applied for use in dose accumulation studies.

Discussion

The validation of DIR was consistent in terms of the volume-based criterion, DSC, and the defor-

tion field analysis, ICE. Accuracy in terms of DSC analysis tended to decrease as the treatment progressed as a result of organs with large-scale deformation causing reduction in the DIR accuracy.¹⁶ The AsyDM method showed the best performance with the highest average DSC value of all ROIs, the mean value of $DSC = 0.804 \pm 0.07$, and also enabled the minimization of the inverse consistency error by the lowest mean value of $ICE = 0.006 \pm 0.002$, as demonstrated in Figure 3.

As regards the weekly dose variation from the initial plan, the results demonstrated that the median, the near-minimum dose, and the near-maximum dose of the target slightly varied, by less than 0.5% of the initial plan. However, with regard to organ doses like the bilateral parotid gland, the discrepancy between the planned and the delivered mean doses was 6.8% (right) and 15.8% (left) higher than the initial plan. The accumulated mean parotid dose increased to be in the range of -0.6 to 12.4 Gy. Lee *et al.*² analysed the changes in the parotid gland dose with reference to the anatomic changes throughout the course of radiotherapy. The daily parotid mean dose of the 10 patients differed from the planned dose by an average of 15%. At the end of the treatment, 3 of the 10 patients were estimated to have received greater than 10% higher mean parotid dose than in the original plan (range: 13–42%), whereas the remaining 7 patients received doses that differed by less than 10% (range: 6–8%).

Regarding the correlation between dose accumulation and DIR accuracy, there was consistency between the accuracy of ROI deformation and discrepancy of dose accumulation. The DIR method that yielded the highest DSC value was considered the best method for dose accumulation with the lowest variation from the reference dose. The AsyDM method demonstrated the best performance for target deformation with the highest mean DSC value of 0.802 ± 0.08 , as presented in Figure 3, and showed the best agreement for target dose accumulation with the lowest average variation of 0.01% with the reference dose, as presented in Figure 5. This method also gave the highest mean DSC value of 0.824 ± 0.05 for the right parotid gland and the lowest mean parotid dose variation with 3.2% of the reference deformed dose, as demonstrated in Figure 6A. However, the SymHS method showed the best performance for left parotid deformation, as demonstrated in Figure 3A, with the highest mean value of $DSC = 0.824 \pm 0.06$, and also showed the lowest mean left parotid dose variation with 2.9% of the reference deformed dose,

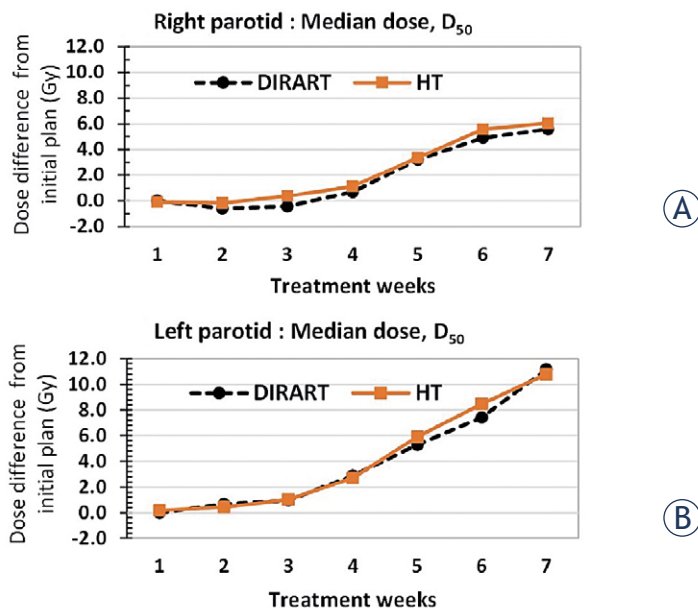


FIGURE 7. Cumulative dose comparison, derived from helical tomotherapy planned adaptive software (HT) and DIRART software in median dose, D_{50} , of (A) right parotid gland and (B) left parotid gland.

as illustrated in Figure 6B. For the spinal cord, the AsyHS method gave the best performance, as presented in Figure 3, with the highest mean value of $DSC = 0.806 \pm 0.05$, and also showed the lowest dose variation with 1.5% of the reference deformed dose, as presented in Figure 6C.

Regarding the uncertainty of dose accumulation, the three DIR methods demonstrated satisfactory volume matching for accumulated dose application with DSC values more than 0.7 for all the methods. Moreover, the one-way ANOVA analysis demonstrated that there was no significant difference between the three DIR methods as regards ROI deformation and dose accumulation. However, when uncertainty was considered (difference between the maximum dose and the minimum dose) in the estimation of the accumulated dose for all the DIR methods, the average of the DSC value of all the targets by the three DIR methods was 0.782 ± 0.04 . The mean uncertainty for estimating the target dose was 0.21 ± 0.11 Gy (range: 0.06–0.32 Gy). Regarding the uncertainty of the parotid dose, the averages of the DSC values by the three DIR methods were 0.805 ± 0.01 (right) and 0.814 ± 0.01 (left). This shows that the mean uncertainty values for estimating the parotid dose were 1.99 ± 0.76 Gy (range: 0.01–3.14 Gy) for the right parotid and 1.19 ± 0.24 Gy (range: 0.01–1.58 Gy) for the left parotid. For the spinal cord, the average of the DSC values was 0.791 ± 0.01 Gy, while the mean uncertainty value for the estimated dose was 0.41

± 0.04 Gy (range: 0.04–0.57 Gy). The results in this study were lower than Rigaud *et al.*¹⁷ who showed the mean uncertainty (difference between the maximum dose and the minimum dose, considering all the 10 DIR methods) to estimate the cumulated mean dose for the parotid gland (PG) was 4.03 Gy (SD = 2.27 Gy, range: 1.06–8.91 Gy).

Further investigation would involve applying this methodology to other treatment areas to identify patients who may benefit from adaptive treatment. DIR on megavoltage computed tomography imaging makes it possible to calculate daily and accumulated doses. Significant dose variations were observed as a result of inter-fractional anatomic changes, which is information that would benefit adaptive treatment strategies.

Acknowledgments

The author offers many thanks to the staff of the Division of Therapeutic Radiology and Oncology, Faculty of Medicine, Chiang Mai University, for supporting this study.

References

1. Hardcastle N, Tome W, Cannon D, Brouwer C, Wittendorp P, Dogan N, et al. A multi-institution evaluation of deformable image registration algorithms for automatic organ delineation in adaptive head and neck radiotherapy. *Radiat Oncol J* 2012; **7**: 1-7. doi: 10.1186/1748-717X-7-90
2. Lee C, Langen KM, Lu W, Haimerl J, Schnarr E, Ruchala KJ, et al. Assessment of parotid gland dose changes during head and neck cancer radiotherapy using daily megavoltage computed tomography and deformable image registration. *Int J Radiat Oncol Biol Phys* 2008; **71**: 1563-71. doi: 10.1016/j.ijrobp.2008.04.013
3. Lee C, Langen KM, Lu W, Haimerl J, Schnarr E, Ruchala KJ, et al. Evaluation of geometric changes of parotid glands during head and neck cancer radiotherapy using daily MVCT and automatic deformable registration. *Radiother Oncol* 2008; **89**: 81-8. doi: 10.1016/j.radonc.2008.07.006
4. Castelli J, Simon A, Louvel G, Henry O, Chajon E, Nassef M, et al. Impact of head and neck cancer adaptive radiotherapy to spare the parotid glands and decrease the risk of xerostomia. *Radiat Oncol J* 2015; **10**: 1-10. doi: 10.1186/s13014-014-0318-z
5. Kupelian PA, Langen KM, Zeidan OA, Meeks SL, Willoughby TR, Wagner TH, et al. Daily variations in delivered doses in patients treated with radiotherapy for localized prostate cancer. *Int J Radiat Oncol Biol Phys* 2006; **66**: 876-82. doi: 10.1016/j.ijrobp.2006.06.011
6. Langen KM, Meeks SL, Poole DO, Wagner TH, Willoughby TR, Kupelian PA, et al. The use of megavoltage CT (MVCT) images for dose recomputations. *Phys Med Biol* 2005; **50**: 4259-76. doi: 10.1088/0031-9155/50/18/002
7. Morin O, Chen J, Aubin M, Gillis A, Aubry JF, Bose S, et al. Dose calculation using megavoltage cone-beam CT. *Int J Radiat Oncol Biol Phys* 2007; **67**: 1201-10. doi: 10.1016/j.ijrobp.2006.10.048
8. Yeo U, Supple J, Taylor M, Smith R, Kron T, Franich R. Performance of 12 DIR algorithms in low-contrast regions for mass and density conserving deformation. *Med Phys* 2013; **40**: 1-12. doi: 10.1118/1.4819945
9. Nie K, Chuang C, Kirby N, Braunstein S, Pouliot J. Site-specific deformable imaging registration algorithm selection using patient-based simulated deformations. *Med Phys* 2013; **40**: 041911. doi: 10.1118/1.4793723
10. Hardcastle N, Elmpot W, Cannon D, Ruyscher D, Bzdusek K, Tomé W. Accuracy of deformable image registration for contour propagation in adaptive lung radiotherapy. *Radiat Oncol J* 2013; **8**: 243-50. doi: 10.1186/1748-717X-8-243
11. Yang D, Brame S, Naqa E. Technical Note: DIRART—A software suite for deformable image registration and adaptive radiotherapy research. *Med Phys* 2011; **38**: 71-7. doi: 10.1118/1.3521468
12. Lee N, Harris J, Garden AS, Straube W, Glisson B, Xia P, et al. Intensity-modulated radiation therapy with or without chemotherapy for nasopharyngeal carcinoma: radiation therapy oncology group phase II trial 0225. *J Clin Oncol* 2009; **27**: 3684-90. doi: 10.1200/JCO.2008.19.9109
13. Kristy KB. *Image processing in radiation therapy*. New York: Taylor & Francis Group; 2013.
14. Zimring D, Talos F, Bhagwat G, Haker J, Black P, Zou K. Statistical validation of brain tumor shape approximation via spherical harmonics for image-guided neurosurgery. *Acad Radiol* 2005; **12**: 459-66. doi: 10.1016/j.acra.2004.11.032
15. Varadhan R, Karangelis G, Krishnan K, Hui S. A framework for deformable image registration validation in radiotherapy clinical applications. *J Appl Clin Med Phys* 2013; **14**: 4066. doi: 10.1120/jacmp.v14i1.4066
16. Luiza B, Mischa SH, Eliana M, Vasquez O, Ben JM. A symmetric nonrigid registration method to handle large organ deformations in cervical cancer patients. *Med Phys* 2010; **37**: 3760. doi: 10.1118/1.3443436
17. Rigaud B, Antoine S, Castelli J, Gobeli M, Arango JO, Cazoulat G, et al. Evaluation of deformable image registration methods for dose monitoring in head and neck radiotherapy. *Biomed Res Int* 2015; 1-16. doi: 10.1155/2015/726268

Long term results of radiotherapy in vulvar cancer patients in Slovenia between 1997-2004

Helena Barbara Zobec Logar

Department of Radiotherapy, Institute of Oncology Ljubljana, Ljubljana, Slovenia

Radiol Oncol 2017; 51(4): 447-454.

Received 2 March 2017
Accepted 24 April 2017

Correspondence to: Helena Barbara Zobec Logar, M.D., M.Sc., Institute of Oncology Ljubljana, Zaloška 2, 1000 Ljubljana, Slovenia. Phone: +386 1 5879 505; Fax: +386 1 5879 857; E-mail: hlogar@onko-i.si

Disclosure: No potential conflicts of interest were disclosed.

Background. The aim of this retrospective single institution study was to analyse long term results of vulvar cancer treatment with conventional 2D radiotherapy in Slovenia between years 1997–2004.

Patients and methods. Fifty-six patients, median age 74.4 years +/- 9.7 years, mainly stage T2 or T3, were included in the study. All patients were treated with radiotherapy, which was combined with surgery (group A), used as the primary treatment (group B) or at the time of relapse (group C). Chemotherapy was added in some patients. Histology, grade, lymph node status, details of surgery, radiation dose to the primary tumour, inguinofemoral and pelvic area as well as local control (LC) and survival were evaluated.

Results. Overall survival (OS), disease specific survival (DSS) and LC rates at 10-years for all patients were as follows: 22.7%, 34.5% and 41.1%, respectively. The best 10-years results of the treatment were achieved in the primary operated patients treated with adjuvant radiotherapy +/- chemotherapy (OS 31.9%, DSS 40.6% and LC 47.6%). Positive lymph nodes had a strong influence on LC. In case of positive nodes LC decreased by 60% ($p = 0.03$) and survival decreased by 50% ($p = 0.2$). There was a trend to a better LC with higher doses ≥ 54.0 Gy ($p = 0.05$).

Conclusions. The best treatment option for patients with advanced vulvar cancer is combined treatment with surgery and radiotherapy +/- chemotherapy, if feasible. Radiotherapy with the dose of ≥ 54.0 Gy should be considered to achieve better LC if positive adverse factors are present.

Key words: vulvar cancer; radiotherapy, surgery; local control; survival

Introduction

Vulvar cancer is a rare gynaecological cancer and it accounts for approximately 3–5% of all gynaecological malignancies. The incidence in Slovenia between years 1997–2004 was 33 to 57 (average 40) patients per year, the highest incidence occurred in women over 60 years of age.¹ Surgery is the most important modality in the treatment of early vulvar cancer, while (chemo)radiotherapy +/- surgery is the most important modality in the treatment of advanced vulvar cancer. Radiotherapy can be used preoperatively, postoperatively, or as the only treatment in locally advanced vulvar cancer with bulky unresectable primary tumour or groin disease. In operated patients positive margins and

positive lymph nodes are the most important indications for adjuvant radiotherapy. Other prognostic factors such as large primary tumour lesion, deep tumour invasion and in recent years also lymphovascular space involvement (LVI) are the factors that are used to determine adjuvant radiotherapy as well.^{2,3} The majority of the patients with vulvar cancer are over 70 years of age, with many additional comorbidities, which also favour radiotherapy as the best treatment option. Recent data are showing improvement of the treatment by adding adjuvant chemotherapy.⁴⁻⁷ In the past different cytotoxic agents were utilized, but nowadays the preferred is weekly cisplatin, an option which was extrapolated from treatment of advanced cervical squamous cell carcinoma (SCC).

Surgical treatment

Classical surgical approach is radical vulvectomy. More conservative surgery which reduced morbidity without compromising prognosis is used in early stage vulvar SCC. Wide local excision of the tumour with sentinel lymph node biopsy (SNB) with or without inguinofemoral lymphadenectomy is an attractive alternative.⁸⁻¹² The most suitable candidates for SNB are patients with tumour diameter < 4 cm and with no palpable groin nodes.^{9,13,14} Patients with positive sentinel-node metastases are candidates for additional treatment.^{8,9} The lymph node status and particularly inguinofemoral lymph node status is the most important prognostic factor for survival, while the tumour free margin is the most important prognostic factor for local recurrence.^{3, 15-17}

Postoperative radiotherapy

Radiotherapy in postoperative adjuvant treatment is used to additionally treat the primary site, groins and/or pelvis. Radiotherapy to the primary site is indicated in case of positive or close margin (≤ 8 mm) and large primary tumour (> 4 cm).^{2,3,18} OS of patients with close/positive margins who received adjuvant radiotherapy was similar to those with negative margins.¹⁸ Radiotherapy to the groins is indicated in case of two or more microscopically positive groin nodes, in case of one or more macroscopically positive node, or in case of extracapsular extension (ECE). When only one microscopically positive groin node is identified, adjuvant radiotherapy can be omitted, although recent recommendations show improvement in disease free survival (DFS) when adding radiotherapy also in a single microscopic node positive disease.^{5, 19-22} Lymph node involvement is the strongest negative predictive factor for survival. The 3-years PFS and OS for node positive disease was 35.2% and 56.2% compared to 75.2% and 90.2% for node negative disease.^{5,11,23} Despite adjuvant radiotherapy in node positive disease and clinical benefit in PFS, OS remains poor (57.7% with adjuvant radiotherapy vs 51.4% without radiotherapy at 3-years, $p = 0.17$).⁵

Locally advanced vulvar cancer

Radiotherapy is the treatment option for bulky primary site and/or extensive groin disease. The addition of chemotherapy to radiotherapy improves survival in several SCC.^{6,7,24,25} As high as 60% of

patients with locally advanced disease can present with nodal metastases, the reason that urge for more aggressive treatment which combines chemotherapy and radiotherapy in locally advanced disease. After primary chemoradiotherapy surgery can be performed in selected cases. There are only a few studies, mainly single institution or phase II studies that report results of such approach.^{4,6,25-28}

In this retrospective single institution study the long term results of vulvar cancer treatment in Slovenia between 1997 and 2004 with radiotherapy alone or combined with surgery or chemotherapy were analysed.

Patients and methods

Patients and tumours

69 patients with vulvar cancer treated with radiotherapy from January 1997 till December 2004 were retrospectively analysed. Thirteen patients were excluded from the study, because the palliative dose was used to treat the cancer. At the end 56 patients with histologically confirmed vulvar cancer treated with curative intent with radiotherapy, +/- surgery, +/- chemotherapy were enrolled and retrospectively analysed.

Mean patient age was 74.4 +/- 9.7 years. All patients were staged according to the FIGO 1988 staging system (13). FIGO stage distribution, available in 94.6% of the patients, was as follows: stage I 5 (8.9%), stage II 4 (7.1%), stage III 33 (58.9%) and stage IV 11 (19.6%) and not specified in 3 patients.

Histological type of the tumour was SCC in all patients included in the study. Other histological types ranging from malignant melanoma (2 patients), adenocarcinoma of the Bartholin's gland (1 patient) and Paget's disease (1 patient) were rare and were excluded from further analysis. The diagnostic work-up before the treatment consisted of clinical examination with biopsy and chest radiography in operated patients, while imaging studies such as abdominal and groin ultrasound or chest/abdominal computer tomography (CT) were only rarely performed.

Patients, tumour and treatment characteristics are listed in Table 1.

The study was approved by the Protocol Review Board at the Institute of Oncology Ljubljana (ERID-KESOPKR-14). The investigation followed recommendations of the Helsinki Declaration (1964, with later amendments) and of the European Council Convention on Protection of Human Rights in Bio-Medicine (Oviedo 1997).

TABLE 1. Patients, tumor and treatment characteristics

Characteristics	All	Primary operated	Primary irradiated	Relapse group
		group A	group B	C
Number of patients (%)	56 (100.0%)	31 (55.4%)	11 (19.6%)	14 (25%)
Mean age (years) (+/-SD)	74.4 (+/-9.7)	74.9 (+/- 9.8)	67.9 (+/-10.8)	87.2 (+/- 6.1)
Median follow-up time (months)	22.5 (2-203)	27 (8-203)	9 (2-72)	44 (5-134)
FIGO stage				
I	5 (8.9%)	0	0	5 (35.7%)
II	4 (7.1%)	0	0	4 (28.6%)
III	33 (58.9%)	23 (74.2%)	6 (54.5%)	4 (28.6%)
IV	11 (19.6%)	7 (22.6%)	4 (36.4%)	0
not specified	3 (5.4%)	1 (3.2%)	1 (9.1%)	1 (7.1%)
Histopathologic grade				
G1	21 (37.5%)	11 (35.5%)	3 (27.3%)	7 (50.0%)
G2	25 (44.6%)	15 (48.4)	7 (63.6%)	3 (21.4%)
G3	5 (8.9%)	3 (9.7%)	1 (9.1%)	1 (7.1%)
not specified	5 (8.9%)	2 (6.5%)	0	3 (21.4%)
T stage				
T1	5 (8.9%)	2 (6.5%)	0	3 (21.4%)
T2	26 (46.4%)	18 (58.1%)	1 (9.1%)	7 (50.0%)
T3	16 (28.6%)	9 (29.0%)	7 (63.6%)	0
T4	3 (5.4%)	1 (3.2%)	2 (18.2%)	0
not specified	6 (10.7%)	1 (3.2%)	1 (9.1%)	4 (28.6%)
Diameter of primary tumor				
≤ 2 cm	10 (17.9%)	7 (22.6%)	0	3 (21.4%)
> 2 and ≤ 4 cm	23 (41.1%)	16 (51.6%)	3 (27.3%)	4 (28.6%)
> 4 cm	12 (21.5%)	5 (16.2%)	6 (54.5%)	1 (7.1%)
not specified	11 (19.6%)	3 (9.7%)	2 (18.2%)	6 (42.9%)
Tumor invasion				
lower urethra	9 (16.1%)	3 (9.7%)	6 (54.5%)	0
vagina	15 (26.8%)	8 (25.8%)	7 (63.6%)	0
anus	1 (1.8%)	0	1 (9.1%)	0
bladder wall	0	0	1 (9.1%)	0
rectal wall	1 (1.8%)	0	1 (9.1%)	0
pelvic bone	2 (7.1%)	1 (3.2%)	1 (9.1%)	0
Tumor location				
clitoris	6 (10.7%)	4 (12.9%)	0	2 (14.3%)
labium major	10 (17.9%)	5 (16.1%)	1 (9.1%)	4 (28.6%)
labium minor	8 (14.3%)	4 (12.9%)	0	4 (28.6%)
comissura/more than one location	28 (50.0%)	16 (51.6%)	10 (90.9%)	2 (14.3%)
not specified	4 (7.1%)	2 (6.5%)	0	2 (14.3%)
Nodal status				
N0	17 (30.3%)	4 (12.9%)	5 (45.5%)	8 (57.1%)
N1	25 (44.6%)	19 (61.3%)	2 (18.2%)	4 (28.6%)
N2	10 (17.9%)	7 (22.6%)	3 (27.3%)	0
not specified	4 (7.1%)	1 (3.2%)	1 (9.1%)	2 (14.3%)
Nodal metastases				
micrometastases	9 (16.1%)	7 (22.6%)	not specified	2 (14.3%)
macrometastases	25 (44.6%)	18 (58.1%)	5 (45.5%)	2 (14.3%)
Extracapsular tumor spread				
positive	10 (17.9%)	8 (25.8%)	not specified	2 (14.3%)
Residual tumor after surgery				
primary tumor site	20 (35.7%)	16 (51.6%)	not specified	4 (28.6%)
nodal site	15 (26.8%)	13 (41.9%)	not specified	2 (14.3%)
nodal site	7 (12.5%)	4 (12.9%)	not specified	3 (21.4%)
Mean dose to the tumor (Gy) (+/-SD)	47.4 (+/-7.9)	47.1 (+/-8.2)	46.7 (+/-8.7)	46.0 (+/-5.2)
Mean dose to the inguinofemoral area (Gy) (+/-SD)				
ipsilateral	47.5 (+/-8.8)	50.7 (+/-7.9)	46.9 (+/-8.4)	40.1 (+/-6.7)
contralateral	49.7 (+/-9.7)	53.4 (+/-7.8)	44.9 (+/-9.8)	37.4 (+/-6.9)
Mean dose to the pelvic area (Gy) (+/-SD)				
ipsilateral	46.2 (+/-6.2)	47.0 (+/-6.8)	45.0 (+/-4.9)	43.5 (+/-6.2)
contralateral	44.6 (+/-10.5)	44.7 (+/-12.5)	45.0 (+/-4.9)	39.1 (+/-4.9)

Treatment

In this retrospective study radiotherapy was used as the part of the treatment in all patients and it was most frequently combined with surgery in 31 patients (55.4%). Chemoradiotherapy was used in 11 patients (17.9%). At that time the most commonly used cytotoxic agent in adjuvant setting was bleomycin or cisplatin. Radiotherapy was also used at the time of relapse in 14 patients (25%): local relapse at the site of primary tumour was detected in 6 patients, and nodal relapse in 10 patients. The majority of relapses developed within two years after the primary treatment.

In order to evaluate LC and survival among different treatment modalities, three treatment groups were formed (Table 1). 31 patients were included in the primary operated group (group A), where the primary treatment modality was surgery with radiotherapy +/- chemotherapy as an adjuvant treatment. This was the largest group, reflecting that operation therapy +/- radiotherapy is the most important treatment modality in the management of advanced vulvar cancer. Chemoradiotherapy was used only in 2/31 patients, respectively. In the primary irradiated group (group B) 11 patients were included. Radiotherapy was used as the only treatment in 4/11 patients, combined with chemotherapy in 7/11 patients, used preoperatively in 1 or pre- and postoperatively in 1 patient, respectively. In the relapse group (group C) radiotherapy alone or combined with surgery was used at the time of relapse in 9/14 patients and 5/14 patients, respectively. Chemoradiotherapy was used in 2/14 patients.

Surgical treatment

Surgery is the cornerstone in the treatment of vulvar cancer. The most frequently used type of operation was radical vulvectomy in 29 and wide local excision in 16 patients. SNB was performed only in 6 patients. Vulvar cancer patients were diagnosed in different gynaecological centres in Slovenia and were mainly operated in the three main centres: University Medical Centre Ljubljana (33.9%), Institute of Oncology Ljubljana (37.5%) and University Medical Centre Maribor (5.4%). Unilateral and bilateral inguinofemoral lymph node dissection was performed in 26.8% and 33.9%, respectively. The mean number of removed lymph nodes was 7 (range 1–19). Among all operated patients adjuvant radiotherapy was used in 65.1%, radiochemotherapy in 6.9% and radiotherapy at the time of relapse in 27.9%.

Radiotherapy

Radiotherapy is an important modality of the treatment in adjuvant setting, as a radical treatment in locally advanced cancer or as a treatment of choice at the time of relapse. External beam radiotherapy was delivered with 5–15 MV linear accelerator or Cobalt-60 machine. In addition, electrons were sometimes applied to boost inguinal areas or primary tumour. Mostly supine position has been used, but “frogleg” position has been used as well, particularly in fat patients. Various two-dimensional (2D) techniques were used to radiate primary tumour and/or inguinal nodes at that time.

First technique used wide anteroposterior (AP) field that included the pelvic and inguinal area, with a narrow posteroanterior (PA) field covering pelvis only. The fields were weighted equally 1:1. The inguinal nodes were boosted to a certain depth determined by a clinician, with a separate anterior field. Bolus material on the primary tumour or inguinal areas was used according to the physician's decision. The physician's determined depth of the inguinal nodes was usually 3 to 4 cm. The second technique used AP/PA field of the same dimension. An alternative technique consisted of a wide AP field and narrow PA field with a partial transmission block at the central portion of the AP field. The dose at a specified depth to the inguinal areas was delivered through the AP field.

The two opposite fields technique was applied in majority of the patients. Other techniques, such as four field (box) technique was used as well (16.2%). There were many variations in the prescribed dose to the inguinal nodes among patients due to different inguinal depth chosen by a physician and different radiation techniques that were used. The daily dose was usually 1.8–2.0 Gy per fraction, a daily dose of 2.5–3.0 Gy per fraction was seldom used as well, with a total dose mainly in the range between 45–60 Gy. In order to enable comparison of the dose to the inguinal area, the depth dose was calculated for all patients at the same depth. The so called “inguinal depth” was determined on CT scans of the fifty women treated with pelvic radiotherapy at the time of collecting data for this study. The mean depth of the inguinal nodes was 5.5 cm (range 2–18 cm), which was more than arbitrary by a physician determined depth.

Chemotherapy

Today chemotherapy combined with radiotherapy is the fundamental strategy in the treatment of

advanced vulvar cancer. At the time of this study it was not so widely used, altogether 11 patients (19.6%) got some kind of chemotherapy. Platinum-based chemotherapy is the treatment of choice in squamous cell carcinomas. In our study cisplatin was used alone or in combination with other cytotoxic drugs such as bleomycin or 5-fluorouracil. Rarely, in case of renal dysfunction, carboplatin was used instead of cisplatin.

Follow up

First follow-up was usually performed 3 months after the treatment. Consecutive follow-ups were usually performed alternately by gynaecologist or radiation oncologist at 3 to 6 month intervals for the first 5 years and once per year later on.

Statistical analysis

The data were analysed using IBM SPSS statistical software package version 23.0 (SPSS Inc., Chicago, IL, USA), p values of <0.05 were considered statistically significant.

Kaplan-Meier method was applied to calculate actuarial survival and loco-regional control rates. The endpoint for OS was death from any cause, for DSS the disease related death and for LC any evidence of loco-regional recurrent disease. Patients without relapse were censored at the time of the last follow-up, visit or death. Surviving patients were censored at the time of the last follow-up. No effort was made to compare results between different treatment groups due to small number of patients in each group and consequently a low power of the test.

The influence of positive lymph nodes, ECE, size of primary tumour and completeness of surgical resection on survival and LC were analysed. Arbitrary cut off points for positive lymph nodes and ECE (negative versus positive), size of primary tumour (up to 4 cm versus ≥ 4 cm) and completeness of surgical resection (complete R0 versus incomplete R1/R2) were used.

The data regarding the side effects of the radiotherapy treatment or surgery were not systematically recorded and were in general missing in the patient's record, therefore the analysis of side effects of the treatment was omitted in this study.

Results

At the time of the last follow up 21 patients (37.5%) proved to be disease free. Median follow-up for

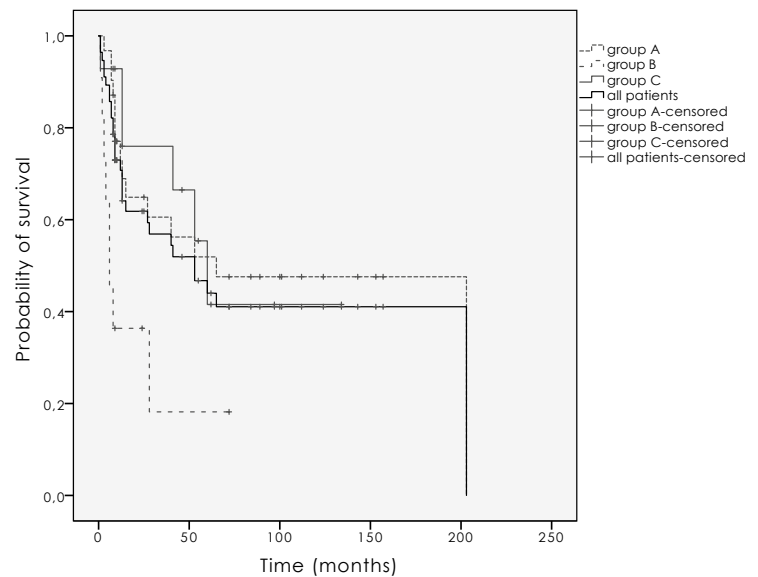


FIGURE 1. Local control for the group A (primary operated patients), B (primary irradiated patients), C (patients with relapse) and all patients.

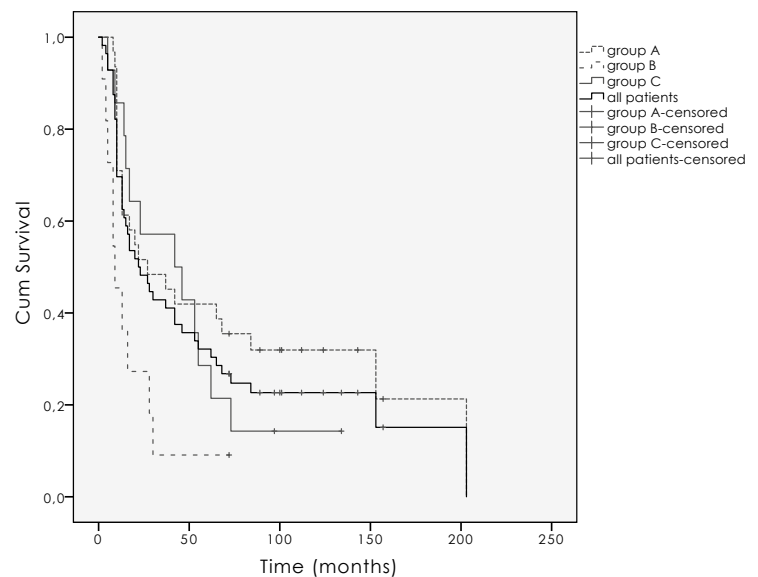


FIGURE 2. Overall survival for the group A, (primary operated patients), B (primary irradiated patients), C (patients with relapse) and all patients.

all patients was 22.5 months (range 2–203) and for surviving patients 101 months (range 72–157). For 4 surviving patients follow-up was lower than 10-years due to lost to follow-up, but according to the national Cancer Registry they were still alive at the close-out time of the study. The pattern of failure at the last follow-up is represented in Table 2. Half of the patients with distant metastases had also locoregional recurrence. The skin was the most common site of metastatic disease, other pos-

TABLE 2. Pattern of failure at the time of last follow-up

	All	Primary operated	Primary irradiated	Relapse group
		group A	group B	C
Local failure	9	5	4	0
Inguinal failure	6	3	1	2
Distant failure	5	3	1	1
Local and inguinal failure	10	5	3	2
Local/inguinal and distant failure	5	2	1	2
Overall failure	35	18	10	7
No evidence of disease	21	13	1	7

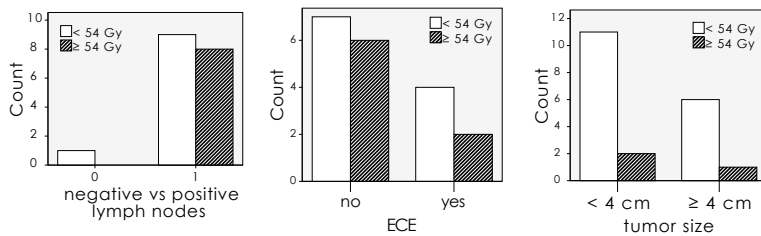


FIGURE 3. Number of patients with the dose applied to the positive lymph nodes, nodes with extracapsular lymph node extension (ECE) and large tumours.

sible sites were pelvic and paraaortic lymph nodes, lungs and bones.

Overall survival (OS), disease specific survival (DSS) and local control (LC) for all vulvar cancer patients at 10-years were 22.7%, 34.5% and 41.1%, for primary operated group 31.9%, 40.6% and 47.6% respectively, in primary irradiated group there were no survivals at 10-years and for the relapse group survivals and LC were as follows 14.3%, 33.9% and 41.5% (Figure 1 and 2). Ten years LC for node negative disease was 57.1% for T1–2 and 55.6% for T3–4. For node positive disease T1–4N1 and T1–4N2 it was 38.4% and 29.2%, respectively. The difference was not statistically significant ($p = 0.5$).

OS, DSS and LC at 10-years for stage III were as follows 30.3%, 35.3% and 44%, and for stage IV 18.2%, 18.2% and 24.9%. Data for stage I and II are not reported, because only 2 patients were alive at 5 years and only 1 patient (FIGO stage II) was alive at 10 years (134 months). Factors that contribute to lower outcome in stage I and II were higher age (mean age 79.9 \pm 6.5, $p = 0.04$) and treatment of the relapsed disease in all stage I and II patients (local relapse 3, inguinal 4, local and inguinal 2 patients).

The mean equivalent dose in 2 Gy per daily fraction (EQD2) applied to the primary tumour was

47.4 Gy \pm 7.9 Gy. The mean equivalent dose to the inguino-femoral area was 47.5 \pm 8.8 Gy and 49.7 \pm 9.7 Gy for the ipsi- and contralateral side. The mean equivalent dose to the primary tumour and to the inguinal area for different treatment groups are listed in Table 1. Significantly higher dose was applied to the macroscopic positive lymph nodes as to the negative or microscopic lymph nodes (54.0 Gy against 40.0 Gy, $p = 0.04$). There was no statistically significant difference between the dose applied to operated or non-operated patients. Despite positive adverse factors, such as positive lymph nodes, ECE or large primary tumour, the dose applied to the primary site or groins was rather low. Only 16% of patients received the dose higher than 54.0 Gy (Figure 3).

ECE had a negative impact on LC ($p = 0.02$; Figure 4). Positive lymph nodes had a strong influence on LC (Figure 5). In case of positive nodes LC decreased by 60% ($p = 0.03$), and OS as well as DSS decreased by 50% ($p = 0.2$). The completeness of surgical resection had an impact on local and regional control in the first two years after the treatment, which did not prove to be statistically significant ($p = 0.6$). There was a trend to a better LC with higher doses over 54.0 Gy ($p = 0.05$).

Vulvar and groin morbidity are important factors which effect quality of life of the patient. It is compromised due to surgical treatment and radiotherapy. In this study acute and late side effects were not systematically recorded and these results were not evaluated.

Discussion

The best treatment option for early stage vulvar cancer is surgery, with adjuvant radiotherapy indicated in high risk disease with positive adverse factors such as large primary tumour size, close or positive surgical margins, positive lymph node/s or ECE. For patients, who are not candidates for primary surgery due to more extensive disease or comorbidities, radiotherapy combined with chemotherapy if feasible, is the preferred treatment option. The distribution of the patients between different treatment groups reflects the treatment strategy which was used most frequently - surgery combined with adjuvant radiotherapy. SNB in patients with early stage disease and negative groin exam as an alternative to inguino-femoral lymphadenectomy, was performed only in 10.7%, reflecting early beginnings of using this method in Slovenia. Radiotherapy as the primary treatment

was used less frequently; concomitant chemotherapy was used in 63.3% (7/11) of patients. The 2D treatment technique that was used frequently at that time, with dose prescription to the groins, usually at 3 cm depth, resulted in under-dosing of the inguinal nodes. Many studies, as well as ours, showed that the inguinal lymph nodes depth is in general more than 3 cm.^{1,29} With the use of 3D and other novel techniques such as intensity modulated radiotherapy (IMRT) or volumetric modulated arc therapy (VMAT), the appropriate higher dose can be delivered to the groins with the dose reduction to the uninvolved tissues.⁴ In the study there was no significant difference between the dose applied to the patients with different risk factors and the patients in different treatment groups. The radiation dose applied after surgery is different after complete tumour removal, it ranges between 45.0 to 50.0 Gy, than after incomplete tumour removal with remaining microscopic or macroscopic disease, where the applied dose should be higher (≥ 60.0 Gy); although recent report showed that for vulvar squamous cell carcinoma with positive margins an adequate dose lies between 54.0 to 59.9 Gy.³⁰ The results from our study showed that rather low dose was applied to the primary irradiated patients group B and relapse group C, which was, besides the existing comorbidity factors, higher age and advanced tumours, the possible reason for lower LC and survival. The risk factors for the worse outcome that were recognized in other studies were proved in this study as well, despite the small number of patients. Positive lymph nodes status proved to be one of the strongest predictor for lower disease control and survival, despite the use of adjuvant therapy.^{7,5,31}

Despite the fact of a low quality data of the retrospective analysis with scarce diagnostic work-up performed before the treatment, the historical 2D radiotherapy technique used in majority of the patients and lacking morbidity data of the treatment, this is up to now the first and the only study of SCC of the vulva treated with radiotherapy in Slovenia. These results can be used as the basis for further analysis and improvement of the treatment of vulvar cancer patients with modern radiotherapy techniques.

Conclusions

The best treatment option for patients with squamous cell vulvar cancer is surgery with adjuvant radiotherapy +/- chemotherapy in case of positive

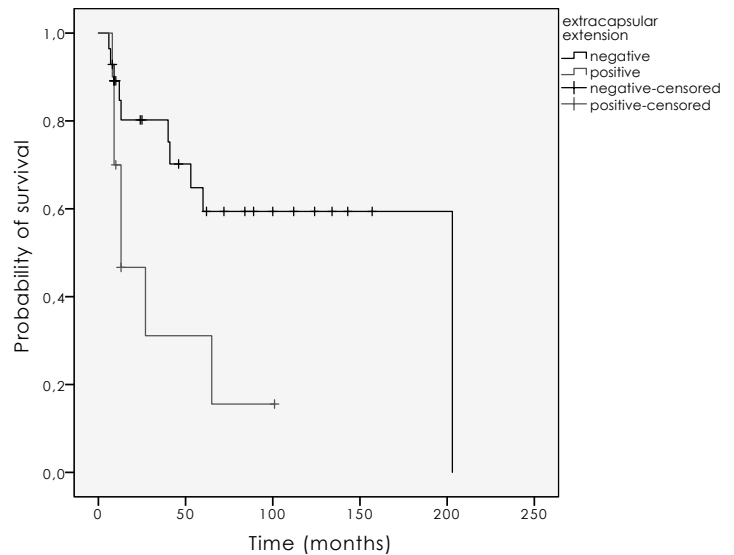


FIGURE 4. The influence of extracapsular nodal extension on local control ($p = 0.02$).

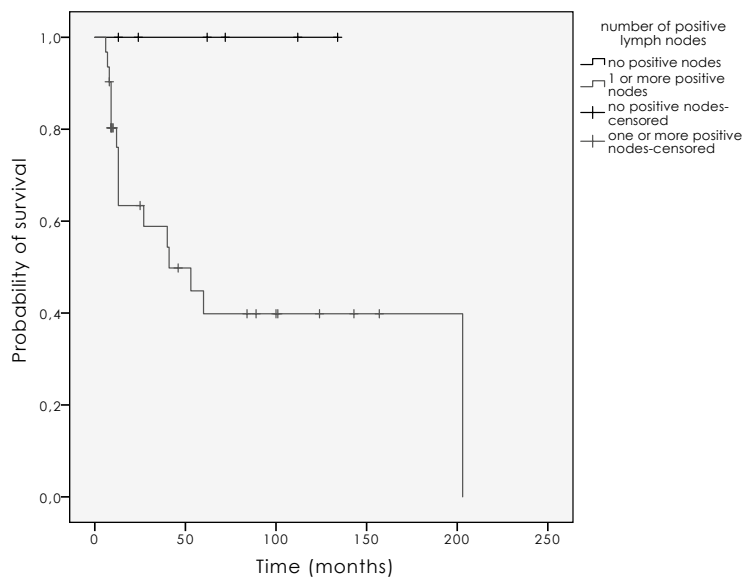


FIGURE 5. The influence of positive nodes on local control ($p = 0.03$).

adverse factors. The dose over 54.0 Gy is associated with better LC. More aggressive treatment with higher doses to the lymph node/s and adjuvant chemotherapy should be offered to the patients with positive lymph node/s. For the patients who are not candidates for primary surgery chemoradiotherapy is the treatment of choice. 2D radiotherapy technique with the dose prescription to the inguinal nodes at certain depth and consequently sometimes inadequate dose distribution to the inguinofemoral region can be bypassed by modern radiotherapy techniques, such as IMRT and

VMAT. With the use of these techniques and more conservative surgery the side effects and cosmetic results of the treatment can be further improved.

References

- Zadnik V, Primic Zakelj M, Lokar K, Jarm K, Ivanus U, Zagar T. Cancer burden in Slovenia with the time trends analysis. *Radiol Oncol* 2017; **51**(4): 447-454.; doi: 10.1515/raon-2017-0008
- Jolly S, Soni P, Gaffney DK, Biagioli M, Elshaikh MA, Jhingran A, et al. ACR Appropriateness Criteria(R) Adjuvant Therapy in Vulvar Cancer. *Oncology* 2015; **29**: 867-75.
- Heaps JM, Fu YS, Montz FJ, Hacker NF, Berek JS. Surgical-pathologic variables predictive of local recurrence in squamous cell carcinoma of the vulva. *Gynecol Oncol* 1990; **38**: 309-14.
- Beriwal S, Coon D, Heron DE, Kelley JL, Edwards RP, Sukumvanich P, et al. Preoperative intensity-modulated radiotherapy and chemotherapy for locally advanced vulvar carcinoma. *Gynecol Oncol* 2008; **109**: 291-5. doi: 10.1016/j.ygyno.2007.10.026
- Mahner S, Jueckstock J, Hilpert F, Neuser P, Harter P, de Gregorio N, et al. Adjuvant therapy in lymph node-positive vulvar cancer: the AGO-CaRE-1 study. *J Natl Cancer Inst* 2015; **107**: 1-12. doi: 10.1093/jnci/dju426
- Montana GS, Thomas GM, Moore DH, Saxer A, Mangan CE, Lentz SS, et al. Preoperative chemo-radiation for carcinoma of the vulva with N2/N3 nodes: a gynecologic oncology group study. *Int J Radiat Oncol Biol Phys* 2000; **48**: 1007-13. doi: 10.1016/S0360-3016(00)00762-8
- Gill BS, Bernard ME, Lin JF, Balasubramani GK, Rajagopalan MS, Sukumvanich P, et al. Impact of adjuvant chemotherapy with radiation for node-positive vulvar cancer: a National Cancer Data Base (NCDB) analysis. *Gynecol Oncol* 2015; **137**: 365-72. doi: 10.1016/j.ygyno.2015.03.056
- Te Grootenhuys NC, van der Zee AG, van Doorn HC, van der Velden J, Vergote I, Zanagnolo V, et al. Sentinel nodes in vulvar cancer: long-term follow-up of the GROningen INternational Study on Sentinel nodes in Vulvar cancer (GROINSS-V) I. *Gynecol Oncol* 2016; **140**: 8-14. doi: 10.1016/j.ygyno.2015.09.077
- Oonk MH, van Hemel BM, Hollema H, de Hullu JA, Ansink AC, Vergote I, et al. Size of sentinel-node metastasis and chances of non-sentinel-node involvement and survival in early stage vulvar cancer: results from GROINSS-V, a multicentre observational study. *Lancet Oncol* 2010; **11**: 646-52. doi: 10.1016/S1470-2045(10)70104-2
- Van Der Zee AGJ, Oonk MH, De Hullu JA, Ansink AC, Vergote I, Verheijen RH, et al. Sentinel node dissection is safe in the treatment of early-stage vulvar cancer. *J Clin Oncol* 2008; **26**: 884-9. doi: 10.1200/JCO.2007.14.0566
- de Hullu JA, van der Zee AG. Surgery and radiotherapy in vulvar cancer. *Crit Rev Oncol Hematol* 2006; **60**: 38-58. doi: 10.1016/j.critrevonc.2006.02.008
- Vakselj A, Bebar S. The role of sentinel lymph node detection in vulvar carcinoma and the experiences at the Institute of Oncology Ljubljana. *Radiol Oncol* 2007; **41**: 167-73. doi: 10.2478/v10019-007-0027-4
- Benedet JL, Bender H, Jones H, Ngan H, Pecorelli S. Staging classifications and clinical practice guidelines of gynaecologic cancers. *Int J Gynaecol Obstet* 2000; **70**: 207-312. doi: 10.1016/S0020-7292(00)90001-8
- Levenback CF, Ali S, Coleman RL, Gold MA, Fowler JM, Judson PL, et al. Lymphatic mapping and sentinel lymph node biopsy in women with squamous cell carcinoma of the vulva: a Gynecologic Oncology Group study. *J Clin Oncol* 2012; **30**: 3786-91. doi: 10.1200/JCO.2011.41.2528
- Homesley HD, Bundy BN, Sedlis A, Adcock L. Radiation therapy versus pelvic node resection for carcinoma of the vulva with positive groin nodes. *Obstet Gynecol* 1986; **68**: 733-40.
- Homesley HD, Bundy BN, Sedlis A, Yordan E, Berek JS, Jahshan A, et al. Assessment of current International Federation of Gynecology and Obstetrics staging of vulvar carcinoma relative to prognostic factors for survival (a Gynecologic Oncology Group study). *Am J Obstet Gynecol* 1991; **164**: 997-1003.
- De Hullu JA, Hollema H, Lolkema S, Boezen M, Boonstra H, Burger MPM, et al. Vulvar carcinoma. The price of less radical surgery. *Cancer* 2002; **95**: 2331-8. doi: 10.1002/cncr.10969
- Ignatov T, Eggemann H, Burger E, Costa SD, Ignatov A. Adjuvant radiotherapy for vulvar cancer with close or positive surgical margins. *J Cancer Res Clin Oncol* 2016; **142**: 489-95. doi: 10.1007/s00432-015-2060-9
- Fons G, Groenen SMA, Oonk MHM, Ansink AC, van der Zee AGJ, Burger MPM, et al. Adjuvant radiotherapy in patients with vulvar cancer and one intra capsular lymph node metastasis is not beneficial. *Gynecol Oncol* 2009; **114**: 343-5. doi: 10.1016/j.ygyno.2009.05.017
- Viswanathan AN, Pinto AP, Schultz D, Berkowitz R, Crum CP. Relationship of margin status and radiation dose to recurrence in post-operative vulvar carcinoma. *Gynecol Oncol* 2013; **130**: 545-9. doi: 10.1016/j.ygyno.2013.05.036
- Parthasarathy A, Cheung MK, Osann K, Husain A, Teng NN, Berek JS, et al. The benefit of adjuvant radiation therapy in single-node-positive squamous cell vulvar carcinoma. *Gynecol Oncol* 2006; **103**: 1095-9. doi: 10.1016/j.ygyno.2006.06.030
- Woelber L, Eulenburg C, Choschzick M, Kruell A, Petersen C, Gieseckig F, et al. Prognostic role of lymph node metastases in vulvar cancer and implications for adjuvant treatment. *Int J Gynecol Cancer* 2012; **22**: 503-8. doi: 10.1097/IGC.0b013e31823eed4c
- Farias-Eisner R, Cirisano FD, Grouse D, Leuchter RS, Karlan BY, Lagasse LD, et al. Conservative and individualized surgery for early squamous carcinoma of the vulva: the treatment of choice for Stage I and II (T1-2 N0-1 M0) Disease. *Gynecol Oncol* 1994; **53**: 55-8. doi: 10.1006/gy.1994.1087
- Green JA, Kirwan JM, Tierney JF, Symonds P, Fresco L, Collingwood M, et al. Survival and recurrence after concomitant chemotherapy and radiotherapy for cancer of the uterine cervix: a systematic review and meta-analysis. *Lancet* 2001; **358**: 781-6. doi: 10.1016/S0140-6736(01)05965-7
- Eifel P. Prolonged continuous infusion cisplatin and 5-fluorouracil with radiation for locally advanced carcinoma of the vulva. *Gynecol Oncol* 1995; **59**: 51-6. doi: 10.1006/gy.1995.1267
- Moore DH, Thomas GM, Montana GS, Saxer A, Gallup DG, Olt G. Preoperative chemoradiation for advanced vulvar cancer: a phase II study of the Gynecologic Oncology Group. *Int J Radiat Oncol Biol Phys* 1998; **42**: 79-85.
- Geisler JP, Manahan KJ, Buller RE. Neoadjuvant chemotherapy in vulvar cancer: avoiding primary exenteration. *Gynecol Oncol* 2006; **100**: 53-7. doi: 10.1016/j.ygyno.2005.06.068
- Gerszten K, Selvaraj RN, Kelley J, Faul C. Preoperative chemoradiation for locally advanced carcinoma of the vulva. *Gynecol Oncol* 2005; **99**: 640-4. doi: 10.1016/j.ygyno.2005.07.126
- Koh WJ, ChiuM, Stelzer KJ, Greer BE, Mastras D, Comsia N, Russell KJ GT. Femoral vessel depth and the implications for groin node radiation. *Int J Radiat Oncol Biol Phys* 1993; **15**: 969-74.
- Chapman B V, Gill BS, Viswanathan AN, Balasubramani GK, Sukumvanich P, Beriwal S. Adjuvant radiation therapy for margin-positive vulvar squamous cell carcinoma: defining the ideal dose-response using the national cancer data base. *Int J Radiat Oncol Biol Phys* 2016; **97**: 1-11. doi: 10.1016/j.ijrobp.2016.09.023
- Chan JK, Sugiyama V, Pham H, Gu M, Rutgers J, Osann K, et al. Margin distance and other clinico-pathologic prognostic factors in vulvar carcinoma: a multivariate analysis. *Gynecol Oncol* 2007; **104**: 636-41. doi: 10.1016/j.ygyno.2006.10.004

Association between *SLC19A1* gene polymorphism and high dose methotrexate toxicity in childhood acute lymphoblastic leukaemia and non Hodgkin malignant lymphoma: introducing a haplotype based approach

Barbara Faganel Kotnik¹, Janez Jazbec¹, Petra Bohanec Grabar²,
Cristina Rodriguez-Antona³, Vita Dolzan²

¹ Department of Oncology and Haematology, University Children's Hospital, University Medical Centre Ljubljana, Ljubljana, Slovenia

² Pharmacogenetics Laboratory, Institute of Biochemistry, Faculty of Medicine, University of Ljubljana, Ljubljana, Slovenia

³ Hereditary Endocrine Cancer Group Human Cancer Genetics Programme, Spanish National Cancer Research Centre, Madrid, Spain

Radiol Oncol 2017; 51(4): 455-462.

Received 14 February 2017

Accepted 18 August 2017

Correspondence to: Prof. Vita Dolžan, M.D., Ph.D., Pharmacogenetics Laboratory, Institute of Biochemistry, Faculty of Medicine, University of Ljubljana, Vrazov trg 2; SI-1000 Ljubljana, Slovenia. Phone: + 386 1 543 7670; E-mail: vita.dolzan@mf.uni-lj.si

Disclosure: No potential conflicts of interest were disclosed.

Background. We investigated the clinical relevance of *SLC19A1* genetic variability for high dose methotrexate (HD-MTX) related toxicities in children and adolescents with acute lymphoblastic leukaemia (ALL) and non Hodgkin malignant lymphoma (NHML).

Patients and methods. Eighty-eight children and adolescents with ALL/NHML were investigated for the influence of *SLC19A1* single nucleotide polymorphisms (SNPs) and haplotypes on HD-MTX induced toxicities.

Results. Patients with rs2838958 TT genotype had higher probability for mucositis development as compared to carriers of at least one rs2838958 C allele (OR 0.226 (0.071–0.725), $p < 0.009$). Haplotype TGTCCG (H4) statistically significantly reduced the risk for the occurrence of adverse events during treatment with HD-MTX (OR 0.143 (0.023–0.852), $p = 0.030$).

Conclusions. *SLC19A1* SNP and haplotype analysis could provide additional information in a personalized HD-MTX therapy for children with ALL/NHML in order to achieve better treatment outcome. However further studies are needed to validate the results.

Key words: acute lymphoblastic leukaemia; genetic polymorphism; haplotype; methotrexate

Introduction

Inter-individual variability in treatment responses and treatment related toxicities is an important issue in clinical practice. It can lead to therapeutic failures or adverse drug events (ADE). Identification and characterization of genetic polymorphisms

and haplotypes involved in drug metabolism, transport and mechanism of action would provide important information about individual inherited differences in drug metabolism and treatment response in order to optimize treatment outcome.¹

The solute carrier 19A1 (*SLC19A1*), trivially referred as reduced folate carrier (*RFC*), located in a

40719 bp region at chromosome 21q22.3, is coding for solute folate carrier (*RFC1*), a major transporter of folates and antifolates into the cell. The antifolate methotrexate (MTX) is a cytotoxic drug which is used in current treatment regimens for childhood acute lymphoblastic leukaemia (ALL)², and non-Hodgkin malignant lymphoma (NHML).^{3,4} The most frequently studied *SLC19A1* polymorphism is rs1051266 in the second exon of the *SLC19A1*, which results in amino acid substitution of arginine for histidine (H27R)⁵ in transmembrane domain 1 (TMD1), a region implicated in substrate binding and/or translocation^{6,7}, is expected to alter SLC transport properties. Other polymorphisms have been described to date, but the functional consequences of other single nucleotide polymorphisms (SNPs) are not known yet.⁸

Several studies so far investigated the association of rs1051266 with high dose MTX (HD-MTX) treatment outcome and treatment related toxicities in ALL patients.⁹⁻¹³ Some of them reported a protective role of rs1051266 AA genotype^{14,15}, while in others either an increased risk of MTX-induced toxicities and fatal outcomes in rs1051266 A carriers^{9,10}, or even no association between *SLC19A1* genotype and MTX-induced toxicities was report-

ed.^{11,13,16,17} Recently, SNPs in microRNAs (miRNAs) that are involved in regulation of *SLC19A1* were investigated. SNP in miR-595 which might affect *SLC19A1* regulation and could affect MTX levels in patients with paediatric B-cell ALL was reported.¹⁸

To date all studies but one¹⁹ evaluated the role of individual *SLC19A1* SNPs in the MTX toxicities and outcomes of ALL treatment. The discovery of HapMap (Humane gene database) made it possible to analyse many SNPs at a time. Between the former and the latter a tagSNP approach has been introduced recently. A tagSNP is a representative SNP in a region of the genome with high linkage disequilibrium. Using the tagSNPs reduces number of SNPs needed to be genotyped to capture the common variations across the genome.²⁰ Relatively small numbers of tagSNPs will therefore mark each of the common haplotypes within the gene region.²¹

In the present study we investigated a possible association between *SLC19A1* haplotypes, defined by common functional variants and tagSNPs, and MTX related toxicities in 88 children and adolescents with ALL/NHML. The aim was to provide additional insight into improved, cost-effective approach for a personalized HD-MTX therapy for children with ALL/NHML based on haplotype analysis in order to achieve better treatment outcome.

TABLE 1. Demographic and clinical characteristics of children with ALL/NHML and MTX treatment toxicity

Characteristic	ALL patients (N = 88)
Gender (%)	
Male	41 (46.6)
Female	47 (53.4)
Median age at diagnosis, years (range)	4.58 (0.3–16.6)
Median body surface area, m ² (range)	0.73 (0.4–1.9)
Leukaemia subtype (%):	
B-cell	72 (81.8)
T-cell	13 (14.7)
Undetermined	3 (3.4)
Median No. leukocytes at diagnosis, 10 ⁹ cells/L (range)	9.35 (1–1650)
Median No. thrombocytes at diagnosis, 10 ⁹ cells/L (range)	72 (3–553)
Median haemoglobin conc., g/l (range)	84 (43–148)
Median % of blasts at diagnosis (range)	23.5 (0–97)
Median MTX dose, mg (range)	3300 (540–9200)
MTX response	Present, N (%)
Relapse	8 (9.2)**
Exitus	4 (4.6)**
All MTX-induced ADEs*	48 (54.5)
Leukopenia	33 (37.5)
Thrombocytopenia	16 (18.2)
Mucositis	15 (17.0)
Neurotoxicity	7 (8.0)**

*data was collected after the first cycle of MTX, **data is missing for one patient

Patients and methods

Study design

The study group included 88 children and adolescents (41 male, 47 female) with ALL/NHML diagnosed and treated in the period from 1990 to 2008 at the Department of oncology and haematology, University Children's Hospital in Ljubljana, Slovenia. All the patients were Central European Caucasians and below the age of 18 years at the time of diagnosis. Clinical and demographic data were obtained from the medical records and a questionnaire by a single abstractor blinded to genotypes and are presented in Table 1. Each patient enrolled in the study received a high MTX dose (77.3% of patients received 5 g/m² and 22.7% received 2 g/m² of MTX, according to treatment protocols) on 4 separate occasions and concomitant leucovorin rescue therapy to reduce MTX toxicity. Overall, 352 courses of HD-MTX applications were analysed.

All patients and/or their parents or legal guardians gave their written informed consent to participate in the study. The study was approved by the Republic of Slovenia National Medical Ethics

Committee and was carried out according to the Helsinki Declaration.

Outcome measurement

Adverse drug events (ADE) were recorded retrospectively from patients' files throughout the course of the HD-MTX treatment. ADEs were classified as (1) leukopenia, defined as white blood cells count less than 5×10^9 per litre, (2) thrombocytopenia, defined as thrombocyte count less than 140×10^9 per litre, (3) mucositis, determined and graded according to the WHO oral toxicity scale classification²² or based on physician's descriptions in medical records, need for analgesia and/or total parenteral nutrition and (4) neurotoxicity, determined and graded according to National Cancer Institute Common Toxicity Criteria Version 1 and included patients with seizures (regardless of grade) and patients with grade 3 or 4.²³ The data on relapse and exitus were also recorded. All the reported ADEs were used for the evaluation of MTX toxicity.

SLC19A1 SNP selection

A total of seven SNPs (rs2838951, rs2838956, rs2838958, rs1051266, rs1131596, rs2838451 and rs17004785) in *SLC19A1* spanning 40 kbp across the chromosomal 21q22.3 region were selected. SNP selection was based on known function from the literature and/or National Center for Biotechnology Information SNP database (NCBI) and block-tagging ability. Among all, two SNPs were a functional variant (rs1051266 and rs1131596), while five (rs2838951, rs2838956, rs2838958, rs2838451, rs17004785) were tagging SNPs, selected based on International HapMap Project CEPH data (phase II, March 2008) with the following criteria: $r^2 > 0.8$, and the frequency of minor allele greater than 5%. Tagging SNP selection was done using HaploView software version 4.1 (Supplementary Table 1).²⁴

SLC19A1 genotyping

In total 5 ml of peripheral blood was collected into tubes with sodium citrate and stored for short term at -20°C until DNA isolation. Genomic DNA was isolated from peripheral blood leukocytes using a Qiagen FlexiGene kit (Qiagen GmbH, Germany). Genotyping was performed using a fluorescence-based competitive allele-specific (KASPar) assay.²⁵ Real time PCR was performed on the ABI 7900HT in a 4 μL reaction mix containing 0.055 μL of

KASPar allele specific PCR assay, 2 μL of KASPar PCR Master Mix (2x concentration, containing KTaQ polymerase and ROX), 2.2 mM MgCl_2 and 10 ng of DNA.

Statistical analysis

SNP based analyses

Binary logistic regression analysis with the addition of independent variables, such as sex, age at time of diagnosis and body surface area (BSA) was done using SPSS for Windows version 16.0.1 software (Statistical Package for the Social Sciences, Chicago, IL). The risk for toxicity of MTX treatment was expressed as odds ratio (OR) with 95% confidence intervals (CI). The level of significance was set to 0.05. Deviation from Hardy-Weinberg equilibrium (HWE) was calculated for each SNP using Chi-square test. The level of deviation was set to 0.05. Power calculations were done using G*Power software version 3.1.0. Our study had an 80% statistical power to detect medium effect sizes (0.331) with an alpha level of 0.05. The correction for false-positive findings was done using a method for detecting false-positive report probability (FPRP) described by Wacholder *et al.*²⁶

The cut-off for noteworthy results was set as 0.5. The expected ORs were based on the previous reports of an association of SNPs in *SLC19A1* with MTX-toxicity.^{9,10,11,14,15} Prior probability was set to high ($\pi = 0.1$) due to well documented association of *SLC19A1* and MTX transport.²⁷

Haplotype based analysis

SLC19A1 haploblocks and linkage disequilibrium (LD) between the selected SNPs were visualized using HaploView software version 4.1.²⁴ *SLC19A1* haplotype construction was performed using Tagger pairwise method.

Results

Patient characteristics

Of the 88 patients recruited, 48 (54.5%) patients suffered from MTX-induced adverse events. Specific MTX-induced ADEs after the first cycle of MTX and their frequencies are presented in Table 1.

Association between individual SNPs and MTX toxicity

The characteristics and the minor allele frequencies (MAF) of the investigated SNPs in *SLC19A1* are

TABLE 2. The influence of rs2838958 genotype on mucositis development - univariate logistic regression analysis

Degree of mucositis	rs2838958 genotype		OR (95% CI)	P
	TT (%)	TC + CC (%)		
0	18 (66.7)	53 (89.8)	reference	
1	4 (14.8)	4 (6.8)	0.340 (0.077–1.500)	0.154
2	4 (14.8)	2 (3.4)	0.170 (0.029–1.007)	0.051
4	1 (3.7)	0 (0.0)	- *	
1–4	9 (33.3)	6 (10.2)	0.226 (0.071–0.725)	0.009
Mean value ± STD	0.59	0.14		0.007

* Calculation was not possible

presented in Supplementary Table 1. In one patient genotyping failed for all SNPs, while genotyping for rs2838951 and rs17004785 failed in two patients. The observed frequencies of the studied SNPs in ALL/NHML patients did not deviate from HWE (data not shown).

With regard to specific ADEs, univariate logistic regression analysis revealed only the association of rs2838958 with the occurrence of mucositis development ($p = 0.009$). We observed that patients with rs2838958 TT genotype had higher probability for mucositis development as compared to carriers of at least one polymorphic rs2838958 C allele (OR 0.226 (0.071–0.725), $p < 0.009$) (Table 2).

We then investigated the possible association between SLC19A1 polymorphisms and MTX-induced ADEs with the multivariate analysis using an additive model (*per allele*), but a statistically significant relationship could be established neither for overall nor for specific ADEs (Table 3). A margin-

ally significant impact on the risk of mucositis was observed for rs2838951 (OR 2.160 (0.909–5.129), $p = 0.081$).

We also performed haplotype analysis to ascertain whether the combination of polymorphisms that define a specific haplotype impacts the occurrence of ADEs. As shown in Figure 1 the investigated polymorphisms were lying in the same haplotype.

The frequencies of SLC19A1 haplotypes in patients with ALL and NHML that were treated with HD-MTX are shown in Table 4. The Haplotype TGTTCCC (H2), which has wild type alleles present on all loci, was selected as the reference haplotype for the analysis. By frequency, it is the second most common haplotype in the patient test group with a frequency of 33.4%. The haplotype CACCCCG (H1) had polymorphic alleles present on the first four and on the last locus, with wild type alleles present on the fifth and sixth loci. The

TABLE 3. The impact of SLC19A1 genotypes on the occurrence of any and specific MTX-induced adverse events using multivariate analysis – an additive model

SNP ID	Any adverse events		Leukopenia		Thrombocytopenia		Mucositis		Neurotoxicity	
	OR (CI 95%)	P								
rs1131596	0.719 (0.354–1.458)	0.360	0.609 (0.310–1.197)	0.150	1.170 (0.532–2.576)	0.696	1.292 (0.525–3.170)	0.579	0.542 (0.146–2.016)	0.361
rs1051266	1.392 (0.686–2.824)	0.360	1.643 (0.836–3.230)	0.150	0.855 (0.388–1.881)	0.696	0.775 (0.316–1.906)	0.579	0.542 (0.146–2.016)	0.361
rs2838958	1.221 (0.599–2.490)	0.583	1.684 (0.849–3.339)	0.136	0.556 (0.240–1.291)	0.172	0.476 (0.182–1.243)	0.130	0.453 (0.122–1.677)	0.236
rs2838956	1.411 (0.686–2.899)	0.349	1.742 (0.878–3.458)	0.113	0.689 (0.303–1.566)	0.374	0.705 (0.283–1.759)	0.454	0.596 (0.163–2.182)	0.434
rs17004785	0.849 (0.280–2.572)	0.772	1.393 (0.476–4.079)	0.545	0.854 (0.218–3.349)	0.821	0.672 (0.148–3.055)	0.606	1.226 (0.255–5.899)	0.800
rs12483377	1.475 (0.504–4.318)	0.478	1.825 (0.672–4.956)	0.238	1.688 (0.540–5.280)	0.368	0.930 (0.249–3.473)	0.914	1.061 (0.232–4.861)	0.939
rs2838951	1.261 (0.666–2.412)	0.483	0.740 (0.392–1.394)	0.351	1.652 (0.786–3.473)	0.185	2.160 (0.909–5.129)	0.081	1.693 (0.577–4.967)	0.337

The estimates for the odds ratio (OR) were adjusted to the following variables: age, sex, and treatment regimen.

TABLE 5. The impact of gender, age, treatment regimen and SLC19A1 haplotypes on the occurrence of any and specific (thrombocytopenia, mucositis, and neurotoxicity) MTX-induced adverse events

	All		Thrombocytopenia		Mucositis		Neurotoxicity	
	OR (95% CI)	P	OR (95% CI)	P	OR (95% CI)	P	OR (95% CI)	P
Gender	2.385 (0.908–6.259)	0.078	1.615 (5.134–5.076)	0.413	1.523 (0.423–5.472)	0.520	0.531 (0.093–3.024)	0.475
Age	1.028 (0.931–1.134)	0.588	9.526 (8.422–1.078)	0.440	1.054 (0.935–1.190)	0.396	1.088 (0.931–1.272)	0.289
Treatment regimen	2.050 (1.065–3.943)	0.031*	9.839 (4.620–2.095)	0.962	1.676 (0.689–4.075)	0.255	1.282 (0.397–4.139)	0.678
H1 = CACCCCG	1.000 (0.472–2.117)	0.943	6.615 (2.769–1.579)	0.352	0.419 (0.150–1.167)	0.096	0.309 (0.070–1.364)	0.120
H3 = TGTTGTC	1.110 (0.335–3.618)	0.844	9.220 (2.254–3.750)	0.891	0.593 (0.122–2.877)	0.515	0.951 (0.175–5.150)	0.934
H4 = TGTTCCC	0.143 (0.023–0.852)	0.030*	3.617 (4.568–2.541)	0.379	0.005 (0.0–NC)	0.985	0.014 (0.0–NC)	0.992
Rare haplotypes	2.002 (0.580–6.775)	0.275	9.113 (2.607–3.171)	0.871	2.002 (0.580–6.775)	0.275	2.002 (0.580–6.775)	0.275

*p < 0.05; H2 was the reference haplotype

statistically significantly reduces the risk for the occurrence of ADEs during treatment with HD-MTX. Since the frequency is low in our sample it is difficult to ascertain its clinical relevance given the number of patients and the small number of individual toxic events.

Haplotype based approaches have been rarely used when investigating HD-MTX induced adverse events in ALL and NHML patients. One study investigated the influence of *MTHFR* SNPs and haplotypes on treatment response²⁹ and HD-MTX toxicity^{30,31}, while the other studies focused on DNA repair and cell cycle processes on risk for leukaemia development using haplotype based approach.^{32–36}

Only study of Lopez-Lopez focused on MTX transporters. This study examined 384 SNPs in 12 transporter genes, including *SLC19A1*, and their relationship to MTX plasma levels and MTX-related toxicities.¹⁹ They found no association between *SLC19A1* haplotypes and MTX plasma levels. However they confound the results of Treviño and colleagues on association between *SLCO1B1* rs11045879 polymorphism and toxicity and observed for the first time a significant association with MTX plasma levels and rs9516519 in *ABCC4*, rs3740065 and haplotype GCGGG in *ABCC2*.¹⁹

However, haplotype based approach has been used in analysing the influence of the polymorphisms in the broader region of *SLC19A1* on the occurrence of low dose MTX-induced ADEs in rheumatoid arthritis (RA) patients in order to facilitate the design of personalized low dose MTX

treatment.^{37,38} Bohanec Grabar *et al.* reported that individual SNP and haplotype analysis suggest that rs1051266 could be a functional variant altering MTX toxicity; rs1051266 and rs1131956 were significantly associated with protection against discontinuation of treatment owing to MTX toxicity. Rs2838956 was significantly associated with protection against skin ADEs, while two common *SLC19A1* haplotypes carrying rs1051266 and rs1131596 minor alleles had a protective effect towards MTX induced ADEs. Significant association was also found for rs1051266 and rs1131596 with infection.³⁷ Lima *et al.* reported that *SLC19A1* and genotypes and haplotypes may help to identify RA patients with increased risk of MTX-related gastrointestinal toxicity since protective effect of carriers of wild type allele of rs1051266 and rs2838956 regarding MTX induced gastrointestinal toxicity as well as association between GGAG haplotype for *SLC19A1* rs7499, rs1051266, rs2838956 and rs3788200 with MTX gastrointestinal toxicity was established.³⁸

The results of the haplotype based analysis indicate, that other polymorphisms that are in linkage disequilibrium with rs1051266 and rs1131596, may impact the functioning of *SLC19A1* via, for example, alterations in *SLC19A1* splicing.^{39,40} As well, other genes coding for proteins that are involved in the transport and metabolism of MTX can also impact pharmacokinetics and the occurrence of MTX-induced AE, such as *SLCO1B1* SNPs that are associated with lower clearance of MTX and *SLCO1A2* as well.⁴¹ Furthermore, SNP in miR-595

which might affect *SLC19A1* regulation and could affect MTX levels in patients with paediatric B-cell ALL was recently reported.¹⁸

The results of our study show that *SLC19A1* genotyping could be one of the factors that could contribute to safer and more effective treatment with HD-MTX, especially for identifying patient groups at risk of mucositis development in Slovenian patients. As the occurrence of ADEs and the treatment outcome could be affected by other genetic factors involved in the transport and metabolism of MTX as well as by concomitant supportive therapy and the current pathophysiological condition of the patient the results of our study should be confirmed in a larger number of patients.

The main limitation of our study, which is probably also one of the reasons for the inconsistent results among studies published so far, is the limited sample size. Since ALL is a rare disease in children, the number of patients that could be as comparable as possible in the entire treatment process is limited. We therefore also included five patients with NHML in the study, who were treated according to the same protocol as patients with ALL.

The great advantage of our study is that all subjects come from a small and very homogeneous population⁴², that the patient group is clinically well defined and very homogeneous given the type and course of treatment, centralized treatment of patients with an established treatment and supportive regimen. The group was treated by the same medical team in a single centre according to standard criteria.

For genotyping, we used a method that would be suitable for genetic testing in clinical practice, as it is easy to perform, fast, affordable, and enables simultaneous analysis of multiple samples and different polymorphisms if they are run under the same conditions, and also require small amounts of DNA for analysis.

Employing a haplotype based approach we tried to examine the impact of genetic variability in the entire region of the studied gene and also included the possible functional polymorphisms that are in linkage disequilibrium with the selected SNPs. With this approach an even stronger influence of genetic variability of *SLC19A1* with MTX-induced ADEs could be shown as opposed to taking into account only individual SNPs.

The observations of our study provide additional information to the ongoing discussion about the most suitable biological markers to be evaluated during treatment with HD-MTX in order to achieve more efficient, safer and more rational

treatment of children and adolescents with ALL. Additional prospective pharmacogenetic studies on higher sample sizes are needed to further evaluate a possible impact of genetic variability of the MTX transporters that have an impact on pharmacokinetics of MTX and enzymes involved in MTX metabolism that could help us to identify patients that are threatened by serious ADEs during HD-MTX treatment.

References

1. Crews KR, Hicks JK, Pui CH, Relling MV, Evans WE. Pharmacogenomics and individualized medicine: Translating science into practice. *Clin Pharmacol Ther* 2012; **92**: 467-75. doi: 10.1038/clpt.2012.120
2. Evans WE, Relling MV, Rodman JH, Crom WR, Boyett JM, Pui CH. Conventional compared with individualized chemotherapy for childhood acute lymphoblastic leukemia. *N Engl J Med* 1998; **338**: 499-505. doi: 10.1056/NEJM199802193380803
3. Murphy SB, Fairclough DL, Hutchison RE, Berard CW. Non-Hodgkin's lymphomas of childhood: an analysis of the histology, staging, and response to treatment of 338 cases at a single institution. *J Clin Oncol* 1989; **7**: 186-93. doi: 10.1200/JCO.1989.7.2.186
4. Anderson JR, Jenkin RD, Wilson JF, Kjeldsberg CR, Spoto R, Chilcote RR, et al. Long-term follow-up of patients treated with COMP or LSA2L2 therapy for childhood non-Hodgkin's lymphoma: a report of CCG-551 from the Childrens Cancer Group. *J Clin Oncol* 1993; **11**: 1024-32. doi: 10.1200/JCO.1993.11.6.1024
5. Shaw GM, Lammer EJ, Zhu HP, Baker MW, Neri E, Finnell RH. Maternal periconceptional vitamin use, genetic variation of infant reduced folate carrier (A80G), and risk of spina bifida. *Am J Med Genet* 2002; **108**: 1-6.
6. Assaraf YG. The role of multidrug resistance efflux transporters in antifolate resistance and folate homeostasis. *Drug Resist Updat* 2006; **9**: 227-46. doi: 10.1016/j.drug.2006.09.001
7. Zeng H, Chen ZS, Belinsky MG, Rea PA, Kruh GD. Transport of methotrexate (MTX) and folates by multidrug resistance protein (MRP) 3 and MRP1: effect of polyglutamylation on MTX transport. *Cancer Res* 2001; **61**: 7225-32.
8. The Pharmacogenomics Knowledgebase. Pharmacogenomics. Knowledge. Implementation. [cited 2017 Feb 06]. Available from: www.pharmgkb.org
9. Laverdiere C, Chiasson S, Costea I, Moghrabi A, Krajcinovic M. Polymorphism G80A in the reduced folate carrier gene and its relationship to methotrexate plasma levels and outcome of childhood acute lymphoblastic leukemia. *Blood* 2002; **100**: 3832-4. doi: 10.1182/blood.V100.10.3832
10. Imanishi H, Okamura N, Yagi M, Noro Y, Moriya Y, Nakamura T, et al. Genetic polymorphisms associated with adverse events and elimination of methotrexate in childhood acute lymphoblastic leukemia and malignant lymphoma. *J Hum Genet* 2007; **52**: 166-71. doi: 10.1007/s10038-006-0096-z
11. Kishi S, Griener J, Cheng C, Das S, Cook EH, Pei D, et al. Homocysteine, pharmacogenetics, and neurotoxicity in children with leukemia. *J Clin Oncol* 2003; **21**: 3084-91. doi: 10.1200/JCO.2003.07.056
12. Shimasaki N, Mori T, Samejima H, Sato R, Shimada H, Yahagi N, et al. Effects of methylenetetrahydrofolate reductase and reduced folate carrier 1 polymorphisms on high-dose methotrexate-induced toxicities in children with acute lymphoblastic leukemia or lymphoma. *J Pediatr Hematol Oncol* 2006; **28**: 64-8. doi: 10.1097/01.mph.0000198269.61948.90
13. Faganel Kotnik B, Dolzan V, Grabnar I, Jazbec J. Relationship of the reduced folate carrier gene polymorphism G80A to methotrexate plasma concentration, toxicity, and disease outcome in childhood acute lymphoblastic leukemia. *Leuk Lymphoma* 2010; **51**: 724-6. doi: 10.3109/10428191003611402
14. Shimasaki N, Mori T, Torii C, Sato R, Shimada H, Tanigawara Y, et al. Influence of MTHFR and RFC1 polymorphisms on toxicities during maintenance chemotherapy for childhood acute lymphoblastic leukemia or lymphoma. *J Pediatr Hematol Oncol* 2008; **30**: 347-52. doi: 10.1097/MPH.0b013e318165b25d

15. Faganel Kotnik B, Grabnar I, Bohanec Grabar P, Dolžan V, Jazbec J. Association of genetic polymorphism in the folate metabolic pathway with methotrexate pharmacokinetics and toxicity in childhood acute lymphoblastic leukaemia and malignant lymphoma. *Eur J Clin Pharmacol* 2011; **67**: 993-1006. doi: 10.1007/s00228-011-1046-z
16. Huang L, Tissing WJ, de Jonge R, van Zelst BD, Pieters R. Polymorphisms in folate-related genes: association with side effects of high-dose methotrexate in childhood acute lymphoblastic leukemia. *Leukemia* 2008; **22**: 1798-800. doi: 10.1038/leu.2008.66
17. Zgheib NK, Akra-Ismael M, Aridi C, Mahfouz R, Abboud MR, Solh H, et al. Genetic polymorphisms in candidate genes predict increased toxicity with methotrexate therapy in Lebanese children with acute lymphoblastic leukemia. *Pharmacogenet Genomics* 2014; **24**: 387-96. doi: 10.1097/FPC.000000000000069
18. Iparraguirre L, Gutierrez-Camino A, Umerez M, Martin-Guerrero I, Astigarraga I, Navajas A, et al. MiR-pharmacogenetics of methotrexate in childhood B-cell acute lymphoblastic leukemia. *Pharmacogenet Genomics* 2016; **26**: 517-25. doi: 10.1097/FPC.0000000000000245
19. Lopez-Lopez E, Ballesteros J, Piñan MA, Sanchez de Toledo J, Garcia de Andoin N, Garcia-Miguel P, et al. Polymorphisms in the methotrexate transport pathway: a new tool for MTX plasma level prediction in pediatric acute lymphoblastic leukemia. *Pharmacogenet Genomics* 2013; **23**: 53-61. doi: 10.1097/FPC.0b013e32835c3b24
20. Ribas G, González-Neira A, Salas A, Milne RL, Vega A, Carracedo B, et al. Evaluating HapMap SNP data transferability in a large-scale genotyping project involving 175 cancer-associated genes. *Hum Genet* 2006; **118**: 669-79. doi: 10.1007/s00439-005-0094-9
21. Johnson GC, Esposito L, Barratt BJ, Smith AN, Heward J, Di Genova G, et al. Haplotype tagging for the identification of common disease genes. *Nat Genet* 2001; **29**: 233-7. doi: 10.1038/ng1001-233
22. World Health Organization. *Handbook for reporting results of cancer treatment*. Geneva: World Health Organization; 1979. p. 15-22.
23. National Cancer Institute. Common Toxicity Criteria Version 1. [cited 2017 Feb 06]. Available from: URL: <http://ctep.cancer.gov/reporting/ctc.html>
24. Broad Institute. HaploView software version 4.1. [cited 2017 Feb 06]. Available from: <http://www.broad.mit.edu/haploview/haploview-downloads>
25. LGC. Science for a safer world. [cited 2017 Feb 06]. Available from: <http://www.kbioscience.co.uk>
26. Wacholder S, Chanock S, Garcia-Closas M, El Ghormli L, Rothman N. Assessing the probability that a positive report is false: an approach for molecular epidemiology studies. *J Natl Cancer Inst* 2004; **17**: 96: 434-42.
27. Moscow JA, Gong M, He R, Sgagias MK, Dixon KH, Anzick SL, et al. Isolation of a gene encoding a human reduced folate carrier (RFC1) and analysis of its expression in transport-deficient, methotrexate-resistant human breast cancer cells. *Cancer Res* 1995; **55**: 3790-4.
28. Whetstine JR, Gifford AJ, Witt T, Liu XY, Flatley RM, Norris M et al. Single nucleotide polymorphisms in the human reduced folate carrier: characterization of a high-frequency G/A variant at position 80 and transport properties of the His(27) and Arg(27) carriers. *Clin Cancer Res* 2001; **7**: 3416-22.
29. Aplenc R, Thompson J, Han P, La M, Zhao H, Lange B, et al. Methylenetetrahydrofolate reductase polymorphisms and therapy response in pediatric acute lymphoblastic leukemia. *Cancer Res* 2005; **65**: 2482-7. doi: 10.1158/0008-5472.CAN-04-2606
30. Kałużna E, Strauss E, Zając-Spychała O, Gowin E, Świątek-Kościelna B, Nowak J, et al. Functional variants of gene encoding folate metabolizing enzyme and methotrexate-related toxicity in children with acute lymphoblastic leukemia. *Eur J Pharmacol* 2015; **769**: 93-9. doi: 10.1016/j.ejphar.2015.10.058
31. Liao QC, Li XL, Liu ST, Zhang Y, Li TY, Qiu JC. [Association between the methylenetetrahydrofolate reductase gene polymorphisms and haplotype with toxicity response of high dose methotrexate chemotherapy]. [Chinese]. *Zhonghua Liu Xing Bing Xue Za Zhi* 2012; **33**: 735-9.
32. Meza-Espinoza JP, Peralta-Leal V, Gutierrez-Angulo M, Macias-Gomez N, Ayala-Madriz ML, Barros-Nuñez P, et al. XRCC1 polymorphisms and haplotypes in Mexican patients with acute lymphoblastic leukemia. *Genet Mol Res* 2009; **8**: 1451-8. doi: 10.4238/vol8-4gmr687
33. Chokkalingam AP, Bartley K, Wiemels JL, Metayer C, Barcellos LF, Hansen HM, et al. Haplotypes of DNA repair and cell cycle control genes, X-ray exposure, and risk of childhood acute lymphoblastic leukemia. *Cancer Causes Control* 2011; **22**: 1721-30. doi: 10.1007/s10552-011-9848-y
34. Mosor M, Ziółkowska I, Januszkiewicz-Lewandowska D, Nowak J. Polymorphisms and haplotypes of the NBS1 gene in childhood acute leukaemia. *Eur J Cancer* 2008; **44**: 2226-32. doi: 10.1016/j.ejca.2008.06.026
35. Semsei AF, Erdélyi DJ, Ungvári I, Kámory E, Csóky B, Andrikovics H, et al. Association of some rare haplotypes and genotype combinations in the MDR1 gene with childhood acute lymphoblastic leukaemia. *Leuk Res* 2008; **32**: 1214-20. doi: 10.1016/j.leukres.2007.12.009
36. Pakakasama S, Sirirat T, Kanchanachumpol S, Udomsubpayakul U, Mahasirimongkol S, Kitpoka P, et al. Genetic polymorphisms and haplotypes of DNA repair genes in childhood acute lymphoblastic leukaemia. *Pediatr Blood Cancer* 2007; **48**: 16-20. doi: 10.1002/pbc.20742
37. Bohanec Grabar P, Leandro-García LJ, Inglada-Pérez L, Logar D, Rodríguez-Antona C, Dolžan V. Genetic variation in the SLC19A1 gene and methotrexate toxicity in rheumatoid arthritis patients. *Pharmacogenomics* 2012; **13**: 1583-94. doi: 10.2217/pgs.12.150
38. Lima A, Bernardes M, Azevedo R, Monteiro J, Sousa H, Medeiros R, Seabra V. SLC19A1, SLC46A1 and SLC01B1 polymorphisms as predictors of methotrexate-related toxicity in Portuguese rheumatoid arthritis patients. *Toxicol Sci* 2014; **142**: 196-209. doi: 10.1093/toxsci/kfu162
39. Williams FM, Flintoff WF. Structural organization of the human reduced folate carrier gene: evidence for 5' heterogeneity in lymphoblast mRNA. *Somat Cell Mol Genet* 1998; **24**: 143-56.
40. Whetstine JR, Flatley RM, Matherly LH. The human reduced folate carrier gene is ubiquitously and differentially expressed in normal human tissues: identification of seven non-coding exons and characterization of a novel promoter. *Biochem J* 2002; **367**: 629-40. doi: 10.1042/BJ20020512
41. Trevino LR, Shimasaki N, Yang W, Panetta JC, Cheng C, Pei D, et al. Germline genetic variation in an organic anion transporter polypeptide associated with methotrexate pharmacokinetics and clinical effects. *J Clin Oncol* 2009; **27**: 5972-8. doi: 10.1200/JCO.2008.20.4156
42. Vidan- Jeras B, Jurca B, Dolzan V, Jeras M, Breskvar K, Bohinjec M. Caucasian Slovenian normal. In: Gjertson DW, Terasaki PI, editors. HLA 1998. Lenexa: American society for histocompatibility and immunogenetics; 1998. p. 180-1.

Impact on radiation dose and volume V57 Gy of the brain on recurrence and survival of patients with glioblastoma multiformae

Igor Stojkovski, Valentina Krstevska, Snezhana Smichkoska

University Clinic of Radiotherapy and Oncology, Skopje, Macedonia

Radiol Oncol 2017; 51(4): 463-468.

Received 11 June 2017

Accepted 11 September 2017

Correspondence to: Igor Stojkovski, University Clinic of Radiotherapy and Oncology - Skopje, Majka Tereza (Vodnjanska) 17, 1000 Skopje, Macedonia. Phone: +389 7 639 7454; Fax: +389 2 311 1430; E-mail: istojkovski@gmail.com

Disclosure: No potential conflicts of interest were disclosed.

Background. The aim of the study was to analyze impact of irradiated brain volume V57 Gy (volume receiving 57 Gy and more) on time to progression and survival of patients with glioblastoma.

Patients and methods. Dosimetric analysis of treatment plan data has been performed on 70 patients with glioblastoma, treated with postoperative radiochemotherapy with temozolomide, followed by adjuvant temozolomide. Patients were treated with 2 different methods of definition of treatment volumes and prescription of radiation dose. First group of patients has been treated with one treatment volume receiving 60 Gy in 2 Gy daily fraction (31 patients) and second group of the patients has been treated with "cone-down" technique, which consisted of two phases of treatment: the first phase of 46 Gy in 2 Gy fraction followed by "cone-down" boost of 14 Gy in 2 Gy fraction (39 patients). Quantification of V57 Gy and ratio brain volume/V57Gy has been done. Average values of both parameters have been taken as a threshold value and patients have been split into 2 groups for each parameter (values smaller/larger than threshold value).

Results. Mean value for V57 Gy was 593.39 cm³ (range 166.94 to 968.60 cm³), mean value of brain volume has been 1332.86 cm³ (range 1047.00 to 1671.90 cm³) and mean value of brain-to-V57Gy ratio was 2.46 (range 1.42 to 7.67). There was no significant difference between two groups for both V57 Gy and ratio between brain volume and V57 Gy.

Conclusions. Irradiated volume with dose 57 Gy or more (V57 Gy) and ration between whole brain volume and 57 Gy had no impact on time to progression and survival of patients with glioblastoma.

Key words: irradiation V57; glioblastoma

Introduction

Glioblastoma is most common and most aggressive brain tumor with incidence of 2-3 per 100 000 population according to GLOBOCAN.¹ Incidence of glioblastoma accounts 12-15% of all intracranial tumors and approximately 50-60 of all astrocytic tumors.^{2,3} Diagnosis, treatment and follow up of patients with glioblastoma and multidisciplinary approach and best results are achieved in specialized centers, which can offer all treatment modalities when it is needed and which are more

experienced with larger volume of cases.⁴ Mutual understanding and collaboration of team of professionals is of paramount importance for obtaining best medical care and best clinical results (tumor control and survival). During last two decades, major advantages have been made in enhancing precision of radiation treatment and shaping of radiation dose to increase dose distribution in target and to decrease radiation dose in organs at risk. Three-dimensional conformal radiotherapy and its derivatives, Intensity Modulated Radiation Therapy (IMRT) and Volumetric Arc Therapy (VMAT) are

now standard of treatment for patients with glioblastoma.⁵⁻⁷ Standard postoperative treatment of patients with glioblastoma consist of postoperative radiotherapy with temozolomide followed by adjuvant temozolomide.⁸⁻¹¹ Radiotherapy is corner-stone of multimodality approach and it is considered as treatment with highest benefit of all three treatment modalities. Despite the major advantages in personalization and precision of the radiotherapy treatment, median survival of patients with glioblastoma is still between 12 and 16 months from diagnosis.⁴

In general there are two major approaches in definition of gross tumor volume (GTV) in patients with glioblastoma. In studies conducted by EORTC (European Organization for Research and Treatment of Cancer) only one contoured gross tumor volume is used which is defined as an enhanced visible tumor on MR images prior the surgery expanded respectively to clinical target volume (CTV) and planning target volume (PTV) according ESTRO-ACROP Guidelines.⁷

In contrast in studies conducted by RTOG (Radiation Therapy Oncology Group) definition of volumes in according to “cone-down” approach, which means that there are virtually two volumes defined on preoperative and/or postoperative MR, one initial (larger) volume and second “cone-down” volume or boost volume (smaller). With “cone-down” approach in some clinical situation it is possible do decrease radiation dose to the brain which could have impact on survivorship of patients with glioblastoma.^{12,13}

Volume of the tumor measured as initial tumor size or preoperative tumor size and residual disease is generally considered as a prognostic factor for survival and recurrence in patients with glioblastoma.^{14,15} There are various approaches and quantification of what is really visible tumor and

consequently, what volume should be irradiated in order to minimize tumor recurrence, but reaching consensus between different research groups is still under debate. Definition of volume of the tumor, depends of imaging modality used, resolution of imaging modality, processing algorithms and various other variables.¹⁵⁻¹⁸

After definition of gross tumor volume there is still debate, what is most appropriate clinical treatment volume (CTV). There are different approaches, which are evolving together with advances of imaging. CTV as concept in glioblastoma is difficult to define and different research groups have various definitions and no-one of these definitions is absolutely true or false.²⁰⁻²⁸

There are more or less well defined criteria for definition of CTV and PTV for patients with glioblastoma specially treated in clinical trial setting, as AVAGlio and Centric trials, recently.^{28,29}

Also it is well known fact that in daily clinical practice clinicians are adopting volume delineation according to their clinical setting and capabilities, and using delineation according to RTOG, EORTC or institutional standards.³⁰

In our study we treated patients with two different approaches on delineation on treatment volumes using one phase treatment EORTC “like” and RTOG “like” approach, but randomization was used for assignment of patients in the group as a part of the standard protocol for treatment developed in the institution.

Patients and methods

This study was approved by the ethical committee of Medical Faculty at University “Ss. Cyril and Methodius” in Skopje and University Clinic of Radiotherapy and Oncology in Skopje (Number: 03-2455/2) and was carried out according to the Declaration of Helsinki.

Total of 70 patients, with glioblastoma multiforme has been included in this study. Patient accrual has been performed in the period from January 2013 to December 2015. All patients have been previously surgically treated with maximal safe resection of the primary tumor and definitive histological diagnosis has been established as a glioblastoma multiforme according to the last World Health Organization classification.³

After referral to radiotherapy treatment, patients have been scheduled for computed tomography (CT) simulation in treatment position. CT scan has encompassed cranial region according to

TABLE 1. Patient characteristics

	Group 1 (1 v) 31 patients	Group 2 (cone-down) 39 patients
Age	Range 29–71, median age 56	Range 27–75, median age 56
Sex	Male - 14 Female - 17	Male - 21 Female - 18
Location of the primary lesion	5 - frontal lobe 6 - temporal lobe 11 - parietal lobe 2 - occipital lobe 7 - overlapping	8 - frontal lobe 15 - temporal lobe 9 - parietal lobe 1 - occipital lobe 6 - overlapping
Average time from surgery to RT (days)	36 (25–55)	39 (24–74)
V57 Gy	< 600 cm ³ - 15 > 600 cm ³ - 16	< 600 cm ³ - 23 > 600 cm ³ - 16

institutional protocol with slice thickness of 2 mm. For immobilization purpose thermoplastics masks and head rests have been used during simulation and treatment.

After computed tomography simulation, image fusion with preoperative and/or postoperative MR scan has been done using automatic MR-CT fusion using non deformable algorithm with manual correction, only if necessary, leaded by decision of radiation oncologist. MR-CT fusion has been done using transversal MR images using T1 with contrast and T2/FLAIR sequence. In the analysis has been included only patents who finished complete treatment, total of 70 patients from included 78 patients. Eight patients did not finish treatment, and were excluded from analysis.

Patients have been randomly assigned to one of the groups on the basis of referral to the department. Patients with odd hospital number have been assigned to the first group, and patients with even hospital number have been assigned to second group. In the first group of the patients (total of 31 patients), delineation was based on T2/FLAIR and T1 with contrast enhancements and only one GTV volume has been contoured. After delineation of GTV, CTV was expanded for 2 cm, taking in account anatomic boundaries and omitting, if possible, organs at risk. CTV was expanded to PTV with addition of margin of 5 mm, which is considered institutional standard. In the second group (total of 39 patients), "cone-down" approach has been used and delineation of target volume has been done in two phases and two GTV volumes have been delineated. First or initial volume GTV46, has been delineated based on MR images using T2/FLAIR abnormalities. Expansion of GTV to CTV has been done with margin of 2 cm, taking in account anatomic boundaries and avoidance of organs at risk, similar as in first group. Further expansion of CTV to PTV was with margin of 5 mm. Cone down volume or boost volume has been delineated on contrasts enhanced T1 MR Image set. CTV has been expanded for 2 cm, and PTV expanded further for 0.5 cm, as initial delineated volume.

Dose prescription for patients in the first group was 60 Gy in 30 daily fractions of 2 Gy and in second group, prescribed dose for initial volume was 46 Gy in 23 fractions and for the "cone-down" volume additional 14 Gy in 7 fractions. Initial and "cone-down" volumes have been treated with 2 Gy daily fractions. Treatment schedules for both groups were 5 fractions on each consecutive day in 7 days week.

Treatment planning has been done using Varian Eclipse planning system version 10.0.45.0 and the most appropriate treatment plan have been selected in order to achieve dose distribution in target(s) and in organs at risk in order to fulfill QUANTEC criteria.³¹⁻³³

Together with radiotherapy all patients were treated according to "Stupp protocol" and received concurrent chemotherapy with temozolomide, followed by adjuvant temozolomide.³⁵

After treatment, patients undergo follow up which consisted of physical examination every month which corresponded with adjuvant chemotherapy cycle, MR every 3-4 months and other clinical examination if necessary. Follow up strategy was in line with ESMO clinical recommendations and modified according to specific clinical situation.⁹

Two volumetric parameters were selected as relevant in order to predict exposure to brain as an organ at risk in our series of patients. First parameter is volume which received 57 Gy and more in cm^3 , "V57Gy", and second parameter is calculated as a ratio between brain volume and "V57Gy", calculated as numeric coefficient, decimal number.

"V57Gy" was calculated using TPS software and using build in algorithms for converting isodose level to structure. This function is standard in majority of modern treatment planning systems available in the market and it is available as a standard option in our institutional TPS.

Patients has been separated in 2 groups for both parameters and threshold values were estimated for "V57Gy" equal to 600 cm^3 and for ratio between brain volume and "V57Gy" equal to 2.4 presented as a decimal number.

Based on the first parameter, patents were split on 2 groups. The first group of patients with "V57Gy" up to 600 cm^3 consisted of 38 patients, and second group of patients with "V57Gy" more than 600 cm^3 consisted of 32 patients.

According to second parameter, ratio between brain volume and "V57Gy", patients were also split into 2 groups: patients with ratio less than 2.4 numeric value (40 patients) and patients with ratio of more than 2.4 (30 patients).

Results

Median follow up of all 70 patients was 12 months (range from 4 to 33 months). Median time to progression (recurrence) was 12 months and median

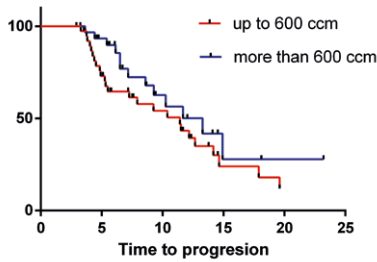


FIGURE 1. Time to progression for "V57Gy" volume. Threshold value was 600 cm³.

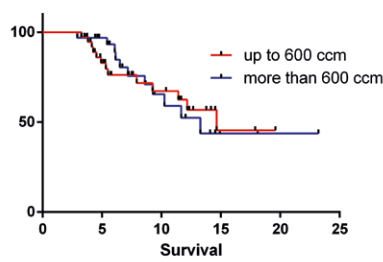


FIGURE 2. Overall survival for "V57Gy" volume. Threshold value was 600 cm³.

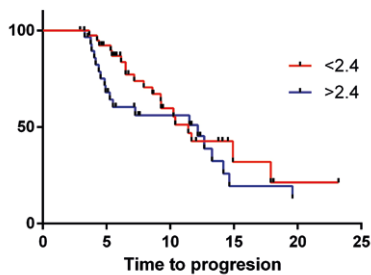


FIGURE 3. Time to progression for ratio between brain volume and "V57Gy" volume. Threshold value was 2.4.

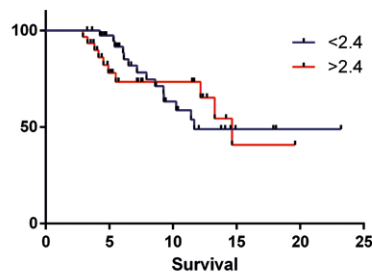


FIGURE 4. Overall survival for ratio between brain volume and "V57Gy" volume. Threshold value was 2.4.

survival was calculated as 24 months using Kaplan Meir method.³⁵

Survival analysis using Kaplan Meir method has been done on two parameters for both time to progression (recurrence) and overall survival. Comparison of survival has been calculated using Matel-Cox and Gehan-Breslow-Wilcoxon (log-rank) tests.^{36,37}

For volumetric parameter of "V57Gy", comparison of patients with "V57 Gy" of less than 600 cm³ (38 patients) and more than 600 cm³ (32 patients) has been done. Time to progression for group of patients with "V57Gy" ≤ 600 cm³ was 11.43 months and for group of patients with "V57Gy" > 600 cm³ was 13.29 and for overall survival, 14.64 and 13.29 months. (Figure 1, 2). There was not any significant difference for both time to progression ($p = 0.2065$) and overall survival ($p = 0.9970$).

For second parameter, calculated as numeric value, ration between whole brain volume and "V57Gy" volume, comparison for time to progression and overall survival for patients with numerical value ≤ 2.4 (40 patients) and numeric value > 2.4 (30 patients) has been done. Median time to progression for group of patients with value ≤ 2.4 was 11.43 months and for group of patients with numeric value > 2.4 was 12.18 months. Overall survival

was 11.68 and 14.64 months respectively. There was no significant difference in time to progression ($p = 0.2881$) and overall survival ($p = 0.8572$) between this two groups (Figure 3, 4).

Discussion

Based on this data we concluded that these volumetric parameters did not have any impact on time to progression and overall survival on patients with glioblastoma, treated with postoperative radiochemotherapy. In general, in malignant tumors, size of the tumor is considered as an independent prognostic factor which is described as a T stage according to UICC Classification³⁸, but due to specific characteristics of brain tumors, TNM classification for prognostic values is not applicable, but rather WHO classification which do not correspond to size of the tumor. According to EORTC and NCIC nomogram for predicting outcome in patients with newly diagnosed glioblastoma, there are several factors which are predicting survival. Following parameters are suggested as potential prognostic factors, which should be reported in all clinical studies: MGMT promoter methylation status, age, performance status, extent of resection, and Mini Mental State Examination (MMSE).³⁹

Volumetric parameters calculated in our study did not have impact on local control and overall survival. In our study threshold value was estimated as an average value from our series of the patients. In the future studies we are planning to include more patients for evaluation of volumetric parameters and to create more strict constraints with higher gradient. In this case we had approximation that there will be difference in both recurrence and survival for patients with smaller irradiated volumes compared with very large irradiated volume, which should be proven in future studies.

Radiation treatment of CNS tumors has been evolved in the past two decades with introduction of more precise imaging and treatment devices in radiation oncology followed by development of more precise treatment techniques. Despite the fact that modern treatment devices are able to deliver higher dose to specified tumor volume, using possibility to conform beams in order to protect critical organs there, are not positive studies to prove that escalation of radiation dose beyond 60 Gy with standard fractionation will have impact of the disease control.⁴⁰ There are some exceptions regarding dose and fractionation for patients with poor performance status. Recent studies showed that

shortening duration of radiotherapy treatment with increasing daily fraction (40 Gy in 15 fractions or 25 Gy in 5 fractions) is with equivalent results regarding survival and quality of life.⁴² In our study we showed that decreasing of treated volume with cone-down approach did not have any impact on marginal recurrence in glioblastoma patients treated with radiotherapy and concurrent and adjuvant temozolomide. These results are in line with recent published studies that reducing treated volume with careful delineation of visible tumor on MR, will not have any impact on marginal recurrence.⁴²⁻⁴⁵

Finally, careful selection of imaging modalities, registration and selection of the most suitable treatment plan is of paramount importance for obtaining best results and obtaining best local control during radiation treatment of patients with glioblastoma.

References

1. Ferlay J, Soerjomataram I, Dikshit R, Eser S, Mathers C, Rebelo M, et al. Cancer incidence and mortality worldwide: sources, methods and major patterns in GLOBOCAN 2012. *Int J Cancer* 2015; **136**: E359-86. doi: 10.1002/ijc.29210
2. Louis DN, Ohgaki H, Wiestler OD, Cavenee WK, Burger PC, Jouvet A, et al. The 2007 WHO classification of tumours of the central nervous system. *Acta Neuropathol* 2007; **114**: 97-109. doi: 10.1007/s00401-007-0243-4
3. Louis DN, Perry A, Reifenberger G, von Deimling A, Figarella-Branger D, Cavenee WK, et al. The 2016 World Health Organization classification of tumors of the central nervous system: a summary. *Acta Neuropathol* 2016; **131**: 803-20. doi: 10.1007/s00401-016-1545-1
4. Thumma SR, Fairbanks RK, Lamoreaux WT, Mackay AR, Demakas JJ, Cooke BS, et al. Effect of pretreatment clinical factors on overall survival in glioblastoma multiforme: a Surveillance Epidemiology and End Results (SEER) population analysis. *World J Surg Oncol* 2012; **10**: 75. doi: 10.1186/1477-7819-10-75
5. Belkacemi Y, Bolle S, Bourdeaut F, Collin P, Cornu P, Delatre JY, et al. Guidelines, 'minimal requirements' and standard of care in glioblastoma around the Mediterranean Area: A report from the AROME (Association of Radiotherapy and Oncology of the Mediterranean arEa) Neuro-Oncology working party. *Crit Rev Oncol Hematol* 2016; **98**: 189-99. doi: 10.1016/j.critrevonc.2015.10.014
6. Mason WP, Maestro RD, Eisenstat D, Forsyth P, Fulton D, Laperriere N, et al. Canadian recommendations for the treatment of glioblastoma multiforme. *Curr Oncol* 2007; **14**: 110-7. doi: http://dx.doi.org/10.3747/co.2007.119
7. Niyazi M, Brada M, Chalmers AJ, Combs SE, Erridge SC, Fiorentino A, et al. ESTRO-ACROP guideline 'target delineation of glioblastomas'. *Radiother Oncol* 2016; **118**: 35-42. doi: 10.1016/j.radonc.2015.12.003
8. Stupp R, Tonn JC, Brada M, Pentheroudakis G. High-grade malignant glioma: ESMO clinical practice guidelines for diagnosis, treatment and follow-up. *Ann Oncol* 2010; **21**(Suppl. 5): 190-3. doi: 10.1093/annonc/mdq187
9. Stupp R, Brada M, van den Bent MJ, Tonn JC, Pentheroudakis G. High-grade glioma: ESMO clinical practice guidelines for diagnosis, treatment and follow-up. *Ann Oncol* 2014; **25**: 93-101. doi: 10.1093/annonc/mdu050
10. Weller M, van den Bent M, Hopkins K, Tonn JC, Stupp R, Falini A, et al. EANO guideline for the diagnosis and treatment of anaplastic gliomas and glioblastoma. *Lancet Oncol* 2014; **15**: e395-403. doi: 10.1016/S1470-2045(14)70011-7
11. National Comprehensive Cancer Network. Central Nervous System Cancers (Version 1.2016). [cited 15 May 2017]. Available at: https://www.nccn.org/professionals/physician_gls/pdf/cns.pdf.
12. Kazda T, Jancalek R, Pospisil P, Sevela O, Prochazka T, Vrzal M, et al. Why and how to spare the hippocampus during brain radiotherapy: the developing role of hippocampal avoidance in cranial radiotherapy. *Radiat Oncol* 2014; **9**: 139. doi: 10.1186/1748-717X-9-139
13. Conson M, Cella L, Pacelli R, Comerci M, Liuzzi R, Salvatore M, et al. Automated delineation of brain structures in patients undergoing radiotherapy for primary brain tumors: From atlas to dose-volume histograms. *Radiother Oncol* 2014; **112**: 326-31. doi: 10.1016/j.radonc.2014.06.006
14. Grabowski MM, Recinos PF, Nowacki AS, Schroeder JL, Angelov L, Barnett GH, et al. Residual tumor volume versus extent of resection: predictors of survival after surgery for glioblastoma. *J Neurosurg* 2014; **121**: 1115-23. doi: 10.3171/2014.7.JNS132449
15. Pessina F, Navarria P, Cozzi L, Tomatis S, Riva M, Ascolese AM, et al. Role of surgical resection in recurrent glioblastoma: prognostic factors and outcome evaluation in an observational study. *J Neurooncol* 2016; **131**: 1-8. doi: 10.1007/s11060-016-2310-y
16. Feng Y, Clayton EH, Okamoto RJ, Engelbach J, Bayly P V, Garbow JR. A longitudinal magnetic resonance elastography study of murine brain tumors following radiation therapy. *Phys Med Biol* 2016; **61**: 6121-31. doi: 10.1088/0031-9155/61/16/6121
17. Molina D, Pérez-Beteta J, Martínez-González A, Sepúlveda JM, Peralta S, Gil-Gil MJ, et al. Geometrical measures obtained from pretreatment post-contrast T1 weighted MRIs predict survival benefits from bevacizumab in glioblastoma patients. *PLoS One* 2016; **11**: e0161484. doi: 10.1371/journal.pone.0161484
18. Sreenivasan S, Madhugiri V, Sasidharan G, Kumar RR. Measuring glioma volumes: A comparison of linear measurement based formulae with the manual image segmentation technique. *J Cancer Res Ther* 2016; **12**: 161. doi: 10.4103/0973-1482.153999
19. Moghaddasi L, Bezak E, Harriss-Phillips W. Evaluation of current clinical target volume definitions for glioblastoma using cell-based dosimetry stochastic methods. *Br J Radiol* 2015; **88**: 1-14. doi: 10.1259/bjr.20150155
20. Chang EL, Akyurek S, Avalos T, Rebueno N, Spicer C, Garcia J, et al. Evaluation of peritumoral edema in the delineation of radiotherapy clinical target volumes for glioblastoma. *Int J Radiat Oncol Biol Phys* 2007; **68**: 144-50. doi: http://dx.doi.org/10.1016/j.ijrobp.2006.12.009
21. Aydin H, Sillenberg I, von Lieven H. Patterns of failure following CT-based 3-D irradiation for malignant glioma. *Strahlenther Onkol* 2001; **177**: 424-31.
22. Bagri PK, Kapoor A, Singh D, Singhal MK, Narayan S, Kumar HS. Addition of magnetic resonance imaging to computed tomography-based three-dimensional conformal radiotherapy planning for postoperative treatment of astrocytomas: Changes in tumor volume and isocenter shift. *South Asian J cancer* 2015; **4**: 18-20. doi: 10.4103/2278-330X.149939
23. Hess CF, Schaaf JC, Kortmann RD, Schabet M, Bamberg M. Malignant glioma: patterns of failure following individually tailored limited volume irradiation. *Radiother Oncol* 1994; **30**: 146-9. doi: http://dx.doi.org/10.1016/0167-8140(94)90044-2
24. Easaw JC, Mason WP, Perry J, Laperrière N, Eisenstat DD, Del Maestro R, et al. Canadian recommendations for the treatment of recurrent or progressive glioblastoma multiforme. *Curr Oncol* 2011; **18**: e126-36.
25. Wallner KE, Galich JH, Krol G, Arbit E, Malkin MG, Concannon JP, et al. Patterns of failure following treatment for glioblastoma multiforme and anaplastic astrocytoma. *Int J Radiat Oncol Biol Phys* 1989; **16**: 1405-9. doi: http://dx.doi.org/10.1016/0360-3016(89)90941-3
26. Halperin EC, Bentel G, Heinz ER, Burger PC. Radiation therapy treatment planning in supratentorial glioblastoma multiforme: an analysis based on post mortem topographic anatomy with CT correlations. *Int J Radiat Oncol Biol Phys* 1989; **17**: 1347-50. doi: http://dx.doi.org/10.1016/0360-3016(89)90548-8
27. Burger PC, Heinz ER, Shibata T, Kleihues P. Topographic anatomy and CT correlations in the untreated glioblastoma multiforme. *J Neurosurg* 1988; **68**: 698-704. doi: 10.3171/2Fjns.1988.68.5.0698
28. Chinot OL, Wick W, Mason W, Henriksson R, Saran F, Nishikawa R, et al. Bevacizumab plus radiotherapy-temozolomide for newly diagnosed glioblastoma. *N Engl J Med* 2014; **370**: 709-22. doi: 10.1056/NEJMoa1308345

29. Stupp R, Hegi ME, Gorlia T, Erridge SC, Perry J, Hong Y-K, et al. Cilengitide combined with standard treatment for patients with newly diagnosed glioblastoma with methylated MGMT promoter (CENTRIC EORTC 26071-22072 study): a multicentre, randomised, open-label, phase 3 trial. *Lancet Oncol* 2014; **15**: 1100-8. doi: 10.1016/S1470-2045(14)70379-1
30. Ghose A, Lim G, Husain S. Treatment for glioblastoma multiforme: current guidelines and Canadian practice. *Curr Oncol* 2010; **17**: 52-8. doi: 10.3747/co.v17i6.574
31. Lawrence YR, Li XA, el Naqa I, Hahn CA, Lawrence BM, Merchant TE, et al. QUANTEC: Radiation dose - volume effects in the brain. *Int J Radiat Oncol* 2010; **76**: S77-85. doi: 10.1016/j.ijrobp.2009.02.091
32. Mayo C, Yorke E, Merchant TE. Radiation associated brainstem injury. *Int J Radiat Oncol Biol Phys* 2010; **76(3 Suppl)**: 36-41. doi: 10.1016/j.ijrobp.2009.08.078
33. Mayo C, Martel MK, Marks LB, Flickinger J, Nam J, Kirkpatrick J. Radiation dose-volume effects of optic nerves and chiasm. *Int J Radiat Oncol Biol Phys* 2010; **76(3 Suppl)**: 28-35. doi: 10.1016/j.ijrobp.2009.07.1753
34. Stupp R, Dietrich PY, Kraljevic SO, Pica A, Maillard I, Maeder P, et al. Promising survival for patients with newly diagnosed glioblastoma multiforme treated with concomitant radiation plus temozolomide followed by adjuvant temozolomide. *J Clin Oncol* 2002; **20**: 1375-82. doi: 10.1200/JCO.2002.20.5.1375
35. Kaplan EL, Meier P. Nonparametric estimation from incomplete observations. *J Am Stat Assoc* 1958; **53**: 457-81. doi: 10.2307/2281868
36. Berty HP, Shi H, Lyons-Weiler J. Determining the statistical significance of survivorship prediction models. *J Eval Clin Pract* 2010; **16**: 155-65. doi: 10.1111/j.1365-2753.2009.01199.x
37. Mantel N. Evaluation of survival data and two new rank order statistics arising in its consideration. *Cancer Chemother Rep* 1966; **50**: 163-70.
38. International Union Against Cancer. *TNM classification of malignant tumours*. Sobin LH, Gospodarowicz MK, Wittekind C, editors. 7th Edition. Oxford: Wiley-Blackwell; 2011.
39. Gorlia T, van den Bent MJ, Hegi ME, Mirimanoff RO, Weller M, Cairncross JG, et al. Nomograms for predicting survival of patients with newly diagnosed glioblastoma: prognostic factor analysis of EORTC and NCIC trial 26981-22981/CE.3. *Lancet Oncol* 2008; **9**: 29-38. doi: http://dx.doi.org/10.1016/S1470-2045(07)70384-4
40. Khan L, Soliman H, Sahgal A, Perry J, Xu W, Tsao MN. External beam radiation dose escalation for high grade glioma. *Cochrane Database Syst Rev* 2016; **8**: CD011475. doi: 10.1002/14651858.CD011475.pub2
41. Roa W, Kepka L, Kumar N, Sinaika V, Matiello J, Lomidze D, et al. International Atomic Energy Agency randomized phase III study of radiation therapy in elderly and/or frail patients with newly diagnosed glioblastoma multiforme. *J Clin Oncol* 2015; **33**: 4145-50. doi: 10.1200/JCO.2015.62.6606
42. McDonald MW, Shu H-KG, Curran WJ, Crocker IR. Pattern of failure after limited margin radiotherapy and temozolomide for glioblastoma. *Int J Radiat Oncol* 2011; **79**: 130-6. doi: 10.1016/j.ijrobp.2009.10.048
43. Minniti G, Amelio D, Amichetti M, Salvati M, Muni R, Bozzao A, et al. Patterns of failure and comparison of different target volume delineations in patients with glioblastoma treated with conformal radiotherapy plus concomitant and adjuvant temozolomide. *Radiother Oncol* 2010; **97**: 377-81. doi: 10.1016/j.radonc.2010.08.020
44. Dobelbower MC, Burnett III OL, Nordal RA, Nabors LB, Markert JM, Hyatt MD, et al. Patterns of failure for glioblastoma multiforme following concurrent radiation and temozolomide. *J Med Imaging Radiat Oncol* 2011; **55**: 77-81. doi: 10.1111/j.1754-9485.2010.02232.x
45. Gebhardt BJ, Dobelbower MC, Ennis WH, Bag AK, Markert JM, Fiveash JB. Patterns of failure for glioblastoma multiforme following limited-margin radiation and concurrent temozolomide. *Radiat Oncol* 2014; **9**: 130. doi: 10.1186/1748-717X-9-130

Quality assurance procedures based on dosimetric, gamma analysis as a fast reliable tool for commissioning brachytherapy treatment planning systems

Grzegorz Zwierzchowski^{1,2}, Grzegorz Bielecki^{1,2}, Janusz Skowronek^{1,3}

¹ Poznan University of Medical Sciences, Faculty of Health Sciences, Poznan, Poland

² Greater Poland Cancer Centre, Medical Physics Department, Poznan, Poland

³ Greater Poland Cancer Centre, Brachytherapy Department, Poznan, Poland

Radiol Oncol 2017; 51(4): 469-474.

Received 25 November 2016

Accepted 10 October 2017

Correspondence to: Dr. Grzegorz Zwierzchowski, Greater Poland Cancer Centre, Medical Physics Department / Brachytherapy Department, Garbary 15 Str, PL 61-855 Poznan, Poland. E-mail: grzegorz.zwierzchowski@gmail.com

Disclosure: No potential conflicts of interest were disclosed.

Background. Fast and easily repeatable methods for commissioning procedures for brachytherapy (BT) treatment planning systems (TPS) are needed. Radiochromic film dosimetry with gamma analysis is widely used in external beam quality assurance (QA) procedures and planar film dosimetry is also increasingly used for verification of the dose distribution in BT applications. Using the gamma analysis method for comparing calculated and measured dose data could be used for commissioning procedures of the newly developed TG-186 and MBDCa calculation algorithms. The aim of this study was dosimetric verification of the calculation algorithm used in TPS when the CT/MRI ring applicator is used.

Materials and methods. Ring applicators with 26 and 30 mm diameters and a 60 mm intra-uterine tube with 60° angle were used for verification. Gafchromic® EBT films were used as dosimetric media. Dose grids, corresponding to each plane (dosimetric film location), were exported from the TPS as a raw data. Gafchromic® films were digitized after irradiation. gamma analysis of the data were performed using the OMNI Pro I'mRT® system, as recommended by the AAPM TG-119 rapport criterion for gamma analysis of 3%, 3 mm and a level of 95%.

Results. For the 26 mm and 30 mm rings, the average gamma ranged, respectively, from 0.1 to 0.44 and from 0.1 to 0.27. In both cases, 99% of the measured points corresponded with the calculated data.

Conclusions. This analysis showed excellent agreement between the dose distribution calculated with the TPS and the doses measured by Gafchromic films. This finding confirms the viability of using film dosimetry in BT.

Key words: brachytherapy; quality assurance; film dosimetry; ring applicator

Introduction

Radiochromic film dosimetry with gamma analysis is widely used in quality assurance procedures for external beam radiotherapy (EBRT). The main advantage of this method is the ability to collect dosimetric data with very high planar resolution in contrast to other methods that are based on point dose measurements.

Introducing fast and easily repeatable methods for commissioning procedures for brachytherapy

(BT) treatment planning systems (TPS) is a complex undertaking in most cases.^{1,2} The relatively low energy range of BT sources induce very high spatial dose gradients in irradiated volumes; as a result, it is difficult to use point dose measurement in high dose volumes because small errors in detector positioning can induce large uncertainties in the measured values.

Planar film dosimetry is increasingly used to verify dose distributions in BT applications. When the stepping source is used, the overall dose distri-

bution in the medium is a product of the contribution from each source position and the modulated step time, which are governed by optimization routines.^{3,4} An advantage of film dosimetry is that it offers the possibility of collecting the dose data in the planar area and using techniques of additive measurements.^{5,6}

Self-developing dosimetry films have long been used to successfully verify dose distributions.^{7,8} Although this approach still needs to be customized—in terms of its technical possibilities and BT TPS realization regime in particular facilities.

Most TPS used for treatment plan preparation are still based on the TG-43 recommendations. These algorithms and optimization routines have been verified by many authors in homogenous conditions.^{9,10} The Sivert integral and modular dose calculation models allow calculations of dose rates under the assumption that the elemental source position is surrounded by a homogenous water environment.^{11,12}

The TG-186 recommendations use the MBDC (Model Based Dose Calculation Algorithm). Because these recommendations deliver accurate tissue segmentation and take into account the elemental composition of the structure, their use continues to make inroads because they provide better accuracy in BT dosimetry.^{13,14,15}

Ring applicators are widely used in high dose rate (HDR) BT applications for patients with cervix cancer. This model is convenient to use due to its fixed geometry and availability in versions com-

patible with computed tomography (CT)/magnetic resonance imaging (MRI) and many variations including additional interstitial needles. The most common observed problems with setup are associated with source positioning uncertainties during treatment compared to the dwell position placements used to calculate the dose distribution. This problem occurs when source path models from libraries are used and can also occur when the path is modeled manually.¹⁶

To our knowledge, no previous studies have attempted to perform dosimetric verification of the calculation algorithm used in TPS when the CT/MRI ring applicator is used. For this reason, we conducted the present study, in which we also sought to develop treatment planning commissioning procedures for current and further use based on the planar film dosimetry.

Materials and methods

For the preparation of the treatment plans Oncentra Brachy[®] 4.3 were used as this is the main treatment planning software used in authors department. This version of the system was equipped with TG43 based calculation algorithms only.

Two treatment plans were prepared for evaluation purposes. Standard CT/MRI ring applicator sets were used. The setup was based on 26 and 30 mm diameter rings and a 60 mm intra-uterine tube with 60° bent angle. Reconstruction of the application geometry was based on the applicator library module in Oncentra Brachy[®] 4.3. The reference dose of 3 Gy was prescribed to the standard Manchester A points using a HDR iridium source.

Gafchromic[®] EBT films were used as the dosimetric media. Irradiation setup was based on a PMMA phantom.

The phantom was build using large PMMA blocks with prepared cavity for intrauterine probe. Blocks of PMMA with different thickness were used to prepare repeatable setup and for assuring dosimetric media flatness and proper (parallel and perpendicular) positioning relative to the applicator. The dose to water in PMMA (calibration) and dose to water in water (measurements and TG43-based dose calculations) are not equivalent. However, $D_{w,w}$ and $D_{w,PMMA}$ differ only by 0.8% for distances of 25 mm from an 192Ir source. For this reason, relative character of the performed measurements and that PMMA is commonly available in radiotherapy facilities this material was chosen and used.

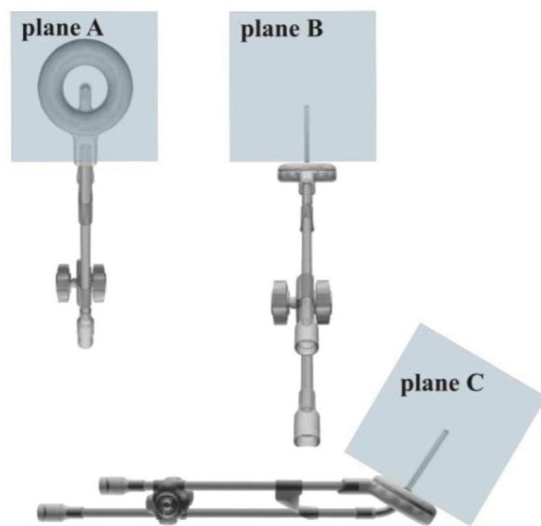


FIGURE 1. Geometry of the measurements, tandem ring applicator and Gafchromic[®] film located in planes (A), (B) and (C), respectively.

Dosimetric films (Gafchromic® EBT) were then placed in three planes. The first plane (plane A) was located at the surface of the ring part of the applicator with a round hole for the intra-uterine probe. Plane B was located on the surface of the probe in parallel orientation to the plane where Manchester A points were located. The third film (plane C) was placed on the surface of the probe perpendicular to the previous (plane B) localization. Geometry of the measurements is presented on the Figure 1.

After preparation of the treatment plan dose grids corresponding to each plane (dosimetric film localization), these were exported from the TPS as a raw data. The smallest available dose grid resolution was 1 mm x 1 mm, although under this condition only a small part of the data collected from film analysis could be used for comparisons. In the plane A area that included the hole data were removed from the analysis to avoid obvious differences in the no-film area. Additionally, the dose limit in the export module of the TPS was set to 400% of the reference dose and any dose values exceeding this limit were exported as 400% value in the dose grid.

After 72 hours, the irradiated Gafchromic® films were digitized with a flat table scanner (Epson® Perfection V750 Pro), all with the same orientation. Bitmap representation of the digitized films was then converted to the dose data and then local gamma analysis of the data were performed using the OMNI Pro I'mRT® package with 3% and 3 mm criteria.

Calibration data for the films were collected by separately irradiating 14 sheets (20 mm x 30 mm) of Gafchromic® EBT (Lot #: 47207-031, ISP) films with doses ranging from 0.25 Gy to 8.0 Gy using an HDR Ir-192 (192-Ir-mHDR-v2) source. To assure homogenous dose distribution, the films were placed between two blocks of 25 mm thick PMMA and two catheters were placed above and below the films at a distance of 25 mm. The doses were prescribed to the dose points in the centre of the film. After 72 hours, the films were digitized with a flat table scanner (Epson® Perfection V750 Pro) with light source on the one side and the detector on the other side of the film, all with the same orientation. Mean values from the most homogenous central part of the film (10 mm x 5 mm) were calculated using the VeriSoft® package. In region of interest of 10 mm x 5 mm the dose variation was estimated below 5%. Then the calibration curve was prepared and used recalculate the optical density (analog to digital conversion value; ADC) to the doses.¹⁷

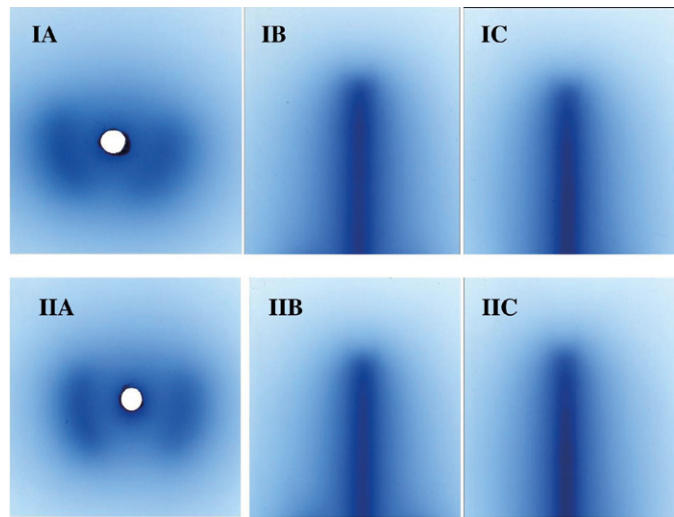


FIGURE 2. Digitized dosimetric films as a visual input data for two applicators setup and for all three analyzed dose planes. (I) Applicator ring diameter 26 mm, Gafchromic® film located in planes (A), (B) and (C), respectively. (II) Applicator ring diameter 30 mm: Gafchromic® film located in planes (A), (B) and (C), respectively.

Results

Co-registration of data imported from TPS and dose distribution from scanned film were guided by centre of the intrauterine probe. Dose was normalized to 400% as maximum measured dose by OmniPro® software for each analyzed film. The films were scanned at 250 DPI (Dots Per Inch) resolution, always with the same orientation. Treatment planning system export files contains dose data with 1 mm resolution therefore the data from film have to be downsampled by analyzing software. The dose inside the hole in the films - prepared for insertion intrauterine probe was manually changed to 0 Gy, in both - film data and TPS exported ones.

We assumed that dose distributions (planned and measured) were consistent if the count of pixel values from 0.00 to 1.00 (blue and green representation) in the gamma analysis was over 95% and the average pixel value was lower than 1.00. Pixel values higher than 1.00 (yellow and red representation) show the regions of inconsistencies (Figures 3–8).

The gamma analysis showed that all measured dose distributions were consistent with the planned distributions. Table 1 presents average and maximum gammas and percentage of the analyzed dose points that met the 3% and 3 mm criteria.

It's difficult to clearly state the uncertainties during realizing this study (based on gamma analysis), the main source of possible error is the mechani-

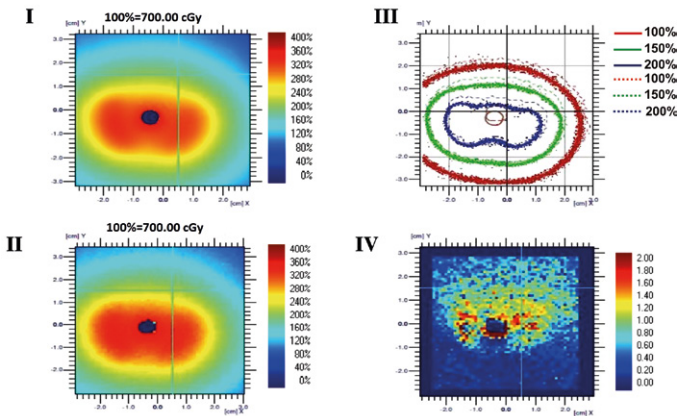


FIGURE 3. Data analysis for the 26 mm ring in plane A. (I) - dose distribution obtained from film, (II) - dose distribution obtained from TPS, (III) - isodoses obtained from film (dots) and TPS (lines), (IV) - gamma factor map.

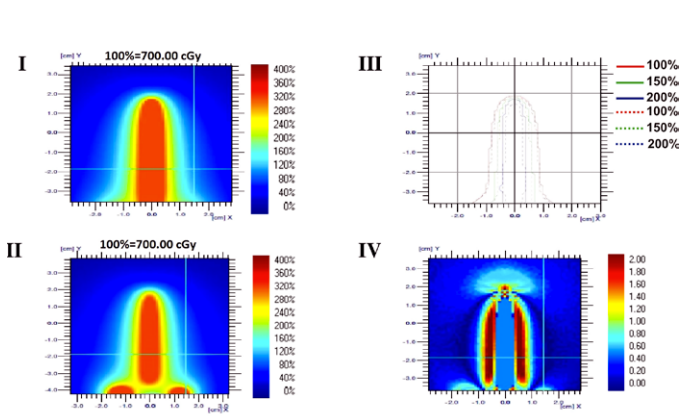


FIGURE 4. Data analysis for the 26 mm ring in plane B. (I) - dose distribution obtained from film, (II) - dose distribution obtained from TPS, (III) - isodoses obtained from film (dots) and TPS (lines), (IV) - gamma factor map.

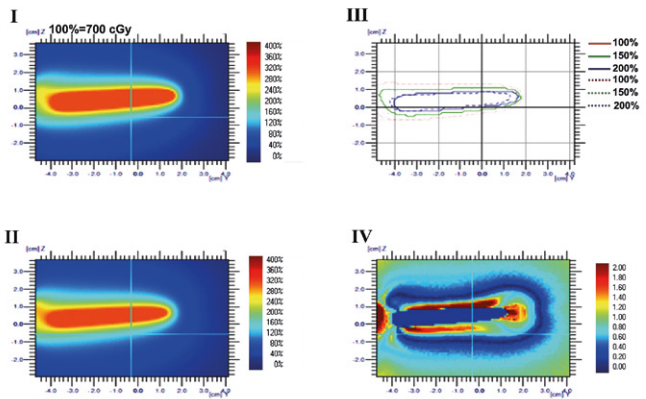


FIGURE 5. Data analysis for the 26 mm ring in plane C. (I) - dose distribution obtained from film, (II) - dose distribution obtained from TPS, (III) - isodoses obtained from film (dots) and TPS (lines), (IV) - gamma factor map.

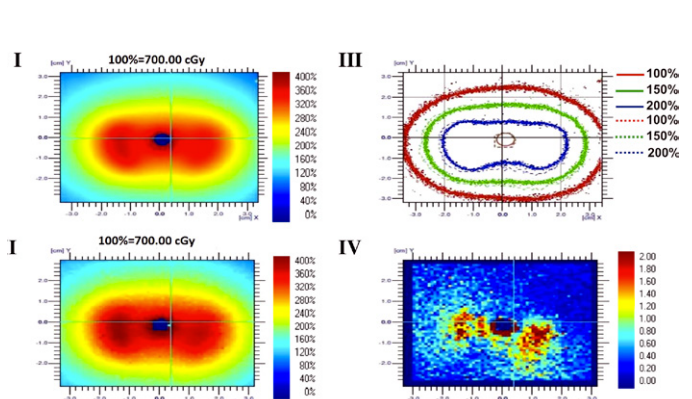


FIGURE 6. Data analysis for the 30 mm ring in plane A. (I) - dose distribution obtained from film, (II) - dose distribution obtained from TPS, (III) - isodoses obtained from film (dots) and TPS (lines), (IV) - gamma factor map.

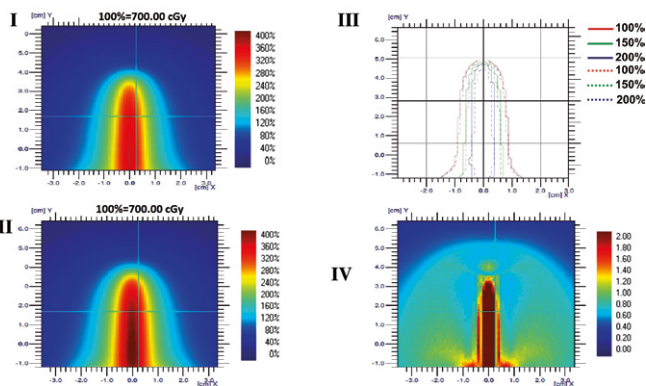


FIGURE 7. Data analysis for the 30 mm ring in plane B. (I) - dose distribution obtained from film, (II) - dose distribution obtained from TPS, (III) - isodoses obtained from film (dots) and TPS (lines), (IV) - gamma factor map.

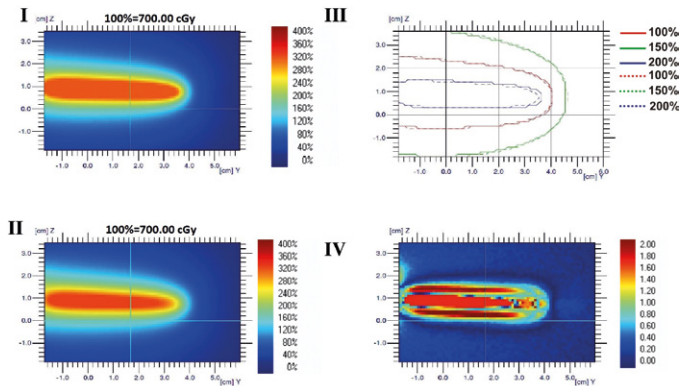


FIGURE 8. Data analysis for the 30 mm ring in plane C. (I) - dose distribution obtained from film, (II) - dose distribution obtained from TPS, (III) - isodoses obtained from film (dots) and TPS (lines), (IV) - gamma factor map.

cal positioning of the films in phantom. Another problem could be found in the spatial alignment of the two types of analyzed data. Authors decided to manually register two data series using intrauterine probe position assuming that the film was flat

and properly placed. Authors estimated possible positioning errors at less than 1 mm level. During the calibration - homogenous irradiation of film detector with a point source in one position isn't achievable, therefore a special arrangement

of irradiation based on Khushdeep Singh's¹⁸ work with two catheters was used, which allowed to deposit not less than 95% with standard deviation of 0,82% of reference dose on a defined film area.

Discussion

In the study, we have attempted to use the typical BT setup with tandem ring applicator as a test platform to develop a commissioning procedure to verify the MBDC algorithm recommended in TG-186. The main finding was that self-developing flat film dosimetry is a fast and reliable commissioning method in TG-43 conditions that could easily be adopted to almost any clinical setup in which point dose dosimetry is difficult to use and cannot provide valuable information.

The data packages obtained from digitizing the Gafchromic[®] films were prepared for comparison with the planar dose distribution data exported from the TPS. The OMNI Pro I[®]mRT software typically used for IMRT was used to perform gamma analysis of the data. In this approach, a commercially available method, typically used for external beam radiotherapy (EBRT), was used to compare the calculated and measured dose distribution. Overall dose distributions from EBDRT and BT is significantly different in terms of the dose gradients.¹⁹ For brachytherapy dose distributions we observe much larger dose ranges in small volumes. As a result, the use of point dose detectors to make measurements is highly difficult due to positioning errors. In contrast, film dosimetry seems to offer a fast and reliable method for commissioning calculation algorithms, and planning and treatment delivery procedure.^{2,20,21}

The common rule for the gamma criterion when BT verification using gafchromic films is performed has not been established. For purposes of this study, we adopted the AAPM TG-119 rapport criterion for gamma analysis: 3%, 3 mm and a level of 95%.

The results of the analysis were acceptable for two applicator size on all three planes at the 95% level and above. This results confirms the correctness of this measuring method and is a positive reference for further analysis in more complex cases with more complicated density and geometry setup.

Another important issue is the use of shields and commissioning of the calculation result for shielded applicators, where high density material is placed in the close proximity of the source.²²

TABLE 1. Results of Gamma analysis for the 26 mm ring and 30 mm ring applicator

Ring, 26 mm	Gamma average	Gamma max	Gamma (0.00 – 1.00)
plane A	0.22	1.42	99.04%
plane B	0.10	1.29	99.31%
plane C	0.44	1.75	98.88%

Ring, 30 mm	Gamma average	Gamma max	Gamma (0.00 – 1.00)
plane A	0.25	1.96	98.11%
plane B	0.27	2.00	97.94%
plane C	0.10	1.22	99.54%

In most TPS in current use, the elemental composition of the structures is not taken into account during the calculation (atomic number - Z) and dose distribution is based on geometric models of the shields. The TG-186 recommendations with MBDC algorithm introduce the need to develop reliable verification methods that are more convenient and accurate, which can be performed in a more repeatable manner than point dose methods.^{23,24}

Better accuracy in BT dosimetry appears to be a common need when the benefits from accurate tissue segmentation and the structure's elemental composition are considered as an important step up.^{13,14,25}

It bears mentioning that for the analysis performed in the present study, we only used a small amount of the data from the digitized dosimetric films. The planar resolution of the films is very high and limited only by the chemical structure of the dosimetric media itself and physical resolution of the scanner. On the other hand, the maximum resolution of the exported dose grid was only 1 mm. But the most important factor for QA in BT is the possibility to export data exactly from the plane where the film was located during the measurements. This allows for the design of very effective phantoms with convenient and repeatable geometry.^{2,26}

The film dosimetry used to verify the dose distribution and also for the direct reconstruction of the source path should be considered the method of choice for commissioning these newly-designed applicators. Precise reconstruction of the real source positions allows the dose distributions calculated by the planning system to be checked and leads to more conformal treatment planning.²⁷ It should be noted that introducing effective, repeatable and easy-to-use QA procedures for BT is es-

sential. Numerous factors, including relatively high doses, dose gradients, limited number of fractions, and advanced optimization algorithms with extensive dwell time modulation, make it nearly impossible to apply *in-vivo* dosimetry, thus leaving virtually no room to implement plan corrections during treatment. In these conditions, developing convenient “offline” methods for commissioning calculation routines, applicators and also for more frequently used QA procedures is very important and merits more study.

Conclusions

The analysis performed in this study showed excellent agreement between the dose distributions calculated using TPS and the doses measured by Gafchromic films. This confirms the viability of using film dosimetry in brachytherapy. The proposed commissioning procedure for further use with the MBDCa algorithm was established for use at the authors' facility, and it seems likely that the same procedure could be replicated at other centers.

References

- Malicki J. The importance of accurate treatment planning, delivery, and dose verification. *Rep Pract Oncol Radiother* 2012; **17**: 63-5. doi: 10.1016/j.rpor.2012.02.001
- Palmer AL, Lee C, Ratcliffe AJ, Bradley D, Nisbet A. Design and implementation of a film dosimetry audit tool for comparison of planned and delivered dose distributions in high dose rate (HDR) brachytherapy. *Phys Med Biol* 2013; **58**: 6623-40. doi: 10.1088/0031-9155/58/19/6623
- Adamczyk M, Zwierzchowski G, Malicki J, Skowronek J. Evaluation of clinical benefits achievable by using different optimization algorithms during real time prostate brachytherapy. *Phys Medica* 2013; **29**: 111-7. doi: 10.1016/j.ejmp.2011.12.005
- Rivard MJ, Beaulieu L, Mourtada F. Enhancements to commissioning techniques and quality assurance of brachytherapy treatment planning systems that use model-based dose calculation algorithms. *Med Phys* 2010; **37**: 2645-58. doi: 10.1118/1.3429131
- Granero D, Vijande J, Ballester F, Rivard MJ. Dosimetry revisited for the HDR 192Ir brachytherapy source model mHDR-v2. *Med Phys* 2011; **38**: 487-94. doi: 10.1118/1.3531973
- Perez-Calatayud J, Ballester F, Das RK, Dewerd LA, Ibbott GS, Meigooni AS, et al. Dose calculation for photon-emitting brachytherapy sources with average energy higher than 50 keV: Report of the AAPM and ESTRO. *Med Phys* 2012; **39**: 2904-29. doi: 10.1118/1.3703892
- Brown T, Hogstrom RK. Dose-response curve of EBT, EBT2 and EBT3 radiochromic films to synchrotron-produced monochromatic x-ray beams. *Med Phys* 2012; **39**: 7412-7. doi: 10.1118/1.4767770
- Chiu-Tsao ST, Ho Y, Shankar R, Wang L, Harrison LB. Energy dependence of response of new high sensitivity radiochromic films for megavoltage and kilovoltage radiation energies. *Med Phys* 2005; **32**: 3350-4. doi: 10.1118/1.20165467
- DeWerd LA, Ibbott GS, Meigooni AS. A dosimetric uncertainty analysis for photon-emitting brachytherapy sources: report of AAPM Task Group No. 138 and GEC-ESTRO. *Med Phys* 2011; **38**: 782-801. doi: 10.1118/1.3533720
- Hyer DE, Sheybani A, Jacobson GM, Kim Y. The dosimetric impact of heterogeneity corrections in high-dose rate (192Ir) brachytherapy for cervical cancer: investigation of both conventional Point-A and volume-optimized plans. *Brachytherapy* 2012; **11**: 515-20. doi: 10.1016/j.brachy.2012.01.011
- de Oliveira CA, Lopes MD, Matos A. Commissioning of brachytherapy module of Oncentra MasterPlan treatment planning system. *J Contemp Brachyther* 2009; **1**: 224-30.
- Palmer A, Bradley D, Nisbet A. Physics-aspects of dose accuracy in high dose rate (HDR) brachytherapy: source dosimetry, treatment planning, equipment performance and in vivo verification techniques. *J Contemp Brachytherapy* 2012; **4**: 81-91. doi: 10.5114/jcb.2012.32558
- Beaulieu L, Carlsson Tedgren A, Carrier JF, Davis SD, Mourtada F, Rivard MJ, et al. Report of the Task Group 186 on model-based dose calculation methods in brachytherapy beyond the TG-43 formalism: current status and recommendations for clinical implementation. *Med Phys* 2012; **39**: 6208-36. doi: 10.1118/1.4747264
- Mikell JK, Klopp AH, Gonzalez GM, Kising KD, Price MJ, Berner PA, et al. Impact of heterogeneity-based dose calculation using a deterministic grid-based Boltzmann equation solver for intracavitary brachytherapy. *Int J Radiat Oncol Biol Phys* 2012; **83**: 417-22. doi: 10.1016/j.ijrobp.2011.12.074
- Oliveira S, Teixeira N, Fernandes L, Teles P, Vaz P. Dosimetric effect of tissue heterogeneity for 125I prostate implants. *Rep Pract Oncol Radiother* 2014; **19**: 392-8.
- Awunor OA, Dixon B, Walker C. Direct reconstruction and associated uncertainties of 192Ir source dwell positions in ring applicators using gafchromic film in the treatment planning of HDR brachytherapy cervix patients. *Phys Med Biol* 2013; **58**: 3207-25. doi: 10.1088/0031-9155/58/10/3207
- Zwierzchowski G, Bieleńda G, Skowronek J, Mazur M. Film based verification of calculation algorithms used for brachytherapy planning-getting ready for upcoming challenges of MBDCa. *J Contemp Brachytherapy* 2016; **8**: 326-35. doi: 10.5114/jcb.2016.61828
- Singh K. Investigation of the energy response of EBT-2 gafchromic film model. Montreal: Department of Medical Physics, McGill University; 2011.
- Manikandan A, Biplab S, David PA, Holla R, Vivek TR, Sujatha N. Relative dosimetric verification in high dose rate brachytherapy using two-dimensional detector array iMatrixX. *J Med Phys* 2011; **36**: 171-5. doi: 10.4103/0971-6203.83491
- Vijande J, Ballester F, Ouhib Z, Granero D, Pujades-Claumarchirant MC, Perez-Calatayud J. Dosimetry comparison between TG-43 and Monte Carlo calculations using the Freiburg flap for skin high-dose-rate brachytherapy. *Brachytherapy* 2012; **11**: 528-35. doi: 10.1016/j.brachy.2011.11.005
- Rivard MJ, Venselaar JL, Beaulieu L. The evolution of brachytherapy treatment planning. *Med Phys* 2009; **36**: 2136-53. doi: 10.1118/1.3125136
- Hira M, Podgorsak MB, Jaggernauth W, Malhotra HK. Measurement of dose perturbation around shielded ovoids in high-dose-rate brachytherapy. *Brachytherapy* 2011; **10**: 232-41. doi: 10.1016/j.brachy.2010.08.008
- Uniyal SC, Sharma SD, Naithani UC. A dosimetry method in the transverse plane of HDR Ir-192 brachytherapy source using gafchromic EBT2 film. *Phys Med* 2012; **28**: 129-33. doi: 10.1016/j.ejmp.2011.03.005
- Landry G, Reniers B, Murrer L, Lutgens L, Gurr EB, Pignol JP, et al. Sensitivity of low energy brachytherapy Monte Carlo dose calculations to uncertainties in human tissue composition. *Med Phys* 2010; **37**: 5188-98. doi: 10.1118/1.3477161
- Kirisits C, Rivard MJ, Baltas D, Ballester F, De Brabandere M, van der Laarse R, et al. Review of clinical brachytherapy uncertainties: analysis guidelines of GEC-ESTRO and the AAPM. *Radiother Oncol* 2014; **110**: 199-212. doi: 10.1016/j.radonc.2013.11.002
- Niatsetski Y, Fekkes S, Vreeken H. Source path measurements for ring applicators. [Abstract]. *Radiother Oncol* 2011; **99**: 278. Poster No. 695
- Berger D, Dimopoulos J, Georg P, Georg D, Pötter R, Kirisits C. Uncertainties in assessment of the vaginal dose for intracavitary brachytherapy of cervical cancer using a tandem-ring applicator. *Int J Radiat Oncol Biol Phys* 2007; **67**: 1451-9. doi: 10.1016/j.ijrobp.2006.11.021

Radiol Oncol 2017; 51(4): 369-377.
doi: 10.1515/raon-2017-0044

Karcinogeneza inducirana z nizkimi dozami sevanja

Piotrowski I, Kulcenty K, Maria Suchorska W, Skrobata A, Skórska M, Kruszyna-Mochalska M, Kowalik A, Jackowiak W, Malicki J

Izhodišča. Učinki visokodoznega sevanja na človeške celice in tkiva so sorazmerno dobro znani, ni pa še enotnega mnenja o učinkih nizkih in ultra nizkih doz sevanja. Znano je, da ionizirajoče sevanje povzroča karcinogenezo z indukcijo genskih mutacij in kromosomskih aberacij. Tako lahko z radioterapijo onkoloških bolnikov povzročimo nastanek sekundarnih rakov. Obsevalne aparature - pri intenzivno modulirani radioterapiji - izpostavijo velika področja zdravih tkiv nizkim dozam sevanja. To bi lahko vplivalo na povečano incidence rakov pri uspešno zdravljenjih bolnikih. Raziskave kažejo, da je tveganje za karcinogenezo večje pri nizkih dozah sevanja, glede na izračune linearnega modela. Tudi epidemiološki podatki delavcev v nuklearnih reaktorjih in preživelih po atomski bombi potrjujejo, da lahko nizke doze sevanja prispevajo k tveganju za nastanek raka. To tveganje morda korelira s starostjo ob izpostavitvi.

Zaključki. Razumevanje molekularnih mehanizmov odgovorov na sevanje z nizko dozo je ključno za pravilno oceno tveganj in dobrot teh sevanj. Upoštevati bi jih bilo potrebno tudi pri planiranju radioterapije in izpostavljenosti zaposlenih, ki delajo v območju sevanja.

Radiol Oncol 2017; 51(4): 378-385.
doi: 10.1515/raon-2017-0045

Klinični pomen ^{18}F -DFG pozitronske emisijske tomografije/računalniške tomografije pri sledenju kolorektalnega raka. Iskanje načinov za povečanje specifičnosti pri odkrivanju ponovitev

Ince S, Okuyucu K, Hancerliogulları O, Alagoz E, San H, Arslan N

Izhodišča. Kolorektalni rak se v 2 letih po resekciji primarnega tumorja ponovi pri skoraj 40 % bolnikov. Slikanje z ^{18}F -FDG pozitronsko emisijsko tomografijo/računalniško tomografijo (PET/CT) je novejša preiskava, ki jo pogosto uporabljamo za oceno metastatskega širjenja v obdobju sledenja. Naš namen je bil raziskati diagnostični pomen podatkov ^{18}F -FDG-PET/CT pri kolorektalnem raku. Ocenjevali smo vrednosti maksimalnega standardiziranega privzema izotopa (SUVmax), vrednosti celokupne glikolize v leziji (TLG) in razlike v SUVmax pri dveh ponovitvah slikanja v določenem časovnem razmiku.

Bolniki in metode. Pri 53 bolnikih s kolorektalnim rakom smo analizirali na kontrolnem ali ponovnem ^{18}F -FDG-PET/CT vrednosti SUVmax posameznih lezij. Vse lezije s povišanimi vrednostmi SUVmax so bile potrjene s kolonoskopijo ali histološko. Rezultate PET/CT smo primerjali s konvencionalnimi slikovnimi načini (CT, MRI) in tumorskimi označevalci (karbohidratni antigen 19-9 [Ca 19-9], karcinoembrionalni antigen [CEA]).

Rezultati. V skupini benignih lezij je bil povprečni SUVmax $6,9 \pm 5,6$ in v skupini malignih lezij $12,7 \pm 6,1$. Povprečna vrednost TLG v skupini benignih in malignih lezij je bila 401 oz. 148. Rezultati preiskave ^{18}F -FDG-PET/CT so bili pravilno pozitivni pri 48 % bolnikov z normalnimi vrednostmi Ca19-9 ali CEA in pravilno negativni pri 10 % primerov s povišanim Ca 19-9 ali CEA. CT ali MRI sta prepoznala sumljivo maligno lezijo pri 32 % bolnikih in rezultati ^{18}F -FDG-PET/CT so bili pravilno negativni pri 35 % primerov. Najpomembnejšo in jasno statistično razliko v vrednosti TLG smo našli med skupinama z benignimi boleznimi in recidivnimi lezijami.

Zaključki. Čeprav je SUVmax močan metabolni pokazatelj ($p = 0,008$), se kaže TLG kot najboljši napovedovalec recidiva pri kolorektalnem raku ($p = 0,001$). Oba zvišujeta specifičnost preiskave z ^{18}F -FDG-PET/CT.

Radiol Oncol 2017; 51(4): 386-392.

doi: 10.1515/raon-2017-0049

Pomen ultrazvoka s kontrastnim sredstvom v zaznavi in biopsiji lezij dojke zaznavnih le s preiskavo MR?

Nykänen A, Arponen O, Sutela A, Vanninen R, Sudah M

Izhodišča. Namen raziskave je bil oceniti uporabnost ultrazvoka s kontrastnim sredstvom (UZKS) in UZKS vodenih posegov v diagnostiki lezij, ki so vidne na MR ampak nezaznavne s klasično ultrazvočno (UZ) preiskavo.

Bolniki in metode. Z retrospektivno raziskavo smo zajeli 10 žensk, ki so imele 10 z UZ nezaznavne lezije in smo jih zdravili v obdobju od julija 2014 do aprila 2017. Vse lezije so bile ponovno ocenjene z UZKS, kjer smo aplicirali 2,4 ml kontrasta SonoVue®. Ko smo lezijo spoznali za pozitivno z UZKS, smo uporabili enako količino kontrastnega sredstva še za UZKS voden poseg.

Rezultati. Z MR smo odkrili 8 lezij, ki so privzemale kontrastno sredstvo s povprečno velikostjo 9 mm (razpon 5–16 mm) in 2 leziji, ki nista privzemali kontrastnega sredstva velikosti 10 ter 20 mm. Z usmerjeno UZ preiskavo nismo odkrili skladnih lezij. Z UZKS smo odkrili 5 od 10 lezij (50 %). Z UZKS vodenim posegom smo vzeli biopsijo 4 lezij in 1 lezija je bila označena s sponko ter kasneje kirurško odstranjena. Štiri lezije so bile histološko potrjeno maligne. Pet lezij ni bilo zaznavnih z UZKS; pri 3 smo opravili MR voden biopsijo; 1 lezija ni bila dostopna za MR voden biopsijo in smo jo sledili; pri 1 leziji smo opravili UZ voden biopsijo z mesta kjer so bile vidne arhitekturne nepravilnosti, čeprav je morfološko nismo z gotovostjo uspeli identificirati. Tri lezije, UZKS nezaznavne, so bile histološko potrjeno maligne.

Zaključki. Na podlagi preliminarnih rezultatov je UZKS možno orodje pri zaznavi lezij, ki so vidne le z MR in lahko odraža finančno in časovno učinkovito prakso. UZKS je bolj priročno nadomestilo MR vodeni biopsiji in bi ga lahko vključili v diagnostični algoritem, ki ocenjuje lezije vidne le z MR.

Radiol Oncol 2017; 51(4): 393-400.;

doi: 10.1515/raon-2017-0030

Izhodiščni privzem Lipiodola po transarterijski kemoembolizaciji pri hepatocelularnih rakih. Določitev praznih vrednosti, ki napovedujejo tumorski odgovor

Matsui Y, Horikawa M, Noudeh YJ, Kaufman JA, Kolbeck KJ, Farsad K

Izhodišča. Namen raziskave je bil oceniti povezavo med izhodiščnimi vrednostmi privzema Lipiodola in zgodnjo ponovitvijo hepatocelularnega raka (HCC) po transarterijski kemoembolizaciji (TACE) ter določiti prazne vrednosti izhodiščnega privzema, ki napoveduje odgovor tumorja.

Bolniki in metode. Retrospektivno smo pregledali bazo podatkov o HCC, pri katerih smo opravili TACE z Lipiodolom. S kemoterapevtsko lipiodolsko emulzijo smo zdravili 46 tumorjev pri 30 bolnikih, nismo pa naredili dodatno embolizacija z majhnimi delci. Izhodiščni privzem lipiodola smo merili kot srednje vrednosti v Hounsfieldovih enotah (HU) s pomočjo računalniške tomografije (CT) 1 teden po TACE. Izračunali smo hitrost izpiranja kot razmerje razlik med izhodiščnimi vrednostmi HU in vrednostmi HU po določenem času sledenja (HU/mesec). Coxov regresijski model sorazmernega tveganja smo uporabili za ugotavljanje povezanosti med izhodiščnim privzemom Lipiodola in drugimi spremenljivkami tumorskega odgovora. Uporabili smo analizo ROC (receiver operating characteristics) za opredelitev izhodiščnega praga privzema Lipiodola, ki napoveduje odgovor tumorjev.

Rezultati. V obdobju spremljanja (povprečno 5,6 mesecev) se je ponovilo 19 (41,3 %) tumorjev (povprečni čas do ponovitve je bil 3,6 mesecev). V multivariatnem modelu sta bila nizki izhodiščni privzem Lipiodola ($P = 0.001$) in večja hitrost izplavljanja ($P < 0.0001$) statistično značilna napovedna dejavnika zgodnje ponovitve tumorja. Analiza ROC je pokazala, da so izhodiščne prazne vrednosti privzema Lipiodola 270,2 HU značilno povezane z odgovorom tumorjev (95 % občutljivost, 93 % specifičnost).

Zaključki. Izhodiščni privzem Lipiodola in hitrost izplavljanja v obdobju sledenja sta neodvisna napovedna dejavnika zgodnje ponovitve tumorja. Prazne vrednosti izhodiščnega privzema Lipiodola več kot 270 HU so imele največjo občutljivost in specifičnost za napoved odgovora tumorja na zdravljenje. Naše ugotovitve bi bile lahko koristne pri odločanju o nadaljnjih strategijah zdravljenja po TACE z Lipiodolom.

Radiol Oncol 2017; 51(4): 401-406.;
doi: 10.1515/raon-2017-0053

Hondromalacija patele, ruptura medialnega meniskusa in medialni periartikularni burzitis pri bolnikih z osteoartrozo

Resorlu M, Doner D, Karatag O, Akgun Toprak C

Izhodišča. V raziskavi smo ocenjevali prisotnost burzitisa v medialnem kompartmentu kolena (burze tetiv *pes anserinus*, semimembranoznega tibialnega kolateralnega ligamenta in medialnega kolateralnega ligamenta) pri osteoartrizi, hondromalaciji patele in raztrganini medialnega meniskusa.

Bolniki in metode. Dva radiologa sta retrospektivno pregledala 100 magnetnoresonančnih preiskav kolena pri bolnikih napotenih zaradi bolečine v kolenu. Prvi radiolog je ocenjeval osteoartrizo, hondromalacijo patele in rupturo medialnega meniskusa. Drugi radiolog je brez podatkov najdb prvega ocenjeval prisotnost burzitisa.

Rezultati. Znake blage osteoartrize (stopnje I in II) je imelo 55 bolnikov, znake težje osteoartrize (stopnje III in IV) pa 45. Ohranjen hrustanec patele je imelo 25 bolnikov, medtem ko je imelo znake blage hondromalacije patele (stopnje I in II) 29 bolnikov in znake izrazite hondromalacije patele (stopnje III in IV) 46 bolnikov. Rupturo medialnega meniskusa je imelo 51 bolnikov. Med težjo osteoartrizo in hondromalacijo patele je obstajala pozitivna korelacija ($p < 0.001$ in $p = 0.018$). Pomembno korelacijo smo ugotovili tudi pri ugotovitvi medialnega burzitisa in rupture medialnega meniskusa ($p = 0.023$). Pozitivno korelacijo smo videli tudi med medialnim burzitisom in stopnjo osteoartrize, ne pa med burzitisom in hondromalacijo patele ($p = 0.023$ in $p = 0.479$). Burzitis lateralnega kolateralnega ligamenta smo našli pri dveh bolnikih, iliotibialni burzitis pa pri petih bolnikih.

Zaključki. Bolniki s težjo osteoartrizo so imeli večjo prevelanco rupture medialnega meniskusa ter burzitisa v medialnem kompartmentu.

Radiol Oncol 2017; 51(4): 407-414.
doi: 10.1515/raon-2017-0048

Fitoterapevtika oridonin in ponigidin imata in vitro aditivni učinek z obsevanjem na celicah raka trebušne slinavke

Liermann J, Naumann P, Fortunato F, E. Schmid TE, Weber KJ, Debus J, Combs SE

Izhodišča. Kemoradioterapija lokalno napredovalega raka trebušne slinavke lahko pripomore k njegovi operabilnosti. V raziskavi smo preučevali radisenzibilizirajoči učinek oridonina in ponigidina na celice raka trebušne slinavke. Obe učinkovini sta bili izolirani iz *Isodon rubescens*, rastline znane iz tradicionalne kitajske medicine, in imata dokazano protitumorsko delovanje.

Materiali in metode. Celice raka trebušne slinavke AsPC-1, BxPC-3, Panc-1 in MIA PaCa-2 smo izpostavili oridoninu ali ponigidinu in jih nato obsevali z 2 Gy ali 6 Gy. Merili smo njihovo klonogenost, vpliv na razporeditev v celičnem ciklusu, nastajanje žarišč γ H2AX kot indikatorja dvojnih DNA prelomov ter izražanje proteinov Ku70 in XRCC4, ki so udeleženi v popravilu dvojnih DNA prelomov.

Rezultati. Oridonin in ponigidin sta imela citotoksičen učinek na celične linije trebušne slinavke in sta povzročala dvojne prelome DNA. V kombinaciji z obsevanjem smo zasledili aditivni učinek in podaljšano fazo zaostanka v G2/M. Nismo zaznali sprememb v izražanju proteinov, ki so udeleženi v popravilu dvojnih prelomov DNA.

Zaključki. Kombinirano zdravljenje celic z oridoninom ali ponigidinom in obsevanjem je imelo aditivni učinek z zaustavitvijo celic v G2/m fazi celičnega ciklusa. Obe učinkovini povzročita dvojne prelome DNA in onemogočata večje popravilo dvojnih prelomov.

Radiol Oncol 2017; 51(4): 415-421.

doi: 10.1515/raon-2017-0051

Usmerjena elektroporacija podganjih jeter s pomočjo slane infuzije v portalno veno. Preliminarni rezultati različne konduktivnosti

Pañella C, Castellví Q, Moll X, Quesada R, Villanueva A, Iglesias M, Naranjo D, Sánchez-Velázquez P, Andaluz A, Grande G, Ivorra A, Burdío F

Izhodišča. Jetrni tumorji in metastaze pogosto niso primerni za kirurško ali ablativno zdravljenje. Namen raziskave je bil preučiti izvedljivost in varnost povečanja konduktivnosti jeter z infuzijo slane raztopine v portalno veno. Predpostavljali smo, da s tem lahko zdravimo več tumorskih nodulov hkrati z ireverzibilno elektroporacijo.

Materiali in metode. Uporabili smo podgane Sprague Dawley (Skupina A, n = 10) in atimične podgane s tumorji v jetrih (Skupina B, n = 8). Slano raztopino smo injicirali v portalno veno, hkrati pa za neutralizacijo hipernatremije dejoniziran serum in furesimid intraarterijsko. Merili smo spremembe konduktivnosti jeter in tumorjev v jetrih. Čas, ko je bila jetrna konduktivnost večja od tumorske konduktivnosti, smo imenovali terapevtsko okno. Živali smo spremljali še en mesec po terapiji, nato smo jih humano usmrtili in izvedli histološko analizo vzorcev.

Rezultati. Večina živali, 82,4 % obravnavanih je preživela postopek. Srednja vrednost največje jetrne konduktivnosti se je povečala za 2,7 in 3,5 krat od bazalne vrednosti v skupini A in skupini B. Tudi jetrna konduktivnost v primerjavi s tumorsko konduktivnostjo se je povečala za 1,4 krat, kar je terapevtsko okno za selektivno aplikacijo ireverzibilne elektroporacije.

Zaključki. Infuzija slane raztopine ob kompenzacije hipernatremije je varna metoda za povečanje jetrne konduktivnosti in za usmerjeno delovanje ireverzibilne elektroporacije na jetrne tumorje.

Radiol Oncol 2017; 51(4): 422-430.

doi: 10.1515/raon-2017-0043

Minimalno invaziven postopek elektrokemoterapije za zdravljenje nosnih tumorjev psov z enoigelnno elektrodo

Maglietti F, Tellado M, Olaiz N, Michinski S, Marshall G

Izhodišča. Tumorje nosne votline odkrijemo pozno, ko že infiltrirajo okoljska tkiva in je zato potrebno agresivno zdravljenje. V raziskavi smo za zdravljenje takih tumorjev uporabili elektrokemoterapijo.

Materiali in metode. V primeru zdravljenja globoko ležečih tumorjev je glavna omejitev elektrokemoterapije pokritost celotnega tumorja s primernim električnim poljem. Zato smo razvili enoigelnno elektrodo (SiNE), ki ob minimalni invazivnosti lahko dobro pokrije tumor z električnim poljem in je enostavna za uporabo. S tako elektrodo smo zdravili 11 psov s spontanimi tumorji ter primerjali učinkovitost z 10 psmi, ki so bili zdravljeni s kirurgijo in adjuvantno kemoterapijo.

Rezultati. Elektrokemoterapije je bil uspešna, pri 27 % tumorjev smo ugotovili popolni odgovorov, pri 64 % delni odgovor in pri 9 % stabilno bolezen. S tem smo dosegli 91 % objektivnih odgovorov in 16,86 mesecev celokupnega preživetja (4–32 mesecev; srednja vrednost 16,5 mesecev), kar pomeni značilno podaljšanje preživetja ($p = 0,0008$) v primerjavi s kontrolno skupino zdravljenih psov. Stranski učinek je bilo vnetje nosne votline, ki se je pomirilo po zdravljenju s kortikosteroidi. Eno leto po zdravljenju je bilo živih 60 % psov zdravljenih z elektrokemoterapijo in 10 % psov v kontrolni skupini, po 32 mesecih pa 30 % po elektrokemoterapiji in 10 % v kontrolni skupini.

Zaključki. Elektrokemoterapija s SiNE elektrodo je varna in učinkovita pri zdravljenju nosnih tumorjev psov.

Radiol Oncol 2017; 51(4): 431-437.
doi: 10.1515/raon-2017-0042

Metformin *in vitro* v glioblastomih poveča občutljivost za obsevanje z zaustavitvijo celičnega cikla v fazi G2/M in s povečanim izražanjem adenozin-5'-monofosfat-aktivirajoče proteinske kinaze

Adeberg S, Bernhardt D, Harrabi SB, Nicolay NH, Hörner-Rieber J, König L, Repka M, Mohr A, Abdollahi A, Weber KJ, Debus J, Rieken S

Izhodišča. Predpostavljamo, da ima metabolizem pomembno vlogo pri nadzoru rakavih celic. Nedavno smo pokazali izboljšano preživetje brez napredovanja bolezni pri bolnikih z glioblastomom, ki so med kemoradioterapijo prejeli metformin kot antidiabetično zdravilo. Čeprav metformin uporabljamo v klinični praksi, je njegov vpliv pri glioblastom še razmeroma slabo raziskan, še posebej v kombinaciji z drugimi načini zdravljenja, kot sta obsevanje in temozolomid.

Materiali in metode. V raziskavi smo proučevali vpliv metformina v kombinaciji z obsevanjem in temozolomidom na preživetje celic (klonogeno preživetje) celični ciklus (rutinska citometrijska analiza FACScan) in nivojem fosforilirane adenozin-5'-monofosfat-aktivirajoče proteinske kinaze (AMPK) (Phospho-AMPK α 1 - ELISA) v glioblastomskih celičnih linijah LN18 in LN229.

Rezultati. Metformin in temozolomid sta izboljšala učinkovitost fotonskega obsevanja v celicah glioblastoma. Toksičnost celic je bila izrazitejša pri celicah LN18 z ne-metiliranim promotorjem za O6-metilgvanin DNK metiltransferazo (MGMT). Zaustavitev celičnega cikla v fazi G2/M z metforminom in kombiniranim zdravljenjem smo opazili v času do 72 ur. Ti učinki po obsevanju, metforminu in temozolomidu so bili povezani s povišanimi vrednostmi aktivirane AMPK v celični liniji LN229, ne pa tudi v celični liniji LN18.

Zaključki. Radiosenzitivni učinki metformina na glioblastomske celice, zdravljene z obsevanjem in temozolomidom *in vitro*, se kaže z zaustavitvijo celičnega cikla v fazi G2/M in spremembami pAMPK.

Radiol Oncol 2017; 51(4): 438-446.;
doi: 10.1515/raon-2017-0033

Ocena metod preoblikovane registracije slik za akumulacijo doze pri bolnikih z rakom nosnega žrela med radioterapijo

Nobnop W, Chitapanarux I, Neamin H, Wanwilairat S, Lorvidhaya V, Sanghangthum T

Izhodišča. Preoblikovano registracijo slik (PRS) uporabljamo za prilagoditev struktur glede na anatomske spremembe pri opazovanju dozimetričnega učinka. V raziskavi smo uporabili slike megavoltnega računalniškega tomografa (MVCT) za izdelavo kumulativnih doz pri bolnikih z rakom nosnega žrela z različnimi metodami PRS. Analizirali smo izvedbo različnih metod PRS in vpliv akumulacije doze.

Bolniki in metode. V raziskavo smo vključili pet bolnikov z rakom nosnega žrela, ki smo jih zdravili s helično tomoterapijo. Za oceno akumulacije doze s štirimi metodami PRS smo uporabili tedenske slike MVCT, ki smo jih posneli ob 1., 6., 11., 16., 21., 26. in 31. frakciji obsevanja. Analizirali smo deviacije kumulativne doze od izhodiščnega obsevalnega načrta in preučene korelacije teh variacij z anatomske spremembami in metodami PRS.

Rezultati. Tarčna doza ob koncu zdravljenja je bila nekoliko različna glede na izhodiščni načrt. Z napredovanjem zdravljenja so razlike v dozah za posamezne organe naraščale in sicer do 6,8 % (razpon: 2,2–10,9 %) za desno parotidno žlezo, do 15,2 % (razpon: -1,7–36,3 %) za levo parotidno žlezo in do 6,4 % (razpon: -1,6–13,2 %) za hrbtenjačo. Povprečne vrednosti nenatančnosti za oceno akumuliranih doz za vse metode PRS so bile $0,21 \pm 0,11$ Gy (tarčna doza), $1,99 \pm 0,76$ Gy (desna parotidna žleza), $1,19 \pm 0,24$ Gy (leva parotidna žleza) in $0,41 \pm 0,04$ Gy (hrbtenjača).

Zaključki. Natančnost metod PRS vpliva na oceno akumuliranja doze. Vpliva tako na tarčno dozo kot na dozo, ki jo prejme organi. Metode PRS vključujejo ustrezno tehniko ocene doze za opazovanje kot rezultat anatomske spremembe med frakcijami obsevanja. Primerne so za uporabo pri adaptivnih terapevtskih strategijah.

Radiol Oncol 2017; 51(4): 447-454.

doi: 10.1515/raon-2017-0024

Dolgoročni rezultati zdravljenja z obsevanjem pri bolnicah z rakom zunanjega spolovila v Sloveniji v letih 1997-2004

Zobec Logar HB

Izhodišča. Namen raziskave je bila retrospektivna analiza bolnic z rakom zunanjega spolovila zdravljenih z dvodimenzionalnim (2D) obsevanjem na Onkološkem inštitutu Ljubljana v letih 1997–2004.

Bolnice in metode. V raziskavo smo vključili 56 bolnic, srednje starosti 74,4 +/- 9,7 let, večinoma stadija T2 in T3. Vse bolnice smo zdravili z obsevanjem, bodisi v kombinaciji z operacijo (skupina A), z obsevanjem kot primarnim zdravljenjem (skupina B) ali z obsevanjem ob ponovitvi bolezni (skupina C). Nekatere bolnice so prejele tudi kemoterapijo. Analizirali smo histološki tip tumorja, stopnjo diferenciacije, število in velikost pozitivnih bezgavk, širjenje bolezni preko bezgavčne kapsule, vrsto operativnega posega, dozo obsevanja na področje primarnega tumorja, dimeljskih in medeničnih bezgavk, lokalno kontrolo bolezni in preživetje bolnic.

Rezultati. 10-letno celokupno preživetje je bilo 22,7 %, za bolezen specifično preživetje 34,5 % in lokalna kontrola bolezni 41,1 %. Najboljše 10-letne rezultate zdravljenja smo dosegli v skupini primarno operiranih bolnic, zdravljenih z dopolnilnim obsevanjem z ali brez kemoterapije (celokupno preživetje 31,9 %, za bolezen specifično preživetje 40,6 %, lokalna kontrola bolezni 47,6 %). Prisotnost pozitivnih bezgavk je imela velik vpliv na lokalno kontrolo bolezni. V primeru pozitivnih bezgavk se je lokalna kontrola zmanjšala za 60 % ($p = 0,03$), preživetje pa za 50 % ($p = 0,2$). Pri dozi, ki je bila enaka ali višja od 54 Gy, se je pokazala težnja k boljši lokalni kontroli bolezni ($p = 0,05$).

Zaključki. Najboljši način zdravljenja lokalno napredovalega raka zunanjega spolovila nudi kombinacija operacije in obsevanja z ali brez kemoterapije. V primeru prisotnosti negativnih dejavnikov tveganja je zaradi boljše lokalne kontrole smiselno obsevanje z dozo ≥ 54 Gy.

Radiol Oncol 2017; 51(4): 455-462.

doi: 10.1515/raon-2017-0040

Povezava med polimorfizmi gena *SLC19A1* in toksičnostjo visokih odmerkov metotreksata pri otrocih z akutno limfoblastno levkemijo in ne-Hodgkinovim malignim limfomom. Uvedba obravnave, ki temelji na haplotipih

Faganel Kotnik B, Jazbec J, Bohanec Grabar P, Rodriguez-Antona C, Dolžan V

Izhodišča. Raziskovali smo klinično pomembnost vpliva genetske variabilnosti *SLC19A1* na z metotreksatom v visokem odmerku (HD-MTX) povzročene toksičnosti pri otrocih in adolescentih, ki smo jih zdravili zaradi akutne limfoblastne levkemije (ALL) in ne-Hodgkinovega malignega limfoma (NHML).

Bolniki in metode. Pri 88 otrocih in mladostnikih z ALL/NHML smo raziskovali vpliv polimorfizmov posameznega nukleotida (SNP) in haplotipov *SLC19A1* na toksičnost, povzročeno s HD-MTX.

Rezultati. Bolniki z genotipom TT rs2838958 so imeli večjo verjetnost za razvoj mukozitisa v primerjavi z nosilci najmanj enega C alela rs2838958 (Razmerje obojev [OR] 0,226 [0,071–0,725], $p < 0,009$). Haplotip TGTCCG (H4) je statistično značilno zmanjšal tveganje za pojav neželenih učinkov med zdravljenjem s HD-MTX (OR 0,143 [0,02274–0,852], $p = 0,0303$).

Zaključki. Analiza *SLC19A1* SNP in haplotipov bi lahko prinesla dodatne informacije za bolniku prilagojeno zdravljenje s HD-MTX pri otrocih z ALL/NHML. To bi lahko omogočilo boljši izid zdravljenja. Za validacijo rezultatov so potrebne nadaljnje raziskave.

Radiol Oncol 2017; 51(4): 463-468.
doi: 10.1515/raon-2017-0041

Vpliv obsevalne doze in možganskega volumna V57 Gy na napredovanje bolezni in preživetje pri bolnikih z multiformnim glioblastomom

Stojkovski I, Krstevska V, Smichkoska S

Izhodišča. Namen raziskave je bil analizirati vpliv obsevanega volumna možgan V57 Gy (volumna, ki je prejel 57 Gy ali več) na čas do napredovanja bolezni in na preživetje pri bolnikih z glioblastomom.

Bolniki in metode. Naredili smo dozimetrično analizo obsevalnih načrtov pri 70 bolnikov z glioblastomom, ki so prejeli pooperativno radiokemoterapijo s temozolamidom in nato še z adjuvantno terapijo prav tako s temozolamidom. Bolnike smo zdravili z dvema različnima načinoma, ki smo ju uporabili pri opredelitvi obsevanega volumna in pri predpisu obsevalne doze. Prvo skupino bolnikov smo obsevali z enim volumnom, ki je prejel 60 Gy v dnevni frakciji po 2 Gy (31 bolnikov). Drugo skupino bolnikov pa smo obsevali s stožčasto tehniko cone-downe, sestavljeno iz dveh faz. Prvi fazi s 46 Gy v frakcijah po 2 Gy je sledil dodatek cone-down s 14 Gy v frakcijah po 2 Gy (39 bolnikov). Določili smo volumen V57 Gy in razmerje med volumnom možgan in V57 Gy. Povprečne vrednosti obeh parametrov smo obravnavali kot prazne vrednosti. Tako smo bolnike razdelili v dve skupini glede na vsak parameter (manjše oz. večje vrednosti od prazne).

Rezultati. Povprečna vrednost volumna V57 Gy je bila 593,39 cm³ (razpon 166,94 do 968,60 cm³), povprečna vrednost volumna možgan 1332,86 cm³ (razpon 1047 do 1671,90 cm³) in povprečna vrednost razmerja možgani/V57 Gy 2,46 (razpon 1,42 do 7,67). Med obama skupinama ni bilo pomembne razlike glede V57 Gy in razmerja med volumnom možgan in V57 Gy.

Zaključki. Volumen, ki smo ga obsevali z dozo več kot 57 Gy (V57 Gy) in razmerje med volumnom celih možgan in V57 Gy nista imela vpliva na čas do napredovanja bolezni in na preživetje pri bolnikih z glioblastomom.

Radiol Oncol 2017; 51(4): 469-474.
doi: 10.1515/raon-2017-0050

Zagotavljanje kakovosti pri uporabi analize gama za radiokromsko filmsko dozimetrijo

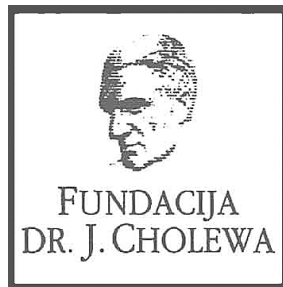
Zwierzchowski G, Bieledda G, Skowronek J

Izhodišča. Za komisioniranje načrtovalnih sistemov v brahiterapiji potrebujemo hitre in enostavno ponovljive postopke. V teleradioterapiji je uporaba analize gama pri radiokromski filmski dozimetriji že dobro uveljavljena metoda pri postopkih za zagotavljanje kakovosti. Obenem to metodo vedno bolj uporabljamo pri preverjanju dvodimenzionalne dozne porazdelitve v brahiterapiji. Analizo gama lahko uporabljamo kot metodo za primerjavo med izračunanimi in izmerjenimi dozami v skladu s poročilom TG-186 in za računske algoritme MBDCA. Namen raziskave je bil dozimetrično preverjanje računskih algoritmov v načrtovalnih sistemih za brahiterapijo, ko uporabljamo krožne aplikatorje CT/MRI.

Materiali in metode. V raziskavi smo uporabljali krožna aplikatorja s polmeroma 26 in 30 mm ter 60 mm maternično sondo. Za same meritve doze pa smo uporabljali filme Gafchromic® EBT. Dozne porazdelitve smo izvozili iz načrtovalnih sistemov za vsako ravnino, v kateri smo uporabili filme, ki smo jih po obsevanju digitalizirali. Za analizo gama smo uporabili kriterij 3 % / 3 mm pri stopnji 95 %, kar je v skladu s priporočili iz AAPM TG-119. Podatke pa smo obdelali s sistemom OMNI Pro l'mRT®.

Rezultati. Povprečne vrednosti gama so bile od 0,1 do 0,44 za 26 mm krožni aplikator in od 0,1 do 0,27 za 30 mm krožni aplikator. V obeh primerih je bila stopnja ujemanja z izračunanimi vrednostmi 99 %.

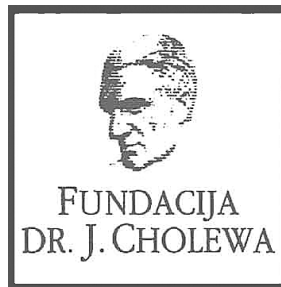
Zaključki. Predstavljena analiza je pokazala odlično ujemanje med doznimi porazdelitvami izračunanimi z načrtovalnimi sistemi in doznimi porazdelitvami, ki smo jih izmerili z gafkromskimi filmi. Naše ugotovitve potrjujejo primernost uporabe filmske dozimetrije v brahiterapiji.



FUNDACIJA "DOCENT DR. J. CHOLEWA"
JE NEPROFITNO, NEINSTITUCIONALNO IN NESTRANKARSKO
ZDRUŽENJE POSAMEZNIKOV, USTANOV IN ORGANIZACIJ, KI ŽELIJO
MATERIALNO SPODBUJATI IN POGLABLJATI RAZISKOVALNO
DEJAVNOST V ONKOLOGIJI.

DUNAJSKA 106
1000 LJUBLJANA

IBAN: SI56 0203 3001 7879 431



Activity of “Dr. J. Cholewa” Foundation for Cancer Research and Education - a report for the final quarter of 2017

Dr. Josip Cholewa Foundation for cancer research and education continues with its planned activities in the final quarter of 2017. Its primary focus remains the provision of grants and scholarships and other forms of financial assistance for basic, clinical and public health research in the field of oncology. In parallel, it also makes efforts to provide financial and other support for the organisation of congresses, symposia and other forms of meetings to spread the knowledge about prevention and treatment of cancer, and finally about rehabilitation for cancer patients. In Foundation's strategy the spread of knowledge should not be restricted only to the professionals that treat cancer patients, but also to the patients themselves and to the general public.

The Foundation continues to provide support for »Radiology and Oncology«, a quarterly scientific magazine with a respectable impact factor that publishes research and review articles about all aspects of cancer. The magazine is edited and published in Ljubljana, Slovenia. »Radiology and Oncology« is an open access journal available to everyone free of charge. Its long tradition represents a guarantee for the continuity of international exchange of ideas and research results in the field of oncology for all in Slovenia that are interested and involved in helping people affected by many different aspects of cancer.

The Foundation will continue with its activities in the future, especially since the problems associated with cancer affect more and more people in Slovenia and elsewhere. Ever more successful treatment results in longer survival in many patients with previously incurable cancer conditions, thus adding many new dimensions in life of cancer survivors and their families.

Viljem Kovač, M.D., Ph.D.
Borut Štabuc, M.D., Ph.D.
Tomaž Benulič, M.D.
Andrej Plesničar, M.D., M.Sc.

Vectibix® + FOLFIRI v 1. liniji zdravljenja bolnikov z mKRR in nemutiranim genom RAS¹

Zdravilo Vectibix® je indicirano za zdravljenje odraslih bolnikov z metastatskim kolorektalnim rakom (mKRR) in nemutiranim genom RAS:

- v 1. liniji zdravljenja v kombinaciji s FOLFOX ali FOLFIRI
- v 2. liniji zdravljenja v kombinaciji s FOLFIRI pri bolnikih, ki so v prvi liniji zdravljenja prejeli kemoterapijo, ki je vključevala fluoropirimidin (vendar ni vključevala irinotekana)
- kot monoterapija po neuspehu shem kemoterapije, ki so vključevale fluoropirimidin, oksaliplatin in irinotekan.

Vectibix® 20 mg/ml koncentrat za raztopino za infundiranje (sterilni koncentrat) (panitumumab) – SKRAJŠAN POVZETEK GLAVNIH ZNAČILNOSTI ZDRAVILA
Samo za strokovno javnost. Pred predpisovanjem si preberite celoten Povzetek glavnih značilnosti zdravila (SmPC).

SESTAVA ZDRAVILA: 1 ml koncentrata vsebuje 20 mg panitumumaba. 1 viala vsebuje 100 mg panitumumabov 5 ml ali 400 mg panitumumabov v 20 ml koncentrata. **TERAPEVTSKE INDIKACIJE:** Zdravljenje odraslih bolnikov z metastatskim kolorektalnim rakom (mKRR) z dvijem tipom RAS in sicer v prvi liniji zdravljenja v kombinaciji s FOLFOX ali FOLFIRI, v drugi liniji zdravljenja v kombinaciji s FOLFIRI pri bolnikih, ki so v prvi liniji zdravljenja prejeli kemoterapijo, ki je vključevala fluoropirimidin (vendar ni vključevala irinotekana), ter kot monoterapija po neuspehu shem kemoterapije, ki so vključevale fluoropirimidin, oksaliplatin in irinotekan. **ODMERJANJE IN NAČIN UPORABE:** Zdravljenje z zdravilom Vectibix® mora nadzirati zdravnik z izkušnjami pri uporabi terapij proti raku. Pred začetkom zdravljenja z zdravilom Vectibix® mora biti potrjeno, da gre za stanje dvijega tipa RAS (KRAS in NRAS). Mutacijsko stanje mora ugotoviti izkusen laboratorij z uporabo validiranih testnih metod za detekcijo mutacij KRAS (aksoni 2, 3 in 4) in NRAS (aksoni 2, 3 in 4). Priporočeni odmerek zdravila Vectibix® je 6 mg/kg telesne mase enkrat na dva tedna. V primeru hudih (≥ 3. stopnja) dermatoloških reakcij je lahko potrebna prilagoditev odmerka zdravila Vectibix®. Bolniki z ovisno ledvico ali jeter: Varnost in učinkovitost zdravila Vectibix® nista raziskani. Starejši bolniki: Ni kliničnih podatkov, ki bi podprli prilagoditev odmerka. **Neželeni učinki:** Zdravilo Vectibix® nima relevantne uporabe za indikacijo zdravljenja kolorektalnega raka. Zdravilo Vectibix® morata aplikirati v intravenski (iv.) infuziji z infuzijsko črpalko. Če se pojavijo z infundiranjem povezane reakcije, je lahko potrebna uporaba infundiranja zdravila Vectibix®. Zdravila Vectibix® ne sme injicirati z intravenskim vbrzganjem ali v bolusu. **CONTRAINDIKACIJE:** Anamneza hude ali smrtne nevarne preobčutljivosti na zdravilno učinkovino ali katere koli pomožne snovi, intersticijski pnevmonitis, pljučna fibroza. Pri bolnikih z mKRR z mutiranim RAS in tisti bolnikih z mKRR, pri katerih stanje RAS ni znano, je kontraindicirana kombinacija zdravila Vectibix® in kemoterapije, ki vključuje oksaliplatin.

POSEBNA OPOZORILO IN PREVIDNOSTNI UKREPI: Dermatološke reakcije in toksičnost mehkih tkiv: Skoraj pri vseh bolnikih (približno 90%), zdravljenih z zdravilom Vectibix®, se pojavijo dermatološke reakcije, ki so farmakološki učinek, opažen pri zavirateljih EGFR. Če se pri bolniku pojavijo dermatološke reakcije 3. ali višje stopnje (po CTCAE verzija 4.0) ali dermatološke reakcije, ocenjene kot neznosne, je priporočljiva naslednja prilagoditev odmerka: Prvi pojav kožnih simptomov z 3. stopnjo: Zadržite 1 ali 2 odmerka zdravila Vectibix®, če se simptomi izboljšajo (< 3. stopnja), nadaljujte infundiranje z 100 % odmerka, ki ste ga aplikirali pred pojavom kožnih simptomov; če izboljšanja ni, prekinite uporabo zdravila Vectibix®. Ob drugem pojavu kožnih simptomov z 3. stopnjo: Zadržite 1 ali 2 odmerka zdravila Vectibix®, če se simptomi izboljšajo (< 3. stopnja), nadaljujte infundiranje z 80 % odmerka, ki ste ga aplikirali pred pojavom kožnih simptomov; če izboljšanja ni, prekinite uporabo zdravila Vectibix®. Ob tretjem pojavu kožnih simptomov z 3. stopnjo: Zadržite 1 ali 2 odmerka zdravila Vectibix®, če se simptomi izboljšajo (< 3. stopnja), nadaljujte infundiranje z 60 % odmerka, ki ste ga aplikirali pred pojavom kožnih simptomov; če izboljšanja ni, prekinite uporabo zdravila Vectibix®. Ob četrtem pojavu kožnih simptomov z 3. stopnjo: Prekinite uporabo. Bolniki s hudimi dermatološkimi reakcijami ali toksičnostjo mehkih tkiv ali poslabšanjem reakcij med uporabo zdravila Vectibix® morate nadzirati zaradi možnih vnetnih ali infekcijskih posledic (vključno s celulitisom in nekrotizirajočim fasciitisom) ter jim nemudoma vnesti ustrezno zdravljenje, če se pojavijo. Če se pojavi dermatološka toksičnost ali toksičnost mehkih tkiv, povezana s hudimi ali življenjsko ogrožujočimi vnetnimi ali infekcijskimi zapleti, zadržite ali prekinite zdravljenje z zdravilom Vectibix®. Zapleti na pljučih: V primeru akutnega nastanka ali poslabšanja pljučnih simptomov morate z zdravljenjem z zdravilom Vectibix® prekiniti in simptome takoj razbiti. Če diagnosticirate intersticijsko pljučno bolezen, morate zdravljenje z zdravilom Vectibix® za stalno prekiniti in bolnika ustrezno zdraviti. Pri bolnikih z anamnezo intersticijskega pnevmonitisa ali pljučne fibroze je potrebno skrbno razmisлити o koristih zdravljenja s panitumumabom v primerjavi s tveganjem za zaplete na pljučih. **Elektrolitske motnje:** Bolnika je treba pred uvedbo zdravljenja, med zdravljenjem in 5a 8 tednov po končanem zdravljenju z zdravilom Vectibix®, redno spremljati glede hipomagnezije in spremljati tudi hipokalciemije. Priporočljivo je dodajanje magnezija, kot je ustrezno. Opaziti so tudi druge elektrolitske motnje, vključno s hipokalciemijo. Priporočljivo je spremljanje, kot opisano zgoraj in dodajanje teh elektrolitov, kot je ustrezno. Z infundiranjem povezane reakcije: Če se kadarkoli med ali po infundiranju pojavi huda ali smrtne nevarne reakcija (npr. z bronhospazmom, angioedemom, hipotenzijo, potrebo po parenteralnem zdravljenju ali anafilakso), je treba uporabo zdravila Vectibix® za stalno prekiniti. Bolnikom, ki se jim pojavi blaga ali zmerna (1. in 2. stopnja po CTCAE verzija 4.0) z infundiranjem povezana reakcija, je treba hitrost infundiranja za 50 % zmanjšati. To manjšo hitrost infundiranja je priporočljivo ohraniti tudi pri vseh nadaljnjih infuzijah. Opazna so preobčutljiva reakcija, ki so se pojavile več kot 24 ur po infundiranju, vključno s smrtimi primeri angioedema, ki so se pojavili več kot 24 ur po infundiranju. Bolnika je potrebno opozoriti na možnost reakcij z posrnim nastankom in jim naročiti, naj se obrnejo na svojega zdravnika, če se jim pojavijo simptomi preobčutljivostne reakcije. **Akutna odpoved ledvic:** Opisana je akutna odpoved ledvic pri bolnikih, ki se jim pojavi huda driska in

dehidracija. Bolnikom, ki se jim pojavi huda driska, je treba naročiti, da se takoj posvetujejo z zdravnikom. Zdravilo Vectibix® v kombinaciji s kemoterapijo na podlagi oksaliplatina pri bolnikih z mKRR z mutiranim RAS oz. bolnikih z mKRR, pri katerih stanje RAS tumorja ni znano: Kombinacija zdravila Vectibix® s kemoterapijo, ki vključuje oksaliplatin, je kontraindicirana pri bolnikih z mKRR z mutiranim RAS ali pri katerih stanje RAS ni znano. Če je predvidena uporaba zdravila Vectibix® v kombinaciji s FOLFOX, je priporočljivo, da mutacijsko stanje določi laboratorij, ki sodeluje v programu Elstamo zagotavljanje kakovosti RAS, ali da se stanje dvijega tipa potrdi z duplikiranjem preiskave. **Očesni toksični učinki:** Bolnika, ki se jim med prejetjem zdravila Vectibix® pojavijo znaki in simptomi, ki kažejo na keratitis, kot so akutni pojav ali poslabšanje: vnetja očesa, solzanje, občutljivost na svetlobo, zamagljenega vida, bolečina v očesu in/ali rdečina oči, je priporočljivo takoj napotiti k specialistu oftalmologu. Če je potrjena diagnoza ulcerativnega keratitisa, je treba zdravljenje z zdravilom Vectibix® začasno ali trajno prekiniti. Če je diagnosticiran keratitis, je treba skrbno preiskati koristi in tveganja nadaljevanja zdravljenja. Zdravilo Vectibix® morate uporabljati previdno pri bolnikih z anamnezo keratitisa, ulcerativnega keratitisa ali zelo suhih oči. Bolniki z zmogljivostnim stanjem 2 po ECOG, zdravljeni z zdravilom Vectibix® v kombinaciji s kemoterapijo: Pri teh bolnikih je pred uvedbo zdravila Vectibix® v kombinaciji s kemoterapijo za zdravljenje mKRR priporočljivo oceniti koristi in tveganja, saj pri njih pozitivno razmerje med koristnostjo in tveganjem ni bilo zaznано. Starejši bolniki: V celoti niso ugotovili razlik v varnosti ali učinkovitosti med starejšimi bolniki (starejši s 65 leti), ki so prejeli monoterapijo z zdravilom Vectibix®, drugi, prvotnostni učinki: Zdravilo vsebuje manj kot 0,150 mmol natrija (kar je 3,45 mg natrija) na mililitr koncentrata. To je treba upoštevati pri bolnikih, ki potrebujejo prehrano z nadzorovano količino natrija. **MESELEJNO DELOVANJE Z DRUGIMI ZDRAVILI IN DRUGE OBKLE INTERAKCIJE:** Podatki študije o medsebojnem delovanju zdravil, ki je vključevala zdravilo Vectibix® in irinotekan, pri bolnikih z mKRR kažejo, da se med sočasno uporabo zdravil farmakokinetika irinotekana in njegovega aktivnega metabolita SN-38 ne spreminjati. Rezultati primerjave v navzdol študij so pokazali, da shema z irinotekanom (IFL ali FOLFIRI) ne vpliva na farmakokinetiko panitumumaba. Zdravila Vectibix® se ne sme uporabljati v kombinaciji s kemoterapijo IFL ali kemoterapijo, ki vključuje bevacizumab. Kombinacija zdravila Vectibix® s kemoterapijo, ki vključuje oksaliplatin, je kontraindicirana pri bolnikih z mKRR z mutiranim RAS ali pri katerih stanje RAS ni znano. **NEŽELENI UČINKI:** Neželeni učinki, zaznani v kliničnih študijah in v spontanih poročilih v obdobju zdravljenja pri bolnikih z mKRR, ki so dobili panitumumab kot edino zdravilo ali v kombinaciji s kemoterapijo, so: zelo pogosti (≥ 1/10): paronihija, anemija, hipokalciemija, anoreksija, hipomagnezija, nespečnost, konjunktivitis, dispneja, kašelj, driska, navzea, bruhanje, bolečina v trebuhu, stomatitis, zaprtost, akneliformni dermatitis, tipična (vključuje splošne temne kožne toksičnosti, ekfoliacije kože, ekfoliativnega tipična, papulozna tipična, pruritična tipična, eritematozna tipična, generalizirana tipična, makularna tipična, makulopapulozna tipična, kožna lezija), eritem, srbenje, suha koža, nesure na koži, akne, alopecija, bolečina v hrbtu, utrujenost, piroksija, znojenje, vnetje sluznice, periferni edem, paronihija, zmanjšanje telesne mase; pogosti (≥ 1/100 do < 1/10): pustulozni tipična, celulitis, okužba s očmi, folikulitis, lokalizirana okužba, levkopenija, preobčutljivost, hipokalciemija, dehidracija, hiperglikemija, hipotenzija, anksioznost, glavobol, omotica, biferaritis, nast trnčinski, močnejša solzanja, očesna hiperemija, suho oko, srbenje oči, draženje oči, tahikardija, globoka venska tromboza, hipertenzija, hipertenzija, zadrževanje pljučne embolije, apneja, krvavitve iz danke, suha usta, dispepsija, atročni stomatitis, helitis, gastroezofagealna refluxna bolezen, sindrom palmarno-plantarne eritrodizostoze, kožni ulkus, krasta, hiperterioza, krampljenje nohtov, bolzani nohtov, hiperhidroza, dermatitis, bolečina v okončinah, bolečina v prsih, bolečina, mrzlica, znižanje magnezija v krvi; Občasni (≥ 1/1.000 do < 1/100): okužba oči, okužba vek, draženje vek, keratitis, dnozoza, bronhospazem, suhost nosu, razpokane ustnice, suha ustnica, angioedem, hrušbetem, vraščanje nohta, oniholiza, z infundiranjem povezane reakcije; Redki (≥ 1/10.000 do < 1/1.000): anafilaktična reakcija, ulcerativni keratitis, nekroza kože, Stevens-Johnsonov sindrom, toksična epidermalna nekroliza; Pogostost naznana (pogostost ni mogoče oceniti iz razpoložljivih podatkov): intersticijska pljučna bolezen. **FARMACEVTSKI PODATKI:** Shranjujte v hladilniku (2 °C - 8 °C). Ne zamrzujte. Zdravilo Vectibix® ne vsebuje nobenih anti mikrobnih konzervansov ali baktericidnih. Zdravilo je treba uporabiti takoj po razreditvi. Razreditve ne sme zamrzniti. Zdravilo Vectibix® je namenjeno za enkratno uporabo. **NAČIN IN REŽIM PREDPISOVANJA TER IZDAJE ZDRAVILA:** Predpisovanje in izdaja zdravila je le na recept s posebnim režimom – N.A.CHIN IN REŽIM PREDPISOVANJA TER IZDAJE ZDRAVILA. Predpisovanje in izdaja zdravila je le na recept s posebnim režimom – N.A.CHIN IN REŽIM PREDPISOVANJA TER IZDAJE ZDRAVILA. **AMGEN EUROPA BV, Minsvur 7061, NL-4817 ZK Breda, Nizozemska.** Dodatna pojavnika lahko dobite v lokalni pisarni: AMGEN zdravila d.o.o., Šmartinska 140, SI-1000 Ljubljana. **DATUM ZA DOLGE REVIZIJE BESSEDIL:** November 2016. **DATUM PRIPRAVE FOLIOKALCIJE:** November 2017. Podrobne informacije o zdravilu so objavljene na spletni strani Evropske agencije za zdravila <https://www.ema.europa.eu>.

Zdravilo za predhodno že zdravljene bolnike z mKRR

Več časa za trenutke, ki štejejo

Lonsurf
trifluridin/tipiracil

Spremeni zgodbo predhodno že zdravljenih bolnikov z mKRR

LONSURF® (trifluridin/tipiracil) je indiciran za zdravljenje odraslih bolnikov z metastatskim kolorektalnim rakom (mKRR), ki so bili predhodno že zdravljeni ali niso primerni za zdravljenja, ki so na voljo. Ta vključujejo kemoterapijo na osnovi fluoropirimidina, oksaliplatina in irinotekana, zdravljenje z zaviralci žilnega endotelijskega rastnega dejavnika (VEGF) in zaviralci receptorjev za epidermalni rastni dejavnik (EGFR).

mKRR = metastatski kolorektalni rak

Družba Servier ima licenco družbe Taiho za zdravilo Lonsurf®. Pri globalnem razvoju zdravila sodelujeta obe družbi in ga tržišta na svojih določenih področjih.

TAIHO TAIHO PHARMACEUTICAL CO., LTD.

SERVIER

Skrajšan povzetek glavnih značilnosti zdravila: Lonsurf 15 mg/6,14 mg filmsko obložene tablete in Lonsurf 20 mg/8,19 mg filmsko obložene tablete

▼ Za to zdravilo se izvaja dodatno spremljanje varnosti. **SESTAVA***: Lonsurf 15 mg/6,14 mg: Ena filmsko obložena tableta vsebuje 15 mg trifluridina in 6,14 mg tipiracila (v obliki klorida). Lonsurf 20 mg/8,19 mg: Ena filmsko obložena tableta vsebuje 20 mg trifluridina in 8,19 mg tipiracila (v obliki klorida). **TERAPEVTSKE INDIKACIJE***: Zdravilo Lonsurf je indicirano za zdravljenje odraslih bolnikov z metastatskim kolorektalnim rakom, ki so bili predhodno že zdravljeni ali niso primerni za zdravljenja, ki so na voljo. Ta vključujejo kemoterapijo na osnovi fluoropirimidina, oksaliplatina in irinotekana, zdravljenje z zaviralci žilnega endotelijskega rastnega dejavnika (VEGF - Vascular Endothelial Growth Factor) in zaviralci receptorjev za epidermalni rastni dejavnik (EGFR - Epidermal Growth Factor Receptor). **ODMERJANJE IN NAČIN UPORABE***: Priporočeni začetni odmerek zdravila Lonsurf pri odraslih je 35 mg/m²/odmerek peroralno dvakrat dnevno na 1. do 5. dan in 8. do 12. dan vsakega 28-dnevnega cikla zdravljenja, najpozneje 1 uro po zaključku jutranjega in večernega obroka. Odmerjanje, izračunano glede na telesno površino, ne sme preseči 80 mg/odmerek. Možne prilagoditve odmerka glede na varnost in prenašanje zdravila: dovoljena so največ 3 zmanjšanja odmerka na najmanjši odmerek 20 mg/m² dvakrat dnevno. Potem ko je bil odmerek zmanjšan, povečanje ni dovoljeno. **KONTRAJNIKACIJE***: Preobčutljivost na zdravilni učinkovini ali katero koli pomožno snov. **OPAZOVANA IN PREVIJENOSTNI UKREPI***: Supresija kostnega mozga; Pred uvedbo zdravljenja, pred vsakim ciklom zdravljenja in po potrebi je treba pregledati celotno krvno sliko. Zdravljenja ne sme začeti, če je absolutno število nevtrilicov < 1,5 x 10⁹/l, če je število trombocitov < 75 x 10⁹/l ali če se je pri bolniku zaradi predhodnih zdravljenj pojavila klinično pomembna nehematološka toksičnost 3. ali 4. stopnje, ki še traja. Bolnike je treba skrbno spremljati zaradi morebitnih okužb, uvesti je treba ustrezne ukrepe, kot je klinično indicirano. **Toksičnost za prebavila**: Potrebna je uporaba antiemetikov, antiacidov ter drugih ukrepov, kot je klinično indicirano. Če je potrebno, prilagodite odmerke. **Ladične okvare**: Zdravilo Lonsurf ni primerno za uporabo pri bolnikih s hudo ledvično okvaro ali krepčo stopno ledvično okvaro. Bolnike z zmerno ledvično okvaro je treba zaradi hematološke toksičnosti bolj pogosto spremljati. **Jatrna okvara**: Uporaba zdravila Lonsurf pri bolnikih z obstoječo zmerno ali hudo jatro okvaro ni priporočljiva. **Proteinurija**: Pred začetkom zdravljenja in med njim je priporočljivo spremljanje proteinurije z urinskimi testnimi lističi. **Pomožne snovi**: Zdravilo vsebuje laktozo. **INTERAKCIJE***: Zdravilo, ki medsebojno delujejo z nukleosidnimi pranašalci CNT1, ENT1 in ENT2, zaviralci OCT2 ali MATE1, substrati humane timidin-kinaze (npr. didovudinom), hormonskimi kontraceptivi. **PLODNOST*, NOSEČNOST IN DOJENJE***: Ni priporočljivo. **KONTRACEPCIJA***: Ženske in moški morajo uporabljati učinkovito metodo kontracepcije med zdravljenjem in do 6 mesecev po zaključku zdravljenja. **YPLIV NA SPOSOBNOST VOŽNJE IN UPRAVLJANJA S STROJI***: Med zdravljenjem se lahko pojavijo utrujenost, omotica ali splošno slabo počutje. **NEZELENI UČINKI***: **Želo pogosti**: nevropenija, levkopenija, anemija, trombocitopenija, zmanjšan apetit, diareja, navzea, bruhanje, utrujenost. **Pogosti**: okužba spodnjih dihal, okužba zgornjih dihal, febrilna nevropenija, limfopenija, monocitoza, hipotalbinemija, nespečnost, disgezija, periferna nevropatija, omotica, glavobol, vročinski oblivi, dispneja, kašelj, bolečina v trebuhu, zaprtje, stomatitis, boleznj ustne votline, hiperbilirubinemija, sindrom palmarne plantarne eritrodizestezije, izpuščaj, alopecija, pruritus, suha koža, proteinurija, pireksija, edem, vnetje sluznice, splošno slabo počutje, zvišanje jetrnih encimov, zvišanje alkalne fosfataze v krvi, zmanjšanje telesne mase. **Občasni**: sepični tok, infekcijski entritis, pljučnica, okužba žolčevoda, gripa, okužba sečil, vnetje dišani, herpes zoster, tinea pedis, kandidaza, bakterijska okužba, okužba, bolečina zaradi raka, pancitopenija, granulocitopenija, monocitopenija, eritropenija, levkocitoza, dehidracija, hiperglikemija, hiperkalemija, hipokalemija, hiponatremija, hipoproteinemija, hipoproteinemija, hipokalciemija, protein, anksioznost, nevrotoksičnost, disestezija, hiperestezija, hiposteziija, sinkopa, parestezija, pekoč občutek, letargija, zmanjšana ostrina vida, zamajen vid, diplopija, katarakta, konjunktivitis, suho oko, vrtoglavica, neugodje v ušesu, angina pectoris, aritmija, palpitacija, embolija, hipertenzija, hipotenzija, pljučna embolija, pleuralni izliv, izcedek iz nosu, distonija, orofaringealna bolečina, epistaksa, hemoragični enterokolitis, krvavitve v prebavilih, akutni pankreatitis, ascites, ileus, subileus, kolitis, gastritis, refluksni gastritis, azobgilitis, moteno praznjenje želodca, abdominalna distenzija, anelno vnetje, razjede v ustih, dispnejska, gastrozofagalna refluksna bolezen, protalgija, bukalni polip, krvavitve dišani, glossitis, parodontalna bolezen, bolezen zob, siljenje na bruhanje, flatulenca, slab zadah, hepatotoksičnost, razširitev žolčnih vodov, luščenje kože, urtikarija, preobčutljivostne reakcije na svetlobo, eritem, akne, hiperhidroza, žuli, boleznj nohtov, otekanje sklepov, artralgiija, bolečina v kosteh, mialgija, mišično-skeletna bolečina, mišična oslabelost, mišični krči, bolečina v okončinah, občutek teže, ledvična odpoved, neinfektivni cistitis, motnje mikcije, hematuzija, levkociturija, motnje menstruacija, poslabšanje splošnega zdravstvenega stanja, bolečina, občutek spremembe telesne temperature, keseroza, zvišanje kreatinina v krvi, podaljšanje intervala QT na elektrokardiogramu, povečanje mednarodnega umerjenega razmerja (INR), podaljšanje aktiviranega parcialnega trombotičnega časa (aPTC), zvišanje sečnine v krvi, zvišanje laktatne dehidrogenaze v krvi, znižanje celokupnih proteinov, zvišanje C-reaktivnega proteina, zmanjšanje hematokrita. **Postmarketske izkušnje**: pri bolnikih, zdravljenih z zdravilom Lonsurf na Japonskem, so poročali o primerih intersticijske bolezni pljuč. **PREVELIKO ODMERJANJE***: Neželene učinki, o katerih so poročali v povezavi s prevetlikim odmerjanjem, so bili v skladu z uveljavljenim varnostnim profilom. Glavni pričakovani zaplet prevetlika odmerjanja je supresija kostnega mozga. **FARMAKODINAMIČNE LASTNOSTI***: Farmakoterapevtska skupina: zdravila z delovanjem na novotvorbe, antiemetična, ciklaza. ATC: L01BC59. Zdravilo Lonsurf sestavljata antineoplastični timidinski nukleosidni analog, trifluridin, in zaviralec timidin-fosforilaze (TPaze), tipiracilijev klorid. Po privzemu v rakave celice timidin-kinaza fosforilira trifluridin. Ta se v celicah nato presnovi v substrat deoksitimbouklesinske kisline (DNA), ki se vgradi neposredno v DNA ter tako preprečuje celično proliferacijo. TPaza hitro razgradi trifluridin in njegova presnova po peroralni uporabi je hitra zaradi učinka prvga prehoda, zato je v zdravilo vključen zaviralec TPaze, tipiracilijev klorid. **PKIRIRANJE***: 20 filmsko obloženih tablet. **NAČIN PREDPISOVANJA IN IZDAJE ZDRAVILA**: Rp/Spec. **Inetnik dovoljenja za promet**: Les Laboratoires Servier, 50, rue Carnot, 92284 Suresnes cedex, Francija. **Številka dovoljenja za promet z zdravilom**: ELV/1/16/1096/001 (Lonsurf 15 mg/6,14 mg), ELV/1/16/1096/004 (Lonsurf 20 mg/8,19 mg). **Datum zadnje revizije besedila**: avgust 2017. * Pred predpisovanjem preberite celoten povzetek glavnih značilnosti zdravila. **Podrobnejše informacije so na voljo pri**: Servier Pharma d.o.o., Podmliščakova ulica 24, 1000 Ljubljana, tel: 01 563 48 11, www.servier.si.

PREMAGATI OVIRE. PRESEČI PRIČAKOVANJA.

Zdravilo ALECENSA[®] (alektinib) izkazuje visoke sistemske odzive in učinkovitost v CŽS pri bolnikih z ALK-pozitivnim napredovalim NDRP, ki so se predhodno zdravili s krizotinibom.¹

CŽS = centralno-živčni sistem, ALK = anaplastična limfomska kinaza, NDRP = nedrobnocelični rak pljuč

SKRAJŠAN POVZETEK GLAVNIH ZNAČILNOSTI ZDRAVILA

▼ Za to zdravilo se izvaja dodatno spremljanje varnosti. Tako bodo hitreje na voljo nove informacije o njegovi varnosti. Zdravstvene delavce naprošamo, da poročajo o katerem koli domnevnem neželenem učinku zdravila. Kako poročati o neželenih učinkih, si poglejte skrajšani povzetek glavnih značilnosti zdravila pod "Poročanje o domnevnih neželenih učinkih".

Ime zdravila: Alecensa 150 mg trde kapsule. **Kakovostna in količinska sestava:** Ena trda kapsula vsebuje alektinibijev klorid, kolikor ga ustreza 150 mg alektiniba. Pomožni snovi z znanim učinkom: vsaka trda kapsula vsebuje 33,7 mg laktoze in 6 mg natrija. **Terapevtske indikacije:** Zdravilo Alecensa je v monoterapiji indicirano za zdravljenje odraslih bolnikov z ALK-pozitivnim (ALK – anaplastična limfomska kinaza), napredovalim nedrobnoceličnim rakom pljuč, ki so se predhodno zdravili s krizotinibom. **Odmerjanje in način uporabe:** Za izbiro bolnikov, ki imajo ALK-pozitivnega nedrobnoceličnega raka pljuč, je treba opraviti validiran preizkus za ALK. Ali je bolnikov nedrobnocelični rak pljuč ALK-pozitiven, je treba ugotoviti pred začetkom zdravljenja z zdravilom Alecensa. **Odmerjanje:** Priporočeni odmerek zdravila Alecensa je 600 mg dvakrat na dan s hrano. **Trajanje zdravljenja:** Zdravljenje z zdravilom Alecensa je treba nadaljevati do napredovanja bolezni ali neprejemljivih toksičnih učinkov. **Prilagoditve odmerka:** Obvladovanje neželenih učinkov lahko obsega zmanjšanje odmerka, začasno prekinitve uporabe ali ukinitve zdravljenja z zdravilom Alecensa. Odmerek zdravila Alecensa je treba zmanjševati v korakih po 150 mg dvakrat na dan, upoštevaje prenašanje. Zdravljenje z zdravilom Alecensa je treba ukiniti, če bolnik ne prenese odmerka 300 mg dvakrat na dan. Smernice za prilagoditev odmerka so opisane v povzetku glavnih značilnosti zdravila. **Način uporabe:** zdravilo Alecensa je namenjeno peroralni uporabi. Trde kapsule mora bolnik pogotiviti cele in jih ne sme odpirati ali raztapljati. Vzeti jih mora s hrano. **Kontraindikacije:** preobčutljivost za alektinib ali katero koli pomožno snov. **Posebna opozorila in previdnostni ukrepi:** Intersticijska bolezen pljuč (IBP)/pnevmonitis: Bolnike je treba kontrolirati glede pljučnih simptomov, ki kažejo na pnevmonitis. Bolnikom, pri katerih je diagnosticirana IBP/pnevmonitis, je treba zdravljenje z zdravilom Alecensa nemudoma prekiniti; če ni mogoče ugotoviti drugih možnih vzrokov za IBP/pnevmonitis, je treba zdravljenje ukiniti. **Hepatotoksičnost:** Delovanje jeter, vključno z ALT, AST in celokupnim bilirubinom, je treba kontrolirati izhodno in nato na 2 tedna prve 3 mesece zdravljenja. Kasneje je treba spremljanje izvajati periodično, kar se dogodi lahko pojavijo po več kot 3 mesecih; pri bolnikih, ki se jim pojavi zvišanje aminotransferaz in bilirubina, morajo biti kontrole pogostejše. Glede na izrazitost neželenega učinka je treba uporabo zdravila Alecensa začasno prekiniti in zdravilo znova uvesti v manjšem odmerku, ali pa ga je treba ukiniti. Huda migalga in zvišanja kreatin-fosfokinaze (CPK): Bolnikom je treba naročiti, naj poročajo o vseh nepojasnjenih mišičnih bolečinah, občutljivosti ali šibkosti. Koncentracije CPK je treba določiti vsaka dva tedna v prvem mesecu zdravljenja, pri bolnikih, ki poročajo o simptomih, pa kot je klinično indicirano. Glede na izrazitost zvišanja CPK je treba uporabo zdravila Alecensa začasno prekiniti in zdravilo znova uvesti v manjšem odmerku. Bradikardija: Srčno frekvenco in krvni tlak je treba kontrolirati, kot je klinično indicirano. Če se bolniku pojavijo simptomatska bradikardija ali življenjsko ogrožujoči dogodek, je treba oceniti sočasna zdravila, za katera je znano, da povzročajo bradikardijo, in antihipertenzivna zdravila, odmerjanje zdravila Alecensa pa je treba prilagoditi. Fotosenzibilnost: Bolnikom je treba naročiti, naj se med jemanjem zdravila Alecensa in vsaj še 7 dni po koncu zdravljenja izogibajo dolgotrajnejšemu izpostavljanju soncu. Prav tako jim je treba naročiti, naj za preprečitev sončnih opeklin uporabljajo širokopspektralno zaščito za sončenje in mazilo za ustnice, ki ščitita pred ultravijoličnimi žarki A in B. Ženske v rodni dobi: zdravilo Alecensa lahko škoduje plodu, če je uporabljeno med nosečnostjo. Bolnice v rodni dobi morajo med zdravljenjem in še vsaj 3 mesece po zadnjem odmerku zdravila Alecensa uporabljati visoko učinkovito kontracepcijsko zaščito. **Medsebojno delovanje z drugimi zdravili in druge oblike interakcij:** Vplivi drugih zdravil na alektinib: **Induktorji CYP3A4:** Glede na učinka na skupno izpostavljenost alektinibu in M4 med sočasno uporabo zdravila Alecensa in induktorjev CYP3A4 odmerka ni treba prilagoditi. Priporočljivo je ustrezno spremljanje bolnikov, ki sočasno jemljejo močne induktorje CYP3A4. **Zaviralci CYP3A4:** Glede na učinka na skupno izpostavljenost alektinibu in M4 med sočasno uporabo zdravila Alecensa in zaviralcev CYP3A4 odmerka ni treba prilagoditi. Priporočljivo je ustrezno spremljanje bolnikov, ki sočasno jemljejo močne zaviralce CYP3A4. **Zdravila, ki zvišujejo pH v želodcu:** večkratni odmerki esomeprazola, zaviralca protonske črpalke, 40 mg ankrat na dan, niso imeli klinično pomembnega vpliva na skupno izpostavljenost alektinibu in M4. **Vpliv pranašalcev na odstranjevanje alektiniba:** M4 je substrat P-gp. Ker alektinib zavira P-gp, ni pričakovati, da bi sočasna uporaba z zaviralci P-gp pomembno vplivala na izpostavljenost M4. **Učinki alektiniba na druga zdravila:** **Substrat P-gp:** Če zdravilo Alecensa uporabljamo sočasno s substrati P-gp, je priporočljiv ustrezen nadzor. **Substrati BCRP:** Če zdravilo Alecensa uporabljamo sočasno s substrati BCRP, je priporočljiv ustrezen nadzor. **Substrati CYP:** Alektinib in M4 in vitro kažejo slabo časovno odvisno zavrtje CYP3A4; alektinib je v kliničnih koncentracijah pokazal šibek indukcijski potencial na CYP3A4 in CYP2B6. Tveganja za indukcijo encimov CYP2B6 in drugih encimov, reguliranih s PXR, razen encima CYP3A4, ni mogoče povsem izključiti. Učinkovitost sočasno uporabljenih peroralnih kontraceptivov se lahko zmanjša. **Neželeni učinki:** Povzetek neželenih učinkov pri bolnikih, zdravljenih z zdravilom Alecensa v ključnih kliničnih preskušanjih faze II. **Zelo pogosti:** anemija, motnje vida, driska, bruhanje, zaprtost, navzea, zvišana AST, ALT in zvišan bilirubin, izpuščaj, fotosenzibilnost, migalga, zvišana kreatin-fosfokinaza v krvi in edemi. **Pogosti:** bradikardija, zvišana alkalna fosfataza in zvišan kreatinin v krvi. **Poročanje o domnevnih neželenih učinkih:** Poročanje o domnevnih neželenih učinkih zdravila po izdaji dovoljenja za promet je pomembno. Omogoča namreč stalno spremljanje razmerja med koristmi in tveganji zdravila. Od zdravstvenih delavcev se zahteva, da poročajo o katerem koli domnevnem neželenem učinku zdravila na: Javna agencija Republike Slovenije za zdravila in medicinska pripomočila, Sektor za farmakovigilanco, Nacionalni center za farmakovigilanco, Slovenčeva ulica 22, SI-1000 Ljubljana, Tel: +386 (0)8 2000 500, Faks: +386 (0)8 2000 510, e-pošta: h-farmakovigilanca@jazmp.si, spletna stran: www.jazmp.si. **Režim izdaje zdravila:** Rp/Spec. **Imetniški dovoljenja za promet:** Roche Registration Limited, 6 Falcon Way, Shire Park, Welwyn Garden City, AL7 1TW, Velika Britanija. **Verzija:** 2.0/17. **Informacije pripravljene:** september 2017. Samo za strokovno javnost.

Literatura: 1. Povzetek glavnih značilnosti zdravila ALECENSA. Dostopano september 2017 na: http://www.ema.europa.eu/docs/en_Si/document_library/EPAR_-_Product_information/human/004164/WC500225707.pdf

DODATNE INFORMACIJE SO NA VOLJO PRI:

Roche farmacevtska družba d.o.o., Vodovodna cesta 109, 1000 Ljubljana



Instructions for authors

The editorial policy

Radiology and Oncology is a multidisciplinary journal devoted to the publishing original and high quality scientific papers and review articles, pertinent to diagnostic and interventional radiology, computerized tomography, magnetic resonance, ultrasound, nuclear medicine, radiotherapy, clinical and experimental oncology, radiobiology, radiophysics and radiation protection. Therefore, the scope of the journal is to cover beside radiology the diagnostic and therapeutic aspects in oncology, which distinguishes it from other journals in the field.

The Editorial Board requires that the paper has not been published or submitted for publication elsewhere; the authors are responsible for all statements in their papers. Accepted articles become the property of the journal and, therefore cannot be published elsewhere without the written permission of the editors.

Submission of the manuscript

The manuscript written in English should be submitted to the journal via online submission system Editorial Manager available for this journal at: www.radioloncol.com.

In case of problems, please contact Sašo Trupej at saso.trupej@computing.si or the Editor of this journal at gsera@onko-i.si

All articles are subjected to the editorial review and when the articles are appropriated they are reviewed by independent referees. In the cover letter, which must accompany the article, the authors are requested to suggest 3-4 researchers, competent to review their manuscript. However, please note that this will be treated only as a suggestion; the final selection of reviewers is exclusively the Editor's decision. The authors' names are revealed to the referees, but not vice versa.

Manuscripts which do not comply with the technical requirements stated herein will be returned to the authors for the correction before peer-review. The editorial board reserves the right to ask authors to make appropriate changes of the contents as well as grammatical and stylistic corrections when necessary. Page charges will be charged for manuscripts exceeding the recommended length, as well as additional editorial work and requests for printed reprints.

Articles are published printed and on-line as the open access (www.degruyter.com/view/j/raon).

All articles are subject to 700 EUR + VAT publication fee. Exceptionally, waiver of payment may be negotiated with editorial office, upon lack of funds.

Manuscripts submitted under multiple authorship are reviewed on the assumption that all listed authors concur in the submission and are responsible for its content; they must have agreed to its publication and have given the corresponding author the authority to act on their behalf in all matters pertaining to publication. The corresponding author is responsible for informing the coauthors of the manuscript status throughout the submission, review, and production process.

Preparation of manuscripts

Radiology and Oncology will consider manuscripts prepared according to the Uniform Requirements for Manuscripts Submitted to Biomedical Journals by International Committee of Medical Journal Editors (www.icmje.org). The manuscript should be written in grammatically and stylistically correct language. Abbreviations should be avoided. If their use is necessary, they should be explained at the first time mentioned. The technical data should conform to the SI system. The manuscript, excluding the references, tables, figures and figure legends, must not exceed 5000 words, and the number of figures and tables is limited to 8. Organize the text so that it includes: Introduction, Materials and methods, Results and Discussion. Exceptionally, the results and discussion can be combined in a single section. Start each section on a new page, and number each page consecutively with Arabic numerals.

The Title page should include a concise and informative title, followed by the full name(s) of the author(s); the institutional affiliation of each author; the name and address of the corresponding author (including telephone, fax and E-mail), and an abbreviated title (not exceeding 60 characters). This should be followed by the abstract page, summarizing in less than 250 words the reasons for the study, experimental approach, the major findings (with specific data if possible), and the principal conclusions, and providing 3-6 key words for indexing purposes. Structured abstracts are required. Slovene authors are requested to provide title and the abstract in Slovene language in a separate file. The text of the research article should then proceed as follows:

Introduction should summarize the rationale for the study or observation, citing only the essential references and stating the aim of the study.

Materials and methods should provide enough information to enable experiments to be repeated. New methods should be described in details.

Results should be presented clearly and concisely without repeating the data in the figures and tables. Emphasis should be on clear and precise presentation of results and their significance in relation to the aim of the investigation.

Discussion should explain the results rather than simply repeating them and interpret their significance and draw conclusions. It should discuss the results of the study in the light of previously published work.

Charts, Illustrations, Images and Tables

Charts, Illustrations, Images and Tables must be numbered and referred to in the text, with the appropriate location indicated. Charts, Illustrations and Images, provided electronically, should be of appropriate quality for good reproduction. Illustrations and charts must be vector image, created in CMYK color space, preferred font "Century Gothic", and saved as .AI, .EPS or .PDF format. Color charts, illustrations and Images are encouraged, and are published without additional charge. Image size must be 2.000 pixels on the longer side and saved as .JPG (maximum quality) format. In Images, mask the identities of the patients. Tables should be typed double-spaced, with a descriptive title and, if appropriate, units of numerical measurements included in the column heading. The files with the figures and tables can be uploaded as separate files.

References

References must be numbered in the order in which they appear in the text and their corresponding numbers quoted in the text. Authors are responsible for the accuracy of their references. References to the Abstracts and Letters to the Editor must be identified as such. Citation of papers in preparation or submitted for publication, unpublished observations, and personal communications should not be included in the reference list. If essential, such material may be incorporated in the appropriate place in the text. References follow the style of Index Medicus, DOI number (if exists) should be included.

All authors should be listed when their number does not exceed six; when there are seven or more authors, the first six listed are followed by "et al.". The following are some examples of references from articles, books and book chapters:

Dent RAG, Cole P. In vitro maturation of monocytes in squamous carcinoma of the lung. *Br J Cancer* 1981; **43**: 486-95. doi: 10.1038/bjc.1981.71

Chapman S, Nakielny R. *A guide to radiological procedures*. London: Bailliere Tindall; 1986.

Evans R, Alexander P. Mechanisms of extracellular killing of nucleated mammalian cells by macrophages. In: Nelson DS, editor. *Immunobiology of macrophage*. New York: Academic Press; 1976. p. 45-74.

Authorization for the use of human subjects or experimental animals

When reporting experiments on human subjects, authors should state whether the procedures followed the Helsinki Declaration. Patients have the right to privacy; therefore the identifying information (patient's names, hospital unit numbers) should not be published unless it is essential. In such cases the patient's informed consent for publication is needed, and should appear as an appropriate statement in the article. Institutional approval and Clinical Trial registration number is required. Retrospective clinical studies must be approved by the accredited Institutional Review Board/Committee for Medical Ethics or other equivalent body. These statements should appear in the Materials and methods section.

The research using animal subjects should be conducted according to the EU Directive 2010/63/EU and following the Guidelines for the welfare and use of animals in cancer research (*Br J Cancer* 2010; **102**: 1555 – 77). Authors must state the committee approving the experiments, and must confirm that all experiments were performed in accordance with relevant regulations.

These statements should appear in the Materials and methods section (or for contributions without this section, within the main text or in the captions of relevant figures or tables).

Transfer of copyright agreement

For the publication of accepted articles, authors are required to send the License to Publish to the publisher on the address of the editorial office. A properly completed License to Publish, signed by the Corresponding Author on behalf of all the authors, must be provided for each submitted manuscript.

The non-commercial use of each article will be governed by the Creative Commons Attribution-NonCommercial-NoDerivs license.

Conflict of interest

When the manuscript is submitted for publication, the authors are expected to disclose any relationship that might pose real, apparent or potential conflict of interest with respect to the results reported in that manuscript. Potential conflicts of interest include not only financial relationships but also other, non-financial relationships. In the Acknowledgement section the source of funding support should be mentioned. The Editors will make effort to ensure that conflicts of interest will not compromise the evaluation process of the submitted manuscripts; potential editors and reviewers will exempt themselves from review process when such conflict of interest exists. The statement of disclosure must be in the Cover letter accompanying the manuscript or submitted on the form available on www.icmje.org/coi_disclosure.pdf

Page proofs

Page proofs will be sent by E-mail to the corresponding author. It is their responsibility to check the proofs carefully and return a list of essential corrections to the editorial office within three days of receipt. Only grammatical corrections are acceptable at that time.

Open access

Papers are published electronically as open access on www.degruyter.com/view/j/raon, also papers accepted for publication as E-ahead of print.

Z ZDRUŽENIMI MOČMI, VEČ KOT 2-LETNO mPFS

S kombinacijo zdravila IBRANCE in letrozola, **prelomnim zdravljenjem 1. linije** za metastatskega raka dojke, je ugotovljeno **več kot 2-letno mPFS**.^{1,2} In v kombinaciji s fulvestrantom prinaša **večjo učinkovitost za širok krog bolnikov**.³

Zdravilo IBRANCE je indicirano za zdravljenje lokalno napredovelega ali metastatskega na hormone receptorje pozitivnega (HR+) in na receptorje humanega epidermalnega rastnega faktorja 2 negativnega (HER2-) raka dojke:

- v kombinaciji z zaviralcem aromataze,
- v kombinaciji s fulvestrantom pri ženskah, ki so prejele predhodno endokrino zdravljenje.

BISTVENI PODATKI IZ POVZETKA GLAVNIH ZNAČILNOSTI ZDRAVILA

IBRANCE 75 mg, 100 mg, 125 mg trde kapsule

▼ Za to zdravilo se izvaja dodatno spremljanje varnosti. Tako bodo hitreje na voljo nove informacije o njegovi varnosti. Zdravstvena delavca naprošamo, da poročajo o katerikoli domnevnem neželenem učinku zdravila. Glejte poglavje 4.8 povzetka glavnih značilnosti zdravila, kako poročati o neželenih učinkih.

Sestava in oblika zdravila: Ena trda kapsula vsebuje 75 mg, 100 mg ali 125 mg palbocikliba in 56 mg, 74 mg ali 93 mg laktoze (v obliki monohidrata). **Indikacije:** Zdravljenje lokalno napredovelega ali metastatskega na hormone receptorje pozitivnega in na receptorje humanega epidermalnega rastnega faktorja 2 (HER2 - Human Epidermal growth factor Receptor 2) negativnega raka dojke v kombinaciji z zaviralcem aromataze ali v kombinaciji s fulvestrantom pri ženskah, ki so prejele predhodno endokrino zdravljenje. Pri ženskah v pred- in perimenopavzi je treba endokrino zdravljenje kombinirati z agonistom gonadolibarina. **Odmerjanje in način uporabe:** Zdravljenje mora uvesti in nadzorovati zdravnik, ki ima izkušnje z uporabo zdravil za zdravljenje rakavih bolezni. Priporočeni odmerek je 125 mg enkrat na dan 21 zaporednih dni, sledi 7 dni brez zdravljenja (shema 3/7), celotni cikelus traja 28 dni. Zdravljenje je treba nadaljevati, dokler ima bolnik od zdravljenja klinično korist ali dokler se ne pojavi nesprejemljiva toksičnost. Pri sočasnem dajanju s palbociklibom je priporočeni odmerek letrozola 2,5 mg peroralno enkrat na dan, neprekinjeno vseh 28 dni ciklusa, glejte SmPC za letrozol. Pri sočasnem dajanju s palbociklibom je priporočeni odmerek fulvestranta 500 mg intramuskularno 1, 15, in 29. dan ter nato enkrat na mesec, glejte SmPC za fulvestrant. **Prilaganja odmerkov:** Za prilaganja odmerkov zaradi hematološke toksičnosti glejte preglednico 2, zaradi nehematološke toksičnosti pa preglednico 3 v SmPC-ju. **Posebne skupine bolnikov:** Starost: Prilaganje odmerka ni potrebno. **Okvara jeter ali ledvic:** Pri bolnikih z blago okvaro jeter ali blago ali zmerno okvaro ledvic prilaganje odmerka ni potrebno. **Podatčne populacije:** Varnost in učinkovitost pri otrocih in mladostnikih, starih 18 let, nista bili dokazani. **Način uporabe:** Peroralna uporaba. Jemanje s hrano, priporočljivo z obrokom. Ne smemo jemati z grenivko ali grenivkinim sokom. Kapsule zdravila je treba pogoltniti cele. **Kontraindikacije:** Preobutljivost na učinkovino ali katerikoli pomožni snov. Uporaba pripravkov s šentjanževko. **Posebna opozorila in previdnostni ukrepi:** Ženske v pred- in perimenopavzi: Kadar zdravilo uporabljamo v kombinaciji z zaviralcem aromataze je obvezna ovarijska ablacija ali supresija z agonistom gonadolibarina. Hematološke bolezni: Pri nevotropiji stopnje 3 ali 4 je priporočljiva prekinitav odmerjanja, zmanjšanje odmerka ali odložitve začetka ciklusa zdravljenja, bolnike pa je treba ustrezno spremljati. **Okužbe:** Zdravilo lahko poveča nagnjenost k okužbam, zato je bolnike treba spremljati glede znakov in simptomov okužbe ter jih ustrezno zdraviti. **Okvara jeter ali ledvic:** Bolnike z zmerno ali hudo okvaro jeter ali hudo okvaro ledvic zdravimo samo po skrbni oceni morebitnih koristi in tveganj, ter jih skrbno spremljamo glede znakov toksičnosti. **Laktoza:** Vsebuje laktozo. Bolniki z redko dedno intoleranco za galaktozo, lipoonsko obliko zmanjšane aktivnosti laktaze ali malabsorpcijo glukoze-galaktoze tega zdravila ne smejo jemati. **Medsebojno delovanje z drugimi zdravili in druge oblike interakcij:** Učinki drugih zdravil na farmakokinetiko palbocikliba: **Zaviralci CYP3A:** Sočasni uporabi močnih zaviralcev CYP3A, med drugim klaritromicina, indinavirja, itrakonazola, ketokonazola, lopinavirja/ritonavirja, nefazodona, neflavinirja, posakonazola, sakvinavirja, telaprevirja, telitromicina, vorikonazola in grenivke ali grenivkinega soka, se je treba izogibati. **Induktorji CYP3A:** Sočasni uporabi močnih induktorjev CYP3A, med drugim karbamazepina, enzalutamida, fenitoina, rifampicina in šentjanževke, se je treba izogibati. **Učinek zdravil za zmanjševanje kislin:** Ni pričakovati nobenega kliničnega pomembnega učinka na izpostavljenost palbociklibu, če palbociklib zaužijemo s hrano. **Učinki palbocikliba na farmakokinetiko drugih zdravil:** Pri sočasni uporabi bo morda treba zmanjšati odmerek občutljivih substratov CYP3A z ozkim terapevtskim indeksom (npr. afeentanil, ciklosporin, dihidroergotamin, ergotamin, everolimus, fentanil, pimoizid, kinidin, sirolimus in takrolimus), saj IBRANCE lahko poveča izpostavljenost tem zdravilom. **Študije in vitro s prenašalci palbocikliba** lahko zavira prenos, posredovan s P-gp v prebavilih in baljskovo odpornosti za raka dojke. Uporaba palbocikliba z zdravili, ki so substrati P-gp (npr. digoksin, dabigatran, kolhicin, pravastatin) ali BCRP (npr. rosuvastatin, sulfasalazin) lahko poveča njihov terapevtski učinek in neželene učinke. **Palbociklib lahko zavira privzorni prenašalec organskih kationov OCT1.** **Plodnost, nosečnost in dojenje:** Med zdravljenjem in vsaj 3 tedne (ženske) oziroma 14 tednov (moški) po koncu zdravljenja je treba uporabljati ustrezne kontracepcijske metode. Zdravila ne uporabljajte pri nosečnicah in ženskah v rodni dobi, ki ne uporabljajo kontracepcije. Bolnice, ki prejemajo palbociklib, ne smejo dojeti. Zdravljenje s palbociklibom lahko ogrozi plodnost pri moških. Pred začetkom zdravljenja naj moški zato razmislijo o hrambi sperme. **Vpliv na sposobnost vožnje in upravljanja s stroji:** Ima blag vpliv na sposobnost vožnje in upravljanja strojev. Bolniki morajo biti pri vožnji in upravljanju strojev previdni. **Neželeni učinki:** Zelo pogosti; okužbe, nevotropenja, levkopenija, anemija, trombocitopenija, pomanjkanje teka, stomatitis, navzea, diarreja, bruhanje, izpuščaji, alopecija, utrujenost. **Način in režim izdaje:** Rp/Spec - Predpisovanje in izdaja zdravila je le na recept zdravnika specialista ustreznega področja medicine ali od njega pooblaščenega zdravnika. **Imetnik dovoljenja za prometo:** Pfizer Limited, Ramsgate Road, Sandwich, Kent CT13 9NJ, Velika Britanija. **Datum zadnje revizije besedila:** 28.03.2017. **Pred predpisovanjem se seznanite s celotnim povzetkom glavnih značilnosti zdravila.**

*Na podlagi rezultatov randomiziranega nadzorovanega preskušanja III. faze.

¹mPFS = mediano preživetje brez napredovanja bolezni.

Literatura: 1. Povzetek glavnih značilnosti zdravila IBRance, 28.3.2017. 2. Finn RS, et al. PALOMA-2: Primary results from a phase 3 trial of palbociklib plus letrozole compared with placebo plus letrozole in postmenopausal women with ER+/HER2- advanced breast cancer. Kongres ASCO 2016, orala predstava. 3. Cristofanilli M, et al. Fulvestrant plus palbociklib versus fulvestrant plus placebo for treatment of hormone-receptor-positive, HER2-negative metastatic breast cancer that progressed on previous endocrine therapy (PALOMA-3): final analysis of the multicentre, double-blind, phase 3 randomised controlled trial. *Lancet Oncol.* 2016;17(4):425-439.

IBR-02-17 "Samo za strokovno javnost"



Pfizer Luxembourg SARL, GRAND DUCHY OF LUXEMBOURG,
51, Avenue J. F. Kennedy, L-1855
Pfizer, podružnica Ljubljana, Letališka cesta 3c, Ljubljana

IBRANCE
palbociklib

